THE EXERTION OF CELL-CELL ADHESIONS

Quint le Duc

Cover image: D. Bastiaanse, Domburg beach, NL

Splashing sea foam during a spring storm. The foam in this image is formed out of the remnants/gelatine of algea like e.g. choanoflagellates. The unicellular choanoflagellates can form multicellular colonies and are the closest living relatives to animals. They express cadherins and are believed to be ancestral to the cadherins in multicellular organisms and therefore my thesis.

The exertion of cell-cell adhesions

De inspanning van cel-cel contacten

(met een samenvatting in het Nederlands)

Proefschrift

ter verkrijging van de graad van doctor aan de Universiteit Utrecht op gezag van de rector magnificus, prof.dr. G.J. van der Zwaan, ingevolge het besluit van het college voor promoties in het openbaar te verdedigen op donderdag 21 januari 2016 des middags te 2.30 uur

door

Quint le Duc

geboren op datum 28 mei 1980

te Meliskerke

Promotor: Prof. dr. J.C. Clevers

Copromotor: Dr. ir. J. de Rooij

Dit proefschrift werd mede mogelijk gemaakt met financiële steun van het KWF

Table of content

Introduction: *General introduction*

1A Mechanotransduction at cadherin-mediated adhesions

1B HGF induced EMT as a model

General introduction

Regulation of cadherin adhesion in tissue organization and malignant transformation.

Cadherins are cell-cell adhesion molecules present in all tissues. Cadherins are transmembrane-proteins that form a homotypic, calcium-dependent complex with cadherins molecules on neighboring cells [1]. Inside the cell, they connect to the actin cytoskeleton[2] and thus mediate a strong physical connection between cells. As such, cadherins are important in the control of a wide range of fundamental biological processes, including embryonic development, tissue morphogenesis and vascular homeostasis. The main epithelial cadherin, E-cadherin, organizes into cell-cell adhesion structures called Adherens Junctions (AJ)[3] and is a tumor suppressor[4], whose loss of expression, mainly through gene-silencing, results in tumor metastasis[5-7]. However, several types of metastatic cancer, like certain agressive breast carcinomas (reviewed in[8-10]), do not show any downregulation of the E-cadherin protein. This implies that alternative mechanisms must exist to (de-) regulate E-cadherin adhesion.

At the start of the research described in this thesis, several reports had shown that cytoskeletal tension is involved in the downregulation of AJs. Tumor tissue was found to be stiffer than normal tissue and artificial increase of tissue stiffness in breast cancer cells resulted in the disorganization of AJs[11]. It was shown in our lab, that HGF-induced scattering of epithelial MDCK cells depends on actomyosin-driven cytoskeletal tension[12]: Myosin activity increased after HGF; the structure of the cytoskeleton changed after HGF; Actin-bundles were formed that connected to cell-cell junctions to pull them apart; inhibitors of myosin activity prevented all of this from happening. Together these observations indicated that E-cadherin's adhesive function is sensitive to cytoskeletal tension, but the underlying mechanisms remained completely elusive.

The dynamic link between E-cadherin and actin.

It had been generally accepted, through a large number of experimental studies, that E-cadherin interacts with actin through β–catenin and the actin-binding protein α–catenin. A number of other proteins had been found associated with the E-cadherin complex, including most notably p120-catenin, α–actinin and vinculin. P120-catenin was known to regulate E-cadherin's stability[13, 14]. The function of α–actinin and vinculin, two proteins that are also present in integrin-based adhesions, was less clear[15].

In the year before this PhD research started, this established view on the linkage between E-cadherin and the cytoskeleton had been challenged in two recent papers from James Nelson and William Weis[16, 17]. They showed that a ternary complex of E-cadherin, β/α-catenin and actin cannot

form in vitro. Furthermore, they showed that α–catenin cannot interact with actin and β–catenin simultaneously: It interacts with β–catenin as a monomer that posesses low affinity for F-actin. Dimerization, which is needed for high affinity for F-actin, excludes the interaction with β–catenin. This discrepancy between old models and the new observations, and the importance of cadherin adhesion for tissue development and cancer, triggered a lot of new research into the linkage between E-cadherin and the actin cytoskeleton.

The emerging role of mechanical forces in cadherin adhesion

The one crucial factor that the Nelson/Weis studies did not address was the role of mechanical forces. From integrin-adhesion research it was known that tension on integrin adhesions, caused by contractility in the associated actomyosin cytoskeleton, is needed for their development from nascent to mature[18]. Furthermore, our data and that of others had just indicated that myosin activity is needed for the formation of stable cadherin adhesions[12]. The research described in this thesis was aimed at further elucidating the molecular details of the link between cadherins and the actomyosin cytoskeleton in order to understand how mechanical tension influences the dynamics and function of cadherin adhesion.

Model systems used in our research

One of the tissue remodeling hormones that induces force on cell-cell junctions is HGF (hepatocyte growth factor). HGF induces branching morphogenesis in 3D cell culture and cell scattering in 2D. As was shown by our lab in 2005, HGF does not induce a classical epithelial mesenchymal transition (EMT) in which expression of E-cadherin is blocked to reduce epithelial cell-cell adhesion. In 2D culture models we showed that cell-cell junctions are disrupted as a result of the physical forces induced by HGF[12]. For the research described in this thesis, we have used HGF-induced scattering of MDCK or DU-145 cells as a means to apply tension on the E-cadherin complex and ask which molecular events are triggered by increased force and how they are involved in cell-cell adhesion remodeling.

Chapter 1A

In this published review, we discuss the (at that time) new insights on the dynamics of E-cadherin complex. The opinion of the Nelson en Weiss labs; that α–catenin is not linked to the actin cytoskeleton is debated in this review. Moreover, we and others suggest that the existing link is mechanoregulated and the emerging role of α–catenin and vinculin as the central players in this is discussed.

Chapter 1B

We review the role of HGF on cell scattering. The general mechanism of HGF signaling is discussed and the scattering effects of this growth factor on specific colony forming cell cultures. This cell-scattering phenothype is of great interest to us, because this hands us a tool to induce the force generated breakdown of E-cadherin mediated cell-cell junctions, that could potentially be relevant in cancer cell dissemination. We also screened for drugs interfering in this process to identify additional signaling intermediates that might regulate cell-cell adhesion.

Chapter 2

In this study, we present direct evidence that the E-cadherin complex is a mechanosensor that probes the mechanical environment to elicit a proportional change in the mechanics of the junctions. Furthermore, we show that vinculin potentiates E-cadherin–mediated mechanosensing and localizes to tension-bearing sites in cell–cell junctions to mediate mechanoregulation of cell–cell adhesion. An in depth review of this study and related articles on this subject, is found in Chapter 1A.

Chapter 3

In this study, we investigated the regulatory role of actomyosin during epithelial barrier formation in calcium switch assays and we investigated which cell–cell junction complexes mediate the functional link to actomyosin. We find that actomyosin-based force promotes epithelial barrier formation independent of the structural supportive role of F-actin. This force-dependent effect is mediated by α-catenin and Vinculin in the Cadherin complex specifically. Radial actin-contacted Focal Adherens Junctions (FAJ) are formed rapidly upon calcium, in which Vinculin responds to force on the E-cadherin complex to induce force-dependent reinforcement of cell–cell adhesion, resulting in accelerated barrier formation. This established a role for vinculin-dependent mechanotransduction in a physiological process that is completely independent from the HGF-induced signals.

Chapter 4

In this study, we investigated whether the recruitment of vinculin to other well-known classical cadherin family members, VE-cadherin and N-cadherin, is also dependent on mechanical tension. We wanted to know if vinculin dependend mechanotransduction is unique to E-cadherin mediated cell-cell junctions or more widespread among the cadherin family. The results show that vinculins

presence in both VE-, and N-cadherin mediated junctions is sensitive to actomyosin contractility, which implies that indeed vinculin based mechanotransduction is commonly utilized among the classical cadherins.

Chapter 5

In this study, we developed an apprehensible screening model for HGF induced cell scattering. The Hepatocyte growth factor (HGF), that causes epithelial cells to dissociate from each other and migrate as single cells, a phenomenon called scattering, which is a model for a developmental process known as the epithelial-mesenchymal transition, which also occurs in some cancers. We developed imaging tools that enabled us to track the scattering of live cells without the need to express fluorescently tagged proteins and in such a way that we could distinguish between changes in cell-cell adhesion and cell motility. We screened a drug library in an epithelial cell line with these imaging tools and uncovered inhibitors of cell-cell dissociation that did not strongly affect cell motility, such as nonsteroidal anti-inflammatory drugs. This assay could be used to identify drugs that prevent cell-cell dissociation, an early step in tumor invasion and metastasis. We did not identify signaling intermediates that are likely to affect the mechanotransduction processes mediated by α–catenin and vinculin in this screen.

Chapter 6

In this general discussion we make a short conclusion of our findings in the previous chapters. The E-cadherin complex is mechanoregulated and vinculin recruitment makes up a big part of the mechanism. Furthermore the implications of these findings are discussed; for instance: how is vinculin activated upon force induction, which proteins in the e-cadherin complex recruit/bind vinculin and are yet unidentified proteins involved within this mechanoregulated process.

This mechanoregulated cell-cell junction process is also observed from an evolutionary stand point. How has this complex been able to form over evolutionary time: is it borrowed from the cell-matrix junctions or has it been developed completely independently?

References

1. Patel, S.D., Chen, C.P., Bahna, F., Honig, B. & Shapiro, L. Cadherin-mediated cell-cell adhesion: sticking together as a family. *Curr Opin Struct Biol* **13**, 690-698 (2003).
2. Gumbiner, B.M. Regulation of cadherin adhesive activity. *J Cell Biol* **148**, 399-404 (2000).
3. Yap, A.S., Brieher, W.M., Pruschy, M. & Gumbiner, B.M. Lateral clustering of the adhesive ectodomain: a fundamental determinant of cadherin function. *Curr Biol* **7**, 308-315 (1997).
4. Derksen, P.W. *et al.* Somatic inactivation of E-cadherin and p53 in mice leads to metastatic lobular mammary carcinoma through induction of anoikis resistance and angiogenesis. *Cancer Cell* **10**, 437-449 (2006).
5. Hirohashi, S. & Kanai, Y. Cell adhesion system and human cancer morphogenesis. *Cancer Sci* **94**, 575-581 (2003).
6. Peinado, H., Portillo, F. & Cano, A. Transcriptional regulation of cadherins during development and carcinogenesis. *Int J Dev Biol* **48**, 365-375 (2004).
7. Yang, J. *et al.* Twist, a master regulator of morphogenesis, plays an essential role in tumor metastasis. *Cell* **117**, 927-939 (2004).
8. Hanby, A.M. Aspects of molecular phenotype and its correlations with breast cancer behaviour and taxonomy. *Br J Cancer* **92**, 613-617 (2005).
9. Kenemans, P., Verstraeten, R.A. & Verheijen, R.H. Oncogenic pathways in hereditary and sporadic breast cancer. *Maturitas* **49**, 34-43 (2004).
10. Knudsen, K.A. & Wheelock, M.J. Cadherins and the mammary gland. *J Cell Biochem* **95**, 488-496 (2005).
11. Paszek, M.J. *et al.* Tensional homeostasis and the malignant phenotype. *Cancer Cell* **8**, 241-254 (2005).
12. de Rooij, J., Kerstens, A., Danuser, G., Schwartz, M.A. & Waterman-Storer, C.M. Integrin-dependent actomyosin contraction regulates epithelial cell scattering. *J Cell Biol* **171**, 153-164 (2005).
13. Davis, M.A., Ireton, R.C. & Reynolds, A.B. A core function for p120-catenin in cadherin turnover. *J Cell Biol* **163**, 525-534 (2003).
14. Xiao, K. *et al.* Cellular levels of p120 catenin function as a set point for cadherin expression levels in microvascular endothelial cells. *J Cell Biol* **163**, 535-545 (2003).
15. Gumbiner, B.M. Regulation of cadherin-mediated adhesion in morphogenesis. *Nat Rev Mol Cell Biol* **6**, 622-634 (2005).
16. Drees, F., Pokutta, S., Yamada, S., Nelson, W.J. & Weis, W.I. Alpha-catenin is a molecular switch that binds E-cadherin-beta-catenin and regulates actin-filament assembly. *Cell* **123**, 903-915 (2005).
17. Pokutta, S., Drees, F., Takai, Y., Nelson, W.J. & Weis, W.I. Biochemical and structural definition of the l-afadin- and actin-binding sites of alpha-catenin. *J Biol Chem* **277**, 18868-18874 (2002).
18. Humphries, J.D. *et al.* Vinculin controls focal adhesion formation by direct interactions with talin and actin. *J Cell Biol* **179**, 1043-1057 (2007).

Available online at www.sciencedirect.com
ScienceDirect
Current Opinion in Cell Biology

Mechanotransduction at cadherin-mediated adhesions

Deborah E Leckband[1], Quint le Duc[2], Ning Wang[3] and Johan de Rooij[2]

Cell-to-cell junctions are crucial mechanical and signaling hubs that connect cells within tissues and probe the mechanics of the surrounding environment. Although the capacity of cell-to-extracellular-matrix (ECM) adhesions to sense matrix mechanics and proportionally modify cell functions is well established, cell–cell adhesions only recently emerged as a new class of force sensors. This finding exposes new pathways through which force can instruct cell functions. This review highlights recent findings, which demonstrate that protein complexes associated with classical cadherins, the principal architectural proteins at cell–cell junctions in all soft tissues, are mechanosensors. We further discuss the current understanding of the rudiments of a cadherin-based mechanosensing and transduction pathway, which is distinct from the force sensing machinery of cell–ECM adhesions.

Addresses
[1] School of Chemical Sciences, University of Illinois, Urbana, IL 61822, USA
[2] Hubrecht Institute and University Medical Centre Utrecht, 3584 CT, Utrecht, The Netherlands
[3] Department of Mechanical Science and Engineering, University of Illinois, Urbana, IL 61822, USA

Corresponding author: Leckband, Deborah E (leckband@illinois.edu)

Current Opinion in Cell Biology 2011, **23**:523–530

This review comes from a themed issue on
Cell-to-cell contact and extracellular matrix
Edited by Arnoud Sonnenberg and Thomas Lecuit

Available online 2nd September 2011

0955-0674/$ – see front matter

DOI 10.1016/j.ceb.2011.08.003

Introduction

Multicellular organisms integrate mechanical and chemical cues at the cellular level to govern processes ranging from embryonic development to tumor progression. Whereas the molecular mechanisms of signaling triggered by soluble factors have been at the center of cell biology research for decades, relatively recent research demonstrated the importance of mechanical signaling (mechanotransduction) [1–5]. Groundbreaking studies of mechanotransduction focused largely on mechanical signaling by integrin-based cell-extracellular matrix (ECM) contacts [1,2,5,6,7,8]. Recently, cell–cell adhesion complexes also emerged as mechanosensors. A key example is the mechanotransduction at cell–cell adhesions that coordinates with cell–ECM adhesions to induce endothelial cell realignment in response to shear flow [9].

Recent studies in model organisms demonstrate the physiological importance of intercellular forces during tissue morphogenesis. Anisotropic, temporally controlled actomyosin contraction, coupled to intercellular adhesions, drives junction remodeling in apical constriction and in embryo elongation through cell intercalation [10,11•,12,13•,14•]. Similarly, contraction of the wing hinge regulates planar cell polarity (PCP) and cell intercalation during *Drosophila* wing elongation [15]. Wnt-driven PCP signaling regulates putative cadherin-dependent tissue tension to regulate ECM organization [16]. Furthermore, differential myosin-dependent cortical tension directs cell sorting in the germ layer of embryos [17], whereas coordinated actomyosin-based tension at the anterior–posterior boundary maintains tissue segmentation later in development [18,19•,20•]. Finally, perturbations of cell–cell adhesion complexes in epithelial sheets [21,22] emphasize the centrality of these junctions for proper transmission of actomyosin-based forces during tissue stratification.

Although strongly anticipated from these studies, it is not possible to infer a mechanosensory role for cell–cell adhesion proteins based on cell morphology, subcellular architecture, or the composition of intercellular junctions. An important challenge is to establish whether intercellular adhesion proteins are merely passive force conduits or active sensors that modulate cell functions in response to mechanical stimuli. So far, this question was not directly addressed, and most current knowledge regarding the interplay of force and adhesion biochemistry is based on two-dimensional cell-culture models, which focused primarily on cell-extracellular matrix adhesions [7]. Determining the forces at cell–cell junctions and their impact on adhesion protein functions has proven more challenging.

This review highlights recent developments in the investigation of intercellular tension and the demonstration that cadherin complexes are mechanosensors at cell–cell junctions that modify cell functions in response to force. Furthermore, we discuss the current understanding of the underlying molecular mechanisms.

Endogenous actomyosin-dependent forces at cadherin-based intercellular junctions

Broad strategies for investigating the effect of mechanical force on cell surface proteins determine cell responses to endogenous actomyosin-dependent contractile force,

contractile stress associated with substrate mechanics (rigidity sensing) or cell responses to direct mechanical stimulation (exogenous force) (Figure 1) [23]. In two-dimensional cell culture models, increases in endogenous mechanical force at E-cadherin-mediated cell–cell contacts were implicated in the phenotypic transformation of epithelial cells by oncogenic growth factors such as Neu [24], HGF [25] and TGFβ [26], although the force at the cell–cell junctions was not determined.

Extended traction force calculations by Maruthamuthu and Gardel [27•] determined the tension at cell–cell junctions within unconstrained cell clusters (Figure 1a and b). Nanonewton cell–cell forces were calculated from

Figure 1

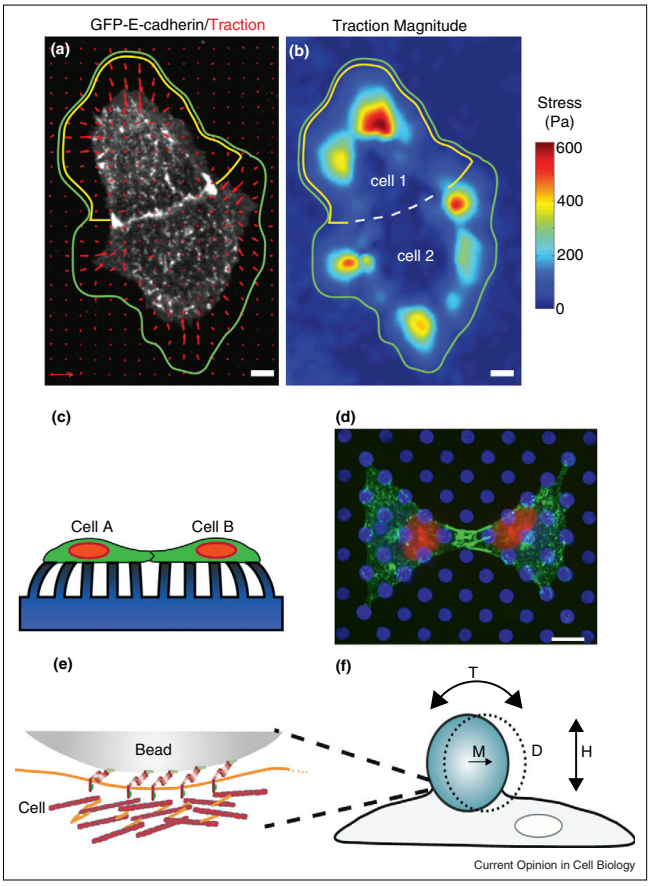

Approaches for investigating intercellular forces and mechanosensing through cell surface adhesion proteins. **(a)** In traction force microscopy, fluorescent particles embedded in soft gels serve as fiduciary markers to quantify the traction force exerted by attached cells. Bead displacement maps are converted to local traction forces, which are represented in heat maps **(b)**, which indicate cell traction force distributions. Here, two cells are in contact, and the cell boundary is indicated in (a) and (b) (from [27•]). **(c)** Micro-arrays of elastomeric pillars are used to determine cell tractions from the cell-induced deflections of the pillars. Figures c and d show two adhering cells on the array. **(d)** Between cell doublets constrained to a bowtie pattern on the array, increases in the net force at the cell–cell contact correlated with an increase in the size of the intercellular junction, indicated by β-catenin (green) (from [29••]). **(e)** In magnetic twisting cytometry (MTC), cadherin-modified beads are attached to the cell surfaces. **(f)** The magnetized beads are subject to an orthogonal, oscillating magnetic field, *H*, which induces a torque, *T*, on the bead. The amplitude of the resulting bead displacement, *D*, reflects the stiffness of the bead-cell-cytoskeletal linkage.

Figure 2

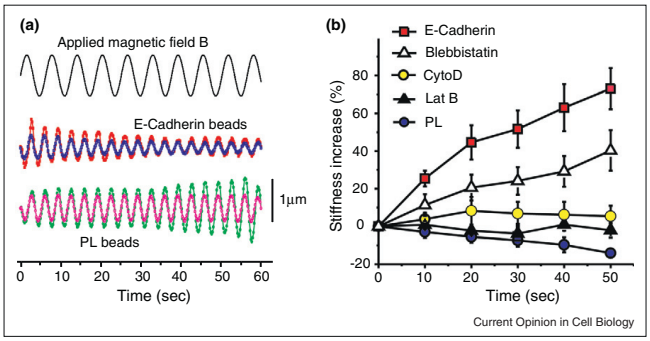

Experimental evidence for cadherin mechanosensing. **(a)** In MTC measurements, a driving magnetic field (top) was correlated with the displacements of beads coated with E-cadherin adhered to F9 cells (middle) and with control beads coated with poly-lysine (PL) adhered to F9 cells (bottom). The decreasing displacement amplitude of the E-cadherin beads with increasing forcing time (middle) is indicative of mechanosensing. **(b)** % Stiffness increase with time in the cases of E-cadherin beads bound to F9 cells (red squares) and after treatment with blebbistatin (white triangles), cytochalasin D (yellow circles), or latrunculin B (black triangles). The black circles show the poly-lysine control (from [35••]).

the balance of all traction forces exerted by each of the cells in the cluster, and the net force at the cell–cell junctions varied in direct proportion to the cell–ECM traction forces. Somewhat surprisingly, the calculated forces at cadherin-based junctions between MDCK epithelial cells [27•] were of the same order of magnitude as at N-cadherin adhesions between myoblasts and N-cadherin-coated elastomeric pillars [28]. Although the similarity in forces may be fortuitous because traction forces depend on the cell-type, extracellular matrix protein, and substrate rigidity, the quantified values indicate that cell–cell adhesions may sustain endogenous forces comparable to focal adhesions (*cf.* Figure 2) [27•,28].

Evidence for mechanosensing at intercellular junctions

Using similar traction force calculations, Liu *et al.* [29••] monitored junction remodeling in response to increased force between endothelial cell pairs, which were geometrically constrained on patterned elastomeric pillar arrays (Figure 1c and d). In contrast to unconstrained cells, the length of contacts between geometrically constrained cells increased with the cell–cell force, even though the tension between unconstrained cells was comparable or slightly greater. This is phenotypically similar to the force-dependent growth of focal adhesions, and further supports the existence of force sensing machinery at endothelial cell junctions. Details of the underlying mechanisms are currently unavailable.

Endogenous contractile forces affect intercellular adhesions in different ways. While the assembly and stability of cadherin adhesions requires myosin II [30], large actomyosin-dependent contractile stress may mechanically destabilize junctions. An example is the reported increase in monolayer gaps and altered dynamics of endothelial junction opening in response to inflammatory mediators, with altered endothelial contractility on rigid versus soft substrata [31•]. An important question is how force-dependent remodeling of junctions within cell clusters relates to broader tissue functions such as barrier permeability.

Direct evidence for mechanosensing by classical cadherins

Traction force microscopy is also commonly used to detect force sensation, insofar as the dependence of traction forces on substrate rigidity signifies a mechanosensory function [32]. In traction force studies of N-cadherin adhesions between C2 myogenic cells and arrays of N-cadherin-coated elastomeric pillars, Ladoux *et al.* [33••] demonstrated that traction forces and cell spreading depended on the pillar stiffness. These characteristic signatures confirmed that cadherin complexes are force sensors.

Alternatively, studies of mechanosensing directly apply force to specific cell surface proteins, using sensitive force probes that stimulate, but do not necessarily break bonds [23]. Advantages of this approach are the specificity of the perturbation, control of the force application, and the rapid stimulus relative to slower changes in contractility. An example is magnetic twisting cytometry (MTC) (Figure 1e and f), which applies acute, exogenous oscillatory shear force to cell surface proteins, on timescales of a few seconds to 1–2 h. MTC determines the effect of force modulation on the viscoelasticity of bead-cell-cytoskeletal connections (Figure 1e) [2,34]. In MTC studies

of cadherin adhesions [35••], 4.5 μm ferromagnetic beads coated with cadherin ectodomains were bound to cell surfaces (Figure 1e) and subjected to an oscillating force, which produces a torque T or shear force on protein bonds (Figure 1f). In mature cells, junctions typically behave elastically, and bead displacement is proportional to the junction stiffness, with smaller displacements D corresponding to stiffer linkages.

With cadherin-coated beads, the modulated shear force induced a rapid increase in junction stiffness (Figure 2a and b) [35••]. In the characteristic signature of a force sensor [1], the relative stiffness change also increased with the magnitude of the applied bond shear, consistent with the traction force results. These findings demonstrate that a force sensing mechanism operates at cadherin-based adhesions, and that this mechanism triggers molecular cascades that modify the local and/or global mechanical properties of the cell. Such mechanical changes could reflect any of several molecular events, which themselves are not apparent from these measurements alone. Altered mechanics could also reflect local and/or global changes. Thus, determining specific molecular mechanisms underlying the mechanoresponse requires the use of biochemical tools in conjunction with mechanical measurements.

Molecular basis of cadherin mechanosensing

Two recent papers revealed the rudiments of a molecular mechanism that may partly explain cadherin mechanosensing. The cytodomain of classical cadherins forms a stoichiometric complex with β-catenin, which in turn binds α-catenin (Figure 3a). In a detailed structure–function analysis, Yonemura *et al.* [36••] showed that α-catenin is an auto-inhibited protein in which a putative inhibitory domain encrypts an adjacent vinculin-binding site in the protein (Figure 3b). When full-length α-catenin is present, myosin II activation and the presumed increase in intercellular tension coincide with vinculin recruitment to cell–cell contacts (Figure 3f) [36••,37]. Deleting the inhibitory domain results in myosin II-independent vinculin accumulation [36••]. In the second study, MTC measurements of vinculin knockout F9 cells showed that vinculin contributes to the force-activated reinforcement of E-cadherin adhesions [35••]. Thus a model emerged in which α-catenin is a stretch-activated tension sensing protein in the complex between E-cadherin and actomyosin, such that increased tension

Figure 3

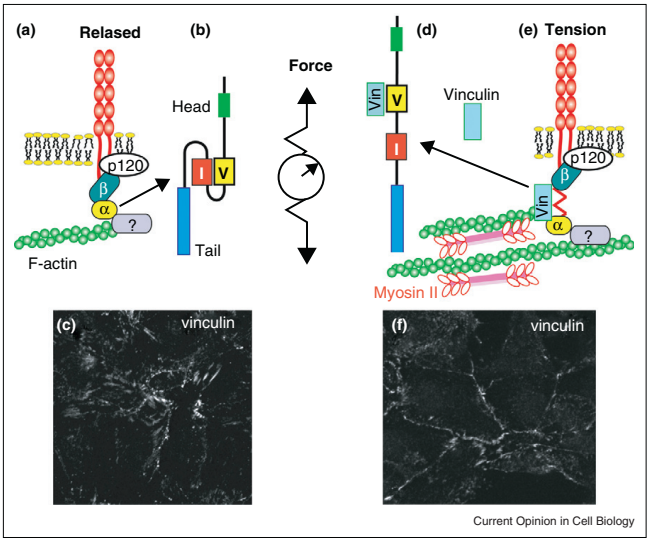

Proposed mechanism of mechanosensing by cadherin complexes. **(a)** Cadherin complex in the absence of tension. The cytoplasmic domain binds to p120 catenin, β-catenin, α-catenin, and possibly other actin-binding proteins (purple). **(b)** In the proposed relaxed conformation, α-catenin is autoinhibited due to the association between the vinculin binding domain and a putative inhibitory domain. **(c)** At unstressed MDCK cell junctions, vinculin is hardly present. **(d)** When cadherins are subject to tension, **(e)** α-catenin undergoes a conformational change that exposes the vinculin binding site and recruits vinculin to junctions. **(f)** Vinculin accumulates at stressed MDCK cell–cell junctions following stimulation of actomyosin contraction by HGF. In this model, α-catenin acts as a strain gauge (center).

relieves the auto-inhibition to expose the cryptic vinculin binding site (Figure 3d and e), with subsequent vinculin recruitment and junction remodeling. This proposed mechanism raises intriguing questions about the mechanical role(s) of proteins in cadherin complexes.

The mechanical connection between actin and cadherin bonds implied by the MTC results might appear to contradict findings that αE-catenin cannot bind actin and β-catenin simultaneously [38,39]. Acute mechanosensing requires mechanical connectivity between cadherin bonds and actomyosin because the force opposing cadherin-bead pulls requires organized actin, and mechanotransduction requires cadherin ligation [35••]. This suggests that the tension sensor lies between two anchor points defined by the cadherin bonds and actin linkage (Figure 3). α-catenin also binds actin and is required for robust cell adhesion [40], for coupling cadherin to actin flow [41], and for cadherin mechanotransduction (Leckband, unpublished observations). These *in vitro* data support an integral role for α-catenin in the mechanotransduction chain, but E-cadherin tethering to cortical actin also requires α-catenin *in vivo* [42]. Moreover, the actomyosin recoil following *in vivo* focal ablation demonstrates that these junctions are under tension [42]. An indirect linkage between α-catenin and actin (Figure 3a and e) could resolve the apparent discrepancy between biochemical and mechanical data. Possible candidates include Eplin [43], Vezatin [44], and ZO-1 [45], which bind to actin and to the appropriate C-terminal region of α-catenin. Their role in cadherin mechanotransduction has yet to be determined.

β-Catenin also binds actin as well as vinculin, and could mechanically link actin and cadherin bonds. However, β-catenin appears to be dispensable for cadherin adhesive function since it could be replaced by α-catenin-cadherin fusions, without significant loss of cadherin function [45,46]. Interestingly, the interaction between β-catenin and vinculin is crucial for maintaining E-cadherin membrane levels [47]. This second vinculin binding site within the cadherin complex raises the possibility that α-catenin and β-catenin cooperate to efficiently recruit vinculin to cell–cell junctions. A current challenge is to demonstrate that vinculin recruitment to α-catenin is caused by a forced conformational change rather than by biochemical changes in α-catenin, due to, for example, phosphorylation by Src or other kinases, which could themselves be downstream targets of a mechanosensor.

Comparison of force-actuated stiffening of E-cadherin junctions in wild type F9 cells with that observed with vinculin knockout F9 cells showed that vinculin loss only attenuates the mechanoresponse [35••]. If stretch-activated vinculin recruitment were the sole mechanosensing mechanism, then vinculin depletion should eliminate cadherin mechanotransduction. Yonemura *et al.* [36••] used vinculin as the principal marker for mechanotransduction, so their results do not address additional mechanisms. Vinculin depletion also alters global cell mechanics [48], which could indirectly modulate force sensation at cadherin junctions. Thus an outstanding question concerns the global versus local role of vinculin in cadherin adhesion mechanics.

Finally, myosin II inhibition only attenuated mechanotransduction (Figure 3b). This differs from force sensation by focal adhesions, for which actomyosin contractility is obligatory [7]. Myosin II is required for cadherin traction force generation [28,33••], but mechanosensing clearly involves additional molecular pathways.

Alternative components and mechanisms

The modest effect of the vinculin knockout suggests the involvement of other pathways or proteins. Known junctional proteins that bind α-catenin and regulate actin dynamics and organization include formins [49], 1-afadin [13•,50], and α-actinin [51]. Intriguingly, vinculin and α-actinin bind overlapping regions of αE-catenin [51]. Formins may participate in mechanosensing [52], and Formin 1 interacts with α-catenin directly [49]. VASP was also implicated in force-dependent adhesion strengthening [53]. Cadherins could also mechanically couple to other adhesion complexes through actin binding partners such as ZO-1 [54]. An example is the coordinate tension sensing at endothelial junctions by a complex of VE-cadherin, PECAM, and vascular endothelial growth factor receptor2 [9].

Conclusions and future directions

Recent findings described in this review identified a new mechanosensing mechanism at cadherin-dependent, cohesive junctions. These cadherin complexes sense force and trigger molecular cascades that remodel adhesions and alter the junction mechanics. Initial studies identified an α-catenin-dependent pathway, in which tension-dependent conformational changes in α-catenin correlate with vinculin recruitment to junctions. Biophysical studies are now needed to directly test whether α-catenin unfolds in direct response to force. It is also unclear how vinculin is activated prior to α-catenin binding. The α-catenin-dependent recruitment of vinculin is unlikely to be the sole mechanotransduction mechanism, however, because vinculin plays only a partial role in the force response, as does myosin II. This strongly suggests the involvement of additional mechanisms and actin binding proteins, which have yet to be implicated in this mechanism.

The current challenge is to establish how intercellular tension instructs both mechanical and biochemical functions *in vivo*. This is especially relevant in development where substantial mechanical forces propagate across tissues through cell–cell junctions to drive large scale,

coordinated cell movements during apical constriction [14•], tissue elongation [11•], and dorsal closure [55]. The coordinated effects of cell–cell cohesion and cell mechanics further regulate gastrulation and define cell shape [56,57]. Studies increasingly demonstrate that mechanical forces are central in development. However, the discovery that essential cadherin complexes modulate cell functions in response to tension raises the intriguing possibility that cadherins play much more significant and diverse roles in coordinating collective cell movements and tissue functions. Examples are now beginning to emerge, as demonstrated by the recent finding that forces exerted at hemidesmosomes by muscle cells are important for muscle and epidermal tissue morphogenesis in *Caenorhabditis elegans* [58]. Studies of *Drosophila* germband extension suggest that the mechanosensation of pulsed actomyosin contractile forces at E-cadherin junctions is critical for tissue morphogenesis [11•]. We further speculate that cadherin mechanotransduction modulates signaling and associated behaviors in a broad range of tissue functions, analogous to integrin-ECM adhesions [1,3,5,15,18,57,59]. This is suggested by the roles of both myosin II and E-cadherin in maintaining stem cell pluripotency [60] and recent findings that regions of minimal shear stress between cells govern the migratory direction of cohorts of cells [61•]. The new findings described in this review clearly open a wide range of exciting new avenues of investigation.

Acknowledgements

DEL is supported by NIH R21 HD059002 and by NSF CMMI 10-29871 (DEL and NW). NW is supported by NIH GM072744, and JdR is supported by AICR 06-0528 and the Dutch Organization for scientific research (NWO-VIDI), Quint le Duc is supported by KWF 2006-3714.

References and recommended reading

Papers of particular interest, published within the period of review, have been highlighted as:

- • of special interest
- •• of outstanding interest

1. Vogel V, Sheetz M: **Local force and geometry sensing regulate cell functions**. *Nat Rev Mol Cell Biol* 2006, **7(4)**:265-275.

2. Wang N, Butler JP, Ingber DE: **Mechanotransduction across the cell surface and through the cytoskeleton**. *Science* 1993, **260(5111)**:1124-1127.

3. Levental KR, Yu H, Kass L, Lakins JN, Egeblad M, Erler JT, Fong SF, Csiszar K, Giaccia A, Weninger W, Yamauchi M *et al.*: **Matrix crosslinking forces tumor progression by enhancing integrin signaling**. *Cell* 2009, **139(5)**:891-906.

4. Wang Y, Boltvinick EL, Zhao Y, Berns MW, Usami S, Tsien RY, Chien S: **Visualizing the mechanical activation of src**. *Nature* 2005, **434**:1040-1045.

5. Engler AJ, Sen S, Sweeney HL, Discher DE: **Matrix elasticity directs stem cell lineage specification**. *Cell* 2006, **126(4)**:677-689.

6. Choquet D, Felsenfeld DP, Sheetz MP: **Extracellular matrix rigidity causes strengthening of integrin-cytoskeleton linkages**. *Cell* 1997, **88(1)**:39-48.

7. Geiger B, Spatz JP, Bershadsky AD: **Environmental sensing through focal adhesions**. *Nat Rev Mol Cell Biol* 2009, **10(1)**:21-33.

8. Pelham RJ Jr, Wang Y: **Cell locomotion and focal adhesions are regulated by substrate flexibility**. *Proc Natl Acad Sci U S A* 1997, **94(25)**:13661-13665.

9. Tzima E, Irani-Tehrani M, Kiosses WB, Dejana E, Schultz DA, Engelhardt B, Cao G, DeLisser H, Schwartz MA: **A mechanosensory complex that mediates the endothelial cell response to fluid shear stress**. *Nature* 2005, **437(7057)**:426-431.

10. Bertet C, Sulak L, Lecuit T: **Myosin-dependent junction remodelling controls planar cell intercalation and axis elongation**. *Nature* 2004, **429(6992)**:667-671.

11. • Rauzi M, Lenne PF, Lecuit T: **Planar polarized actomyosin contractile flows control epithelial junction remodelling**. *Nature* 2010, **468(7327)**:1110-1114.
This study shows that germband extension in *Drosophilla* embryos is governed by pulsed, actomyosin-dependent contractile forces, which require alpha-catenin to couple to DE-cadherin-based cell–cell junctions.

12. Rauzi M, Verant P, Lecuit T, Lenne PF: **Nature and anisotropy of cortical forces orienting *Drosophila* tissue morphogenesis**. *Nat Cell Biol* 2008, **10(12)**:1401-1410.

13. • Sawyer JK, Harris NJ, Slep KC, Gaul U, Peifer M: **The *Drosophila* afadin homologue canoe regulates linkage of the actin cytoskeleton to adherens junctions during apical constriction**. *J Cell Biol* 2009, **186(1)**:57-73.
This paper shows that Canoe/Afadin is essential for connecting radial actomyosin to cadherin during apical constriction, which is essential for tissue invagination, but not for cell–cell junction establishment.

14. • Martin AC, Gelbart M, Fernandez-Gonzalez R, Kaschube M, Wieschaus EF: **Integration of contractile forces during tissue invagination**. *J Cell Biol* 2010, **188(5)**:735-749.
This work shows that tissue morphogenesis depends on supracellular contractile actomyosin networks in which cadherin-based junctions play a key role.

15. Aigouy B, Farhadifar R, Staple DB, Sagner A, Roper JC, Julicher F, Eaton S: **Cell flow reorients the axis of planar polarity in the wing epithelium of *Drosophila***. *Cell* 2010, **142(5)**:773-786.

16. Dzamba BJ, Jakab KR, Marsden M, Schwartz MA, DeSimone DW: **Cadherin adhesion, tissue tension, and noncanonical wnt signaling regulate fibronectin matrix organization**. *Dev Cell* 2009, **16(3)**:421-432.

17. Krieg M, Arboleda-Estudillo Y, Puech PH, Kafer J, Graner F, Muller DJ, Heisenberg CP: **Tensile forces govern germ-layer organization in zebrafish**. *Nat Cell Biol* 2008, **10(4)**:429-436.

18. Sawyer JM, Harrell JR, Shemer G, Sullivan-Brown J, Roh-Johnson M, Goldstein B: **Apical constriction: a cell shape change that can drive morphogenesis**. *Dev Biol* 2010, **341(1)**:5-19.

19. • Monier B, Pelissier-Monier A, Brand AH, Sanson B: **An actomyosin-based barrier inhibits cell mixing at compartmental boundaries in *Drosophila* embryos**. *Nat Cell Biol* 2010, **12(1)**:60-65 sup 61–69.
During cell division in *Drosophila* embryos, actomyosin cables at the boundaries of tissue compartments prevent cells from invading neighboring compartments, apparently by pushing the cells back into their compartment of origin after division. This process requires myosin II.

20. • Landsberg KP, Farhadifar R, Ranft J, Umetsu D, Widmann TJ, Bittig T, Said A, Julicher F, Dahmann C: **Increased cell bond tension governs cell sorting at the *Drosophila* anteroposterior compartment boundary**. *Curr Biol* 2009, **19(22)**:1950-1955.
This study shows that a 2.5-5 fold increase in bond tension at cell–cell junctions at the anteroposterior boundary relative to bond tension in other tissues is required to maintain the separation between anterior and posterior compartments following cell division.

21. Vaezi A, Bauer C, Vasioukhin V, Fuchs E: **Actin cable dynamics and rho/rock orchestrate a polarized cytoskeletal architecture in the early steps of assembling a stratified epithelium**. *Dev Cell* 2002, **3(3)**:367-381.

22. Danjo Y, Gipson IK: **Actin 'purse string' filaments are anchored by e-cadherin-mediated adherens junctions at the leading edge of the epithelial wound, providing coordinated cell movement**. *J Cell Sci* 1998, **111(Pt 22)**:3323-3332.

23. Lele TP, Sero JE, Matthews BD, Kumar S, Xia S, Montoya-Zavala M, Polte T, Overby D, Wang N, Ingber DE: **Tools to study cell mechanics and mechanotransduction**. *Methods Cell Biol* 2007, **83**:443-472.

24. Chausovsky A, Tsarfaty I, Kam Z, Yarden Y, Geiger B, Bershadsky AD: **Morphogenetic effects of neuregulin (neu differentiation factor) in cultured epithelial cells**. *Mol Biol Cell* 1998, **9(11)**:3195-3209.

25. de Rooij J, Kerstens A, Danuser G, Schwartz MA, Waterman-Storer CM: **Integrin-dependent actomyosin contraction regulates epithelial cell scattering**. *J Cell Biol* 2005, **171(1)**:153-164.

26. Gomez EW, Chen QK, Gjorevski N, Nelson CM: **Tissue geometry patterns epithelial–mesenchymal transition via intercellular mechanotransduction**. *J Cell Biochem* 2010, **110(1)**:44-51.

27. • Maruthamuthu V, Sabass B, Schwarz US, Gardel ML: **Cell–ECM traction force modulates endogenous tension at cell–cell contacts**. *Proc Natl Acad Sci U S A* 2011.
Extended traction force measurements used to calculate the tension at intercellular junctions demonstrated that cell–cell force increases in proportion to traction forces exerted at integrin-based adhesions to extracellular matrix, but the size of junctions between unconstrained cells did not appear to increase with intercellular force.

28. Ganz A, Lambert M, Saez A, Silberzan P, Buguin A, Mege RM, Ladoux B: **Traction forces exerted through n-cadherin contacts**. *Biol Cell* 2006, **98(12)**:721-730.

29. •• Liu Z, Tan JL, Cohen DM, Yang MT, Sniadecki NJ, Ruiz SA, Nelson CM, Chen CS: **Mechanical tugging force regulates the size of cell–cell junctions**. *Proc Natl Acad Sci U S A* 2010, **107(22)**:9944-9949.
Traction forces exerted by geometrically constrained cell doublets on patterned elastomeric pillar arrays were used to determine the force at cell–cell junctions, following myosin 2 activation. This report showed that the length of cell–cell contacts increased with intercellular tension, analogous to integrin-based focal adhesions.

30. Shewan AM, Maddugoda M, Kraemer A, Stehbens SJ, Verma S, Kovacs EM, Yap AS: **Myosin 2 is a key rho kinase target necessary for the local concentration of e-cadherin at cell–cell contacts**. *Mol Biol Cell* 2005, **16(10)**:4531-4542.

31. • Krishnan R, Klumpers DD, Park CY, Rajendran K, Trepat X, van Bezu J, van Hinsbergh VW, Carman CV, Brain JD, Fredberg JJ, Butler JP *et al.*: **Substrate stiffening promotes endothelial monolayer disruption through enhanced physical forces**. *Am J Physiol Cell Physiol* 2011, **300(1)**:C146-C154.
Increased endogenous contractility in an endothelial monolayer in 2D cell culture correlated with an increase in gaps between cells in the monolayer, and altered dynamics of intercellular gap formation in response to thrombin.

32. Beningo KA, Lo CM, Wang YL: **Flexible polyacrylamide substrata for the analysis of mechanical interactions at cell-substratum adhesions**. *Methods Cell Biol* 2002, **69**:325-339.

33. •• Ladoux B, Anon E, Lambert M, Rabodzey A, Hersen P, Buguin A, Silberzan P, Mege RM: **Strength dependence of cadherin-mediated adhesions**. *Biophys J* 2010, **98(4)**:534-542.
Traction force measurements of myogenic C2 cells on elastomeric pillars coated with N-cadherin ectodomains demonstrated that traction forces at homophilic N-cadherin bonds increased with the pillar rigidity, and demonstrated that a mechanosensory mechanism operates at cadherin adhesions.

34. Puig-De-Morales M, Grabulosa M, Alcaraz J, Mullol J, Maksym GN, Fredberg JJ, Navajas D: **Measurement of cell microrheology by magnetic twisting cytometry with frequency domain demodulation**. *J Appl Physiol* 2001, **91(3)**:1152-1159.

35. •• le Duc Q, Shi Q, Blonk I, Sonnenberg A, Wang N, Leckband D, de Rooij J: **Vinculin potentiates e-cadherin mechanosensing and is recruited to actin-anchored sites within adherens junctions in a myosinii dependent manner**. *J Cell Biol* 2010, **189**:1107-1115.
Complementary nanomechanics and high resolution imaging studies demonstrated directly that cadherin complexes are mechanosensors. Mechanical studies demonstrated that the force-activated reinforcement of cadherin junctions requires actin, and is modulated by vinculin and myosin 2. Imaging studies confirmed the myosin 2-dependent recruitment of vinculin to junctions.

36. •• Yonemura S, Wada Y, Watanabe T, Nagafuchi A, Shibata M: **Alpha-catenin as a tension transducer that induces adherens junction development**. *Nat Cell Biol* 2010, **12**:533-542.
This study provides compelling evidence that α-catenin is a mechanosensor at cadherin-based cell–cell adhesions. Detailed structure-function analyses of α-catenin identified an inhibitory domain, which appears to encrypt a vinculin binding site in relaxed cells. Myosin 2 activation correlates with a conformational change in α-catenin and the exposure of the vinculin site, which in turn recruits to cadherin complexes.

37. Miyake Y, Inoue N, Nishimura K, Kinoshita N, Hosoya H, Yonemura S: **Actomyosin tension is required for correct recruitment of adherens junction components and zonula occludens formation**. *Exp Cell Res* 2006, **312(9)**:1637-1650.

38. Drees F, Pokutta S, Yamada S, Nelson WJ, Weis WI: **Alpha-catenin is a molecular switch that binds e-cadherin-beta-catenin and regulates actin-filament assembly**. *Cell* 2005, **123(5)**:903-915.

39. Yamada S, Pokutta S, Drees F, Weis WI, Nelson WJ: **Deconstructing the cadherin-catenin-actin complex**. *Cell* 2005, **123(5)**:889-901.

40. Nagafuchi A, Ishihara S, Tsukita S: **The roles of catenins in the cadherin-mediated cell adhesion: functional analysis of e-cadherin-alpha catenin fusion molecules**. *J Cell Biol* 1994, **127(1)**:235-245.

41. Bard L, Boscher C, Lambert M, Mege RM, Choquet D, Thoumine O: **A molecular clutch between the actin flow and n-cadherin adhesions drives growth cone migration**. *J Neurosci* 2008, **28(23)**:5879-5890.

42. Cavey M, Rauzi M, Lenne PF, Lecuit T: **A two-tiered mechanism for stabilization and immobilization of e-cadherin**. *Nature* 2008, **453(7196)**:751-756.

43. Abe K, Takeichi M: **Eplin mediates linkage of the cadherin catenin complex to f-actin and stabilizes the circumferential actin belt**. *Proc Natl Acad Sci U S A* 2008, **105(1)**:13-19.

44. Sousa S, Cabanes D, El-Amraoui A, Petit C, Lecuit M, Cossart P: **Unconventional myosin viia and vezatin, two proteins crucial for listeria entry into epithelial cells**. *J Cell Sci* 2004, **117(Pt 10)**:2121-2130.

45. Imamura Y, Itoh M, Maeno Y, Tsukita S, Nagafuchi A: **Functional domains of alpha-catenin required for the strong state of cadherin-based cell adhesion**. *J Cell Biol* 1999, **144(6)**:1311-1322.

46. Pacquelet A, Rorth P: **Regulatory mechanisms required for de-cadherin function in cell migration and other types of adhesion**. *J Cell Biol* 2005, **170(5)**:803-812.

47. Peng X, Cuff LE, Lawton CD, DeMali KA: **Vinculin regulates cell-surface e-cadherin expression by binding to beta-catenin**. *J Cell Sci* 2011, **123(Pt 4)**:567-577.

48. Goldmann WH, Galneder R, Ludwig M, Kromm A, Ezzell RM: **Differences in f9 and 5.51 cell elasticity determined by cell poking and atomic force microscopy**. *FEBS Lett* 1998, **424(3)**:139-142.

49. Kobielak A, Pasolli HA, Fuchs E: **Mammalian formin-1 participates in adherens junctions and polymerization of linear actin cables**. *Nat Cell Biol* 2004, **6(1)**:21-30.

50. Pokutta S, Drees F, Takai Y, Nelson WJ, Weis WI: **Biochemical and structural definition of the l-afadin- and actin-binding sites of alpha-catenin**. *J Biol Chem* 2002, **277(21)**:18868-18874.

51. Kobielak A, Fuchs E: **Alpha-catenin: at the junction of intercellular adhesion and actin dynamics**. *Nat Rev Mol Cell Biol* 2004, **5(8)**:614-625.

52. Kozlov MM, Bershadsky AD: **Processive capping by formin suggests a force-driven mechanism of actin polymerization**. *J Cell Biol* 2004, **167(6)**:1011-1017.

53. Kris AS, Kamm RD, Sieminski AL: **Vasp involvement in force-mediated adherens junction strengthening**. *Biochem Biophys Res Commun* 2008, **375(1)**:134-138.

54. Ikeda W, Nakanishi H, Miyoshi J, Mandai K, Ishizaki H, Tanaka M, Togawa A, Takahashi K, Nishioka H, Yoshida H, Mizoguchi A *et al.*: **Afadin: a key molecule essential for structural organization of cell–cell junctions of polarized epithelia during embryogenesis**. *J Cell Biol* 1999, **146(5)**:1117-1132.

55. Solon J, Kaya-Copur A, Colombelli J, Brunner D: **Pulsed forces timed by a ratchet-like mechanism drive directed tissue movement during dorsal closure**. *Cell* 2009, **137(7)**:1331-1342.

56. Manning ML, Foty RA, Steinberg MS, Schoetz EM: **Coaction of intercellular adhesion and cortical tension specifies tissue surface tension**. *Proc Natl Acad Sci U S A* 2010, **107(28)**:12517-12522.

57. Lecuit T, Lenne PF: **Cell surface mechanics and the control of cell shape, tissue patterns and morphogenesis**. *Nat Rev Mol Cell Biol* 2007, **8(8)**:633-644.

58. Zhang H, Landmann F, Zahreddine H, Rodriguez D, Koch M, Labouesse M: **A tension-induced mechanotransduction pathway promotes epithelial morphogenesis**. *Nature* 2011, **471(7336)**:99-103.

59. Hayashi T, Carthew RW: **Surface mechanics mediate pattern formation in the developing retina**. *Nature* 2004, **431(7009)**:647-652.

60. Li D, Zhou J, Wang L, Shin ME, Su P, Lei X, Kuang H, Guo W, Yang H, Cheng L, Tanaka TS *et al.*: **Integrated biochemical and mechanical signals regulate multifaceted human embryonic stem cell functions**. *J Cell Biol* 2010, **191(3)**:631-644.

61. • Tambe DT, Hardin CC, Angelini TE, Rajendran K, Park CY, Serra-Picamal X, Zhou EH, Zaman MH, Butler JP, Weitz DA, Fredberg JJ *et al.*: **Collective cell guidance by cooperative intercellular forces**. *Nat Mater* 2011, **10(6)**:469-475.
This study mapped stresses within a migrating cohort of cells, and demonstrated that collective migration is guided by differences in tensile and shear stress at cell–cell junctions, with regions of minimal shear stress determining the migratory direction.

HGF induced EMT as a model.

Epithelial Mesenchymal Transition.

Epithelial Mesenchymal Transition (EMT) is a process throughout development and adopted by some invasive cancer cells. In this process, epithelial cells transit through several stages wherein they lose their cell-cell junctions and gain the capacity to migrate individually. For migration the cell creates a leading edge where the cell can protrude, with the help of the actin cytoskeleton, into the direction of interest. For traction purposes, the protrusions adhere to the extracellular matrix (ECM) by integrin mediated connections. Following initial adhesion, a whole complex of proteins is gathered around the intracellular part of the integrins to form focal adhesions, a site for cytoskeletal anchoring and regulation [1, 2]. In order to migrate, actomyosin driven contractility pulls the cell forward via the anchoring focal adhesions at the leading edge. Concomitantly, the integrin mediated adhesions detach at the trailing edge of the cell.

Before cells can migrate away from the surrounding tissue, cellular contacts have to be broken. Therefore, the expression of the cell-cell contact mediator E-cadherin is downregulated. This is the most characteristic event of EMT [3]. Regulation of migratory and cell adhesion processes during EMT are orchestrated by several factors, well known examples are the transcription regulators: slug and snail [4, 5].

HGF-MET signalling induces EMT.

Upstream of transcription factors, like snail and slug, several EMT promoting/inducing growth factors have been identified. Factors like TGFβ, FGF and WNT are primary examples of factors that can induce EMT in a wide range of tissues. Besides those general EMT inducing factors, other factors are known that induce only facets of the EMT pathway. A well-known example within this class of partial EMT inducers is the Hepatocyte Growth Factor (HGF), also known as Scatter Factor. The transmembrane receptor for HGF is MET, MET was discovered in the 1980's in three independent research lines, through its suggested involvement in Metastasis it owes its name MET. The receptor, a heterodimer of an extracellular chain bound to a transmembrane chain, is expressed by melanocytes, chondrocytes, skeletal muscle, hematopoietic, lymphoid and neural cells. The deletion of both ligand and receptor genes in mice revealed the importance of this couple in many other physiological processes like growth, migration and survival [6, 7, 8].

HGF-cMET in tissues

MET activation and subsequent intracellular signaling pathways direct myogenic progenitor cells through EMT in order to migrate over great lengths during embryonic development [8, 9]. Similarly, the HGF dependent EMT mechanism is hijacked in tumor metastasis and invasion. However in other non-oncogenic processes like wound healing and tissue regeneration HGF signaling is also of great importance. Infliction of Liver damage results in the onset of extracellular HGF release leading to tissue regeneration by the remaining hepatocytes [10]. Concurrently, inhibition of the HGF-MET pathway hampers the hepatocyte proliferation and therefore complete liver regeneration. [11, 12]. In skin the regeneration after wounding is also HGF dependent. In mice experiments wherein a subpopulation of the keratinocytes was conditionally deprived of functional MET, skin regeneration after wounding was only possible by the subpopulation of cells that did contain the functional protein [13]. Moreover, HGF and MET show elevated expression patterns in keratinocytes during wound repair in an autocrine manner. Upregulation of HGF-signaling is not limited to just the organs liver and skin, in

regeneration tests after wounding in epithelial tissues of the kidney, lung and muscle, the same reliance on HGF-MET signaling was reported [14].

HGF-MET signalling in cancer development.

Whereas controlled HGF-MET activity is exploited during development and wound healing, deregulated HGF-MET signalling is exploited during cancer. Besides transcriptional upregulation of the protein couple, other cases leading to increased activity have been observed; aberrant degradation, receptor crosstalk and even activating point mutations. In human head and neck cancers, the subpopulation of cells with MET activating mutations are significantly enriched in metastases (50%) when compared to the primary tumor (2%). Hereby supporting the suggestion that deregulation of the MET signaling can be causal to metastasis [15]. Numerous studies in which HGF-MET overexpression was forced show that elevated activity of this couple can result in the onset of metastasis in cells originating from diverse organ tissues [16][17][18][19][20].

As a possible explanation for the metastatic activity of MET, people have implicated the RAS-MAPK and RAC1 pathways, their involvement in metastasis is clearly established [21][22][23] . Furthermore, the well-known cancer associated WNT pathway and the normally independent MET cascade interconnect in colon cancer. The PI3K/AKT pathway regulates beta-catenin translocation to the nucleus, a mechanism shared by the canonical WNT signalling. This HGF induced effect of β-catenin translocation, activates the WNT signalling cascade constitutively and therefore helps to maintain the stemness of these cancer stemcells[24].

A big aspect in cancer progression is the increasing demand of nutrients and signaling ques, therefore the expansion of the endothelial network by angiogenesis is essential. Although the vascular endothelial growth factor (VEGF) and its receptor (VEGFR) take the lead, HGF-MET signaling is also important in the regulation of angiogenesis [25][26][27]. The blocking of MET by inhibitors of its kinase activity and docking sites resulted in a reduction of the number of blood vessels in experimental tumors [28][29]. Through activation of the ERK/MAPK, PI3K/AKT and FAK pathways, HGF-MET mediate a cooperative effect with VEGF-VEGFR.

Epithelial cell scattering as a model for metastasis.

To study HGF-MET induced cellular processes, several cultured cell lines have been used as model systems. The HGF induced mitogenic, motogenic and morphogenic activities on cultured epithelial cells is termed cell scattering. Several cell lines show a scattering response to HGF; the Madin_Darby Canine Kidney (MDCK) [30], the human lung carcinoma A549 [31], human liver carcinoma HEP G2 [32] and the human prostate carcinoma DU145 [33]. These cell-types are able to aggregate and form colonies in culture that can disperse/scatter upon HGF addition. However, although this scattering behaviour might suggest an EMT phenotype, the molecular paths to establish this phenotype do differ from traditional EMT. Especially in the 2D culture models, there is little evidence for an induction of EMT by HGF: the hallmark of EMT, downregulation of E-cadherin, seems not to be the basis of HGF induced cell-scattering. In the HGF induced cell scattering of MDCK's, E-cadherin remains at the surface while cellular junctions are broken. Forces transduced via the cytoskeleton connected with the matrix plays a significant role in cell-cell junction breakage during scattering [34]. Although this differs from regular EMT, carcinogenesis is known to use alternative modes for E-cadherin regulation, besides surface levels expression [35]. During tumor development cellular tension is utilized for several processes in order to progress [36]. Thus

the lack of specific EMT features does not necessarily disqualify these cell lines as valuable model system in the study of tumor metastasis. The specific HGF induced processes do mimic events taking place during physiological tumorigenesis. Using cell culture models is very beneficial for the use of experimental based manipulations. The findings from these experiments can be extrapolated to the in vivo situation and therefore aid in our understanding of HGF-MET signalling during physiological events and carcinogenesis in general.

References

1. Arnaout, M.A., Goodman, S.L. & Xiong, J.P. Structure and mechanics of integrin-based cell adhesion. *Current opinion in cell biology* **19**, 495-507 (2007).
2. Wehrle-Haller, B. Structure and function of focal adhesions. *Current opinion in cell biology* **24**, 116-124 (2012).
3. Kalluri, R. & Weinberg, R.A. The basics of epithelial-mesenchymal transition. *The Journal of clinical investigation* **119**, 1420-1428 (2009).
4. Becker, K.F. *et al.* Analysis of the E-cadherin repressor Snail in primary human cancers. *Cells, tissues, organs* **185**, 204-212 (2007).
5. Alves, C.C., Carneiro, F., Hoefler, H. & Becker, K.F. Role of the epithelial-mesenchymal transition regulator Slug in primary human cancers. *Frontiers in bioscience : a journal and virtual library* **14**, 3035-3050 (2009).
6. Schmidt, C. *et al.* Scatter factor/hepatocyte growth factor is essential for liver development. *Nature* **373**, 699-702 (1995).
7. Uehara, Y. *et al.* Placental defect and embryonic lethality in mice lacking hepatocyte growth factor/scatter factor. *Nature* **373**, 702-705 (1995).
8. Bladt, F., Riethmacher, D., Isenmann, S., Aguzzi, A. & Birchmeier, C. Essential role for the c-met receptor in the migration of myogenic precursor cells into the limb bud. *Nature* **376**, 768-771 (1995).
9. Dietrich, S. *et al.* The role of SF/HGF and c-Met in the development of skeletal muscle. *Development* **126**, 1621-1629 (1999).
10. Michalopoulos, G.K. & DeFrances, M.C. Liver regeneration. *Science* **276**, 60-66 (1997).
11. Borowiak, M. *et al.* Met provides essential signals for liver regeneration. *Proceedings of the National Academy of Sciences of the United States of America* **101**, 10608-10613 (2004).
12. Huh, C.G. *et al.* Hepatocyte growth factor/c-met signaling pathway is required for efficient liver regeneration and repair. *Proceedings of the National Academy of Sciences of the United States of America* **101**, 4477-4482 (2004).
13. Chmielowiec, J. *et al.* c-Met is essential for wound healing in the skin. *The Journal of cell biology* **177**, 151-162 (2007).
14. Nakamura, T., Mizuno, S., Matsumoto, K., Sawa, Y. & Matsuda, H. Myocardial protection from ischemia/reperfusion injury by endogenous and exogenous HGF. *The Journal of clinical investigation* **106**, 1511-1519 (2000).
15. Di Renzo, M.F. *et al.* Somatic mutations of the MET oncogene are selected during metastatic spread of human HNSC carcinomas. *Oncogene* **19**, 1547-1555 (2000).
16. Rong, S., Segal, S., Anver, M., Resau, J.H. & Vande Woude, G.F. Invasiveness and metastasis of NIH 3T3 cells induced by Met-hepatocyte growth factor/scatter factor autocrine stimulation. *Proceedings of the National Academy of Sciences of the United States of America* **91**, 4731-4735 (1994).
17. Meiners, S., Brinkmann, V., Naundorf, H. & Birchmeier, W. Role of morphogenetic factors in metastasis of mammary carcinoma cells. *Oncogene* **16**, 9-20 (1998).

18. Gallego, M.I., Bierie, B. & Hennighausen, L. Targeted expression of HGF/SF in mouse mammary epithelium leads to metastatic adenosquamous carcinomas through the activation of multiple signal transduction pathways. *Oncogene* **22**, 8498-8508 (2003).
19. Jeffers, M. *et al.* The mutationally activated Met receptor mediates motility and metastasis. *Proceedings of the National Academy of Sciences of the United States of America* **95**, 14417-14422 (1998).
20. Moshitch-Moshkovitz, S. *et al.* In vivo direct molecular imaging of early tumorigenesis and malignant progression induced by transgenic expression of GFP-Met. *Neoplasia* **8**, 353-363 (2006).
21. Muschel, R.J., Williams, J.E., Lowy, D.R. & Liotta, L.A. Harvey ras induction of metastatic potential depends upon oncogene activation and the type of recipient cell. *The American journal of pathology* **121**, 1-8 (1985).
22. Webb, C.P. *et al.* Evidence for a role of Met-HGF/SF during Ras-mediated tumorigenesis/metastasis. *Oncogene* **17**, 2019-2025 (1998).
23. Ridley, A.J., Comoglio, P.M. & Hall, A. Regulation of scatter factor/hepatocyte growth factor responses by Ras, Rac, and Rho in MDCK cells. *Molecular and cellular biology* **15**, 1110-1122 (1995).
24. Vermeulen, L. *et al.* Wnt activity defines colon cancer stem cells and is regulated by the microenvironment. *Nature cell biology* **12**, 468-476 (2010).
25. Abounader, R. & Laterra, J. Scatter factor/hepatocyte growth factor in brain tumor growth and angiogenesis. *Neuro-oncology* **7**, 436-451 (2005).
26. Bussolino, F. *et al.* Hepatocyte growth factor is a potent angiogenic factor which stimulates endothelial cell motility and growth. *The Journal of cell biology* **119**, 629-641 (1992).
27. Grant, D.S. *et al.* Scatter factor induces blood vessel formation in vivo. *Proceedings of the National Academy of Sciences of the United States of America* **90**, 1937-1941 (1993).
28. Puri, N. *et al.* A selective small molecule inhibitor of c-Met, PHA665752, inhibits tumorigenicity and angiogenesis in mouse lung cancer xenografts. *Cancer research* **67**, 3529-3534 (2007).
29. Cantelmo, A.R. *et al.* Cell delivery of Met docking site peptides inhibit angiogenesis and vascular tumor growth. *Oncogene* **29**, 5286-5298 (2010).
30. Stoker, M. & Perryman, M. An epithelial scatter factor released by embryo fibroblasts. *Journal of cell science* **77**, 209-223 (1985).
31. Shiratori, M. *et al.* Hepatocyte growth factor stimulates DNA synthesis in alveolar epithelial type II cells in vitro. *American journal of respiratory cell and molecular biology* **12**, 171-180 (1995).
32. Neaud, V. *et al.* Human hepatic myofibroblasts increase invasiveness of hepatocellular carcinoma cells: evidence for a role of hepatocyte growth factor. *Hepatology* **26**, 1458-1466 (1997).
33. Humphrey, P.A. *et al.* Hepatocyte growth factor and its receptor (c-MET) in prostatic carcinoma. *The American journal of pathology* **147**, 386-396 (1995).
34. de Rooij, J., Kerstens, A., Danuser, G., Schwartz, M.A. & Waterman-Storer, C.M. Integrin-dependent actomyosin contraction regulates epithelial cell scattering. *The Journal of cell biology* **171**, 153-164 (2005).
35. Gumbiner, B.M. Regulation of cadherin adhesive activity. *The Journal of cell biology* **148**, 399-404 (2000).
36. Egeblad, M., Rasch, M.G. & Weaver, V.M. Dynamic interplay between the collagen scaffold and tumor evolution. *Current opinion in cell biology* **22**, 697-706 (2010).

Vinculin potentiates E-cadherin mechanosensing and is recruited to actin-anchored sites within adherens junctions in a myosin II-dependent manner

Published June 28, 2010

Vinculin potentiates E-cadherin mechanosensing and is recruited to actin-anchored sites within adherens junctions in a myosin II–dependent manner

Quint le Duc, Quanming Shi, Iris Blonk, Arnoud Sonnenberg, Ning Wang, Deborah Leckband, and Johan de Rooij

Vol. 189 No. 7, June 28, 2010. Pages 1107–1115.

The authors regret an error in the Materials and methods section of this paper pertaining to the use of a certain antibody. The correct sentence appears below:

Alternatively, beads were labeled with monoclonal anti–E-cadherin antibodies (also used as a blocking antibody in these experiments; DECMA-1; Sigma-Aldrich) using an identical protocol.

Vinculin potentiates E-cadherin mechanosensing and is recruited to actin-anchored sites within adherens junctions in a myosin II–dependent manner

Quint le Duc,[1] Quanming Shi,[2] Iris Blonk,[1] Arnoud Sonnenberg,[5] Ning Wang,[3] Deborah Leckband,[2,4] and Johan de Rooij[1]

[1]Hubrecht Institute, University Medical Centre Utrecht, 3584 CT Utrecht, Netherlands
[2]Department of Chemical and Biomolecular Engineering, [3]Department of Mechanical Science and Engineering, and [4]Department of Chemistry, University of Illinois at Urbana-Champaign, Champaign, IL 61801
[5]Division of Cell Biology, The Netherlands Cancer Institute, 1066 CX Amsterdam, Netherlands

Cell surface receptors integrate chemical and mechanical cues to regulate a wide range of biological processes. Integrin complexes are the mechanotransducers between the extracellular matrix and the actomyosin cytoskeleton. By analogy, cadherin complexes may function as mechanosensors at cell–cell junctions, but this capacity of cadherins has not been directly demonstrated. Furthermore, the molecular composition of the link between E-cadherin and actin, which is needed to sustain such a function, is unresolved. In this study, we describe nanomechanical measurements demonstrating that E-cadherin complexes are functional mechanosensors that transmit force between F-actin and E-cadherin. Imaging experiments reveal that intercellular forces coincide with vinculin accumulation at actin-anchored cadherin adhesions, and nanomechanical measurements show that vinculin potentiates the E-cadherin mechanosensory response. These investigations directly demonstrate the mechanosensory capacity of the E-cadherin complex and identify a novel function for vinculin at cell–cell junctions. These findings have implications for barrier function, morphogenesis, cell migration, and invasion and may extend to all soft tissues in which classical cadherins regulate cell–cell adhesion.

Introduction

Cell surface receptors integrate both chemical and mechanical cues to regulate biological processes as diverse as differentiation, vascular development, tumor growth, and malignancy (Bershadsky et al., 2003; Discher et al., 2005; Vogel and Sheetz, 2006; Lecuit and Lenne, 2007; Kumar and Weaver, 2009). Integrin-based adhesion complexes are sensors of force between the ECM and the contractile actomyosin cytoskeleton (Bershadsky et al., 2003). Direct assays for integrin mechanosensing apply external force to ligand-coated beads bound to the cell surface and determine force-dependent reinforcement (or force-induced cell stiffening) from the reduction in bead displacement upon prolonged application of force (Wang et al., 1993; Choquet et al., 1997). Talin and vinculin are strongly implicated in this mechanoresponse (Giannone et al., 2003). In vitro force-dependent unfolding of talin opens up binding sites for vinculin (del Rio et al., 2009). In intact cells, recruitment of vinculin to tensile focal adhesions (FAs) is mediated by paxillin rather than direct talin binding (Pasapera et al., 2010). Overexpressing vinculin deletion mutants uncouples integrin-mediated adhesion from its regulation by cytoskeletal force (Humphries et al., 2007), and the absence of vinculin reduces cell stiffness (Mierke et al., 2008).

During morphogenesis, contractile forces at intercellular junctions direct cell patterning, drive convergence and extension

Q. le Duc and Q. Shi contributed equally to this paper.

Correspondence to Ning Wang: nwangrw@illinois.edu; Deborah Leckband: leckband@illinois.edu; or Johan de Rooij: j.derooij@hubrecht.eu

N. Wang, D. Leckband, and J. de Rooij contributed equally to this paper.

Abbreviations used in this paper: COMP, cartilage oligomerizing protein; CSK, cytoskeleton preserving; FA, focal adhesion; FRET, fluorescence resonance energy transfer; HGF, hepatocyte growth factor; IF, immunofluorescence; IP, immunoprecipitation; ko, knockout; MTC, magnetic twisting cytometry; pMLC, phosphorylated myosin light chain; ROI, region of interest; TIRF, total internal reflection fluorescence; wt, wild type.

The Rockefeller University Press $30.00
J. Cell Biol. Vol. 189 No. 7 1107–1115
www.jcb.org/cgi/doi/10.1083/jcb.201001149

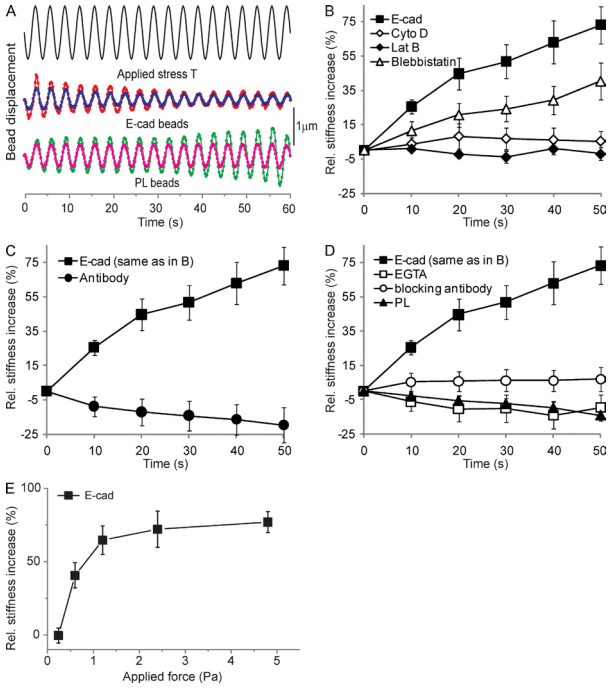

Figure 1. **E-cadherin is a mechanosensor.** (A) Continuous driving field modulation at 0.3 Hz for 60 s (2.4 Pa stress) and representative time course of the displacement of two E-cadherin– and poly-L-lysine (PL)–coated beads. (B) The force-induced stiffening of Fc–E-cadherin–coated beads relative to unperturbed bead–cell contacts in the absence (E-cad) or presence of latrunculin B (Lat B), cytochalasin D (Cyto D), or blebbistatin. (C) Fc–E-cadherin–coated beads versus beads coated with monoclonal E-cadherin antibody. (D) Fc–E-cadherin–coated beads in the absence or presence of 3 mM EGTA added just before MTC or blocking anti–E-cadherin antibody versus beads coated with poly-L-lysine. (E) The percent change in E-cadherin junction stiffness relative to unperturbed cells as a function of applied shear stress is shown. After 20 min of bead–cell contact, the beads were subjected to a modulated 0.3-Hz magnetic field for 60 s. The elastic shear modulus was determined at 50 s as a function of the amplitude of the applied shear stress. (B–E) Each data point represents >300 beads. Error bars represent SD.

movements, and regulate germ cell migration (Lecuit, 2005; Kardash et al., 2010). Also, endothelial cells coordinately align with shear flow (Tzima et al., 2005). Classical cadherins are good candidates for mechanosensing at cell–cell junctions. Myosin II activity is required for accumulation and stability of cadherins at junctions (Shewan et al., 2005; Miyake et al., 2006; Lambert et al., 2007). However, actomyosin contraction disrupts epithelial cell–cell adhesion in response to hepatocyte growth factor (HGF; de Rooij et al., 2005) or oncogenes such as Ras and Src (Zhong et al., 1997; Krendel et al., 1999; Avizienyte et al., 2004; Ayollo et al., 2009). The defining characteristic of mechanosensors is the capacity to both sense force and generate a proportional cell response (Vogel and Sheetz, 2006). As none of the prior investigations actually probed forces to demonstrate this, direct evidence for mechanosensing by cadherins is lacking (Schwartz and DeSimone, 2008). Moreover, the existence of a mechanical link between the E-cadherin complex and cytoskeleton, a necessity for mechanosensing, was challenged by recent findings (Drees et al., 2005; Yamada et al., 2005).

In this study, we present direct evidence that the E-cadherin complex is a mechanosensor that probes the mechanical environment to elicit a proportional change in the mechanics of the junctions. Furthermore, we show that vinculin potentiates E-cadherin–mediated mechanosensing and localizes to tension-bearing sites in cell–cell junctions to mediate mechanoregulation of cell–cell adhesion.

Results and discussion

The E-cadherin complex is a mechanosensor

We used magnetic twisting cytometry (MTC; Fig. 1 A; Wang and Ingber, 1995) to test whether mechanical stimulation affects the viscoelastic properties of junctions between F9 cells and Fc–E-cadherin–coated beads. All measurements were performed after 20 min of bead–cell contact to resolve force-dependent from force-independent changes in stiffening, which plateaus after ~15 min (see Fig. 4 B). During continuous shear modulation, bead displacement amplitude decreased with the forcing time (Fig. 1 A), amounting to a force-actuated 70% increase in stiffness, which is relative to previously unperturbed cells (Fig. 1 B). Latrunculin B, cytochalasin D, and blebbistatin strongly affected this response, demonstrating that cadherin force transmission requires a direct mechanical link to an organized and contractile actin cytoskeleton.

Beads coated with an anti–E-cadherin antibody bound strongly to the cell surface but did not display any force-actuated stiffening (Fig. 1 C). Moreover, addition of EGTA or an

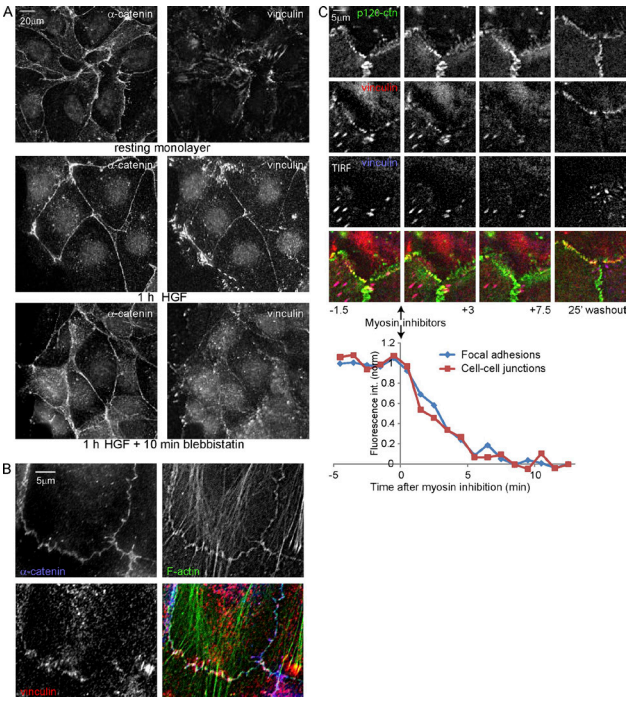

Figure 2. **Vinculin is recruited to active cell–cell junctions in a myosin-dependent manner.** (A) IF after CSK buffer extraction shows HGF-induced and myosin II–dependent α-catenin and vinculin distribution. (B) Magnified view of vinculin in cell–cell junctions of HGF-stimulated cells. (C) Cells expressing EGFP-vinculin (stably) and mCherry–p120-catenin (p120-ctn; transiently) analyzed by widefield and TIRF microscopy 1 h after HGF treatment. 3 μM ML-7 and 10 μM Y27632 were added 15 min after the start of imaging and washed out after another 10 min. EGFP-vinculin fluorescence intensity was measured in FAs (15 ROIs, each containing two to four FAs from seven time lapses) and cell–cell contacts (eight ROIs from seven time lapses).

E-cadherin–blocking antibody after 20 min of Fc–E-cadherin bead–cell contact just before the MTC measurements completely abolished the force-actuated stiffening (Fig. 1 D). Finally, poly-L-lysine–coated beads showed no stiffening (Fig. 1, A and D). This argues that contaminating integrin–bead contacts (because of nonspecific protein adsorption to beads) are not affecting our results and demonstrates that specific cadherin ligation is required. This is similar to integrins (Choquet et al., 1997) and highlights the importance of using proper ligands to elicit the mechanoresponse.

Finally, the relative stiffness increase at cadherin junctions increases with the applied bond shear up to a limiting plateau at stresses >2 Pa (Fig. 1 E). This increase in junction stiffness in proportion to the applied stress ultimately confirms that E-cadherin complexes are bona fide mechanosensors. Although regulation of E-cadherin complexes by contractile force is suggested by the myosin II requirement, direct evidence for force-dependent reinforcement of E-cadherin adhesions had not been presented to our knowledge. Thus, our data show for the first time that the E-cadherin complex is a mechanosensor.

Myosin-dependent recruitment of vinculin to active cell–cell junctions

We investigated the localization of putative cadherin–actin linker proteins after HGF stimulation, which increases tension on cell–cell junctions (see Fig. 5 A; de Rooij et al., 2005). As shown in Fig. 2 A and Fig. S1, E-cadherin, α-, β-, p120-catenin, and EPLIN (Abe and Takeichi, 2008) are localized at similar levels in steady-state and HGF-stimulated cell–cell adhesions. Interestingly, vinculin scarcely localizes to steady-state cell–cell adhesions, whereas its colocalization with α-catenin is much more evident in junctions after HGF (Fig. 2 A). Treatment with blebbistatin for 10 min largely abolished vinculin localization to cell–cell junctions, suggesting that this localization is indeed tension dependent. We conclude that vinculin is recruited to cell–cell junctions in a myosin II–dependent manner.

Closer analysis of Fig. 2 B shows that vinculin does not colocalize with the E-cadherin complex all over cell–cell junctions but is restricted to those sites in which junctions contact F-actin bundles and, thus, likely experience increased tension. Moreover, dual-color imaging of GFP-vinculin and mCherry–p120-catenin shows that cell spreading induced by HGF is followed by an increase in contraction, which marks the onset of vinculin accumulation at discrete sites within cell–cell junctions (Video 1). Finally, Fig. 2 C and Video 2 show that EGFP-vinculin, but not mCherry–p120-catenin, rapidly disappears from cell–cell junctions when tension is relieved by inhibitors. Upon inhibitor washout, tension is restored concomitant with a relocalization of vinculin to cell–cell junctions (Fig. 2 C and Video 2). Quantification

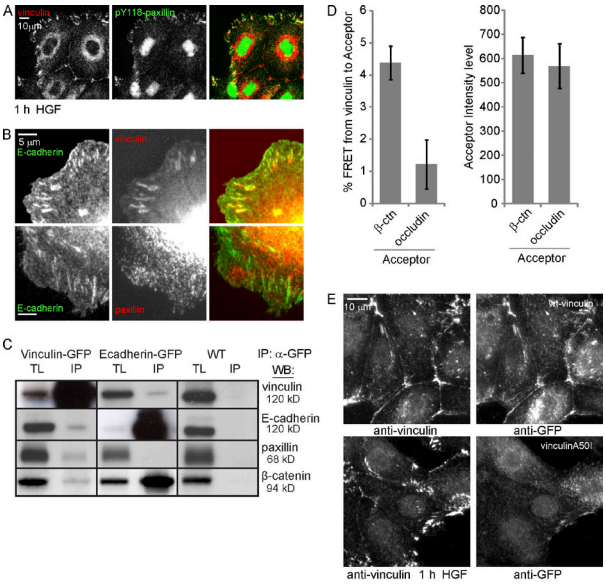

Figure 3. **Vinculin closely interacts with the E-cadherin complex.** (A) Recruitment of vinculin but not pY118-paxillin to cell–cell junctions in HGF-stimulated cells shown by IF. (B) Colocalization of vinculin but not paxillin with GFP–E-cadherin in E-cadherin–COMP adhesions revealed by IF. (C) Western blot (WB) analyses of total lysates (TL) and IP of endogenous E-cadherin, vinculin, paxillin, and β-catenin co-IP with GFP-tagged vinculin or E-cadherin from cell lysates after cross-linking. Black lines indicate that intervening lanes have been spliced out. (D, left) FRET from immunolabeled GFP-vinculin (Alexa Fluor 488) to immunolabeled β-catenin (β-ctn) or occludin (rhodamine). Error bars represent SEM (n = 18). (right) Mean acceptor fluorescence intensity in the ROIs used for calculating FRET. (E) MDCK cells transfected with GFP-vinculin or GFP–vinculin A50I were washed with CSK buffer, fixed, and immunostained for vinculin and GFP simultaneously.

of the EGFP-vinculin intensity shows that the loss of vinculin from cell–cell junctions upon myosin inhibition follows the same time curve as the loss of vinculin from FAs. We conclude that during activation of cell–cell adhesions by HGF, a pool of vinculin accumulates at discrete, actin-anchored sites in cell–cell junctions, which is concurrent with increased myosin II–dependent tension.

Vinculin interacts with the E-cadherin complex at cell–cell junctions

Total internal reflection fluorescence (TIRF) microscopy (Fig. 2 C and Video 2) shows that the pool of vinculin in cell–cell junctions is distinct from the vinculin in FAs. Furthermore, the FA protein paxillin does not colocalize with vinculin at cell–cell contacts after HGF (Video 3). Finally, tyrosine-118–phosphorylated (pY118) paxillin, which mediates myosin II–dependent recruitment of vinculin to FAs (Pasapera et al., 2010), shows no colocalization with the cell–cell junction pool of vinculin (Fig. 3 A). Thus, we conclude that vinculin is recruited to cell–cell junction complexes, which do not contact the basal ECM, through intermediates that are distinct from those that mediate recruitment of vinculin to FAs.

To separate E-cadherin adhesions from other cell–cell adhesion complexes, we plated MDCK cells on coverslips coated with E-cadherin–cartilage oligomerizing protein (COMP), a pentamerizing fusion of the ectodomain of E-cadherin and COMP (Tomschy et al., 1996), to induce the formation of actin-anchored E-cadherin adhesions (Fig. S1 A). These E-cadherin–COMP adhesions contain E-cadherin (Fig. 3 B) and α-, β-, and p120-catenin (Fig. S2, A and F) but not proteins found at other types of cell–cell junctions (nectin and claudin; Fig. S2 F) or FAs (paxillin; Fig. 3 B). Furthermore, they depend on actomyosin activity and calcium (Fig. S2, B and C) and are insensitive to blocking antibodies to β1- and α6-integrins, which mediate basal ECM adhesion in MDCK cells (Fig. S2, D and E). The fact that vinculin strongly localizes to E-cadherin–COMP adhesions (Fig. 3 B) leads to the conclusion that vinculin is recruited to the E-cadherin complex that forms a direct and functional interaction with actomyosin in cells on E-cadherin–COMP.

In immunoprecipitation (IP) after reversible chemical cross-linking followed by boiling and trituration of insoluble material that includes the cell–cell junctions (Hinck et al., 1994), endogenous vinculin precipitates with GFP–E-cadherin, and endogenous E-cadherin precipitates with GFP-vinculin (Fig. 3 C). Compared with total protein levels, β-catenin more efficiently precipitates with E-cadherin, whereas paxillin more efficiently precipitates with vinculin. We could not reproduce the efficient co-IP of vinculin and E-cadherin observed in other cell lines (Hazan et al., 1997; Maddugoda et al., 2007; Peng et al., 2010). Nevertheless, the inefficient co-IP of vinculin and E-cadherin from MDCK cells correlates well with the low abundance of vinculin in their cell–cell adhesions observed by fluorescence (Figs. 2 and 3). Thus, E-cadherin and vinculin reside in one complex, which, in MDCK cells, is not very abundant compared with other complexes in which these proteins reside. The amount of coprecipitated E-cadherin and vinculin

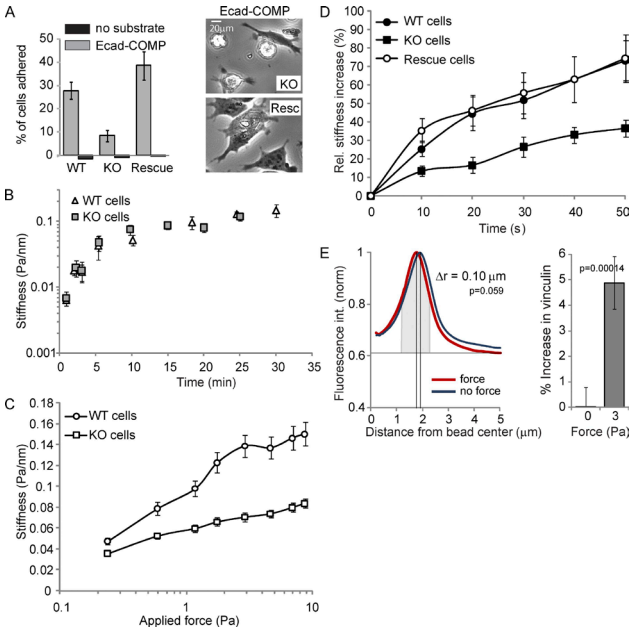

Figure 4. **Vinculin modulates E-cadherin mechanosensing.** (A, left) The relative number of wt, ko, and vinculin-reconstituted F9 cells that adhered to E-cadherin–COMP-coated wells after 45 min is shown. (right) Phase-contrast images of ko and reconstituted cells on E-cadherin–COMP. (B) The force-independent stiffening of E-cadherin junctions as a function of the bead–cell contact time. After increasing periods of bead–cell contact, the oscillating field (0.3 Hz at 10 Gauss) was switched on for 10 s to quantify the elastic shear modulus (Pa/nm). (C) Junctional stiffness in wt versus ko cells in response to increasing applied shear stress. After 20 min of bead–cell contact, the field strength was increased stepwise in 10-s intervals with no pause between successive changes in the magnetic field. Each data point represents the mean. (D) The force-induced stiffening of Fc–E-cadherin–coated beads bound for 20 min to wt, ko, and vinculin-reconstituted F9 cells was measured using a modulated 0.3-Hz field (20 Gauss) for 50 s. (E, left) The mean intensity profile of vinculin IF plotted against the distance from the bead center for ∼80 unforced and forced beads. (right) Total vinculin intensity above baseline at unforced and forced beads measured in a 1-µm-wide area around the maximum of fluorescence intensity (gray). Error bars represent SD (A, triplicates; B–D, $n > 300$ [approximately one bead/cell]; E, $n = \sim 80$).

did not increase after stimulation by HGF (unpublished data). It is possible that the low levels of vinculin that interact with E-cadherin, or the cross-linking method used, preclude the detection of changes in the complex. Alternatively, E-cadherin–vinculin complexes may form before translocation to cell–cell junctions.

Finally, we measured fluorescence resonance energy transfer (FRET) between vinculin and cell–cell junction complex members by means of acceptor photobleaching (see Materials and methods; Fig. S3). GFP-vinculin–expressing cells, stimulated for 1 h with HGF, were extracted in cytoskeleton-preserving (CSK) buffer, fixed, and stained for vinculin as donor (Alexa Fluor 488) and β-catenin or occludin as acceptor (rhodamine). Clear colocalization was found between vinculin and β-catenin at cell–cell junctions, whereas vinculin and occludin colocalized less often. FRET was measured in regions of colocalization. Higher FRET values were found for vinculin and β-catenin compared with vinculin and occludin (Fig. 3 D, left). This difference does not reflect a difference in acceptor concentration because regions were chosen with equal levels of acceptor as judged by rhodamine intensity (Fig. 3 D, right). The close proximity of vinculin to β-catenin suggests a specific association with the E-cadherin complex at cell–cell junctions.

Mutating alanine 50 to isoleucine resulted in a strong loss of vinculin's localization to cell–cell junctions and to integrin-dependent FAs (Fig. 3 E). This indicates that vinculin associates with the E-cadherin complex through mechanistically conserved interactions in its head domain (Bakolitsa et al., 2004). Whether β-catenin is the main recruiter of vinculin, as previously described in a different cell type (Peng et al., 2010), remains to be investigated.

Vinculin potentiates mechanosensing by the E-cadherin complex

To investigate the functional importance of vinculin for E-cadherin adhesion, we determined the adhesion of a panel of F9 cells (Xu et al., 1998) to E-cadherin–COMP. Vinculin knockout (ko) F9 cells showed reduced adhesion to E-cadherin–COMP when compared with wild-type (wt) F9 cells or vinculin ko F9 cells reconstituted with chicken vinculin (Fig. 4 A). This difference is because of impaired cell spreading, as indicated by the morphology of the few ko cells that remained bound to E-cadherin–COMP (Fig. 4 A, right). Functional E-cadherin was present at the plasma membrane because Fc–E-cadherin–coated beads readily adhered to the ko F9 cells (Fig. 4 B). Thus, vinculin is needed to form E-cadherin–dependent adhesive contacts that can support cell spreading.

This suggests that mechanical force is a principal conduit through which vinculin regulates E-cadherin adhesion. We further tested this using MTC. In Fig. 4 B, the force-independent increases in the local stiffness around E-cadherin–coated beads were similar for wt and ko F9 cells, indicating that basal E-cadherin adhesion is not affected by vinculin. In contrast, the stiffness increase in proportion to the applied force was clearly reduced in ko cells (Fig. 4 C). Furthermore,

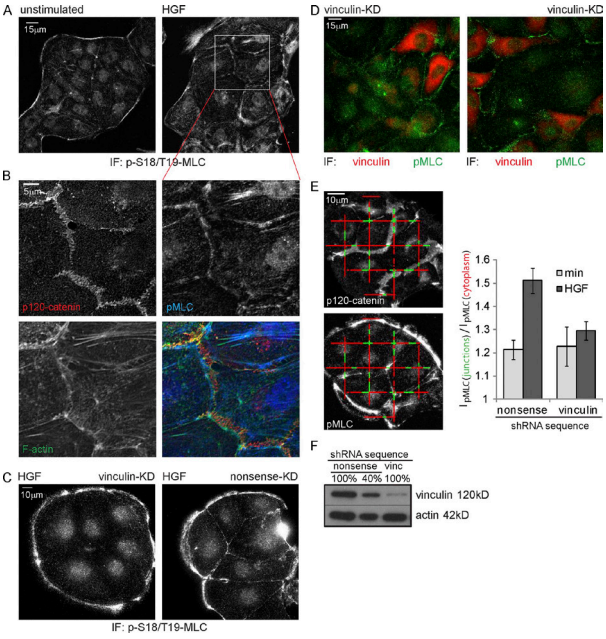

Figure 5. **Vinculin knockdown prevents HGF-induced pMLC accumulation near cell–cell junctions.** (A) HGF (2 h) induced increase in pMLC near cell–cell junctions revealed by IF. (B) A magnified view of A, showing that pMLC accumulates at F-actin structures that connect to p120-labeled cell–cell junctions. (C) IF shows a reduction of pMLC recruited to cell–cell junctions in vinculin knockdown (KD) cells after 2 h of HGF. (D) Overlay of the vinculin channel (smoothed with a Gaussian; $r = 40$) and pMLC channel of a dual-color IF staining of vinculin knockdown cells after 2 h of HGF. (E, left) Representative image automatically generated by custom software, displaying the line fragments used to measure pMLC levels near cell–cell junctions (green) and in the cytoplasm (red). (right) The relative intensity of pMLC near cell–cell junctions (a value of 1 means equal levels) shows an increase after 2 h of HGF that is largely abolished by vinculin knockdown. Error bars represent SEM. 25 images were analyzed for each condition.

ko cells displayed an ∼50% reduction in force-dependent reinforcement of cadherin junctions, which was fully restored by reconstitution with chicken vinculin (Fig. 4 D). Thus, loss of vinculin significantly reduces the mechanoresponse by the E-cadherin complex.

By immunofluorescence (IF), we noticed that vinculin and F-actin are already recruited to unforced beads. For quantification, we measured the fluorescence intensity at an increasing radius from the bead center, which was normalized to the peak level for each bead so that background levels, instead of peak intensity levels, vary. As shown in Fig. 4 E, the vinculin signal condenses around beads upon force. Furthermore, the intensity of vinculin (the curve area above background at 1-µm width around the intensity peak; Fig. 4 E, gray) slightly increases upon force. Clearly, this situation is quite different from the situation at intercellular junctions, where we observed de novo recruitment of vinculin. It is possible that the vinculin levels around unforced beads represent the buildup of intrinsic contractile actomyosin around larger beads (Choquet et al., 1997). Indeed, there was no evidence of either actin or vinculin accumulation near smaller E-cadherin–coated beads (Perez et al., 2008). In conclusion, these data show that vinculin potentiates the E-cadherin mechanoresponse concurrent with its strong increase at intercellular junctions, which experience increased tension, and with a moderate increase around forced beads.

Vinculin mediates the recruitment of active myosin to cell–cell junctions

We have previously shown that HGF signaling increases the presence of active myosin II (phosphorylated myosin light chain [pMLC]) in areas of cell–cell adhesion (de Rooij et al., 2005). A closer inspection of Fig. 5 B reveals that pMLC is present at F-actin structures that are just adjacent to cell–cell junctions and connect to the E-cadherin complex through thin actin bundles. As we show in Fig. 2, inhibition of myosin activity results in a loss of these actin-connected, vinculin-containing junctions. Conversely, we now investigated whether a loss of vinculin would affect these contractile actomyosin structures connected to cell–cell junctions. An ∼90% knockdown of vinculin (Fig. 5 F) resulted in a strong reduction in vinculin levels in the cytoplasm but did not completely deplete vinculin from FAs or intercellular junctions in MDCK cells. Although depletion of vinculin from cell–cell junctions was not complete, we observed a significant effect on the reorganization of junctions in response to HGF, which resulted in a strong loss of pMLC recruitment to cell–cell adhesions (Fig. 5 C). Fig. 5 D shows that this loss is specific for cells with a strongly reduced amount of vinculin. To quantify this, we used custom software that automatically divides the pixel intensity of the pMLC image in areas of cell–cell adhesion (Fig. 5 E, $I_{pMLC(junctions)}$, green) by the pixel intensity of the pMLC signal in the cytoplasm (Fig. 5 E, $I_{pMLC(cytoplasm)}$, red). As shown in Fig. 5 E, there is a strong reduction of the HGF-induced recruitment of

pMLC to cell–cell junctions in vinculin knockdown cells. Thus, we conclude that the recruitment of vinculin to active cell–cell junctions upon HGF is important for the remodeling of the cytoskeleton that connects to these junctions.

In conclusion, our nanomechanical experiments show that the E-cadherin complex is a bona fide mechanosensor. Furthermore, we uncover a novel role for vinculin in modulating E-cadherin–cytoskeleton mechanics and force-induced remodeling of cell–cell junctions. Because stiffness measured by MTC is a complex process, it is impossible to pinpoint the exact molecular mechanism that explains vinculin's role in E-cadherin mechanoregulation from these experiments. It is tempting to speculate similarity to integrin adhesion, but the molecules involved in vinculin recruitment to integrin adhesions (talin and paxillin) are not present at cell–cell contacts. Moreover, the proposed integrin mechanism (vinculin recruitment to stretched talin) would predict full inhibition of mechanosensing in the absence of vinculin, whereas we measure only partial inhibition. Furthermore, our MTC measurements show a strong effect on the stress–strain relation for E-cadherin junctions (Fig. 4 C), which is not found for integrin junctions (Mierke et al., 2008). All of this indicates that the mechanism of integrin-dependent force sensing may differ from mechanosensing at E-cadherin junctions. Thus, our data uncover a novel role for vinculin in E-cadherin mechanosensing, but, as for integrins, the exact mechanism remains to be established. Our findings have broad implications because of the central role of E-cadherin in the development and maintenance of epithelial tissues. Given the similarities in structure and binding characteristics among classical cadherins, it is tempting to speculate that cadherins may constitute a new family of tension sensors. The involvement of vinculin in cadherin mechanosensing and its localization to subdomains in activated cell–cell junctions opens the door for further investigations of molecular mechanisms underlying E-cadherin mechanoregulation.

Materials and methods

Cell lines and culture

MDCK and F9 cells were routinely cultured in high glucose DME (Invitrogen) supplemented with 10% FCS (Sigma-Aldrich) and penicillin/streptomycin (Invitrogen) in standard tissue culture dishes coated with 0.1% gelatin (Sigma-Aldrich) in the case of F9s. F9 ko cells were the γ229 cells, and chicken vinculin-reconstituted R16 cells were described previously (Xu et al., 1998). MDCK cell lines stably expressing EGFP- or mCherry-tagged constructs were generated by nucleofection (Lonza), G418 (Invitrogen) selection, and FACS sorting for intermediate levels of fluorescence. For imaging experiments, cells were grown on glass coverslips, glass-bottom dishes (WillCo Wells B.V.), or chamber coverslips (Thermo Fisher Scientific) coated with 10 µg/ml collagen type 1 (Sigma-Aldrich) or 20 µg/ml E-cadherin–COMP in medium supplemented with 0.5% FCS. 5 ng/ml HGF (Sigma-Aldrich) concentration was used.

Adhesion assays

Both MDCK cells and F9 cells were prepared by trypsinization from the culture dish, washed once in DME containing 10% FCS, incubated for 1 h under rotation in suspension in DME plus 10% FCS at 37°C, pelleted, and resuspended at the appropriate concentration in DME containing 0.5% FCS. MDCK adhesion assays were performed in 48-well plates coated with 20 µg/ml E-cadherin–COMP at a concentration of 100,000 cells per well. F9 cell adhesion was in 96-well plates coated with 20 µg/ml E-cadherin–COMP at a concentration of 100,000 cells per well. Adhesion was allowed for 45 min followed by three steps of rigorous washing in PBS supplemented with 1 mM $CaCl_2$ and quantified by measuring acid phosphatase activity (de Rooij et al., 2005).

Immunocytochemistry and microscopy

For immunocytochemistry, cells were washed three times in PBS (containing 1 mM $CaCl_2$ in the case of growth on E-cadherin–COMP) and fixed using 4% paraformaldehyde in PBS. Alternatively, if indicated, cells were washed two times for 1 min in CSK buffer (300 mM sucrose, 0.5% TX-100, 10 mM Pipes, pH 7, 50 mM NaCl, 3 mM $CaCl_2$, and 2 mM $MgCl_2$) before fixation. Live cell imaging, E-cadherin–COMP IF, and the colocalization imaging of α-catenin and EPLIN in Fig. S2 were performed on a microscope (Ti; Nikon) in a climate-controlled culture chamber using a 60× 1.49 NA Apo TIRF objective lens and an electron microscopy charge-coupled device camera (Luka; Andor). To image cell–cell junctions in Fig. 2 and Fig. S2, immunostained cells on collagen were imaged using a confocal microscope (TCS-SP2; Leica) with a 63× 1.32 NA objective lens and a pinhole setting of 1 airy disk. For FRET measurements, cells were imaged on a confocal microscope (TCS-SP5; Leica) with a 63× 1.32 NA objective lens using a four times zoom and a pinhole setting of 3 mm. Acceptor photobleaching was achieved by scanning the central area of the image with a 20 times zoom using a 561 laser at full power. All widefield images, unless specifically indicated otherwise, and with the exception of the E-cadherin–COMP images in Fig. 3 B and Fig. 2 (A and F), were sharpened for display with an unsharp mask filter in ImageJ (National Institutes of Health; r = 3; weight = 0.6) and background subtracted by rolling ball (r = 40).

Quantification of fluorescence imaging

To measure the decay of vinculin from cell–cell junctions and FAs after inhibition of actomyosin contractility, we cleaned up the time-lapse image series using the unsharp mask filter and background subtraction. Regions of interest (ROIs) were drawn that encompassed two to four closely grouped FAs or a vinculin-containing area of cell–cell adhesion. The decay in each of these ROIs was corrected for bleaching and fluctuations by neighboring background ROIs and normalized between 0 (background level at the end of the curve) and 1 (mean vinculin ROI intensity before addition of inhibitors). Normalized intensities from individual ROIs were averaged per frame and displayed in Fig. 2 C.

To quantify changes in pMLC intensity at cell–cell junctions, a custom function was written in MATLAB (MathWorks) that draws a grid of 9-pixel-wide horizontal and vertical lines on the images, which were first flattened by background subtraction. These lines are spaced 170 pixels apart and from the edges of the image. Thresholding was used to determine the edges of cell islands, and lines were shortened to end at least 100 pixels from these edges (on the inside of the island) or from the edge of the image (Fig. 5 E, red). Peaks in pixel intensity in the p120-catenin image were used to automatically define the location of cell–cell junctions along these lines and mark 60-pixel fragments on the lines that span peaks (Fig. 5 E, green). Pixel intensities along these line fragments in the pMLC image were divided by pixel intensities along the rest of the red lines to calculate the relative pMLC levels near cell–cell junctions.

Acceptor photobleaching (FRET)

FRET efficiencies were measured by acceptor photobleaching. Donor (GFP-vinculin stained by anti-GFP with Alexa Fluor 488–labeled secondary antibodies) and acceptor (indicated primary with rhodamine-labeled secondary antibodies) confocal images were collected before and after photobleaching of the acceptor in a defined region of the image (Fig. S3). Laser, microscope, and scanhead settings were identical throughout these experiments, and the images were corrected for background and nonspecific bleaching during scanning. The FRET values were calculated from the mean fluorescent values from ROIs. Three to five ROIs comprising cell–cell junctions outside the bleach area were used to calculate bleaching caused by imaging, and three to five ROIs inside the bleach area were used to calculate the percent loss in acceptor fluorescence and the gain in donor fluorescence upon acceptor bleaching. The postbleach donor values were corrected for acceptor photo conversion. Photo conversion of the acceptor was measured by imaging in 20 ROIs in five independent images of cells that were stained only with acceptor antibodies (β-catenin + anti–mouse rhodamine) and determined to be 1.12 ± 0.3%. The donor fluorescence loss in the prebleach donor image was calculated by subtracting the prebleach donor image from the corrected postbleach donor image and dividing this by the fraction of acceptor bleaching to correct for incomplete acceptor bleaching (in all experiments >0.8). The FRET percent was calculated by relating the donor fluorescence loss in the prebleach donor image to the total donor fluorescence (prebleach donor image plus donor fluorescence loss in the prebleach donor image).

Antibodies and DNA constructs

Mouse monoclonal vinculin antibody (hVin-1) and rabbit polyclonal α-catenin antibody were obtained from Sigma-Aldrich. Mouse monoclonal

E-cadherin (clones 36 and 34), β- and p120-catenin, paxillin, and EPLIN antibodies were obtained from BD. Polyclonal pMLC antibody (pS18/T19) was obtained from Cell Signaling Technology. Mouse monoclonal occludin antibody was obtained from Invitrogen. Alexa Fluor 488 phalloidin and Alexa Fluor 488, Alexa Fluor 594, or Texas red–labeled secondary antibodies were obtained from Invitrogen. The EGFP–E-cadherin construct was provided by A. Kusumi (Japan Science and Technology Corporation, Chiyoda, Nagoya, Japan; Iino et al., 2001). Chicken vinculin was cloned in the pEGFP-C3 vector, resulting in expression of full-length N-terminal EGFP-tagged vinculin. Murine p120-catenin was cloned in the mCherry-N1 vector (identical to pEGFP-N1, with EGFP replaced by mCherry) to express full-length C-terminal mCherry-tagged p120-catenin. pEGFP-N1-paxillin was provided by M.H. Ginsberg (University of California, San Diego, La Jolla, CA; Nishiya et al., 2005) and was cloned into the mCherry-N1 vector. EGFP-nectin1 was provided by C. Krummenacher (University of Pennsylvania, Philadelphia, PA; Krummenacher et al., 2003), GFP-claudin3 was provided by M. Furuse (Jichi Medical University, Shimotsuke, Tochigi, Japan; Matsuda et al., 2004), and vinculin A50I was provided by C. Ballestrem (University of Manchester, Manchester, England, UK). Vinculin knockdown was performed by nucleofection of a mix of two pSuper vectors containing vinculin-directed shRNA inserts, 5′-AAGAGTTGCTGCCAGTTCTC-ATT-3′ and 5′-AAACCAAGGAATAGAAGAAGCTT-3′. Control (nonsense) knockdown used the identical procedure with a pSuper vector with none-coding insert.

E-cadherin–COMP expression and purification

The E-cadherin–COMP-His6 expression construct was provided by O. Pertz (University of Basel, Basel, Switzerland; Pertz et al., 1999). Expression was performed by transient transfection in HEK293T cells followed by culturing for 2 d on low serum medium and Ni-NTA affinity purification of the secreted E-cadherin–COMP-His6 from the culture medium.

IP

Cells were grown for 24 h on 3 µg/ml collagen-coated tissue culture dishes in DME supplemented with 0.5% FCS (HGF was added for 2 h when indicated) or for 14 h in 60 µM $CaCl_2$ containing EpiLife followed by 1 h addition of up to 1.8 mM $CaCl_2$. Cells were washed twice with PBS containing 1 mM $CaCl_2$ at RT before adding 3 ml PBS with 1 mM $CaCl_2$ containing 200 µg/ml DSP (DSP prepared as 100× stock in DMSO diluted immediately before use) per 10-cm dish. Next, cells were incubated on a rocking platform for 20 min at RT and washed twice with PBS at RT before washing four times with ice-cold quenching buffer (10 mM Tris, pH 7.5, in PBS). Excess liquid was removed, and cells were scraped in 800 µl of ice-cold lysis buffer (25 mM Tris, pH 7.5, 1% NP-40, 1% deoxycholic acid, 150 mM NaCl, protease inhibitor cocktail (1:1000; Roche), 10 µl/ml leupeptin, 1 mM sodium fluoride, and 1 mM sodium orthovanadate). The lysate was spun at 4°C for 10 min at 16,100 relative centrifugal force, the supernatant was removed, and the pellet was triturated in 100 µl SDS-IP buffer (15 mM Tris, pH 7.5, 5 mM EDTA, 2.5 mM EGTA, and 1% SDS) by use of a 23-G needle and subsequently a 29-G insulin needle. The sample was put at 100°C for 10 min, diluted with 900 µl of lysis buffer, and spun at 4°C for 10 min at 16,100 relative centrifugal force. Supernatant was added to protein A–Sepharose beads (GE Healthcare) precoupled with GFP antibody (custom-made rabbit polyclonal) and incubated for 2 h at 4°C. The beads were washed four times with cold lysis buffer and remnant liquid was removed and boiled for 10 min in 50 µl of Laemmli sample buffer (containing 5% β-mercaptoethanol). Samples were run on a 4–12% gradient SDS-PAGE gel (NuPage; Invitrogen), blotted onto PVDF membranes, and analyzed with the indicated primary antibodies followed by HRP-coupled secondary antibodies and ECL detection. Monoclonal E-cadherin (clone 36), monoclonal paxillin, and monoclonal β-catenin were obtained from BD. Polyclonal vinculin (hVin-1) was obtained from Sigma-Aldrich.

MTC

MTC measurements were performed with a home-built instrument. F9 cells were cultured on mixed laminin/poly-L-lysine substrates and grown to confluence. 4.5-µm ferromagnetic beads (Spherotech) were covalently modified with Fc-tagged human E-cadherin. The latter recombinant protein (Niessen and Gumbiner, 2002) was expressed by stably transfected CHO cells cultured in DME containing 10% FBS and 0.4 mg/ml geneticin. During the protein collection phase, the culture medium was switched to serum-free DME to simplify the purification and increase protein yields. Fc–E-cadherin was purified from the serum-free conditioned medium on a protein A affinity column (Affigel; Bio-Rad Laboratories; Prakasam et al., 2006b). Before immobilization, the carboxyl groups on the beads were activated with ethyl-3-(dimethylaminopropyl)-carbodiimide/*N*-hydroxysuccinimide treatment (Prakasam et al., 2006a,b). Incubating the activated beads with soluble E-cadherin covalently linked the protein to the beads. Alternatively, beads were labeled with monoclonal anti–E-cadherin antibodies (also used as a blocking antibody in these experiments; clone 34; BD) using an identical protocol. The E-cadherin–coated beads were incubated with a confluent cell monolayer on a heated microscope stage at 37°C. All MTC imaging was performed on an inverted microscope (Leica) using a 20× 0.6 NA objective and a cooled charge-coupled device camera (Orca2; Hamamatsu Photonics). Control beads were similarly modified with poly-L-lysine. In all measurements, an initial, brief high field was applied to magnetize the beads. After defined time periods, the oscillating magnetic field perpendicular to the bead magnetic moment was turned on for a defined period to induce a modulating shear stress on the beads. Inhibitors in Fig. 1 were added 10 min before MTC measurements. EGTA was added just before MTC measurements. The bead magnetic moment constant was calibrated in a viscosity standard by rotating the beads in the fluid and measuring the bead angular strain (Wang et al., 1993), determined to be 0.12 Pa/Gauss magnetic field. The bead displacements were directly measured and converted to the complex modulus/stiffness by taking the ratio of the applied stress (bead magnetic moment constant × applied magnetic field) to the bead displacement (Wang et al., 1993). Fourier transforms of the bead displacements and the specific torque were used to determine the complex modulus of the bead–cell junction (Fabry et al., 2001). Decreases in the amplitude of bead displacements at a given torque reflect increases in local junction stiffness, which can arise from such processes as adhesion protein accumulation, mechanical reinforcement of the bonds, increased cell contractility, or actin reorganization. Force-independent changes could arise from processes such as E-cadherin accumulation at bead–cell contacts (Perez et al., 2008). Each measurement (experimental condition) represents measurements with $n > 300$ cells at approximately bead per cell. The data follow a log normal distribution from which we obtained the mean and standard deviation. The Student's *t* test was used to compare measurements, with $P < 0.05$ indicative of a statistically significant difference.

Quantification of vinculin around Fc–E-cadherin–coated beads

To investigate the effect of force on vinculin recruitment, the cells were incubated with beads and fixed without applying force or after force application. The cells were stained with either vinculin antibody or rhodamine-conjugated phalloidin. Imaging was performed on a microscope (200M; Carl Zeiss, Inc.) using a 100× 1.3 NA objective and a cooled charge-coupled device camera (AxioCam; Carl Zeiss, Inc.). For each cell-attached bead, the fluorescent image was divided into concentric rings centered at the bead center, and the mean fluorescent intensity was calculated at a different ring radius or position. This fluorescent intensity profile of each bead was subtracted by the background, normalized to its maximum, and averaged for ∼80 beads.

Online supplemental material

Fig. S1 shows localization of E-cadherin–actin linkers after HGF. Fig. S2 shows that E-cadherin–COMP adhesions are cadherin- and myosin II–dependent structures that contain the core E-cadherin complex. Fig. S3 further explains the FRET data shown in Fig. 3 D. Video 1 shows that vinculin is recruited to p120-catenin containing cell–cell junctions after HGF. Video 2 shows that the cell–cell junction pool of vinculin is distinct from the vinculin pool at the basal FAs and that they are both localized in an actomyosin-dependent manner. Video 3 shows that vinculin at cell–cell contacts does not overlap with paxillin-positive FAs. Online supplemental material is available at http://www.jcb.org/cgi/content/full/jcb.201001149/DC1.

We thank Eileen Adamson for the F9 cell lines and Jacco van Rheenen for advice on FRET.

This work was supported by The American Institute for Cancer Research (grant 06-0528), The Dutch Foundation for Cancer Research (KWF; grant 2006-3714 to J. de Rooij), and The National Institutes of Health (grant GM 072744 to N. Wang). D. Leckband was supported by The Reid T. Milner Professorship and The National Science Foundation (Chemical, Bioengineering, Environmental, and Transport Systems; grant 0853705).

Submitted: 27 January 2010
Accepted: 2 June 2010

References

Abe, K., and M. Takeichi. 2008. EPLIN mediates linkage of the cadherin catenin complex to F-actin and stabilizes the circumferential actin belt. *Proc. Natl. Acad. Sci. USA.* 105:13–19. doi:10.1073/pnas.0710504105

Avizienyte, E., V.J. Fincham, V.G. Brunton, and M.C. Frame. 2004. Src SH3/2 domain-mediated peripheral accumulation of Src and phospho-myosin is linked to deregulation of E-cadherin and the epithelial-mesenchymal transition. *Mol. Biol. Cell.* 15:2794–2803. doi:10.1091/mbc.E03-12-0879

Ayollo, D.V., I.Y. Zhitnyak, J.M. Vasiliev, and N.A. Gloushankova. 2009. Rearrangements of the actin cytoskeleton and E-cadherin-based adherens junctions caused by neoplasic transformation change cell-cell interactions. *PLoS One.* 4:e8027. doi:10.1371/journal.pone.0008027

Bakolitsa, C., D.M. Cohen, L.A. Bankston, A.A. Bobkov, G.W. Cadwell, L. Jennings, D.R. Critchley, S.W. Craig, and R.C. Liddington. 2004. Structural basis for vinculin activation at sites of cell adhesion. *Nature.* 430:583–586. doi:10.1038/nature02610

Bershadsky, A.D., N.Q. Balaban, and B. Geiger. 2003. Adhesion-dependent cell mechanosensitivity. *Annu. Rev. Cell Dev. Biol.* 19:677–695. doi:10.1146/annurev.cellbio.19.111301.153011

Choquet, D., D.P. Felsenfeld, and M.P. Sheetz. 1997. Extracellular matrix rigidity causes strengthening of integrin-cytoskeleton linkages. *Cell.* 88:39–48. doi:10.1016/S0092-8674(00)81856-5

de Rooij, J., A. Kerstens, G. Danuser, M.A. Schwartz, and C.M. Waterman-Storer. 2005. Integrin-dependent actomyosin contraction regulates epithelial cell scattering. *J. Cell Biol.* 171:153–164. doi:10.1083/jcb.200506152

del Rio, A., R. Perez-Jimenez, R. Liu, P. Roca-Cusachs, J.M. Fernandez, and M.P. Sheetz. 2009. Stretching single talin rod molecules activates vinculin binding. *Science.* 323:638–641. doi:10.1126/science.1162912

Discher, D.E., P. Janmey, and Y.L. Wang. 2005. Tissue cells feel and respond to the stiffness of their substrate. *Science.* 310:1139–1143. doi:10.1126/science.1116995

Drees, F., S. Pokutta, S. Yamada, W.J. Nelson, and W.I. Weis. 2005. Alpha-catenin is a molecular switch that binds E-cadherin-beta-catenin and regulates actin-filament assembly. *Cell.* 123:903–915. doi:10.1016/j.cell.2005.09.021

Fabry, B., G.N. Maksym, S.A. Shore, P.E. Moore, R.A. Panettieri Jr., J.P. Butler, and J.J. Fredberg. 2001. Selected contribution: time course and heterogeneity of contractile responses in cultured human airway smooth muscle cells. *J. Appl. Physiol.* 91:986–994.

Giannone, G., G. Jiang, D.H. Sutton, D.R. Critchley, and M.P. Sheetz. 2003. Talin1 is critical for force-dependent reinforcement of initial integrin–cytoskeleton bonds but not tyrosine kinase activation. *J. Cell Biol.* 163:409–419. doi:10.1083/jcb.200302001

Hazan, R.B., L. Kang, S. Roe, P.I. Borgen, and D.L. Rimm. 1997. Vinculin is associated with the E-cadherin adhesion complex. *J. Biol. Chem.* 272:32448–32453. doi:10.1074/jbc.272.51.32448

Hinck, L., I.S. Näthke, J. Papkoff, and W.J. Nelson. 1994. Dynamics of cadherin/catenin complex formation: novel protein interactions and pathways of complex assembly. *J. Cell Biol.* 125:1327–1340. doi:10.1083/jcb.125.6.1327

Humphries, J.D., P. Wang, C. Streuli, B. Geiger, M.J. Humphries, and C. Ballestrem. 2007. Vinculin controls focal adhesion formation by direct interactions with talin and actin. *J. Cell Biol.* 179:1043–1057. doi:10.1083/jcb.200703036

Iino, R., I. Koyama, and A. Kusumi. 2001. Single molecule imaging of green fluorescent proteins in living cells: E-cadherin forms oligomers on the free cell surface. *Biophys. J.* 80:2667–2677. doi:10.1016/S0006-3495(01)76236-4

Kardash, E., M. Reichman-Fried, J.L. Maître, B. Boldajipour, E. Papusheva, E.M. Messerschmidt, C.P. Heisenberg, and E. Raz. 2010. A role for Rho GTPases and cell-cell adhesion in single-cell motility in vivo. *Nat. Cell Biol.* 12:47–53: 1–11. doi:10.1038/ncb2003

Krendel, M., N.A. Gloushankova, E.M. Bonder, H.H. Feder, J.M. Vasiliev, and I.M. Gelfand. 1999. Myosin-dependent contractile activity of the actin cytoskeleton modulates the spatial organization of cell-cell contacts in cultured epitheliocytes. *Proc. Natl. Acad. Sci. USA.* 96:9666–9670. doi:10.1073/pnas.96.17.9666

Krummenacher, C., I. Baribaud, R.J. Eisenberg, and G.H. Cohen. 2003. Cellular localization of nectin-1 and glycoprotein D during herpes simplex virus infection. *J. Virol.* 77:8985–8999. doi:10.1128/JVI.77.16.8985-8999.2003

Kumar, S., and V.M. Weaver. 2009. Mechanics, malignancy, and metastasis: the force journey of a tumor cell. *Cancer Metastasis Rev.* 28:113–127. doi:10.1007/s10555-008-9173-4

Lambert, M., O. Thoumine, J. Brevier, D. Choquet, D. Riveline, and R.M. Mège. 2007. Nucleation and growth of cadherin adhesions. *Exp. Cell Res.* 313:4025–4040. doi:10.1016/j.yexcr.2007.07.035

Lecuit, T. 2005. Adhesion remodeling underlying tissue morphogenesis. *Trends Cell Biol.* 15:34–42. doi:10.1016/j.tcb.2004.11.007

Lecuit, T., and P.F. Lenne. 2007. Cell surface mechanics and the control of cell shape, tissue patterns and morphogenesis. *Nat. Rev. Mol. Cell Biol.* 8:633–644. doi:10.1038/nrm2222

Maddugoda, M.P., M.S. Crampton, A.M. Shewan, and A.S. Yap. 2007. Myosin VI and vinculin cooperate during the morphogenesis of cadherin cell–cell contacts in mammalian epithelial cells. *J. Cell Biol.* 178:529–540. doi:10.1083/jcb.200612042

Matsuda, M., A. Kubo, M. Furuse, and S. Tsukita. 2004. A peculiar internalization of claudins, tight junction-specific adhesion molecules, during the intercellular movement of epithelial cells. *J. Cell Sci.* 117:1247–1257. doi:10.1242/jcs.00972

Mierke, C.T., P. Kollmannsberger, D.P. Zitterbart, J. Smith, B. Fabry, and W.H. Goldmann. 2008. Mechano-coupling and regulation of contractility by the vinculin tail domain. *Biophys. J.* 94:661–670. doi:10.1529/biophysj.107.108472

Miyake, Y., N. Inoue, K. Nishimura, N. Kinoshita, H. Hosoya, and S. Yonemura. 2006. Actomyosin tension is required for correct recruitment of adherens junction components and zonula occludens formation. *Exp. Cell Res.* 312:1637–1650. doi:10.1016/j.yexcr.2006.01.031

Niessen, C.M., and B.M. Gumbiner. 2002. Cadherin-mediated cell sorting not determined by binding or adhesion specificity. *J. Cell Biol.* 156:389–399. doi:10.1083/jcb.200108040

Nishiya, N., W.B. Kiosses, J. Han, and M.H. Ginsberg. 2005. An alpha4 integrin-paxillin-Arf-GAP complex restricts Rac activation to the leading edge of migrating cells. *Nat. Cell Biol.* 7:343–352. doi:10.1038/ncb1234

Pasapera, A.M., I.C. Schneider, E. Rericha, D.D. Schlaepfer, and C.M. Waterman. 2010. Myosin II activity regulates vinculin recruitment to focal adhesions through FAK-mediated paxillin phosphorylation. *J. Cell Biol.* 188:877–890. doi:10.1083/jcb.200906012

Peng, X., L.E. Cuff, C.D. Lawton, and K.A. DeMali. 2010. Vinculin regulates cell-surface E-cadherin expression by binding to beta-catenin. *J. Cell Sci.* 123:567–577. doi:10.1242/jcs.056432

Perez, T.D., M. Tamada, M.P. Sheetz, and W.J. Nelson. 2008. Immediate-early signaling induced by E-cadherin engagement and adhesion. *J. Biol. Chem.* 283:5014–5022. doi:10.1074/jbc.M705209200

Pertz, O., D. Bozic, A.W. Koch, C. Fauser, A. Brancaccio, and J. Engel. 1999. A new crystal structure, Ca2+ dependence and mutational analysis reveal molecular details of E-cadherin homoassociation. *EMBO J.* 18:1738–1747. doi:10.1093/emboj/18.7.1738

Prakasam, A., Y.H. Chien, V. Maruthamuthu, and D.E. Leckband. 2006a. Calcium site mutations in cadherin: impact on adhesion and evidence of cooperativity. *Biochemistry.* 45:6930–6939. doi:10.1021/bi060213m

Prakasam, A.K., V. Maruthamuthu, and D.E. Leckband. 2006b. Similarities between heterophilic and homophilic cadherin adhesion. *Proc. Natl. Acad. Sci. USA.* 103:15434–15439. doi:10.1073/pnas.0606701103

Schwartz, M.A., and D.W. DeSimone. 2008. Cell adhesion receptors in mechanotransduction. *Curr. Opin. Cell Biol.* 20:551–556. doi:10.1016/j.ceb.2008.05.005

Shewan, A.M., M. Maddugoda, A. Kraemer, S.J. Stehbens, S. Verma, E.M. Kovacs, and A.S. Yap. 2005. Myosin 2 is a key Rho kinase target necessary for the local concentration of E-cadherin at cell-cell contacts. *Mol. Biol. Cell.* 16:4531–4542. doi:10.1091/mbc.E05-04-0330

Tomschy, A., C. Fauser, R. Landwehr, and J. Engel. 1996. Homophilic adhesion of E-cadherin occurs by a co-operative two-step interaction of N-terminal domains. *EMBO J.* 15:3507–3514.

Tzima, E., M. Irani-Tehrani, W.B. Kiosses, E. Dejana, D.A. Schultz, B. Engelhardt, G. Cao, H. DeLisser, and M.A. Schwartz. 2005. A mechanosensory complex that mediates the endothelial cell response to fluid shear stress. *Nature.* 437:426–431. doi:10.1038/nature03952

Vogel, V., and M. Sheetz. 2006. Local force and geometry sensing regulate cell functions. *Nat. Rev. Mol. Cell Biol.* 7:265–275. doi:10.1038/nrm1890

Wang, N., and D.E. Ingber. 1995. Probing transmembrane mechanical coupling and cytomechanics using magnetic twisting cytometry. *Biochem. Cell Biol.* 73:327–335. doi:10.1139/o95-041

Wang, N., J.P. Butler, and D.E. Ingber. 1993. Mechanotransduction across the cell surface and through the cytoskeleton. *Science.* 260:1124–1127. doi:10.1126/science.7684161

Xu, W., J.L. Coll, and E.D. Adamson. 1998. Rescue of the mutant phenotype by reexpression of full-length vinculin in null F9 cells; effects on cell locomotion by domain deleted vinculin. *J. Cell Sci.* 111:1535–1544.

Yamada, S., S. Pokutta, F. Drees, W.I. Weis, and W.J. Nelson. 2005. Deconstructing the cadherin-catenin-actin complex. *Cell.* 123:889–901. doi:10.1016/j.cell.2005.09.020

Zhong, C., M.S. Kinch, and K. Burridge. 1997. Rho-stimulated contractility contributes to the fibroblastic phenotype of Ras-transformed epithelial cells. *Mol. Biol. Cell.* 8:2329–2344.

le Duc et al., http://www.jcb.org/cgi/content/full/jcb.201001149/DC1

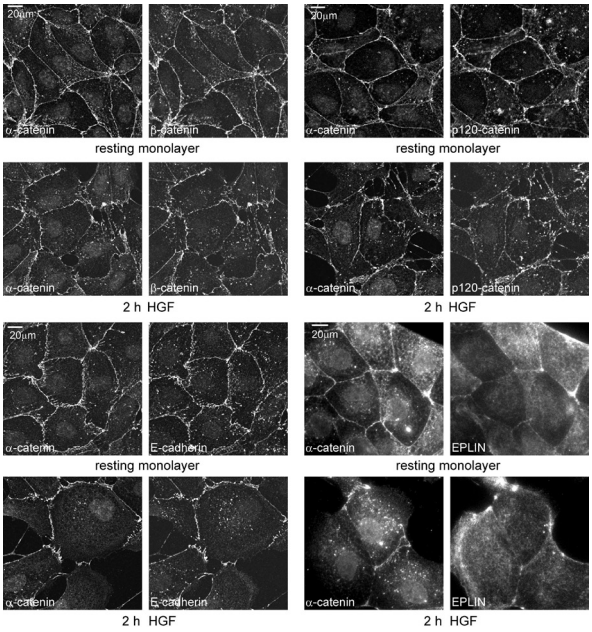

Figure S1. **Localization of E-cadherin complex proteins after HGF stimulation.** Cells were grown for 20 h and treated with HGF for 2 h. Cells were washed two times in CSK buffer before fixation to remove cytosolic proteins and stained as indicated.

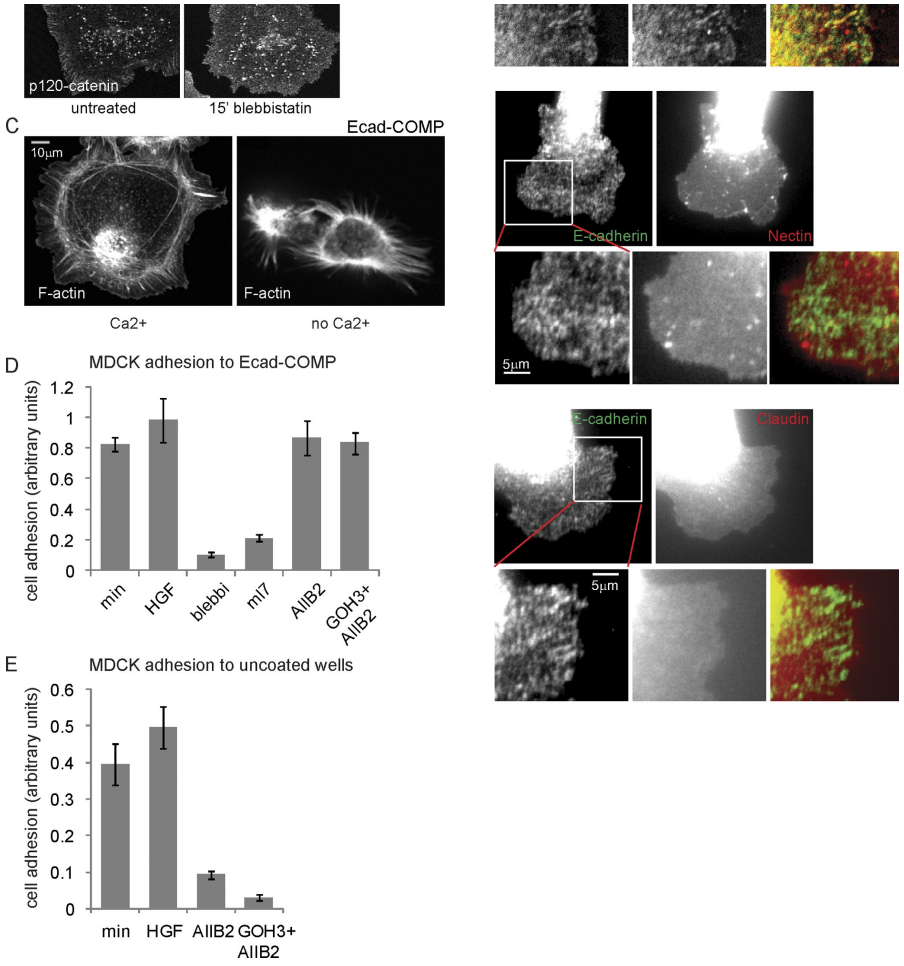

E-cadherin–COMP adhesions are cadherin and myosin II–dependent structures that contain the core E-cadherin cc
ells on E-cadherin–COMP-coated coverslips reveals elongated adhesion structures containing the E-cadherin complex.
ate at these adhesions. (B) Treatment with blebbistatin for 15 min after cell spreading abrogates the elongated E-cad
eatment results in cell rounding and detachment (not depicted). (C) Washing MDCK cells adhering to E-cadherin–CO*M*
s of adhesion, as shown by phalloidin staining of the few remaining cells, whereas cells on collagen or uncoated co
he absence of calcium (not depicted). (D) Adhesion of MDCK cells to E-cadherin–COMP depends on myosin II activity
ns. MDCK cells were allowed to adhere for 45 min in the presence of inhibitors of myosin II activity or ~20 μg/ml int
, AIIB2; α6-integrins, GOH3) followed by rigorous washing. Quantification was performed by acid phosphatase acti
here mainly through β1- and α6-integrins, as indicated by the complete loss of adhesion in the presence of ~20 μg/
CK cells were allowed to adhere for 3 h to uncoated, BSA-blocked wells in the presence of the indicated antibodies.
erformed as described in D. (F) α-Catenin and β-catenin colocalize to E-cadherin–COMP adhesions, whereas GFP-n
udin3 (stably expressed) do not localize to E-cadherin–COMP adhesions, as shown by GFP imaging and IF staining
n–COMP. GFP-nectin1 and GFP-claudin3 do display membrane targeting and localize to junctions between neighb
t these fusion proteins do behave as their wt counterparts and are properly used in this study to conclude that nectin
e not recruited to E-cadherin–COMP adhesions. Error bars represent SD in triplicate samples.

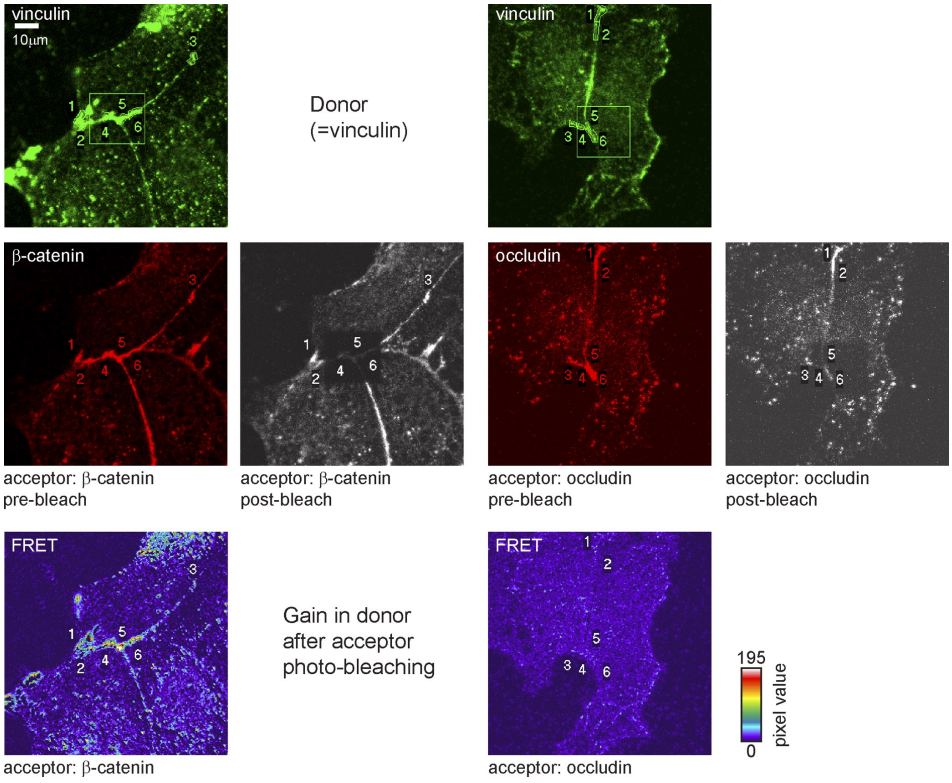

Figure S3. **FRET in cell–cell junctions between Alexa Fluor 488– and rhodamine-labeled proteins.** To measure FRET, GFP-vinculin–expressing MDCK cells were CSK extracted, paraformaldehyde fixed, and stained with polyclonal anti-GFP followed by Alexa Fluor 488–labeled secondary antibodies as the donor. To function as the acceptor, β-catenin or occludin was detected with monoclonal antibodies followed by a rhodamine-labeled secondary antibody. Donor and acceptor images were taken before and after bleaching a central area (boxed regions) of the acceptor using high laser power. ROIs were drawn around vinculin-containing areas, as outlined and numbered in the top panels, of cell–cell junctions both outside and inside the bleach area to calculate bleaching caused by imaging and the percentage of acceptor bleaching. Gain in donor fluorescence as a result of acceptor photobleaching was calculated by correcting the postbleach donor image for imaging bleaching and subtracting, from the photobleach area of this image, the photoconversion fraction of the prebleach acceptor image (1.12%). This is followed by subtraction of the prebleach donor image, and the resulting gain in donor image is displayed in pseudocolor (color scale). The ROIs inside the bleach area were used to calculate the FRET values explained and displayed in Fig. 3.

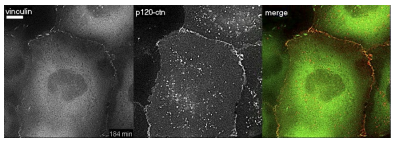

Video 1. **Vinculin is recruited to p120-catenin–containing cell–cell junctions upon HGF stimulation.** Cells stably expressing GFP-vinculin were transiently transfected with mCherry–p120-catenin, grown for 20 h in a collagen-coated glass-bottom chamber, transferred to an epifluorescence microscope, and imaged at 8 min/frame. At 32 min after the start of imaging, 5 ng/ml HGF was added to the medium. At each time point, four consecutive images at increasing z steps were taken (200-nm step size). These images were deconvoluted using Huygens software (Scientific Volume Imaging), and the plane displayed is focused ∼400 nm above the basal cell surface. Bar, 5 µm.

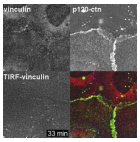

Video 2. **Vinculin presence at FAs as well as suprabasal cell–cell junctions depends on actomyosin contractility.** Cells stably expressing GFP-vinculin and transiently expressing mCherry–p120-catenin were grown for 20 h in a collagen-coated glass-bottom chamber, stimulated with HGF for 1 h, transferred to an epifluorescence microscope, and imaged at 90 s/frame. At 15 min after the start of imaging, 3 µM ML-7 and 10 µM Y27632 were added to inhibit all actomyosin contractility. 10 min after their addition, the inhibitors were removed, and fresh medium was added. At each time point, widefield images and TIRF images were taken (using a steep angle; ∼100 nm was illuminated).

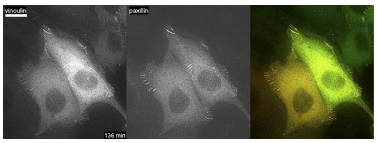

Video 3. **Vinculin is present in paxillin-marked FA and appears in paxillin-devoid cell–cell adhesions upon HGF stimulation.** Cells stably expressing GFP-vinculin were transiently transfected with mCherry-paxillin, grown for 20 h in a collagen-coated glass-bottom chamber, transferred to an epifluorescence microscope, and imaged at 8 min/frame. At 32 min after the start of imaging, 5 ng/ml HGF was added to the medium. At each time point, three consecutive images at increasing z steps were taken (200-nm step size). These images were deconvoluted using Huygens software (Scientific Volume Imaging), and the plane displayed is focused ∼400 nm above the basal cell surface. Bar, 10 µm.

Vinculin-dependent cadherin mechanosensing regulates efficient epithelial barrier formation

Vinculin-dependent Cadherin mechanosensing regulates efficient epithelial barrier formation

Floor Twiss[1], Quint le Duc[1], Suzanne van der Horst[1], Hamid Tabdili[2,3], Gerard van der Krogt[1], Ning Wang[4], Holger Rehmann[5], Stephan Huveneers[1,*], Deborah E. Leckband[2,3] and Johan de Rooij[1,‡]

[1]Hubrecht Institute for Developmental Biology and Stem Cell Research and University Medical Centre Utrecht, PO Box 85164, 3508 AD Utrecht, The Netherlands
[2]Department for Chemical and Biomolecular Engineering, University of Illinois at Urbana-Champaign, Champaign, IL 61801, USA
[3]Department of Chemistry, University of Illinois at Urbana-Champaign, Champaign, IL 61801, USA
[4]Department of Mechanical Science and Engineering, University of Illinois at Urbana-Champaign, Champaign, IL 61801, USA
[5]Department of Molecular Cancer Research, Centre of Biomedical Genetics and Cancer Genomics Centre, University Medical Centre Utrecht, 3584 CG Utrecht, The Netherlands

*Present address: Sanquin Research, Department of Molecular Cell Biology and University of Amsterdam, Swammerdam Institute for Life Sciences, 1098 XH Amsterdam, The Netherlands
‡Author for correspondence (j.derooij@hubrecht.eu)

Biology Open 1, 1128–1140
doi: 10.1242/bio.20122428
Received 2nd July 2012
Accepted 13th August 2012

Summary

Proper regulation of the formation and stabilization of epithelial cell–cell adhesion is crucial in embryonic morphogenesis and tissue repair processes. Defects in this process lead to organ malformation and defective epithelial barrier function. A combination of chemical and mechanical cues is used by cells to drive this process. We have investigated the role of the actomyosin cytoskeleton and its connection to cell–cell junction complexes in the formation of an epithelial barrier in MDCK cells. We find that the E-cadherin complex is sufficient to mediate a functional link between cell–cell contacts and the actomyosin cytoskeleton. This link involves the actin binding capacity of α-catenin and the recruitment of the mechanosensitive protein Vinculin to tensile, punctate cell–cell junctions that connect to radial F-actin bundles, which we name Focal Adherens Junctions (FAJ). When cell–cell adhesions mature, these FAJs disappear and linear junctions are formed that do not contain Vinculin. The rapid phase of barrier establishment (as measured by Trans Epithelial Electrical Resistance (TER)) correlates with the presence of FAJs. Moreover, the rate of barrier establishment is delayed when actomyosin contraction is blocked or when Vinculin recruitment to the Cadherin complex is prevented. Enhanced presence of Vinculin increases the rate of barrier formation. We conclude that E-cadherin-based FAJs connect forming cell–cell adhesions to the contractile actomyosin cytoskeleton. These specialized junctions are sites of Cadherin mechanosensing, which, through the recruitment of Vinculin, is a driving force in epithelial barrier formation.

Key words: E-cadherin, Vinculin, Actomyosin, Mechanotransduction, Junction formation, Cell–cell adhesion

Introduction

Multicellular epithelial tissues line all cavities in an organism and they serve as a selective permeability barrier. In polarized epithelial cells, junctions are organized in an adhesion belt in which they are connected to the actomyosin cytoskeleton. Tight Junctions (TJs) are located most apically, and serve as a selective barrier that limits water, solutes and immune cells from passing between cells. The tightness of the barrier is dependent on the expression of different combinations of transmembrane proteins in the TJs, such as Claudins, Occludin, and Junctional Adhesion Molecule (JAM) (Turksen and Troy, 2004). Adherens Junctions (AJs) and Nectin-based Junctions (NJs) are also part of the adhesion belt, and are located immediately below the TJs. AJs and NJs are also found outside the adhesion belt in both epithelial and non-epithelial cells, in a more discontinuous pattern (Niessen, 2007).

During tissues remodeling, the barrier function must remain intact and is therefore tightly regulated. The junctional complexes that connect to the actomyosin cytoskeleton (AJs, NJs, and TJs) are the targets of many signaling pathways that regulate tissue remodeling. One of the most used model systems for junction remodeling is the formation of epithelial cell–cell junctions in tissue culture. This entails a complex interplay between actomyosin and junctional complexes. As lamellipodia of two cells come into contact with each other, small adhesive puncta are formed, with thin actin bundles extending from the circumferential actin belt to these puncta. As the contact extends, more adhesive puncta arise, which merge and are still connected to radial actin bundles. These actin bundles are proposed to stabilize the adhesive puncta. Finally, the puncta mature into cell–cell junctions, and actin is remodeled back into the circumferential belt (Adams and Nelson, 1998; Meng and Takeichi, 2009). Although mainly studied in 2D cell culture models, it is likely that junction formation *in vivo* (for instance during dorsal closure, angiogenesis, immune responses, wound healing and tumorigenesis) is governed by the same basic principles (Cavey and Lecuit, 2009).

Engagement of cell–cell junction receptors activates several signaling pathways that regulate actin conformation. For instance, nectin–nectin engagement results in activation of c-Src, Rap1, Cdc42, and Rac small GTPases (Ogita et al., 2010; Takai et al., 2008). Engagement of Cadherin adhesion induces Myosin II activation, which in turn promotes the accumulation of Cadherins at sites of cell–cell adhesion (Shewan et al., 2005). Cadherin-induced activation of PI3-kinase and Rac1 leads to membrane and actin dynamics to further stimulate junction formation along the membrane (Noren et al., 2001). Furthermore, Cadherin adhesion leads to recruitment and activation of several actin regulators such as the Arp2/3 complex (Kovacs et al., 2002), cortactin (Helwani et al., 2004), N-WASP (Kovacs et al., 2011), formin (Kobielak et al., 2004) and Ena/VASP (Vasioukhin et al., 2000). Thus, much is known about the regulation of actin dynamics downstream of cell–cell junction formation. Conversely, however, the conformation of the actin cytoskeleton also influences cell–cell adhesion complexes. For example, perturbing actomyosin contractility strongly affects cell–cell adhesion formation and maturation (Angres et al., 1996; de Rooij et al., 2005; Gloushankova et al., 1998; Lambert et al., 2007; Miyake et al., 2006; Shewan et al., 2005), indicating that actomyosin based forces play a promoting or stabilizing role in this process. Exactly how physical forces from contractile actomyosin are transmitted to cell–cell junctions and by which mechanisms this influences their formation is not well understood.

Recently, we showed by magnetic twisting cytometry (MTC) that the E-cadherin complex is a mechanosensor that directly responds to forces exerted on it and that the actin-binding protein Vinculin is important in this process (le Duc et al., 2010). Concomitantly, it was shown that in apical Adherens Junctions force-dependent stretching of the E-cadherin-actin linker α-catenin results in recruitment of Vinculin to these junctions (Yonemura et al., 2010).

During junction formation it is not clear which of the different adhesion complexes forms a functional link with actomyosin. Early experiments showed that the E-cadherin complex is a master regulator of cell–cell adhesion, because the formation of all junctions can be inhibited by E-cadherin-blocking antibodies (Gumbiner et al., 1988). However, Nectins are also crucial for the formation of all other cell–cell junctions (Honda et al., 2003; Ikeda et al., 1999; Sakisaka et al., 2007). As TJ complexes form only after Nectin and Cadherin junctions have formed it is not likely that these complexes are crucial in the actin-dependent initial formation of cell–cell adhesion. Nevertheless, the TJ complex actin linker proteins Zonula Occludens-1 (ZO-1) and ZO-2 have been found in early junctions (Ooshio et al., 2010) preceding the formation of apical TJs (Fanning and Anderson, 2009).

For Cadherin–actin linkage, α-catenin is crucial, but additional proteins, including EPLIN and Vinculin could be needed as well (Abe and Takeichi, 2008; Watabe-Uchida et al., 1998). The latter two seem to be involved in specific phases of junction dynamics as their presence in junctions is not ubiquitous (le Duc et al., 2010; Miyake et al., 2006; Taguchi et al., 2011). For Nectin–actin linkage, Afadin is crucial (Takahashi et al., 1999) and for TJs the ZO proteins are vital (Fanning et al., 1998; Itoh et al., 1999). Complicating the understanding of early junction formation, Afadin, α-catenin and ZO proteins can interact among each other and a number of proteins, including α-actinin, LMO7 (Ooshio et al., 2004), ADIP (Asada et al., 2003), and ponsin (Ikeda et al., 1999), can make additional links by binding two of these proteins simultaneously. Because these actin-connected cell–cell junction complexes are not well separated in space during junction formation and because of the complicated interaction profile between their intracellular components it is not clear whether they can be functionally separated during junction formation.

In this study, we investigated the regulatory role of actomyosin during epithelial barrier formation in calcium switch assays and we investigated which cell–cell junction complexes mediate the functional link to actomyosin. We find that actomyosin-based force promotes epithelial barrier formation independent of the structural supportive role of F-actin. This force-dependent effect is mediated by α-catenin and Vinculin in the Cadherin complex specifically. Radial actin-contacted Focal Adherens Junctions (FAJ) are formed rapidly upon calcium, in which Vinculin responds to force on the E-cadherin complex to induce force-dependent reinforcement of cell–cell adhesion, resulting in accelerated barrier formation.

Results

E-cadherin and F-actin are inter-dependently remodeled upon calcium switch

To pinpoint the proteins most likely involved in connecting cell–cell junctions to F-actin in junction formation, we subjected MDCK cells to a calcium switch assay to induce the formation of Cadherin based adhesions. We fixed the cells at different time-points and performed immunofluoresence (IF) staining for key proteins from AJs, TJs and NJs including the main actin-binding proteins in these complexes. In MDCK cells in low calcium conditions (20 μM), no members of the Cadherin complex are present at cell–cell contact sites, and the actin cytoskeleton is present in bundles that run parallel to the cell–cell contacts (Fig. 1A). Surprisingly, in this experimental setup, Tight Junction- and Nectin Junction complexes were visible at many cell–cell contact sites in low calcium as shown by the presence of Occludin (TJs) and Afadin (NJs) (Fig. 1A). We considered the possibility that the low concentration of FBS used in this setup induced unusual responses. Nevertheless, increasing the serum content to 5%, which has been used in several previous calcium switch studies, did not affect the localization of either Afadin, Occludin, E-cadherin or actin (supplementary material Fig. S1). After the calcium switch (by adding 2 mM Calcium Chloride) Cadherin complex members appeared in small structures that orientated perpendicular to the plane of cell–cell contact. The actin cytoskeleton also remodeled significantly as the parallel bundles disappeared and radial bundles now extended to the cell–cell contact zone terminating in the Cadherin positive structures (Fig. 1B). This confirms earlier studies showing that the formation of Cadherin-dependent cell–cell junctions is a driving force in the remodeling of actin through the recruitment of actin regulating proteins like VASP, formins, cortactin, ARP2/3 and α-actinin (DeMali and Burridge, 2003; Helwani et al., 2004; Kobielak et al., 2004; Ooshio et al., 2004; Tang and Brieher, 2012; Vasioukhin et al., 2000). Conversely, the altered cytoskeleton appears to have profound effects on the morphology of cell–cell junctions in general, because also the pre-assembled NJ and TJ complexes re-orientated into perpendicular junctions upon calcium (Fig. 1B).

As the junctions matured, the AJ, TJ and NJ complexes lost their perpendicular orientation and changed into a linear junction, concomitant with a re-organization of the actin cytoskeleton to

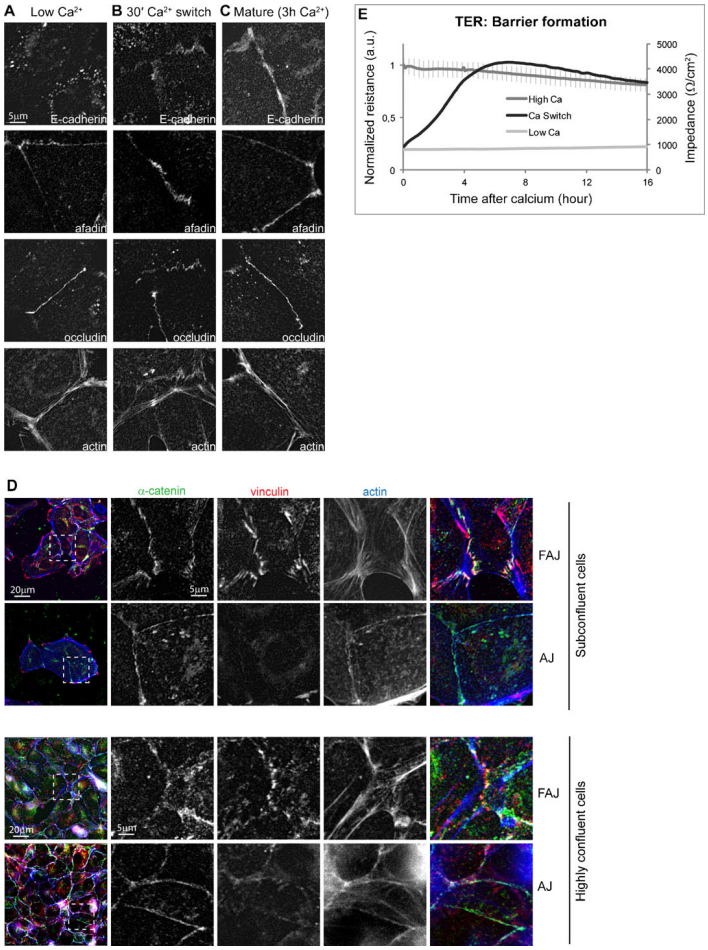

Fig. 1. E-cadherin and actin are inter-dependently remodeled upon calcium switch. (**A–C**) IF images of AJ (E-cadherin), NJ (Afadin), TJ (Occludin) markers and actin (from the same cells as the Occludin staining) during a calcium switch in MDCK cells. (**D**) IF images of FAJs and mature AJs after a calcium switch (30 min. for FAJs, 3 hours for AJs) stained for α-catenin (green) F-actin (blue) and Vinculin (red) in subconfluent and highly confluent conditions. (**E**) TER measurement of MDCK cells seeded in low calcium medium (light grey line), normal calcium medium (dark grey line) or during a calcium switch (black line). Like in all further TER experiments in this study, values normalized to the maximum value of the control sample are shown on the left Y-axis. Actual values in Ohm/cm^2 are shown on the right Y-axis for comparison. Error bars indicate standard error, $n>3$. Scale bar = 5 µm or 20 µm as indicated.

form bundles running parallel to them (Fig. 1C). The actin-driven regulation of junction morphology in the early phases after calcium strongly indicates that a physical link exists between the newly formed radial actin bundles and cell–cell junction complexes. Indeed, there is visible overlap between the radial actin bundles and adhesion proteins (Fig. 1B,D) and the actin binding and junctional protein Vinculin is present in the perpendicular nascent adhesions (Fig. 1D). These structures are very much like the Focal Adherens Junctions (FAJs) we characterized recently in endothelial cells (Huveneers et al., 2012). In that paper, we proposed the name FAJ to emphasize their distinction from stable AJs and their analogy to Focal

Adhesions; typical punctate morphology, connection to radial actin bundles and dependence on cytoskeletal tension. Structures like these have been described under various names in literature (Adams et al., 1998); adhesions zippers described during junction formation in sparse epithelial cells (Vasioukhin et al., 2000); spot-like Adherens Junctions in epithelial cells and fibroblasts (Yonemura et al., 1995); punctate Adherens Junctions in epithelial cells in wound healing (Taguchi et al., 2011). It is very likely that all of these structures are very similar in nature to the FAJs we describe here and in HUVECs.

The fact that TJ and NJ complexes did assemble at cell–cell contacts in low calcium led us to determine Trans Epithelial Electrical Resistance (TER), as a measure for epithelial barrier function of the MDCK monolayer. A confluent monolayer in low calcium showed very low barrier compared to a confluent monolayer grown in normal calcium conditions (Fig. 1E), indicating that although the TJ protein Occludin is present at sites of cell–cell contact (Fig. 1A), the monolayer has no barrier function. After the addition of calcium, a barrier function was gradually established (Fig. 1E). The phase of most rapid barrier increase (between 1 and 4 hours post calcium) coincided remarkably with the phase in which FAJs are observed. The number of FAJs after 4 hours of calcium is very low, whereas barrier function is then maximal. We confirmed that also in the highly confluent conditions that cells are seeded in for TER measurements, FAJs are formed in the first few hours after calcium switching that contain high levels of Vinculin, while Vinculin levels became very low when junctions matured into linear Adherens Junctions (Fig. 1D). Also junctional localization of Occludin and Afadin under low calcium conditions was clearly observed in these conditions (supplementary material Fig. S2). Finally, raising the serum concentration to 5%, did not strongly affect the speed of barrier formation (supplementary material Fig. S3).

In conclusion, upon the induction of E-cadherin adhesion by means of a calcium switch, the actin cytoskeleton is remodeled to form radial bundles, which in turn determine the organization of cell–cell junction complexes into perpendicular orientated FAJs. In this transient phase of active actin and junction remodeling the fastest increase in epithelial barrier function takes place.

Coupling of F-actin to cell–cell junctions requires α-catenin and is necessary for the establishment of the barrier

To understand the requirement of an intact actin cytoskeleton for both the formation and maintenance of the barrier, we treated MDCK cells with Cytochalasin D (CytoD), to induce the breakdown of actin filaments. This resulted in a failure to form a barrier after a calcium switch (Fig. 2A, dashed green line), or in a disruption of the barrier function of a pre-existing monolayer (Fig. 2A, dark green line). As expected from its crucial role in E-cadherin adhesion, MDCK cells with a constitutive α-catenin knockdown to levels below 10% (supplementary material Fig. S4) failed to form cell–cell junctions and consequently did not build any barrier function upon calcium (Fig. 2D, red line). We used this α-catenin-depleted MDCK cell line to further investigate the domains and interactions of α-catenin that are needed for efficient epithelial barrier formation. First of all, we tested an α-catenin mutant that lacks the C-terminal α-helix that is essential for F-actin binding (α-catenin-1-848) (Pokutta et al., 2002) (Fig. 2B). Contrary to rescues with α-catenin WT, this mutant, expressed at relatively high levels (Fig. 2C), could not

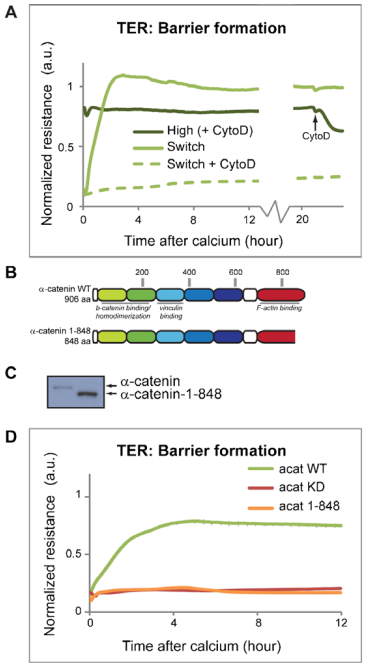

Fig. 2. Coupling of actin to cell–cell junctions requires α-catenin and is necessary for the establishment of the barrier. (**A**) Effect of Cytochalasin D on barrier formation in MDCK cells. CytoD was added during a calcium switch (dashed green line) or to a pre-existing monolayer (dark green line). Error bars indicate standard error, $n>3$. (**B**) Schematic representation of α-catenin-WT construct and α-catenin-1-848 mutant lacking the C-terminal F-actin binding site. (**C**) Expression levels of α-catenin-WT or α-catenin-1-848 in α-catenin depleted MDCK cells assessed by Western Blotting with α-catenin specific antibodies. (**D**) TER measurement in α-catenin depleted MDCK cells (red line), or the same cells rescued with α-catenin-WT (green line) or α-catenin-1-848 (orange line). Error bars indicate standard error, $n>3$.

rescue the formation of the barrier even under the high density plating conditions of the TER measurement (Fig. 2D, orange line). These results show that both intact F-actin and the actin binding region of α-catenin are needed to support epithelial barrier formation.

Coupling of F-actin to the Cadherin complex is sufficient for the induction of cell–cell adhesion

Since α-catenin can bind to the NJ complex through Afadin (Takai et al., 2008), is a key component of the E-cadherin complex in AJs, and can associate with the TJ complex via ZO-1, it was not *a priori* clear which of these complexes recruited α-catenin for a functional link to actin in barrier formation. To further investigate this, we performed IF on MDCKs fixed during a calcium switch. The images and linescans in Fig. 3A show that both α-catenin and Vinculin are in perpendicular structures that

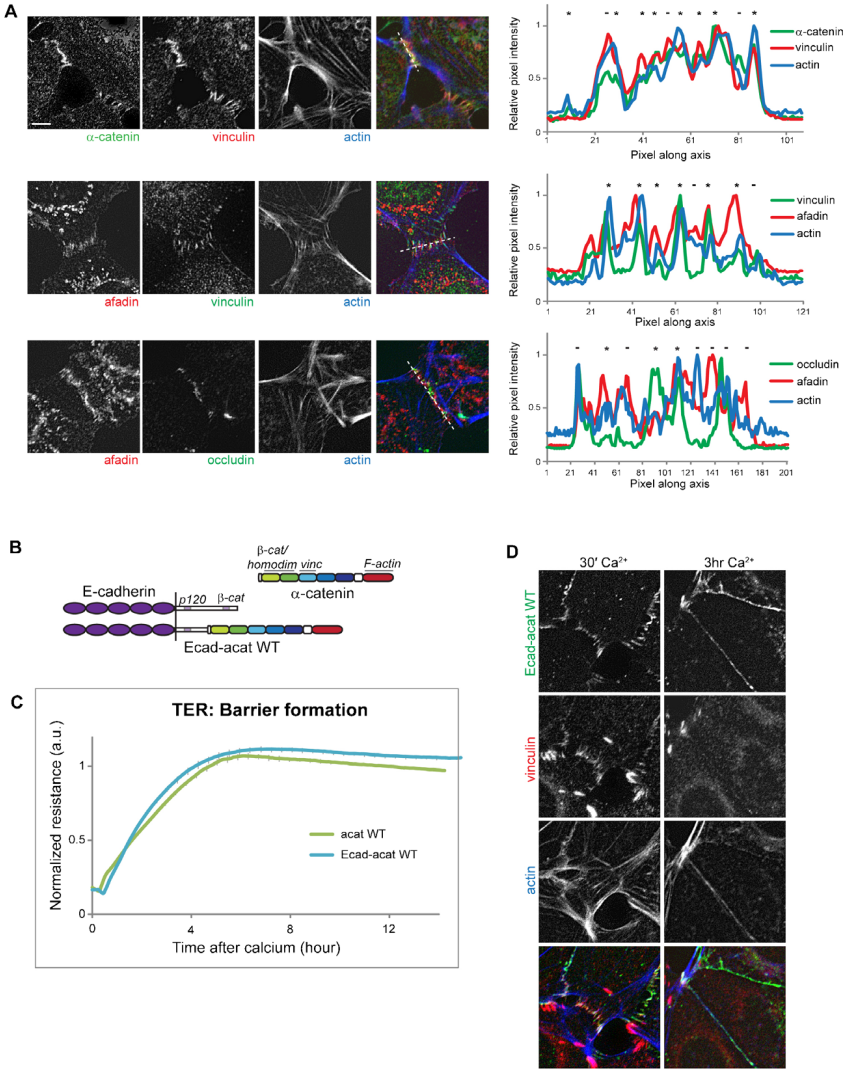

Fig. 3. Coupling of actin to the E-cadherin complex is sufficient for induction of cell–cell adhesion. (**A**) IF images of FAJs and radial actin bundles during a calcium switch. Top row: α-catenin (green) and Vinculin (red) show substantial overlap with radial actin bundles (blue). Middle row: Afadin (red) and Vinculin (green) also show overlap with radial actin bundles (blue). Bottom row: Afadin (red) shows more overlap with radial actin (blue) than Occludin (green). Right panels: linescan through the remodeling junctions showing overlap between α-catenin, Afadin, Vinculin, Occludin and radial actin bundles. (**B**) Schematic representation of the E-cadherin-α-catenin fusion construct used. E-cadherin is C-terminally truncated so that it lacks the β-catenin binding site, and fused to full length α-catenin. (**C**) TER measurement of α-catenin-depleted MDCK cells rescued with either α-catenin-WT (green) or Ecad-αcat (turquoise). (**D**) IF images of FAJs in α-catenin-depleted MDCK cells rescued with Ecad-αcat (green), containing vinculin (red) and connecting to radial actin bundles (blue). Scale bar = 5 µm.

often also overlap with radial actin bundles (Fig. 3A, top row). Similar to this, the main actin linker of NJs, Afadin, also showed a perpendicular staining that overlapped with Vinculin and was often localized at the terminus of radial actin bundles (Fig. 3A, middle row). Although TJ proteins like Occludin and the actin linker ZO-1 also remodeled during a calcium switch, their localization showed less overlap with Afadin or the radial actin bundles (Fig. 3A, bottom row). Because of these data, E-cadherin and Nectin complexes are the primary candidates for functional linkage to the actin cytoskeleton during junction formation.

To further decipher the importance of AJs or NJs in α-catenin-dependent F-actin coupling during junction formation, we expressed a fusion between E-cadherin and α-catenin (Fig. 3B, Ecad-αcat WT) in the α-catenin negative MDCK cells to bypass the possibility of α-catenin associating with the NJ complex. Such fusions have been used before and were shown fully functional in rescuing (D)E-cadherin negative cell lines and epithelial cell clones in organisms (*Drosophila*) (Gottardi et al., 2001; Pacquelet and Rørth, 2005). The fusion used here contained the extracellular and most of the intracellular domains of E-cadherin, except for the β-catenin binding domain. This domain was replaced by full length α-catenin. When α-catenin negative MDCK cells were rescued with this Ecad-αcat fusion, their ability to form junctions was restored to be very similar to that of WT MDCK cells: During early stages of junction formation, Vinculin-containing FAJs that were formed connected to radial actin bundles (Fig. 3D) and when the junctions matured, actin remodeled into the parallel conformation and Vinculin was mostly absent (Fig. 3D). The formation of the barrier function was also restored to be very similar to that in cells rescued with α-catenin-WT (Fig. 3C). Since there was no detectable endogenous α-catenin available in these cells to bind to NJ or TJ complexes, this demonstrates that recruitment of α-catenin to the E-cadherin complex is sufficient for a functional link between actin and cell–cell junctions during epithelial barrier formation. The transient participation of Vinculin in junction formation is also fully restored by the E-cadherin-α-catenin fusion. This suggests that indeed Vinculin recruitment and function at early cell–cell junctions depends on the Cadherin complex specifically.

Myosin II activity promotes epithelial barrier formation

Previously we have shown that FAJs are linked to radial actin bundles and are under actomyosin-dependent tension during junction remodeling in endothelial cells (Huveneers et al., 2012). To test whether contractile cytoskeletal force is important in the process of junction formation, we performed the calcium switch in the presence of the myosin inhibitor blebbistatin. As shown in Fig. 4 (dashed line), the establishment of the barrier is strongly delayed, but the final resistance reached is equal between control and blebbistatin treated samples. This shows that the rate of epithelial barrier formation is enhanced by actomyosin contractility and suggests that besides a structural role in the maintenance of cell–cell adhesions, the actomyosin cytoskeleton also has an instructive function that regulates the efficiency of cell–cell junction formation. It is likely that this response to force is generated at the FAJs where contractile radial actin bundles terminate and where the presence of Vinculin indeed indicates that tensile forces apply (le Duc et al., 2010; Miyake et al., 2006; Yonemura et al., 2010).

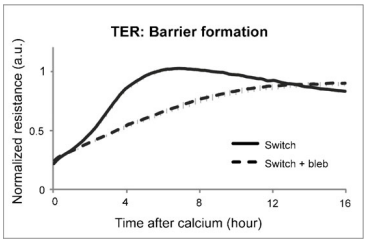

Fig. 4. Actomyosin contractility promotes barrier formation. TER measurement of MDCK cells in the presence or absence of 50 μM blebbistatin. Error bars indicate standard error, $n>3$.

Loss of Vinculin from FAJs does not disturb their physical connection to actomyosin

Vinculin is present at FAJs that are under tension, but Vinculin is also involved in overall F-actin organization and myosin-based contraction (Mierke et al., 2008), both of which likely depend on its role in integrin-based Focal Adhesions (FAs) (Puklin-Faucher and Sheetz, 2009). To specifically perturb Vinculin's role at FAJs, we used the α-catenin-ΔVBS mutant recently developed in our lab. In this construct, the Vinculin binding site (VBS) in α-catenin is replaced with the homologous domain from Vinculin (domain 3A), the closest homolog of α-catenin (Fig. 5A). This leaves α-catenin's structural conformation intact, but prevents Vinculin recruitment to tensile FAJs (Huveneers et al., 2012). To specifically enhance Vinculin's function at cell–cell junctions, we used a truncated version of α-catenin (Fig. 5A, α-catenin-1-402) that constitutively binds and recruits Vinculin (Yonemura et al., 2010).

First, to biochemically characterize the interactions between Vinculin and the α-catenin mutants in more detail, they were co-expressed in and immunoprecipitated (IP) from Cos7 cells. As expected from previous work (Johnson and Craig, 1995) full length Vinculin did not co-IP with any of the α-catenin-GFP constructs (Fig. 5B, lanes 12–15), whereas a truncated mutant that lacks the tail domain (Vinculin 1-881) showed strong α-catenin binding (Fig. 5B, lanes 17, 19). Importantly, all α-catenin-ΔVBS constructs showed a strong reduction in Vinculin 1-881 binding (Fig. 5B, lanes 18, 20). Thus indeed replacement of the Vinculin binding domain in α-catenin strongly perturbs its interaction with Vinculin. Interestingly, whereas α-catenin in cell–cell junctions clearly requires an activation step involving contractile actomyosin before it can recruit Vinculin (Yonemura et al., 2010), in these cell lysates, over-expressed full length α-catenin pulls down Vinculin with similar efficiency as the α-catenin-1-402 mutant that constitutively recruits Vinculin to cell–cell junctions. This suggests that at cell–cell junctions a specifically folded α-catenin is retained or that additional proteins interacting with α-catenin at the junction prevent Vinculin binding. Moreover, in these lysates it is clear that Vinculin also requires an activation step for its interaction with α-catenin. To investigate if β-catenin could be involved in such inactivation of α-catenin or activation of Vinculin, we co-expressed also β-catenin-mCherry in these cells and performed the same IP for α-catenin-GFP. A ternary complex containing α-catenin, β-catenin and Vinculin 1-881 was readily precipitated

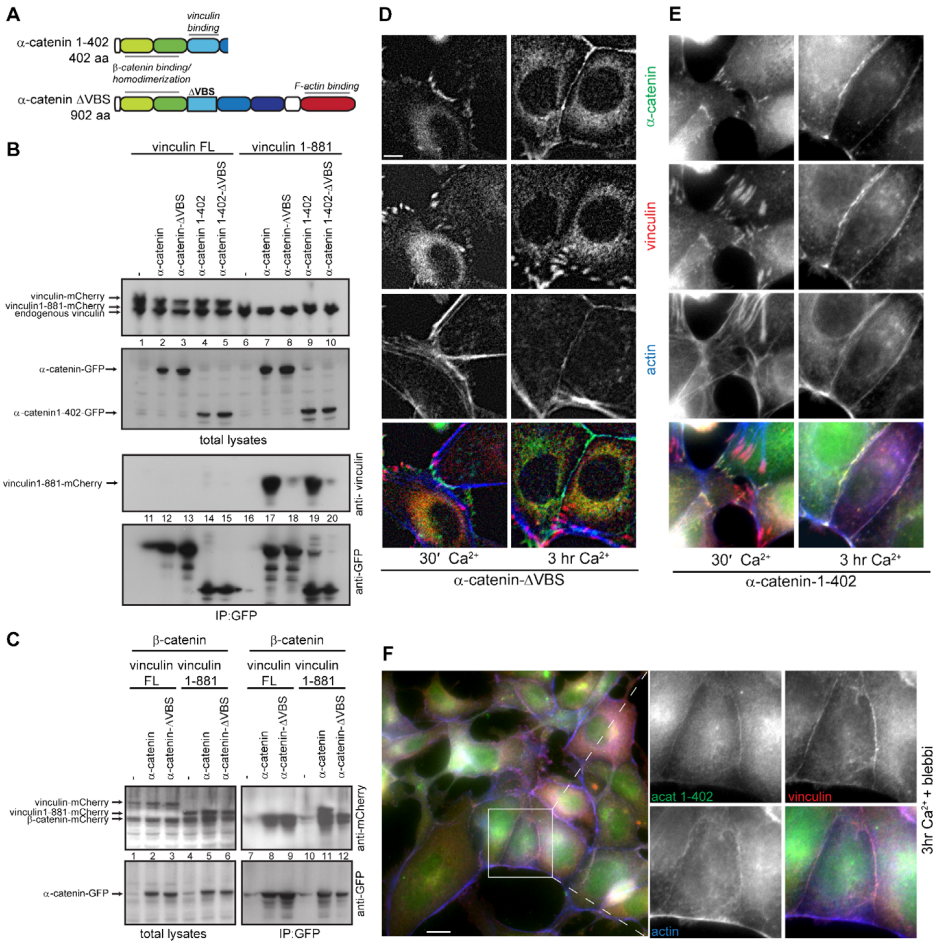

Fig. 5. α-catenin mutants that abolish or enhance Vinculin recruitment to cell–cell junctions. (**A**) Schematic representation of the α-catenin-1-402 truncation mutant and α-catenin-ΔVBS mutant in which the vinculin binding site (VBS) from α-catenin is replaced by the homologous domain from vinculin. (**B**,**C**) Western Blot results of IP of the indicated GFP-α-catenin constructs from MDCK cells and coprecipitation of mCherry-vinculin or mCherry-vinculin 1-881 in the absence (B) or presence of co-expressed mCherry-β-catenin (C). (**D**,**E**) IF images of FAJs and mature junctions that are formed during a calcium switch in α-catenin negative MDCK cells rescued with α-catenin-ΔVBS or α-catenin-1-402 (green), showing absence (D) or constitutive presence of Vinculin (red, E). (**F**) IF images show vinculin (red) recruitment to α-catenin-1-402 (green) is tension-independent, it still occurs in the presence of 50 µM blebbistatin. Scale bars: (D) 5 µm; (F) 10 µm.

(Fig. 5C, lane 11), while a complex between full length Vinculin and α-catenin did still not form in the presence of β-catenin (Fig. 5C, lane 8). This indicates that β-catenin is not directly regulating the interaction between α-catenin and Vinculin.

Next, to assess their capacity to mediate junction formation, we expressed these α-catenin mutants in α-catenin negative MDCK cells. As shown in Fig. 5D, in a calcium switch assay, FAJs are still formed in α-catenin-ΔVBS cells: α-catenin-ΔVBS is present in typical perpendicular structures, and F-actin staining shows radial bundles that terminate at these α-catenin structures. Nevertheless, Vinculin is completely absent from these junctions. In these α-catenin-ΔVBS-rescued cells, junctions do mature and

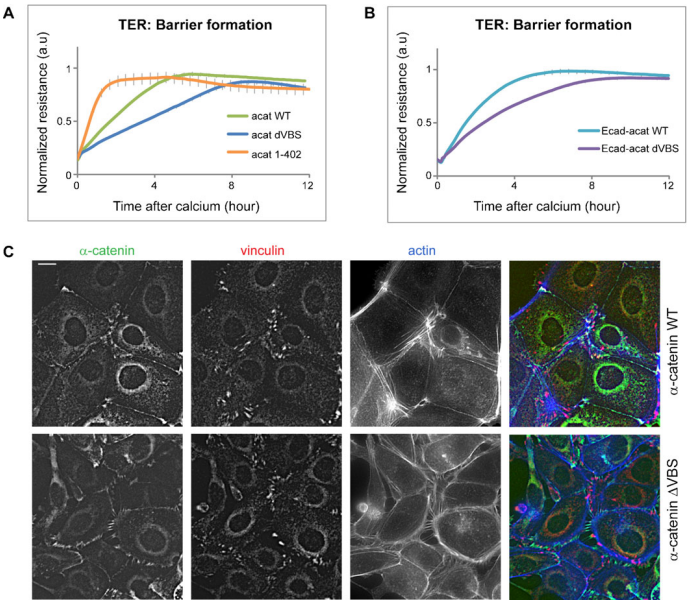

Fig. 7. Vinculin recruitment enhances the efficiency of barrier formation. (**A**) TER measurements after a calcium switch in α-catenin-depleted MDCK cells rescued with the indicated constructs. Error bars indicate standard error, $n>3$. (**B**) TER measurements after a calcium switch in α-catenin-depleted MDCK cells rescued with Ecad-αcat fusions that contain α-catenin-WT or α-catenin-ΔVBS show that mechanosensing at the Cadherin complex is sufficient for force-enhanced barrier formation. Error bars indicate standard error, $n>3$. (**C**) IF images of α-catenin-depleted MDCK cells, rescued with α-catenin-WT or α-catenin-ΔVBS, fixed at 3 hours after calcium showing the delayed maturation into AJs when vinculin cannot be recruited. Scale bar = 10 µm.

recruitment by α-catenin-1-402 leads to enhanced barrier formation suggests that Vinculin recruitment invokes downstream biochemical processes that enhance barrier formation independent of force.

Discussion

In this study we have shown that actomyosin contractility regulates efficient barrier formation through Cadherin dependent Vinculin recruitment. Upon a calcium switch, Tight Junction-, Nectin- and E-cadherin complexes as well as the actomyosin cytoskeleton itself all participate in irregular or punctate cell–cell junctions. Nevertheless, functional, α-catenin-dependent coupling of actomyosin to the E-cadherin complex specifically is sufficient for normal barrier formation. Actomyosin connects to the E-cadherin complex in FAJs that are characterized by the presence of Vinculin. Vinculin is not essential for FAJ formation, their actin linkage or final barrier formation, but mediates the force-dependent reinforcement that determines the rate of epithelial sealing. Constitutive junctional Vinculin recruitment, uncoupled from cytoskeletal pulling forces, enhances epithelial barrier formation independent of cytoskeletal force. Thus pulling forces from contractile actomyosin on the Cadherin complex directly, are a driving factor in epithelial barrier formation, through Vinculin dependent Cadherin mechanotransduction.

The connection between E-cadherin and actin

The simple model in which E-cadherin is connected to F-actin via β- and α-catenin was challenged by the Nelson and Weis labs when they showed that α-catenin cannot bind to F-actin and β-catenin simultaneously (Drees et al., 2005). Nevertheless, α-catenin is required for tight epithelial cell–cell adhesion and this depends on the domain that is essential for its F-actin binding activity (Fig. 2) (Pokutta et al., 2002; Yonemura et al., 2010). Using an E-cadherin-α-catenin fusion, we showed that the interaction of α-catenin with the Cadherin complex is sufficient for a functional link between early cell–cell junctions and contractile actomyosin that sustains apparently normal barrier formation (Fig. 3). Although intermediates between α-catenin and F-actin cannot be excluded, the most obvious candidates EPLIN (Taguchi et al., 2011) and Vinculin (Fig. 5) can be absent from FAJs without perturbing their connection to F-actin, so they are clearly not obligatory. The most straightforward hypothesis to explain all current observations is that a conformational activation of α-catenin occurs in mammalian cells that allows simultaneous binding to the Cadherin complex and actomyosin, which cannot be recapitulated in lysates with mammalian expressed α-catenin proteins.

Vinculin recruitment to cell–cell adhesions

Vinculin has been shown to be present in punctate basolateral cell–cell junctions, which we now call FAJs, in keratinocytes (Vasioukhin et al., 2000), MCF10 cells (Peng et al., 2010) and MDCK cells (le Duc et al., 2010; Miyake et al., 2006; Taguchi et al., 2011). In other studies in tissues (Geiger et al., 1980), MCF7 (Maddugoda et al., 2007), DLD-1 (Taguchi et al., 2011; Yonemura et al., 2010) and MDCK cells (Miyake et al., 2006; Yonemura et al., 2010), Vinculin has been found in the apical zonula adherens (ZA). Several pieces of evidence show that

Vinculin is needed for the structural integrity of this apical ZA (Maddugoda et al., 2007; Watabe-Uchida et al., 1998). In both early junctions and mature apical junctions, the presence of Vinculin depends on myosin activity (le Duc et al., 2010; Miyake et al., 2006; Yonemura et al., 2010). In this study we have only investigated the role of Vinculin in early cell–cell junctions, not in ZA formation. Within the 24 hours after calcium addition that our experiments maximally lasted, there is no clear apical ZA formed in MDCK cells and after the initial phase, Vinculin is mostly absent from cell–cell junctions (Fig. 1). This may reflect reduced tension on these junctions compared to early junctions and ZA junctions, but this has not been experimentally addressed so far. Notably, in DLD1-R2/7 cells rescued with α-catenin, Vinculin is recruited in a myosin dependent manner to the apical-most ZA regions of these cells only, even though E-cadherin and α-catenin are present along the basolateral membrane as well. Force-independent binding of Vinculin to α-catenin-1-402 occurs along the entire lateral membrane (Yonemura et al., 2010). Clearly, the magnitude and direction of the mechanical stresses at different cell–cell junction areas remain to be established to fully understand how junctions are regulated by force.

The role of Vinculin in early junctions remained unclear so far, and there is also conflicting evidence as to which protein recruits it to the Cadherin complexes. Both β-catenin and α-catenin have binding sites for Vinculin and it was shown in MDA_MB-468 cells, lacking α-catenin, that Vinculin could still associate with the Cadherin complex, and this is mediated through β-catenin. This study suggested that Vinculin may be able to replace α-catenin in cell–cell adhesion (Hazan et al., 1997). Vinculin recruitment via β-catenin was also shown to regulate cell surface E-cadherin expression in MCF10a cells (Peng et al., 2010). On the other hand Weiss and colleagues demonstrated that Vinculin can be recruited to the junctional complex through α-catenin (Weiss et al., 1998). Vinculin recruitment via either α- or β-catenin may have different functions in different cell types or at certain stages of junction formation. In MDCKs, we find no evidence for the hypothesis that Vinculin can be recruited to junctions by β-catenin to perform α-catenin-independent functions: KD of α-catenin in MDCK was not rescued by recruitment of Vinculin to junctions. In our α-catenin-ΔVBS mutant, we do not see any Vinculin present in any of the junction types. Furthermore, the E-cadherin-α-catenin fusion protein shows no obvious defects despite the fact that it lacks the β-catenin binding site. Apparently, how Vinculin is recruited to cell–cell junctions is dependent on the cell type and state of the junctions, and more details need to be known for all observations to be reconciled. Speculatively, one could envision a cell-type specific situation in which junction maturation is prevented and all Cadherin-based adhesions remain in the tensile FAJ stage. Loss of Vinculin could render these junctions less stable and result in their overall reduction and as a consequence a reduction of E-cadherin retained at the plasma membrane. We conclude from our present work that the presence and function of Vinculin during cell–cell junction formation in MDCK cells mainly depends on myosin activity and α-catenin connected to the E-cadherin complex.

Regulation of the Vinculin–α-catenin interaction

Whereas F-actin binding by α-catenin may require an elusive activation step (see above), force-dependent recruitment of Vinculin by α-catenin (Yonemura et al., 2010) may first require an inactivation step: our IP results (Fig. 5) show that full length α-catenin binds the Vinculin head domain in the cytoplasm of highly expressing Cos-7 cells quite efficiently (similar to truncated α-catenin-1-402). This is in apparent contrast to the very inefficient co-IPs between Cadherin complex members and Vinculin in MDCK cells (le Duc et al., 2010). It is highly unlikely that forces act on α-catenin in the cytoplasm of Cos-7 cells. Moreover, also when purified from cell lysates, α-catenin does not have the same globular conformation as Vinculin (Drees et al., 2005), indicating that α-catenin is in a more open conformation. This suggests that specifically at cell–cell junctions a closed conformation of α-catenin is stabilized or that α-catenin is bound to another protein that blocks the VBS domain to exclude Vinculin binding. Even though β-catenin does influence α-catenin conformation in solution (Drees et al., 2005) and the interaction between the two is clearly observed in Cos-7 cells (Fig. 5), there is no apparent effect on Vinculin binding to α-catenin in these Cos-7 lysates (Fig. 5). Thus, an elusive inactivation step of α-catenin might occur at cell–cell junctions to prevent constitutive Vinculin recruitment and enable force-sensing.

One alternative explanation would be that not α-catenin, but Vinculin is activated by myosin-dependent force to induce their interaction. Indeed full length Vinculin in solution or in Cos-7 cells (Fig. 5) does not bind α-catenin, whereas the head domain of Vinculin binds to α-catenin very efficiently (Watabe-Uchida et al., 1998; Weiss et al., 1998; Yamada et al., 2005). By inserting a tension sensing FRET element in Vinculin, it was shown that in integrin-based Focal Adhesions Vinculin itself is under actomyosin-based tension (Grashoff et al., 2010). It is difficult to envision, however, how force at cell–cell junctions can activate Vinculin prior to its visible presence. Moreover, recent work by DeMali shows that the presence of unforced F-actin already stimulates the interaction between full length Vinculin and α-catenin (Peng et al., 2012). Thus it is not clear how Vinculin gets activated for α-catenin binding in cell–cell junctions and this means that there is an additional elusive signaling step that participates in Cadherin mechanosensing. Taken together, it is likely that the Yonemura model in which α-catenin is the force-activated molecule at the Cadherin complex applies to FAJs in junction formation, but it is clear that several key details are missing to fully understand the mechanism of Cadherin mechanosensing.

Function of Vinculin at cell–cell junctions

Vinculin has been found at forming cell–cell junctions (Vasioukhin et al., 2000; this study), remodeling junctions (Huveneers et al., 2012; le Duc et al., 2010) and apical adhesions (Watabe-Uchida et al., 1998; Yonemura et al., 2010). The main common theme in all of these instances appears to be the increased presence of contractile actomyosin, but the precise function of Vinculin's presence at such diverse adhesion sites remains somewhat unclear. Vinculin is involved in compaction of epithelial apical junctions (Maddugoda et al., 2007; Watabe-Uchida et al., 1998) and protects FAJs from opening in thrombin-treated HUVEC cells (Huveneers et al., 2012). We now show that Vinculin enhances the efficiency of epithelial junction sealing upon early contact formation. Combining these observations, a general function for Vinculin in force-dependent junction reinforcement becomes apparent. This is in agreement with the force-dependent reinforcement of the junctions between cells and

E-cadherin-coated beads measured in MTC (le Duc et al., 2010) that is lost in α-catenin-ΔVBS expressing cells (Fig. 6). The next question is how exactly Vinculin can bring about this reinforcement. Vinculin can bind to α-catenin and F-actin and could potentially simply reinforce adhesion by supplying additional bonds between E-cadherin and F-actin. In analogy to integrin dependent force sensing, this would increase the adhesive clutch between E-cadherin and retrograde flowing contractile F-actin, thus slowing this retrograde movement at FAJs and enhancing local membrane protrusion, which is also driven by actin polymerization (Gardel and Schwarz, 2010; Hu et al., 2007; Moore et al., 2010). This in turn would enhance the formation of new Cadherin–Cadherin interactions and result in more efficient epithelial barrier formation. On the other hand, Vinculin can also affect actin polymerization itself (Le Clainche et al., 2010; Wen et al., 2009) or by bringing in additional factors such as VASP (Brindle et al., 1996) and ARP2/3 (DeMali and Burridge, 2003). Especially the enhanced barrier formation in the α-catenin-1-402 expressing cells, that have a reduced number of F-actin binding sites in the Cadherin complex due to the truncation of α-catenin, suggests that increased actin polymerization downstream of Vinculin recruitment could indeed a driving factor for barrier formation. To further investigate this, one would need to develop a system in which Vinculin mutants can be used to specifically rescue the absence of Vinculin at cell–cell junctions. Replacing overall Vinculin with mutants is likely to affect FAs and cytoskeletal integrity and will have indirect effects on the mechanics of cell–cell junctions. Clearly integration of the different observations so far into a complete model for Vinculin function awaits further experiments.

Concluding remarks

In conclusion, we have shown that actomyosin contractility is a driving factor in epithelial barrier formation. The crucial involvement of Vinculin at radial actin contacted FAJs shows that force-generated signaling at the Cadherin complex mediates this function of actomyosin. This has implications for embryogenesis, tissue morphogenesis, wound healing and endothelial remodeling processes where mechanical forces and cell–cell junction formation converge to build and maintain properly functioning tissues (Cavey and Lecuit, 2009).

Materials and Methods

Cell lines and culture

Madin Darby Canine Kidney strain II (MDCK-II) cells were cultured in high glucose DMEM containing GlutaMAX (Gibco) and supplemented with 10% Fetal Bovine Serum (FBS, Sigma) and Penicillin/Streptomycin (Gibco) in standard 10 cm culture dishes. MDCK cells negative for α-E-catenin were a kind gift from James Nelson and used previously by Loerke et al. (Loerke et al., 2012). They were selected by neomycin upon integration of a lentiviral vector containing a specific shRNA sequence against α-E-catenin. These cells were cultured under constant neomycin selection (250 μg/ml). α-E-catenin negative MDCK cells stably rescued with α-catenin mutants or E-cadherin-α-catenin fusions were generated by lentiviral transduction, followed by continuous puromycin (1.3 μg/ml) and neomycin (250 μg/ml) selection. These rescue cell lines were kept in culture for a maximum of 6 passages after selection, to prevent endogenous α-catenin from being re-expressed. DLD-1 R2/7 cells were cultured in high glucose DMEM containing GlutaMAX (Gibco) and supplemented with 10% Fetal Bovine Serum (FBS, Sigma) and Penicillin/Streptomycin (Gibco) in standard 10 cm culture dishes.

Immunocytochemistry and microscopy

For immunofluorescence, cells were plated overnight on glass coverslips, coated with 30 mg/ml collagen type I (Calf collagen I, Sigma) in DMEM lacking calcium (Gibco), supplemented with L-glutamine, Sodium Pyruvate (Gibco), 0.5% FBS (Sigma) or 5% FBS (10 kDa dialyzed, Gibco) and 20 μM $CaCl_2$. Calcium switch was performed by adding $CaCl_2$ to a final concentration of 2 mM. At different time-points, cells were washed with PBS and fixed in 2% paraformaldehyde in PBS for 20 min. at RT, permeabilized with 0.4% Triton X-100 for 5 min. and blocked in 2% BSA for 1 hour. Phalloidin, primary and secondary antibody stainings were performed in 2% BSA for 1 hour. Coverslips were mounted in Mowiol4-88/DABCO solution (Sigma). Fixed cells were imaged using a widefield microscope (Nikon Eclipse Ti) with a 60× 1.49 NA Apo TIRF objective and an EMCCD camera (Luka, Andor). Images were enhanced for display with a background subtraction by rolling ball (r=20), unsharp mask (r=3, weight=0.6), gaussian blur (r=1) and brightness/contrast adjustments in ImageJ (National Institutes of Health). Linescans were made on background-subtracted images, using Metamorph 7.5 software.

DNA constructs and viral transduction

GFP-α-catenin-ΔVBS was generated as described before (Huveneers et al., 2012). α-catenin-1-402 was made by digesting α-catenin with ScaI and XbaI, filling in the recessed 3′ ends of the XbaI sites, followed by blunt-ended ligation. This yields a new stop codon after amino acid 402 of α-catenin. Constructs were cloned into the self-inactivating lentiviral pLV-CMV-ires-puro vector using NdeI and HpaI, or SnaBI and XbaI sites. A-catenin 1-848 was cloned directly into the lentiviral vector by ligating the PCR product into the NdeI/HpaI restriction sites. A stop codon and the HpaI site were inserted after amino acid 848 of α-catenin using the following primers: 5′-GTGTATCATATGCCAAGTACGCCC-3′ (Fw) and 5′-CAGAGTTAACTTACCCCTGTGACTT CTGGTATTTGG-3′ (Rv). mCherry-vinculin was made by replacing EGFP for mCherry in the previously described pEGFP-C3-vinculin vector (le Duc et al., 2010). mCherry-vinculin 1-881 and mCherry-vinculin 1-258 were made by digesting the PCR product of truncated mCh-vinculin with AgeI and KpnI and ligating it into the pEGFP-C1 vector. PCR primers used: 5′-CGCTACCGGTATGGTGAGCAA-3′ (Fw) and either 5′-CAGAGGTACCTTATTTTTCTTCAGG GGGTGGTGGTC-3′ (Rv), introducing a stop codon after amino acid 881 of vinculin, followed by a KpnI restriction site, or 5′- CAGAGGTACCTTACCAGGCATCTT CATCCCAGG-3′ (Rv), introducing a stop codon after amino acid 258 of vinculin, followed by a KpnI restriction site. β-catenin-mCherry was made by replacing EGFP with mCherry in the previously published pEGFP-β-catenin vector (Yamada et al., 2005). E-cadherin-α-catenin fusions were generated by fusing either full length α-catenin WT or ΔVBS in frame after amino acid 811 of mouse E-cadherin (Ecad-DEIGN-RS-MTAVH-acat), thereby replacing part of the intracellular domain, including the β-catenin binding domain of E-cadherin. PCR product of E-cadherin was obtained using the following primers: 5′-CAGAGCTAGCATGGGAGCCCG-GTGCC-3′ (Fw) and 5′-CAGAAGATCTGTTTCCAATTTCATCAGGATTGGC-AGG-3′ (Rv), introducing a BglII site behind E-cadherin. PCR product of α-catenin was obtained using the following primers: 5′-CAGAAGATCTATGAC-TGCCGTCCACGCAG-3′ (Fw) and 5′-CAGACCGCGGGATGCTGTCCAT-GGCTTTGAACTC-3′ (Rv). All clones were verified by sequencing. Lentiviral particles were isolated from HEK293T cells transiently transfected with third-generation packaging constructs and the lentiviral expression vectors. MDCK cells were transduced with supernatant containing lentiviral particles in the presence of 8 μg/ml polybrene overnight. To create stable cell lines, cells were selected with puromycin (1.3 μg/ml) for at least two weeks before being used in experiments.

Trans Epithelial Electrical Resistance (TER)

To measure epithelial barrier formation, collagen-I coated E-plate 16 electrodes (Roche) were incubated with medium for 30 min., and a background measurement was taken. Then, 0.5×10^5 α-catenin negative MDCK cells rescued with indicated constructs were plated the electrodes, and measurement on the xCELLigence Real Time Cell Analyzer (RTCA) DP instrument (Roche) was started immediately. After 24 hours, junction formation was induced by adding $CaCl_2$ to a concentration of 2 mM, while the measurement continued for another 24 hours. For each well, the measured impedance value was divided by the individual background values, yielding the dimensionless parameter Cell Index (CI). Alternatively, 1.5×10^3 MDCK WT cells were plated onto L-cysteine reduced, collagen-I coated 8W10E electrodes (Applied Biophysics) and grown for 24 hours in low calcium medium before starting measurement. Electrical impedance during a calcium switch was measured in real time at 37℃ and 5% CO_2 using a 1600R Electrical Cell Impedance Sensing (ECIS) system (Applied Biophysics) at 4000 Hz. Importantly, results obtained by these two were almost identical and in displayed experiments values were normalized to the maximum value of the control sample measured in the same experiment.

Antibodies and reagents

Vinculin was stained using mouse monoclonal vinculin antibody hVIN1 (Sigma–Aldrich). Mouse monoclonal E-cadherin and afadin antibodies were obtained from BD Biosciences. Rabbit polyclonal α-catenin antibody was obtained from Sigma. Rabbit polyclonal occludin antibody was obtained from Invitrogen. Rabbit polyclonal GFP antibody was from Covance and rabbit polyclonal mCherry

antiserum was home-made and a gift from Jacques Neefjes. Secondary antibodies coupled to Alexa fluor 488 and 594 were obtained from Molecular Probes. Phalloidin coupled to Promofluor 415 was obtained from Promokine. To check the expression of α-catenin 1-848 on blot, we used mouse monoclonal α-catenin antibody (BD Biosciences). Blebbistatin (used at 50 μM) was from Calbiochem, Cytochalasin D (used at 0.2 μg/ml) was from Sigma–Aldrich.

Immunoprecipitation

Cos-7 cells were transfected with the indicated constructs by standard transfection using polyethyleneimine (PEI). 48 hours post transfection, cells were lysed at 4℃ for 10 min. in lysis buffer (1% Nonidet P-40, 25 mM Tris pH 7.4, 100 mM NaCl, 10 mM $MgCl_2$, 10% glycerol, protease and phosphatase inhibitors). Lysates were cleared by centrifugation at 14,000 rpm for 1 min. GFP-tagged α-catenin was precipitated from the lysates using GFP-Trap beads (Chromotek) for 1 hour at 4℃. Precipitations were washed 3 times in lysis buffer and dissolved in Laemmli sample buffer for standard Western blot analysis.

Magnetic Twisting Cytometry

MTC measurements were performed as described (le Duc et al., 2010; Wang et al., 1993). Briefly, DLD1-R2/7 cells were cultured on collagen substrates and incubated with Spherotech, 4.5 μm ferromagnetic beads, covalently modified with Fc-tagged human E-cadherin on a heated microscope stage at 37℃. MTC imaging was done on a Leica inverted microscope using a 20×, NA 0.6 objective and a cooled CCD camera (Orca2, Hamamatsu). In all measurements, an initial, brief high field was applied to magnetize the beads. After defined time periods, the oscillating magnetic field perpendicular to the bead magnetic moment was turned on for a defined period in order to induce a modulating shear stress on the beads. The bead magnetic moment constant was calibrated in a viscosity standard by rotating the beads in the fluid and measuring the bead angular strain and determined to be 0.12 Pa per Gauss magnetic field. The bead displacements were directly measured and converted to the complex modulus/stiffness by taking the ratio of the applied stress (the bead magnetic moment constant times the applied magnetic field) to the bead displacement. Fourier transforms of the bead displacements and the specific torque were used to determine the complex modulus of the bead–cell junction. Each measurement (experimental condition) represents measurements with N>300 cells at ~1 bead/cell. The data follow a log-normal distribution, from which we obtain the mean and standard deviation.

Acknowledgements

We thank Niels Bovenschen and Roel Broekhuizen of the Pathology Department, University Medical Center Utrecht for help with the Roche xCELLigence Real Time Cell Analyzer (RTCA) DP instrument. We thank James Nelson for the α-catenin depleted MDCK cell line. We thank Sander Mertens for critically reading the manuscript. F.T. is funded by an NWO-VIDI grant to J.d.R., S.H. is funded by an NWO-VENI, Q.l.D. is funded by a KWF grant to J.d.R. This work was further funded by the following grants: NIH 1 R01 GM097443 (D.E.L. and N.W.), NIH grant GM072744 (N.W.), and NSF IGERT Grant 0965918 (H.T.).

Competing Interests

The authors have no competing interests to declare.

References

Abe, K. and Takeichi, M. (2008). EPLIN mediates linkage of the cadherin catenin complex to F-actin and stabilizes the circumferential actin belt. *Proc. Natl. Acad. Sci. USA* **105**, 13-19.

Adams, C. L. and Nelson, W. J. (1998). Cytomechanics of cadherin-mediated cell-cell adhesion. *Curr. Opin. Cell Biol.* **10**, 572-577.

Adams, C. L., Chen, Y. T., Smith, S. J. and Nelson, W. J. (1998). Mechanisms of epithelial cell-cell adhesion and cell compaction revealed by high-resolution tracking of E-cadherin-green fluorescent protein. *J. Cell Biol.* **142**, 1105-1119.

Angres, B., Barth, A. and Nelson, W. J. (1996). Mechanism for transition from initial to stable cell-cell adhesion: kinetic analysis of E-cadherin-mediated adhesion using a quantitative adhesion assay. *J. Cell Biol.* **134**, 549-557.

Asada, M., Irie, K., Morimoto, K., Yamada, A., Ikeda, W., Takeuchi, M. and Takai, Y. (2003). ADIP, a novel Afadin- and alpha-actinin-binding protein localized at cell-cell adherens junctions. *J. Biol. Chem.* **278**, 4103-4111.

Brindle, N. P., Holt, M. R., Davies, J. E., Price, C. J. and Critchley, D. R. (1996). The focal-adhesion vasodilator-stimulated phosphoprotein (VASP) binds to the proline-rich domain in vinculin. *Biochem. J.* **318**, 753-757.

Cavey, M. and Lecuit, T. (2009). Molecular bases of cell-cell junctions stability and dynamics. *Cold Spring Harb. Perspect. Biol.* **1**, a002998.

de Rooij, J., Kerstens, A., Danuser, G., Schwartz, M. A. and Waterman-Storer, C. M. (2005). Integrin-dependent actomyosin contraction regulates epithelial cell scattering. *J. Cell Biol.* **171**, 153-164.

DeMali, K. A. and Burridge, K. (2003). Coupling membrane protrusion and cell adhesion. *J. Cell Sci.* **116**, 2389-2397.

Drees, F., Pokutta, S., Yamada, S., Nelson, W. J. and Weis, W. I. (2005). Alpha-catenin is a molecular switch that binds E-cadherin-beta-catenin and regulates actin-filament assembly. *Cell* **123**, 903-915.

Fanning, A. S. and Anderson, J. M. (2009). Zonula occludens-1 and -2 are cytosolic scaffolds that regulate the assembly of cellular junctions. *Ann. N. Y. Acad. Sci.* **1165**, 113-120.

Fanning, A. S., Jameson, B. J., Jesaitis, L. A. and Anderson, J. M. (1998). The tight junction protein ZO-1 establishes a link between the transmembrane protein occludin and the actin cytoskeleton. *J. Biol. Chem.* **273**, 29745-29753.

Gardel, M. and Schwarz, U. (2010). Cell-substrate interactions. *J. Phys. Condens. Matter* **22**, 190301.

Geiger, B., Tokuyasu, K. T., Dutton, A. H. and Singer, S. J. (1980). Vinculin, an intracellular protein localized at specialized sites where microfilament bundles terminate at cell membranes. *Proc. Natl. Acad. Sci. USA* **77**, 4127-4131.

Gloushankova, N. A., Krendel, M. F., Alieva, N. O., Bonder, E. M., Feder, H. H., Vasiliev, J. M. and Gelfand, I. M. (1998). Dynamics of contacts between lamellae of fibroblasts: essential role of the actin cytoskeleton. *Proc. Natl. Acad. Sci. USA* **95**, 4362-4367.

Gottardi, C. J., Wong, E. and Gumbiner, B. M. (2001). E-cadherin suppresses cellular transformation by inhibiting β-catenin signaling in an adhesion-independent manner. *J. Cell Biol.* **153**, 1049-1060.

Grashoff, C., Hoffman, B. D., Brenner, M. D., Zhou, R., Parsons, M., Yang, M. T., McLean, M. A., Sligar, S. G., Chen, C. S., Ha, T. et al. (2010). Measuring mechanical tension across vinculin reveals regulation of focal adhesion dynamics. *Nature* **466**, 263-266.

Gumbiner, B., Stevenson, B. and Grimaldi, A. (1988). The role of the cell adhesion molecule uvomorulin in the formation and maintenance of the epithelial junctional complex. *J. Cell Biol.* **107**, 1575-1587.

Hazan, R. B., Kang, L., Roe, S., Borgen, P. I. and Rimm, D. L. (1997). Vinculin is associated with the E-cadherin adhesion complex. *J. Biol. Chem.* **272**, 32448-32453.

Helwani, F. M., Kovacs, E. M., Paterson, A. D., Verma, S., Ali, R. G., Fanning, A. S., Weed, S. A. and Yap, A. S. (2004). Cortactin is necessary for E-cadherin-mediated contact formation and actin reorganization. *J. Cell Biol.* **164**, 899-910.

Honda, T., Shimizu, K., Kawakatsu, T., Yasumi, M., Shingai, T., Fukuhara, A., Ozaki-Kuroda, K., Irie, K., Nakanishi, H. and Takai, Y. (2003). Antagonistic and agonistic effects of an extracellular fragment of nectin on formation of E-cadherin-based cell-cell adhesion. *Genes Cells* **8**, 51-63.

Hu, K., Ji, L., Applegate, K. T., Danuser, G. and Waterman-Storer, C. M. (2007). Differential transmission of actin motion within focal adhesions. *Science* **315**, 111-115.

Huveneers, S., Oldenburg, J., Spanjaard, E., van der Krogt, G., Grigoriev, I., Akhmanova, A., Rehmann, H. and de Rooij, J. (2012). Vinculin associates with endothelial VE-cadherin junctions to control force-dependent remodeling. *J. Cell Biol.* **196**, 641-652.

Ikeda, W., Nakanishi, H., Miyoshi, J., Mandai, K., Ishizaki, H., Tanaka, M., Togawa, A., Takahashi, K., Nishioka, H., Yoshida, H. et al. (1999). Afadin: A key molecule essential for structural organization of cell-cell junctions of polarized epithelia during embryogenesis. *J. Cell Biol.* **146**, 1117-1132.

Itoh, M., Furuse, M., Morita, K., Kubota, K., Saitou, M. and Tsukita, S. (1999). Direct binding of three tight junction-associated MAGUKs, ZO-1, ZO-2, and ZO-3, with the COOH termini of claudins. *J. Cell Biol.* **147**, 1351-1363.

Johnson, R. P. and Craig, S. W. (1995). F-actin binding site masked by the intramolecular association of vinculin head and tail domains. *Nature* **373**, 261-264.

Kobielak, A., Pasolli, H. A. and Fuchs, E. (2004). Mammalian formin-1 participates in adherens junctions and polymerization of linear actin cables. *Nat. Cell Biol.* **6**, 21-30.

Kovacs, E. M., Goodwin, M., Ali, R. G., Paterson, A. D. and Yap, A. S. (2002). Cadherin-directed actin assembly: E-cadherin physically associates with the Arp2/3 complex to direct actin assembly in nascent adhesive contacts. *Curr. Biol.* **12**, 379-382.

Kovacs, E. M., Verma, S., Ali, R. G., Ratheesh, A., Hamilton, N. A., Akhmanova, A. and Yap, A. S. (2011). N-WASP regulates the epithelial junctional actin cytoskeleton through a non-canonical post-nucleation pathway. *Nat. Cell Biol.* **13**, 934-943.

Lambert, M., Thoumine, O., Brevier, J., Choquet, D., Riveline, D. and Mège, R. M. (2007). Nucleation and growth of cadherin adhesions. *Exp. Cell Res.* **313**, 4025-4040.

Le Clainche, C., Dwivedi, S. P., Didry, D. and Carlier, M. F. (2010). Vinculin is a dually regulated actin filament barbed end-capping and side-binding protein. *J. Biol. Chem.* **285**, 23420-23432.

le Duc, Q., Shi, Q., Blonk, I., Sonnenberg, A., Wang, N., Leckband, D. and de Rooij, J. (2010). Vinculin potentiates E-cadherin mechanosensing and is recruited to actin-anchored sites within adherens junctions in a myosin II-dependent manner. *J. Cell Biol.* **189**, 1107-1115.

Loerke, D., le Duc, Q., Blonk, I., Kerstens, A., Spanjaard, E., Machacek, M., Danuser, G. and de Rooij, J. (2012). Quantitative imaging of epithelial cell scattering identifies specific inhibitors of cell motility and cell-cell dissociation. *Sci. Signal.* **5**, rs5.

Maddugoda, M. P., Crampton, M. S., Shewan, A. M. and Yap, A. S. (2007). Myosin VI and vinculin cooperate during the morphogenesis of cadherin cell cell contacts in mammalian epithelial cells. *J. Cell Biol.* **178**, 529-540.

Meng, W. and Takeichi, M. (2009). Adherens junction: molecular architecture and regulation. *Cold Spring Harb. Perspect. Biol.* **1**, a002899.
Mierke, C. T., Kollmannsberger, P., Zitterbart, D. P., Smith, J., Fabry, B. and Goldmann, W. H. (2008). Mechano-coupling and regulation of contractility by the vinculin tail domain. *Biophys. J.* **94**, 661-670.
Miyake, Y., Inoue, N., Nishimura, K., Kinoshita, N., Hosoya, H. and Yonemura, S. (2006). Actomyosin tension is required for correct recruitment of adherens junction components and zonula occludens formation. *Exp. Cell Res.* **312**, 1637-1650.
Moore, S. W., Roca-Cusachs, P. and Sheetz, M. P. (2010). Stretchy proteins on stretchy substrates: the important elements of integrin-mediated rigidity sensing. *Dev. Cell* **19**, 194-206.
Niessen, C. M. (2007). Tight junctions/adherens junctions: basic structure and function. *J. Invest. Dermatol.* **127**, 2525-2532.
Noren, N. K., Niessen, C. M., Gumbiner, B. M. and Burridge, K. (2001). Cadherin engagement regulates Rho family GTPases. *J. Biol. Chem.* **276**, 33305-33308.
Ogita, H., Rikitake, Y., Miyoshi, J. and Takai, Y. (2010). Cell adhesion molecules nectins and associating proteins: Implications for physiology and pathology. *Proc. Jpn. Acad., Ser. B, Phys. Biol. Sci.* **86**, 621-629.
Ooshio, T., Irie, K., Morimoto, K., Fukuhara, A., Imai, T. and Takai, Y. (2004). Involvement of LMO7 in the association of two cell-cell adhesion molecules, nectin and E-cadherin, through afadin and alpha-actinin in epithelial cells. *J. Biol. Chem.* **279**, 31365-31373.
Ooshio, T., Kobayashi, R., Ikeda, W., Miyata, M., Fukumoto, Y., Matsuzawa, N., Ogita, H. and Takai, Y. (2010). Involvement of the interaction of afadin with ZO-1 in the formation of tight junctions in Madin-Darby canine kidney cells. *J. Biol. Chem.* **285**, 5003-5012.
Pacquelet, A. and Rørth, P. (2005). Regulatory mechanisms required for DE-cadherin function in cell migration and other types of adhesion. *J. Cell Biol.* **170**, 803-812.
Peng, X., Cuff, L. E., Lawton, C. D. and DeMali, K. A. (2010). Vinculin regulates cell-surface E-cadherin expression by binding to β-catenin. *J. Cell Sci.* **123**, 567-577.
Peng, X., Maiers, J. L., Choudhury, D., Craig, S. W. and DeMali, K. A. (2012). α-Catenin uses a novel mechanism to activate vinculin. *J. Biol. Chem.* **287**, 7728-7737.
Pokutta, S., Drees, F., Takai, Y., Nelson, W. J. and Weis, W. I. (2002). Biochemical and structural definition of the l-afadin- and actin-binding sites of α-catenin. *J. Biol. Chem.* **277**, 18868-18874.
Puklin-Faucher, E. and Sheetz, M. P. (2009). The mechanical integrin cycle. *J. Cell Sci.* **122**, 179-186.
Sakisaka, T., Ikeda, W., Ogita, H., Fujita, N. and Takai, Y. (2007). The roles of nectins in cell adhesions: cooperation with other cell adhesion molecules and growth factor receptors. *Curr. Opin. Cell Biol.* **19**, 593-602.
Shewan, A. M., Maddugoda, M., Kraemer, A., Stehbens, S. J., Verma, S., Kovacs, E. M. and Yap, A. S. (2005). Myosin 2 is a key Rho kinase target necessary for the local concentration of E-cadherin at cell-cell contacts. *Mol. Biol. Cell* **16**, 4531-4542.
Taguchi, K., Ishiuchi, T. and Takeichi, M. (2011). Mechanosensitive EPLIN-dependent remodeling of adherens junctions regulates epithelial reshaping. *J. Cell Biol.* **194**, 643-656.
Takahashi, K., Nakanishi, H., Miyahara, M., Mandai, K., Satoh, K., Satoh, A., Nishioka, H., Aoki, J., Nomoto, A., Mizoguchi, A. et al. (1999). Nectin/PRR: an immunoglobulin-like cell adhesion molecule recruited to cadherin-based adherens junctions through interaction with Afadin, a PDZ domain-containing protein. *J. Cell Biol.* **145**, 539-549.
Takai, Y., Ikeda, W., Ogita, H. and Rikitake, Y. (2008). The immunoglobulin-like cell adhesion molecule nectin and its associated protein afadin. *Annu. Rev. Cell Dev. Biol.* **24**, 309-342.
Tang, V. W. and Brieher, W. M. (2012). α-Actinin-4/FSGS1 is required for Arp2/3-dependent actin assembly at the adherens junction. *J. Cell Biol.* **196**, 115-130.
Turksen, K. and Troy, T. C. (2004). Barriers built on claudins. *J. Cell Sci.* **117**, 2435-2447.
Vasioukhin, V., Bauer, C., Yin, M. and Fuchs, E. (2000). Directed actin polymerization is the driving force for epithelial cell-cell adhesion. *Cell* **100**, 209-219.
Vogel, V. and Sheetz, M. (2006). Local force and geometry sensing regulate cell functions. *Nat. Rev. Mol. Cell Biol.* **7**, 265-275.
Wang, N. and Ingber, D. E. (1995). Probing transmembrane mechanical coupling and cytomechanics using magnetic twisting cytometry. *Biochem. Cell Biol.* **73**, 327-335.
Wang, N., Butler, J. P. and Ingber, D. E. (1993). Mechanotransduction across the cell surface and through the cytoskeleton. *Science* **260**, 1124-1127.
Watabe-Uchida, M., Uchida, N., Imamura, Y., Nagafuchi, A., Fujimoto, K., Uemura, T., Vermeulen, S., van Roy, F., Adamson, E. D. and Takeichi, M. (1998). α-Catenin-vinculin interaction functions to organize the apical junctional complex in epithelial cells. *J. Cell Biol.* **142**, 847-857.
Weiss, E. E., Kroemker, M., Rüdiger, A. H., Jockusch, B. M. and Rüdiger, M. (1998). Vinculin is part of the cadherin-catenin junctional complex: complex formation between α-catenin and vinculin. *J. Cell Biol.* **141**, 755-764.
Wen, K. K., Rubenstein, P. A. and DeMali, K. A. (2009). Vinculin nucleates actin polymerization and modifies actin filament structure. *J. Biol. Chem.* **284**, 30463-30473.
Yamada, S., Pokutta, S., Drees, F., Weis, W. I. and Nelson, W. J. (2005). Deconstructing the cadherin-catenin-actin complex. *Cell* **123**, 889-901.
Yonemura, S., Itoh, M., Nagafuchi, A. and Tsukita, S. (1995). Cell-to-cell adherens junction formation and actin filament organization: similarities and differences between non-polarized fibroblasts and polarized epithelial cells. *J. Cell Sci.* **108**, 127-142.
Yonemura, S., Wada, Y., Watanabe, T., Nagafuchi, A. and Shibata, M. (2010). α-Catenin as a tension transducer that induces adherens junction development. *Nat. Cell Biol.* **12**, 533-542.

Biology Open

Supplementary Material

Floor Twiss et al. doi: 10.1242/bio.20122428

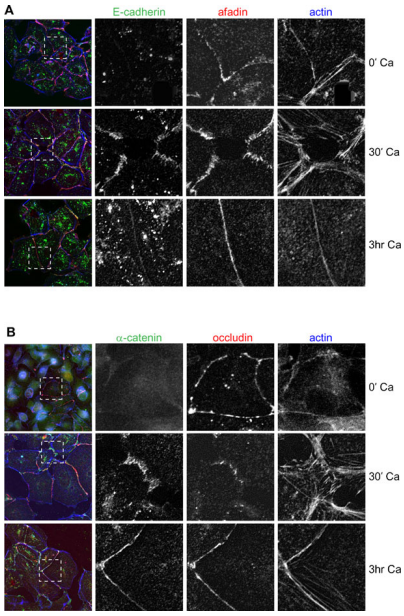

Fig. S1. Serum conditions do not affect Afadin and Occludin localization during a calcium switch. (**A**,**B**) IF images of AJ (E-cadherin, α-catenin), NJ (Afadin) and TJ (Occludin) markers and actin during a calcium switch in subconfluent MDCK cells in 5% FBS low calcium medium.

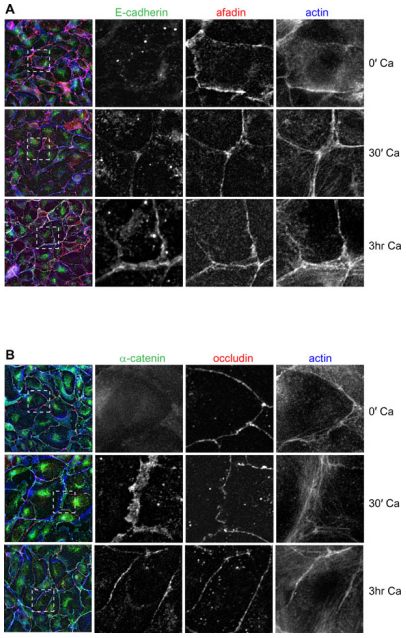

Fig. S2. Cell density does not affect Afadin and Occludin localization during a calcium switch. (**A**,**B**) IF images of AJ (E-cadherin, α-catenin), NJ (Afadin) and TJ (Occludin) markers and actin during a calcium switch in MDCK cells seeded at high confluency in 0.5% FBS low calcium medium.

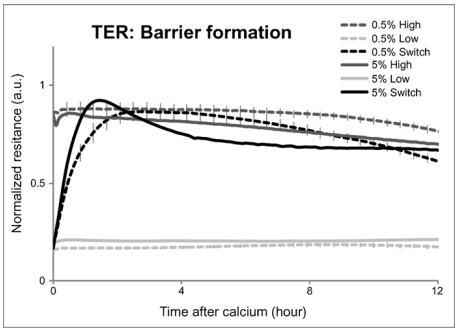

Fig. S3. Serum conditions do not affect barrier formation. TER measurement of MDCK cells seeded in low calcium medium (light grey line), normal calcium medium (dark grey line) or during a calcium switch (black line), containing either 0.5% FBS (dashed lines) or 5% FBS (solid lines). Error bars indicate standard error, $n>3$.

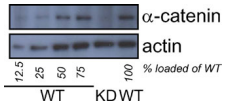

Fig. S4. α-catenin knockdown levels in MDCK cells. Western Blot result of MDCK α-catenin knockdown cells compared to α-catenin levels in MDCK WT cells.

Vinculin localization is conserved among the classical cadherins; E-, VE- and N- cadherin

Vinculin localization is conserved among the classical cadherins

E-,VE- and N- cadherin.

Q. le Duc, G. van der Krogt, S. Huveneers, J. de Rooij

Hubrecht Institute for Developmental Biology and Stem Cell Research, University Medical Center Utrecht, 3584 CT Utrecht, Netherlands

A**bstract**

In this study, we investigated whether the recruitment of vinculin to the classical cadherin family members, VE-cadherin and N-cadherin, is dependent on mechanical tension. We wanted to know if vinculin dependent mechanotransduction is unique to E-cadherin mediated cell-cell junctions or more widespread among the cadherin family. The results show that vinculins presence in both VE-, and N-cadherin mediated junctions is sensitive to actomyosin contractility, which implies that indeed vinculin based mechanotransduction is commonly utilized among the classical cadherins.

Introduction

Cadherins are glycoprotein receptors spanning the cell membrane. Most of these proteins are involved in calcium dependent cell adhesion, hence their name cadherin. Although discovered in multicellular vertebrates, cadherins are also present in simple unicellular choanoflagellates that form colonies (during stages of their life cycle) when triggered by specific bacteria [1, 2]. Since the first appearance in these primitive premetazoan organisms, cadherins have evolved among multicellular metazoans into a superfamily consisting of more than 350 known genes. The cadherin superfamily members are unified by the presence of characteristic extracellular cadherin (EC) repeats, additional structural features that vary, define the different subfamilies; classical cadherins, protocadherins, desmosomal cadherins and atypical cadherins.

The first identified and best studied is the group of the classical cadherins; they are defined by a conserved cytoplasmic region capable of binding cytoplasmic partners. The classical cadherins associate with a core complex of three catenins. B- and p120 -catenin bind directly to the cytoplasmic tail of the classical cadherin and α catenin is indirectly bound to cadherin via βcatenin. In vertebrates the extracellular region of classical cadherins is comprised of five EC domains and further subdivided in type I and II. Type I is distinct from type II by sequence differences in EC1, the main adhesion mediating domain (reviewed in [3, 4]. In general five "type 1" and thirteen "type II" are found in vertebrate genomes, most are named according to the tissues from which they were first isolated. Examples from the classical cadherin type I group are E (Epithelial) cadherin, N (Neural) cadherin and P (Placental) cadherin and examples of type II are VE (Vascular Endothelial) cadherin and K (Kidney) cadherin.

The existence of such a variety of classical cadherins suggest a specific function for each individual member. Cadherins are homophilic binding molecules, and the specificity of their interactions is thought to underlie the sorting out or segregation of cells into specific tissue layers and the formation of tissue boundaries [4, 5]. In vitro experiments show that cells expressing different types of classical type I cadherins sorted out into distinct aggregates [6]

The sorting function of classical cadherins is attributed to the extracellular domain, especially the sequence specificity of the N-terminal EC1 repeat [6] However in vitro studies have shown that heterophilic interactions occur among several type I and II classical cadherins [7-9]. Although there is not much evidence of their occurrence in vivo, the possibility of heterophilic interactions undermines the model in which the mechanism of tissue segregation was based solely on homophilic cadherin interactions. Indeed several observations suggest that tissue segregation is based on alternative mechanisms. For instance in zebrafish the differential actomyosin-dependent cell-cortex tension of different germ layer cells governs the segregation of the germ layers [10]. Furthermore, coordinated actomyosin-based tension at the anterior–posterior boundary maintains tissue segmentation later in development [11, 12]. Additionally, segregation or boundary functions by junctions between cells with the same cadherin are common: Tension-dependent germ layer segregation in zebrafish [10] is exclusively dependent on the E-cadherin member of the classical cadherins, because member substitution disrupts the segregation [13, 14]. Forced overexpression of N- or C-cadherin in *Xenopus* led to disruptions of the ectoderm, suggesting that only E-cadherin, which is the endogenous cadherin in this tissue, can maintain the integrity of this tissue [13, 14]

One possible mechanism explaining segregation of cell expressing different cadherins is that individual member of the classical cadherins can establish a distinct cell-cortex tension. All classical cadherins are linked to the contractile actomyosin network via α-catenin. It has recently become clear from studies

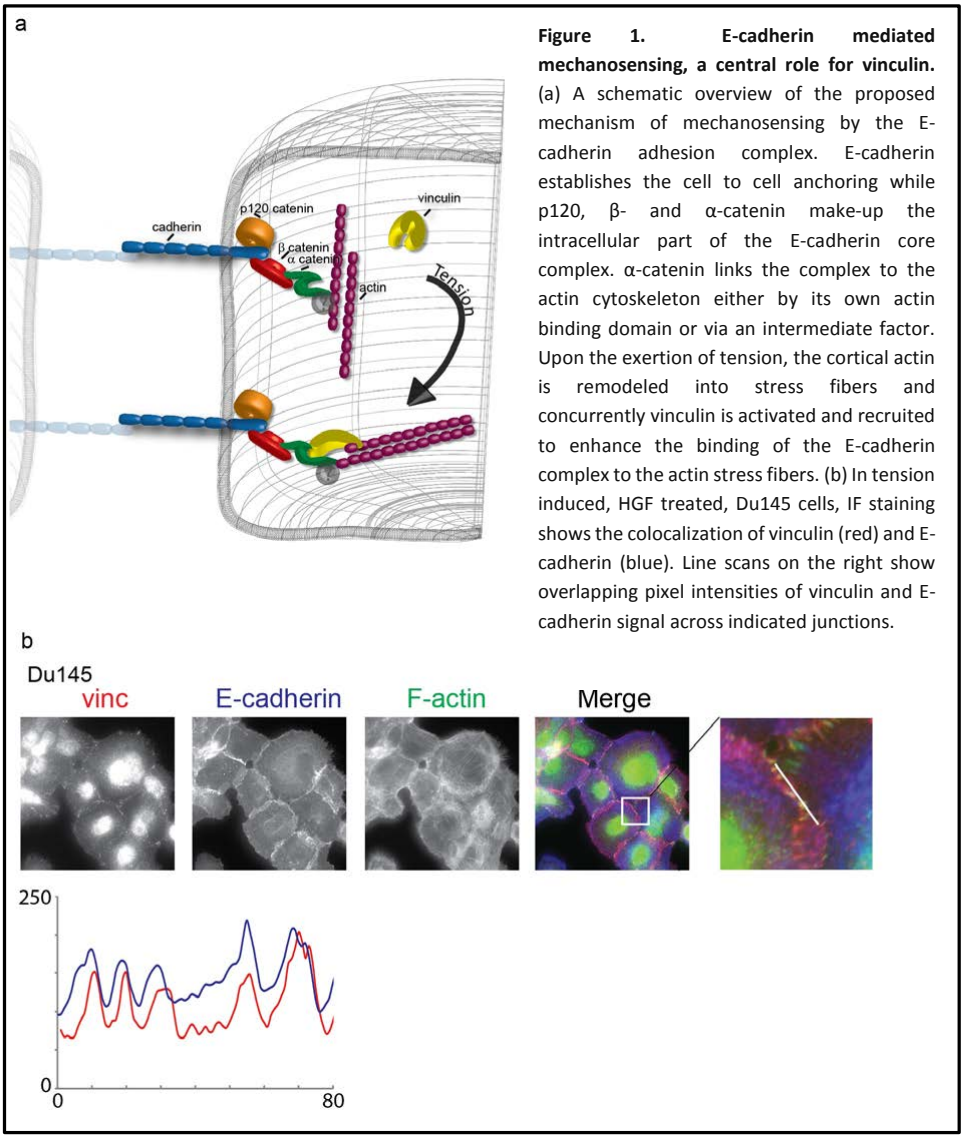

Figure 1. E-cadherin mediated mechanosensing, a central role for vinculin. (a) A schematic overview of the proposed mechanism of mechanosensing by the E-cadherin adhesion complex. E-cadherin establishes the cell to cell anchoring while p120, β- and α-catenin make-up the intracellular part of the E-cadherin core complex. α-catenin links the complex to the actin cytoskeleton either by its own actin binding domain or via an intermediate factor. Upon the exertion of tension, the cortical actin is remodeled into stress fibers and concurrently vinculin is activated and recruited to enhance the binding of the E-cadherin complex to the actin stress fibers. (b) In tension induced, HGF treated, Du145 cells, IF staining shows the colocalization of vinculin (red) and E-cadherin (blue). Line scans on the right show overlapping pixel intensities of vinculin and E-cadherin signal across indicated junctions.

by us and others that classical E-, N- and VE-cadherin complexes not only transmit, but also sense tensile forces across the link between the junctions and the cytoskeleton and respond to increased tension by positive feedback leading to alterations in the junction associated actin: E-cadherin complexes respond to increased tension by stiffening the cortical actomyosin cytoskeleton [15]. Actomyosin-dependent traction forces of C2 cells on N-cadherin coated elastomeric pillars were dependent on pillar stiffness[16]. Cytoskeletal pulling forces on VE-cadherin based cell-cell junctions lead to an increased in junction size, which is an actomyosin dependent process [17]. This newly discovered cadherin mechanosensing raises the possibility that differential regulation of cortical actomyosin-

based tension by different cadherin members, rather than the trans-homophilic recognition of different cadherins per se, is responsible for cell-sorting behaviour.

One mechanism of mechanosensing was recently uncovered for the E-cadherin complex by us and Yonemura. Even though many details still remain unknown, a basic working model puts α-catenin in the centre as the monitor of the tensile forces and mediator of the cortex stiffening feedback step, wherein vinculin is recruited to form an extra link to the actin cytoskeleton (fig 1a) [15, 18]. According to this model, the E-cadherin mediated junction complex adopts different states in response to tensile forces. When the junctional complex is not exposed to tensile forces, the junction complex is in a steady- state and does not incorporate vinculin, this is congruent with data where vinculin is not observed at steady state junctions (fig. 1b). In contrast, E-cadherin complexes in a "tensile" state do recruit vinculin, resulting in the colocalization of vinculin to a tensed subfraction of the E-cadherin mediated junctions. This subfraction is increased when actomyosin contraction and junction (fig 1b).

The differential adhesion and sorting behaviours observed among cells expressing different members of the three mechanosensitive classical cadherins raise the question if these cadherins can all engage the same, vinculin-dependent mechanotransduction mechanism. We investigated this using a combination of IF and live cell imaging and we found that: Vinculin is localized at N-cadherin and VE-cadherin junctions in astrocytes and HUVEC's respectively. Moreover, vinculin localization is dependent on actomyosin functioning as localization was abrogated through perturbations of myosin II or F-actin. This is in correspondence with the observations made on the E-cadherin dependent mechanosensor, indicating that the vinculin dependent mechanosensing capacity is conserved among classical cadherins.

So the question remains if these suggested mechanosensing capacities observed for N- and VE-cadherin depend on the same mechanism as reported for E-cadherin? The E-cadherin mechanosensor is based upon interactions with its cytoplasmic tail, due to the high conservation of the cytoplasmic tails among classical cadherins, similarities in interactions are to be expected. However subtle sequence differences of the cytoplasmic tail do exist and small differences in binding affinities can result in substantial effects. The structural integrity of the cadherin/catenin complex is positively and negatively regulated by phosphorylation sites at the cytoplasmic tail. Three serine residues in the E-cadherin cytoplasmic domain (S684, S686, S692) are phosphorylated which generates additional interactions with β-catenin resulting in a large increase in affinity between the two proteins[19].

Results

Vinculin is abundantly present in N-cadherin junctions of rat astrocytes.

Immuno-fluorescent (IF) co-staining of p120-catenin and N-cadherin in primary rat astrocytes (fig 2a) showed that the junctional pattern of N-cadherin is identical to the p120-catenin staining. This colocalization in the IF images between N-cadherin and P120-catenin, which is bound to all classical cadherins, confirms the notion from literature that N-cadherin [20] is the main cadherin expressed in these cells. This observation was corroborated by IF staining and western blotting, which showed no presence of other classical cadherins in these cells (not shown). Thus, the cell-cell junctions in these rat astrocytes are clearly based on N-cadherin mediated interactions.

Co-staining of N-cadherin and Vinculin (fig 2a) showed that Vinculin is abundantly present at N-cadherin junctions, but the distribution is not uniform. While p120-catenin (fig 2b), N-cadherin and other junction markers (not shown) concentrate along the entire cell-cell contact area, Vinculin concentrates only in areas that are in close proximity to the actomyosin network. The thick radial stress fibers, of the actomyosin network (indicating contractile and tensile networks), run perpendicular into the spot like, vinculin containing junctions. In figure 2b vinculin locates solely to the central region of the cell-cell contact while the peripheral sides, where the junctions resides in the steady state, radial stress fibers cannot be observed and vinculin is absent.

As can be observed (fig 1b,2b,c), next to cell-cell junctions, vinculin is also present in Focal Adhesions (FA), which are integrin-mediated cell matrix adhesions [21] To show that the pool of vinculin in cell–cell junctions is distinct from the vinculin in FAs, the astrocytes were IF stained for both vinculin and the constitutive FA protein paxillin. Staining for tyrosine-118–phosphorylated (pY118) paxillin, which mediates myosin II–dependent recruitment of vinculin to FAs [22], shows no co-localization with the cell–cell junction pool of vinculin (fig 2c). Thus, vinculin is recruited to cell–cell junction complexes that are devoid of vinculins main interactors in integrin-based adhesion contacts.

In conclusion, in astrocytes vinculin is recruited to a subset of N-cadherin-based cell-cell junctions. The specific organization of the associated actomyosin network and the strong abundance of vinculin

Vinculin is recruited to VE-cadherin mediated junctions in primary Human endothelial cells

Live imaging of HUVEC's expressing Lifeact-mCherry (characterized in [23]) and VE-cadherin–GFP (characterized in [24] (Fig. 3 a) shows junctional complexes in both a steady-state and a remodelling-state. The steady-state junctions are marked by faint cortical actin and are aligned by thick parallel actin bundles that do not overlap with VE-cadherin (fig. 3 a). In contrast, remodelling junctions show discontinuous VE-cadherin organisation resulting in elongated adhesion structures oriented perpendicularly to the plane of cell-cell adhesion. In these junctions, cadherins are attached to radial actin bundles from both cells participating in the cell–cell junction (Fig. 3a). Thus, within an endothelial monolayer in 2D culture, two states of VE-cadherin adhesions can be distinguished: the steady state junction (where tension is likely low) and the remodelling junctions where VE-cadherin locates to fragmented adhesion structures contacted by radial actin bundles from both sides (and therefore likely experiences high tension).

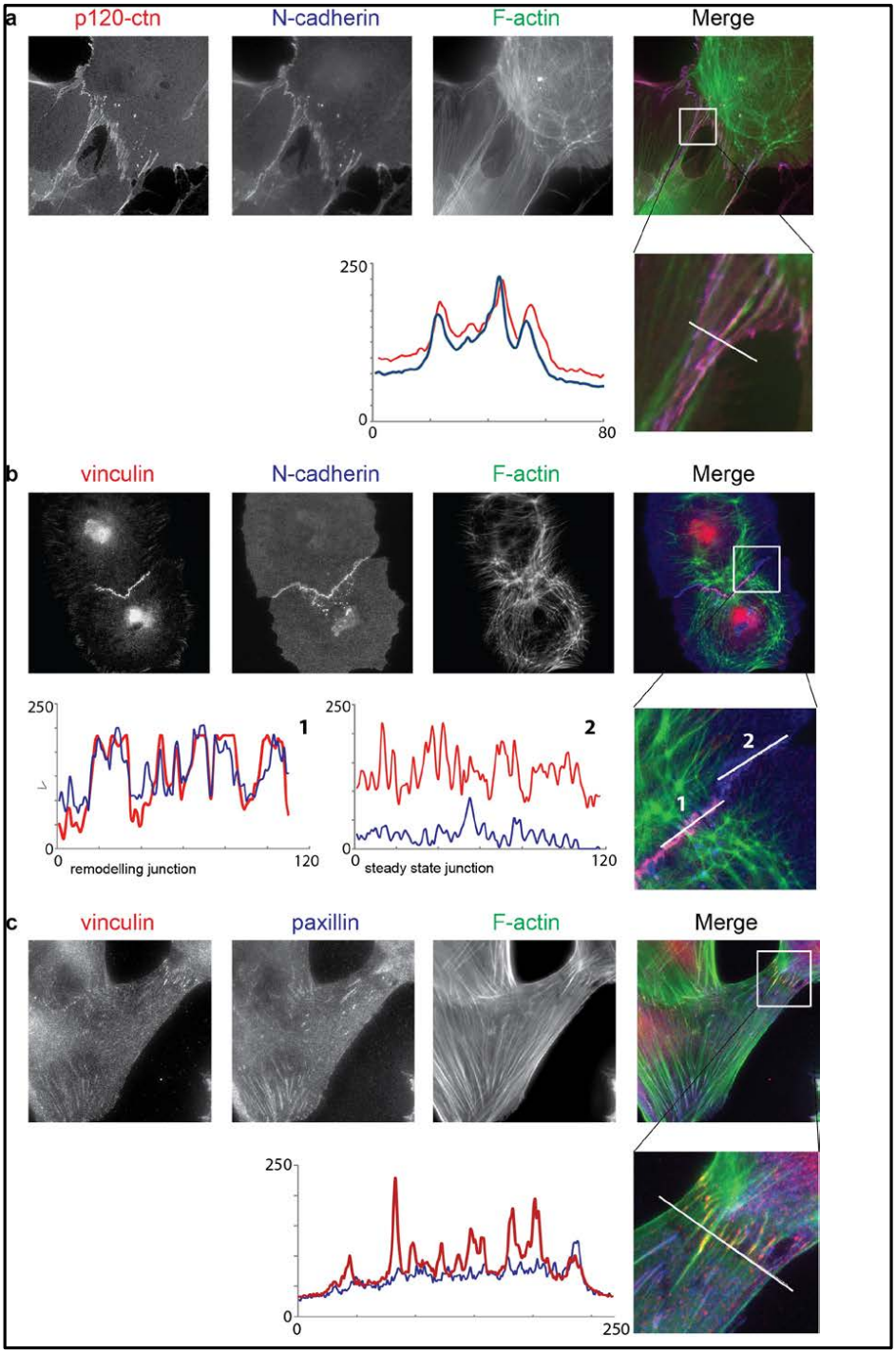
a
p120-ctn
N-cadherin
F-actin
Merge
250
0
0
80
b
vinculin
N-cadherin
F-actin
Merge
250
0
1
0
remodelling junction
120
250
0
2
0
steady state junction
120
2
1
c
vinculin
paxillin
F-actin
Merge
250
0
0
250

Figure 2. N-cadherin specifically colocalizes with vinculin in cell-cell junctions in rat astrocytes. (a) The IF images for p-120-catenin (red) and N-cadherin (blue) in rat astrocytes show a corresponding pattern, supported by the line scan of the indicated junctional area. (b) Furthermore does the co-staining of N-cadherin (blue) and vinculin (red) show a specific colocalization of the two in cell-cell junctions, while this is absent in cell-matrix adhesions where vinculin also resides, indicated by the linescans in the cell-cell and cell-matrix adhesion areas. (c) The IF staining for both vinculin (red) and the cell-matrix adhesion marker paxillin (blue) rule out that vinculin localization in cell-cell junctions is due to the presence of cell-matrix adhesions in the cell-cell junctional area.

The stainings of vinculin, VE-cadherin phalloidin (F-actin) in HUVEC's (fig3b) showed the presence of vinculin in remodelling (tensile) cell-cell junctions. Even though vinculin localizes to VE-cadherin positive spots in IF-stainings, it does not exclude that N-cadherin is also present at these spots and therefore does not fully proof that vinculin localization is VE-cadherin mediated. Although VE-cadherin is highly expressed in HUVEC's, N-cadherin is also expressed in these cells, which is common for endothelial cells [25]. To further investigate if the observed vinculin localization is VE-cadherin dependent, a VE-cadherin blocking antibody was administered to the cells (fig 3c). This blocking antibody did not abolish cell-cell junctions altogether in HUVECs, indicating that other cell-cell junction proteins can support junction integrity in these cells. Interestingly however; vinculin localization was absent at cell-cell junctions when this VE-cadherin blocking antibody was added. Thus in VE-cadherin blocked cell-cell junctions where N-cadherin function is not manipulated, vinculin does not localize to the cell-cell junctions. These observations supports the conclusion that vinculins localisation to cell-cell junctions in HUVEC's is VE-cadherin based.

Although vinculin appears to locate to VE-cadherin mediated junctions, it still has to be proven that this localization is specific for cell-cell junctions and not dependent of FA junction localization. In analogy to what we have shown for N-cadherin, HUVECS were stained for a specific FA marker, paxillin, and vinculin. In figure 3d, even when FAs are located close to endothelial junctions, we find no co-localization of the phospho-Paxillin (pY118), with VE-cadherin at perpendicularly oriented junctions. Co-IF stainings of Paxillin and vinculin in HUVECs show that vinculin is located at integrin- as well as cadherin-based adhesions, which are clearly separate structures. Collectively, these results show that vinculin marks a molecularly (presence of vinculin) and morphologically (perpendicular orientation) distinct subset of VE-cadherin adhesions, which are attached to radial actin bundles and display increased remodelling compared with stable adherens junctions that are paralleled by actin bundles and do not contain vinculin.

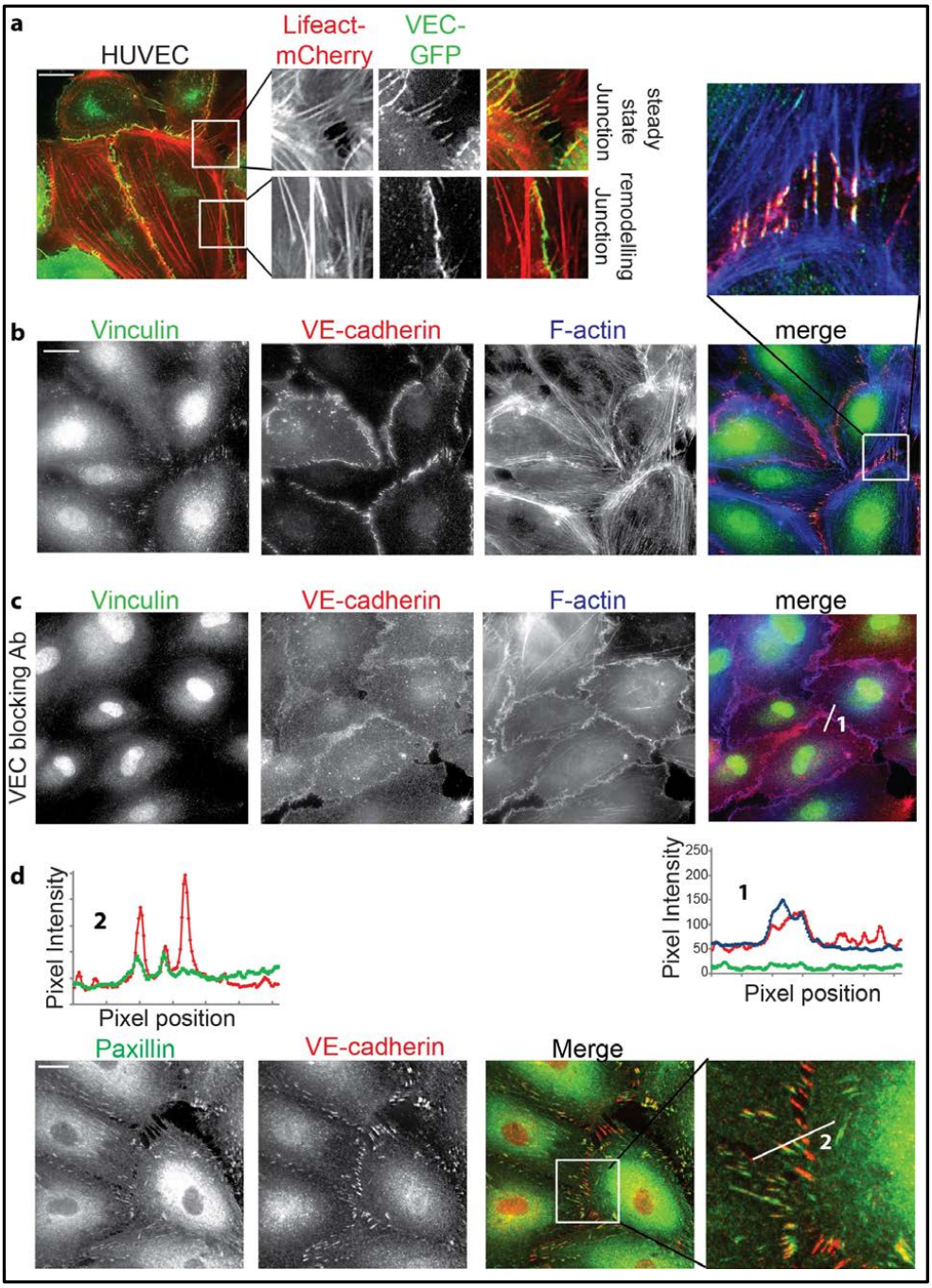
a
HUVEC
Lifeact-mCherry
VEC-GFP
steady state Junction
remodelling Junction
b
Vinculin
VE-cadherin
F-actin
merge
c
VEC blocking Ab
Vinculin
VE-cadherin
F-actin
merge
1
d
Pixel Intensity
2
Pixel position
Pixel Intensity
250
200
150
100
50
0
1
Pixel position
Paxillin
VE-cadherin
Merge
2

Figure 3. Vinculin marks distinct, remodeling cell–cell junctions attached to radial actin bundles. (a) Still images and enlarged views from time-lapse recordings showing perpendicularly oriented remodeling cell–cell junctions and linear stable/mature cell–cell junctions in a monolayer of HUVECs expressing VE-cadherin–GFP (green) and the F-actin probe Lifeact-mCherry (red). (b) IF images of HUVECs stained for vinculin (green), VE-cadherin (red), and F-actin (blue) that were treated with VE-cadherin blocking antibody for 2 h. Line scan on the right show intensities of vinculin, VE-cadherin, and F-actin signal across indicated junctions.(c) IF images of HUVECs stained for vinculin (green), VE-cadherin (red), and F-actin (blue) showing specific colocalization of Vinculin with non-linear, remodeling cell-cell junctions. (d) The IF staining in HUVEC's for both vinculin (green) and the cell-matrix adhesion marker paxillin (red) rule out that vinculin localization in cell-cell junctions is due to the presence of cell-matrix adhesions in the cell-cell junctional area.

Vinculin recruitment is actomyosin sensitive and vinculin positive junctions are tensile.

So far we have shown that vinculin localizes to both N-cadherin and VE-cadherin mediated junctions, specifically when they are connected to radial actin bundles. To directly test whether this localization is dependent on actomyosin-based tension on these junctions, we used the myosin inhibitor blebbistatin [15]. Treatment with blebbistatin for 10 min largely abolished vinculin localization to cell–cell junctions in IF stainings of both rat astrocytes and HUVECs (fig4 a and b), suggesting that this localization is indeed myosin dependent. We conclude that vinculin is recruited to cell–cell junctions in a myosin II–dependent manner. To further corroborate that vinculin-positive cell–cell junctions indeed experience tension from attached actin bundles, we used low doses of the barbed end actin capping agent Cytochalasin D, a method previously validated by the Nelson laboratory [26]. As shown in Fig. 4 b, Cytochalasin D induces a rapid (within 30–60 s) displacement of cell–cell junctions marked by vinculin-GFP and p120-catenin–mCherry in rat astrocytes and HUVEC's. In contrast, p120-positive but vinculin-negative junction sections, hardly show any displacement after Cytochalasin D (shown for HUVECs). These results show that vinculin-containing junctions are biophysically distinct from vinculin-negative steady state junctions. The displacement of the junction in the direction of the attached contractile F-actin bundles suggests that they experienced pulling forces from both sides that were no longer balanced in the presence of Cytochalasin D. We conclude from these experiments that, for both N- and VE-cadherin, vinculin recruitment is dependent on both tension generation via myosin II and an organized actin cytoskeleton

Discussion

We have shown that in N-cadherin and VE-cadherin based junctions the conditions for vinculin localization are highly similar to what is found in E-cadherin based junctions. In junctional complexes of all three classical cadherin members, vinculin localization is isolated to spots where radial actin bundles terminate. We suggest that actomyosin generated force is transduced through these spots. This is corroborated by our experiments that showed an elastic retraction of specifically the vinculin containing junction spots when low doses of cytoD were used to sever the cytoskeletal network. Moreover, the inhibition of myosin-II generated cytoskeletal contractility abolishes the recruitment of vinculin to the junctions in all three cadherin types. Therefore we conclude that the force-induced cytoskeletal feedback signalling is similar in these three members of the classical cadherin sub-family. Thus in both the type I and II members, N- and VE-cadherin respectively, the mechanotransduction mechanism is highly conserved. Notably, the VE-cadherin amino acid sequence shows considerable differences compared to other classical cadherin (only 23% identity when compared with E-, N-, and P- cadherin) [27, 28]. So even in one of the most distant members of the classical cadherins the vinculin-dependent mechanotransduction mechanism is present. Altogether, our data clearly suggest that the

tension dependent junction reinforcement through recruitment of vinculin is conserved among all members of the classical cadherin subfamily.

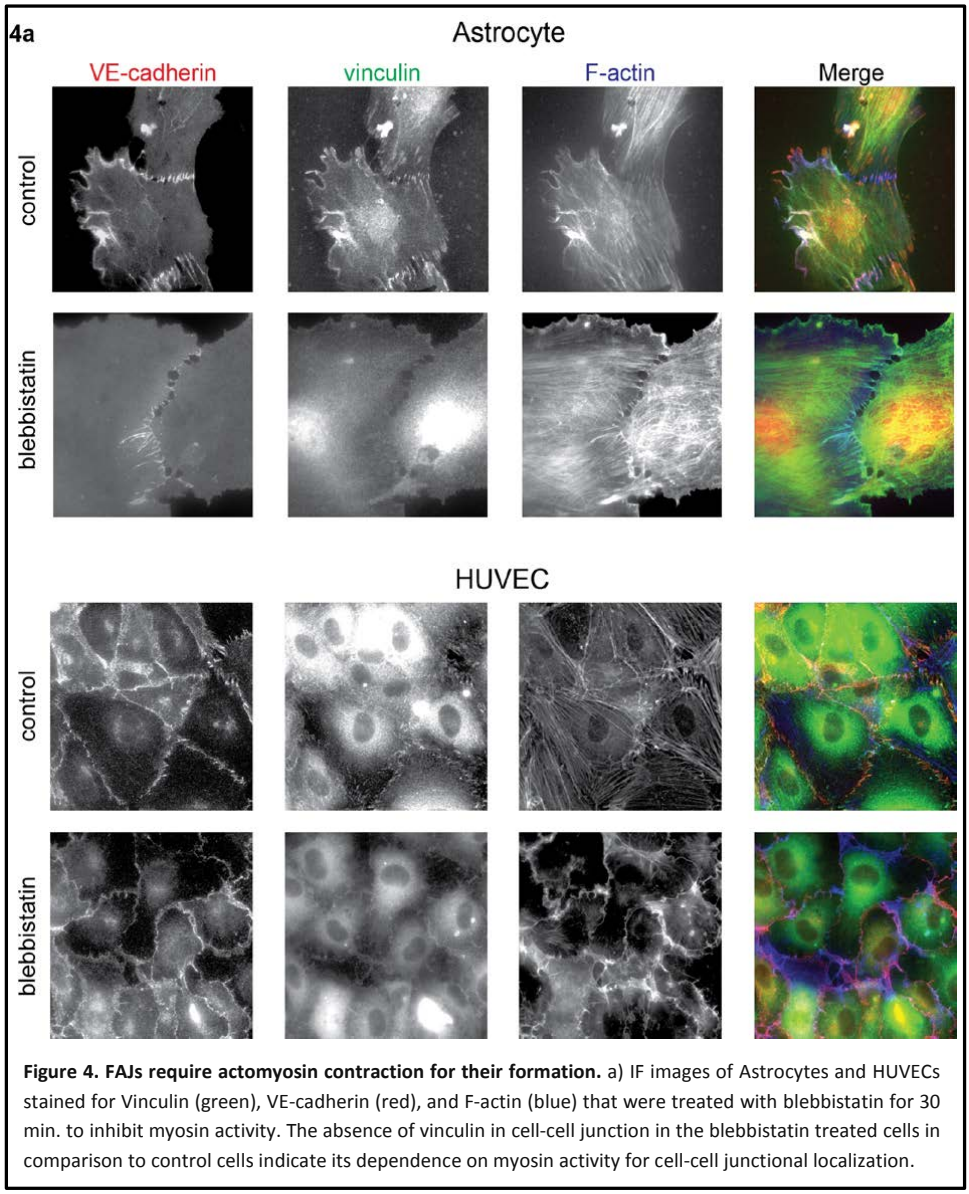

Figure 4. FAJs require actomyosin contraction for their formation. a) IF images of Astrocytes and HUVECs stained for Vinculin (green), VE-cadherin (red), and F-actin (blue) that were treated with blebbistatin for 30 min. to inhibit myosin activity. The absence of vinculin in cell-cell junction in the blebbistatin treated cells in comparison to control cells indicate its dependence on myosin activity for cell-cell junctional localization.

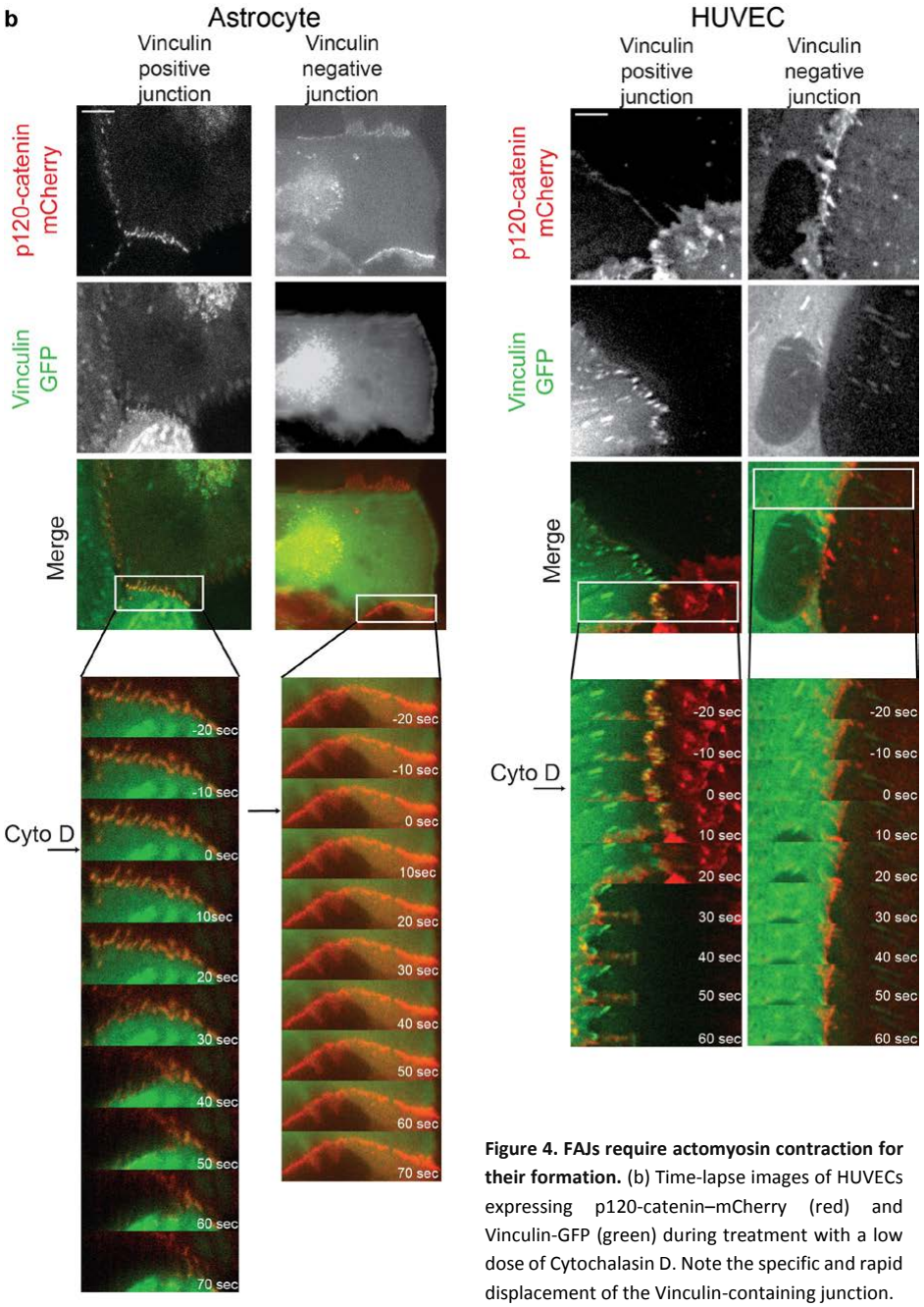

Figure 4. FAJs require actomyosin contraction for their formation. (b) Time-lapse images of HUVECs expressing p120-catenin–mCherry (red) and Vinculin-GFP (green) during treatment with a low dose of Cytochalasin D. Note the specific and rapid displacement of the Vinculin-containing junction.

This conservation would suggest that processes like for instance the earlier described tension dependent sorting of germ layers in zebrafish, are not based upon distinctive tension regulation of different classical cadherin members. Indeed, the mentioned germ layer sorting in zebrafish appears solely based upon E-cadherin mediated junctions [10]. Furthermore, differential cytoskeletal-tension can be regulated independent of cadherins [12, 29] by for instance differential activity of the Rho-ROCK pathway that regulates myosin activity. Nevertheless, even though tension-dependent vinculin recruitment appears grosso modo conserved, other or more subtle differences in mechanotransduction could exist among different members. For instance the exact mechanisms of activation of both α-catenin and vinculin, needed for vinculin binding to α-catenin and actin, remain so far unresolved. Moreover, Yonemura has shown that α-catenin is of great importance within this mechanosensing mechanism [18]. However, different α-catenin subtypes exist: α-E-catenin is the most common form, mainly expressed in epithelium [30], α-T-catenin is predominantly expressed in cardiac tissue [31] and α-N-catenin is neural specific [32]. Although the subtypes are not exclusively bound to one specific cadherin member, they could still contribute to a functional distinction between classical cadherin members. For instances differences in function have been detected between α-E-catenin and α-N-catenin during Xenopus embryogenesis [33]. Indeed, the crystal structure of E- and α -N catenin suggest that they are differently folded in non-tensed conditions (α -N-catenin being more open). So far no one has yet investigated if these other α-catenin subtypes are capable of mediating a similar mechanosensing mechanism as α-E-catenin. Possibly the incorporation of α-catenin subtype could be influential on the function of the mechanosensing mechanism.

Beside a-catenin and vinculin, yet unidentified mechanically regulated proteins could lead to differences in mechanotransduction functioning among classical cadherins. Cell-cell junctions in the different cell lines used here have a clearly distinct appearance. Maybe the abundance of vinculin-rich, tensile junctions found in the astrocytes could give a clue to possible differential regulation of cadherin subtypes. The hexagonal actin mesh suggests the influence of spectrin; a protein that directs actin-bundles in a hexagonal network. In strong support of differences in mechanotransduction between classical cadherins, the Trepat lab has recently shown that E-cadherin, but not P-cadherin can mediate mechano-regulated collective behaviour in epithelial monolayers [34]. Future investigations should be directed at identifying further tension regulated events at the classical cadherin junction. These may lead to understanding how different classical cadherins drive tissue development and remodelling.

Materials and Methods

Cell culture and cells

Pooled HUVECs (cultured up to passage 6) from different donors (Lonza) and HMEC-1 were cultured in EBM-2 culture medium supplemented with EGM-2 bulletkit (Lonza) on gelatin-coated tissue flasks. Primary Astrocytes were obtained from the neurology department at the Vrije Univesity in Amsterdam and cultured in high glucose DME (Invitrogen) supplemented with 10% FCS (Sigma-Aldrich) and penicillin/streptomycin (Invitrogen) in standard tissue culture dishes.

Antibodies and other reagents

Mouse monoclonal Vinculin antibody hVIN-1 used in IF experiments was obtained from Sigma-Aldrich. Mouse monoclonal Talin 8D4 and rabbit polyclonal α-catenin antibodies were obtained from Sigma-Aldrich. Rabbit polyclonal antibody paxillin (pY118) was from Invitrogen, and antibodies for VE-cadherin were from Cell Signaling Technology. Mouse monoclonal VE-cadherin antibody clone 75 (used at 12.5 μg/ml to block VE-cadherin adhesion) was purchased from BD. Rabbit polyclonal clonal anti-GFP antibody was obtained from Covance. Blebbistatin (used at 100 μM) was from EMD, and Cytochalasin D (used at 0.2 μg/ml) was from Sigma-Aldrich. Fibronectin was purchased from Sigma-Aldrich. Human recombinant $VEGF_{165}$ (used at 50 ng/ml in serum-free medium) was from PeproTech.

DNA constructs and viral transductions

Adenoviral transductions of HUVECs for the experiments with human VE-cadherin fused to GFP (characterized in Allingham et al., 2007; the virus was a gift from J. van Buul, Sanquin, Amsterdam, Netherlands) were performed using a Virapower Adenoviral Expression system (Invitrogen). For lentiviral transductions (all other experiments), human VE-cadherin–GFP was cut out of a peGFP–VE-cadherin vector (provided by J. van Buul) using NdeI and XbaI restriction enzymes and cloned into a self-inactivating lentiviral pLV-CMV-ires-puro vector using the NdeI and NheI restriction sites. The same cloning strategy was used to transfer full-length mouse p120-catenin–mCherry from a pmCherry-n1 vector [15]. Lentiviral expression constructs pRRL-Lifeact-mCherry and pRRL-Vinculin-GFP were a gift of O. Pertz (University of Basel, Basel, Switzerland). HUVECs were infected with supernatant containing lentiviral particles in the presence of 8 μg/ml polybrene overnight

Wide-field IF and live cell microscopy

For live-cell microscopy, cells were plated on Lab-Tek chambered 1.0 borosilicate coverglass slides coated with 3 μg/ml Fibronectin and cultured in EBM-2 culture medium supplemented with EGM-2 bulletkit. For IF stainings, cells were plated on coverslips coated with 3 μg/ml Fibronectin or 1ug/ml Collagen for HUVEC and Astrocytes respectively, and after culture fixed for 15 min in 4% paraformaldehyde, permeabilized with 0.4% Triton X-100 for 5 min, and blocked in 2% BSA for 1 h. Phalloidin, primary, and secondary antibody stainings were performed in 2% BSA for 1 h, and coverslips were mounted in Mowiol4-88/DABCO solution (Sigma-Aldrich). Live (at 37°C) and fixed cells were imaged using an inverted research wide-field microscope (Eclipse Ti; Nikon) with perfect focus system, equipped with a 20× 0.75 NA Plan-Apochromat VC differential interference contrast or a 60× 1.49 NA Apochromat total internal reflection fluorescence (oil) objective lens (all other wide-field experiments), a microscope cage incubator (OkoLab), and an EM charge-coupled device (CCD) camera (Andor Technology) controlled with NIS-Elements Ar 3.2 software. All images were enhanced for display with an unsharp mask filter and/or background subtraction by rolling ball, and brightness/contrast adjustments in ImageJ (National Institutes of Health). Line scans were made from original images using MetaMorph 7.5 software.

Acknowledgements

We would like to thank all members of the de Rooij- group for their intellectual input and Andrea Goudriaan and Mark Verheijen for generous supply of primary astrocytes. This research was financed by the Dutch foundation for cancer research (KWF; grant 2006-3714).

References

1. Alegado, R.A. *et al.* A bacterial sulfonolipid triggers multicellular development in the closest living relatives of animals. *Elife* **1**, e00013 (2012).
2. King, N., Hittinger, C.T. & Carroll, S.B. Evolution of key cell signaling and adhesion protein families predates animal origins. *Science* **301**, 361-363 (2003).
3. Pouliot, Y. Phylogenetic analysis of the cadherin superfamily. *BioEssays : news and reviews in molecular, cellular and developmental biology* **14**, 743-748 (1992).
4. Takeichi, M. Morphogenetic roles of classic cadherins. *Current opinion in cell biology* **7**, 619-627 (1995).
5. Redies, C. Cadherins in the central nervous system. *Progress in neurobiology* **61**, 611-648 (2000).
6. Nose, A., Tsuji, K. & Takeichi, M. Localization of specificity determining sites in cadherin cell adhesion molecules. *Cell* **61**, 147-155 (1990).
7. Volk, T., Cohen, O. & Geiger, B. Formation of heterotypic adherens-type junctions between L-CAM-containing liver cells and A-CAM-containing lens cells. *Cell* **50**, 987-994 (1987).
8. Murphy-Erdosh, C., Yoshida, C.K., Paradies, N. & Reichardt, L.F. The cadherin-binding specificities of B-cadherin and LCAM. *The Journal of cell biology* **129**, 1379-1390 (1995).
9. Shapiro, L. *et al.* Structural basis of cell-cell adhesion by cadherins. *Nature* **374**, 327-337 (1995).
10. Krieg, M. *et al.* Tensile forces govern germ-layer organization in zebrafish. *Nature cell biology* **10**, 429-436 (2008).
11. Landsberg, K.P. *et al.* Increased cell bond tension governs cell sorting at the Drosophila anteroposterior compartment boundary. *Current biology : CB* **19**, 1950-1955 (2009).
12. Monier, B., Pelissier-Monier, A., Brand, A.H. & Sanson, B. An actomyosin-based barrier inhibits cell mixing at compartmental boundaries in Drosophila embryos. *Nature cell biology* **12**, 60-65; sup pp 61-69 (2010).
13. Detrick, R.J., Dickey, D. & Kintner, C.R. The effects of N-cadherin misexpression on morphogenesis in Xenopus embryos. *Neuron* **4**, 493-506 (1990).
14. Levine, E., Lee, C.H., Kintner, C. & Gumbiner, B.M. Selective disruption of E-cadherin function in early Xenopus embryos by a dominant negative mutant. *Development* **120**, 901-909 (1994).
15. le Duc, Q. *et al.* Vinculin potentiates E-cadherin mechanosensing and is recruited to actin-anchored sites within adherens junctions in a myosin II-dependent manner. *The Journal of cell biology* **189**, 1107-1115 (2010).
16. Ladoux, B. *et al.* Strength dependence of cadherin-mediated adhesions. *Biophysical journal* **98**, 534-542 (2010).
17. Liu, Z. *et al.* Mechanical tugging force regulates the size of cell-cell junctions. *Proceedings of the National Academy of Sciences of the United States of America* **107**, 9944-9949 (2010).
18. Yonemura, S., Wada, Y., Watanabe, T., Nagafuchi, A. & Shibata, M. alpha-Catenin as a tension transducer that induces adherens junction development. *Nature cell biology* **12**, 533-542 (2010).
19. Huber, A.H., Stewart, D.B., Laurents, D.V., Nelson, W.J. & Weis, W.I. The cadherin cytoplasmic domain is unstructured in the absence of beta-catenin. A possible mechanism for regulating cadherin turnover. *The Journal of biological chemistry* **276**, 12301-12309 (2001).
20. Schnadelbach, O. *et al.* N-cadherin influences migration of oligodendrocytes on astrocyte monolayers. *Mol Cell Neurosci* **15**, 288-302 (2000).
21. Humphries, J.D. *et al.* Vinculin controls focal adhesion formation by direct interactions with talin and actin. *The Journal of cell biology* **179**, 1043-1057 (2007).
22. Pasapera, A.M., Schneider, I.C., Rericha, E., Schlaepfer, D.D. & Waterman, C.M. Myosin II activity regulates vinculin recruitment to focal adhesions through FAK-mediated paxillin phosphorylation. *The Journal of cell biology* **188**, 877-890 (2010).
23. Riedl, J. *et al.* Lifeact: a versatile marker to visualize F-actin. *Nature methods* **5**, 605-607 (2008).

24. Allingham, M.J., van Buul, J.D. & Burridge, K. ICAM-1-mediated, Src- and Pyk2-dependent vascular endothelial cadherin tyrosine phosphorylation is required for leukocyte transendothelial migration. *J Immunol* **179**, 4053-4064 (2007).
25. Salomon, D., Ayalon, O., Patel-King, R., Hynes, R.O. & Geiger, B. Extrajunctional distribution of N-cadherin in cultured human endothelial cells. *Journal of cell science* **102 (Pt 1)**, 7-17 (1992).
26. Yamada, S. & Nelson, W.J. Localized zones of Rho and Rac activities drive initiation and expansion of epithelial cell-cell adhesion. *The Journal of cell biology* **178**, 517-527 (2007).
27. Breviario, F. *et al.* Functional properties of human vascular endothelial cadherin (7B4/cadherin-5), an endothelium-specific cadherin. *Arteriosclerosis, thrombosis, and vascular biology* **15**, 1229-1239 (1995).
28. Breier, G. *et al.* Molecular cloning and expression of murine vascular endothelial-cadherin in early stage development of cardiovascular system. *Blood* **87**, 630-641 (1996).
29. Fernandez, F.S., Alvarez Vega, M.A., Antuna Ramos, A., Fernandez Gonzalez, F. & Lozano Aragoneses, B. Lead Fractures in Deep Brain Stimulation during Long-Term Follow-Up. *Parkinson's disease* **2010**, 409356 (2010).
30. Nagafuchi, A., Takeichi, M. & Tsukita, S. The 102 kd cadherin-associated protein: similarity to vinculin and posttranscriptional regulation of expression. *Cell* **65**, 849-857 (1991).
31. Janssens, B. *et al.* alphaT-catenin: a novel tissue-specific beta-catenin-binding protein mediating strong cell-cell adhesion. *Journal of cell science* **114**, 3177-3188 (2001).
32. Hirano, S., Kimoto, N., Shimoyama, Y., Hirohashi, S. & Takeichi, M. Identification of a neural alpha-catenin as a key regulator of cadherin function and multicellular organization. *Cell* **70**, 293-301 (1992).
33. Nandadasa, S., Tao, Q., Shoemaker, A., Cha, S.W. & Wylie, C. Regulation of classical cadherin membrane expression and F-actin assembly by alpha-catenins, during Xenopus embryogenesis. *PloS one* **7**, e38756 (2012).
34. Bazellieres, E. *et al.* Control of cell-cell forces and collective cell dynamics by the intercellular adhesome. *Nature cell biology* **17**, 409-420 (2015).

Quantitative imaging of epithelial cell-scattering identifies specific inhibitors of cell motility and cell-cell dissociation

CELL BIOLOGY

Quantitative Imaging of Epithelial Cell Scattering Identifies Specific Inhibitors of Cell Motility and Cell-Cell Dissociation

Dinah Loerke,[1*†] Quint le Duc,[2*] Iris Blonk,[2] Andre Kerstens,[1‡] Emma Spanjaard,[2] Matthias Machacek,[1§] Gaudenz Danuser,[1¶‖] Johan de Rooij[1,2‖]

The scattering of cultured epithelial cells in response to hepatocyte growth factor (HGF) is a model system that recapitulates key features of metastatic cell behavior in vitro, including disruption of cell-cell adhesions and induction of cell migration. We have developed image analysis tools that do not require fluorescence tagging and that automatically track and characterize three aspects of scattering in live cells: increase in cell motility, loss of cell-cell adhesion, and spatial dispersion of cells (the redistribution of cells during scattering). We used these tools to screen a library of drugs, and we identified several efficient inhibitors of scattering, which we classified as selective inhibitors of either motility or loss of cell-cell adhesion, or as nonselective inhibitors. We validated the inhibitors and putative targets from this screen in two unrelated model cell lines. Using pharmacological treatments and RNA interference (RNAi), we found that nonsteroidal anti-inflammatory drugs inhibited cell-cell dissociation, that indirubins inhibited cell motility, and that cyclin-dependent kinase 1 and ribosomal S6 kinase were signaling intermediates in HGF-induced cell scattering. This assay is suitable for larger-scale screenings of chemical compounds or RNAi libraries.

INTRODUCTION

During malignant transformation of locally restricted, benign epithelial tumors, cells lose cell-cell adhesions and develop a motile phenotype that facilitates invasion (*1*). Drugs intended to prevent metastasis in cancer patients are generally designed to inhibit cell migration, for example, by targeting matrix metalloproteinases (MMPs) (*2*). Inhibitors that specifically target the initial loss of cell-cell adhesion have not been identified so far. Such drugs may have clinical potential, but both they and their targets are hard to pinpoint, in part because of a lack of an assay to accurately measure in a high-throughput fashion the state of cell-cell adhesion, which would allow the probing of related signaling pathways by small-molecule inhibitors and RNA interference (RNAi).

A well-established in vitro model system that captures key aspects of malignant transformation in two-dimensional cell culture is the scattering of Madin-Darby canine kidney (MDCK) cells in response to hepatocyte growth factor (HGF) (*3*). HGF is a metastasis-promoting hormone that binds to the receptor cMET, which has been implicated in various malignant human cancers (*4*). This model has been used to investigate pathways involved in tumor invasion, leading to the identification of oncogenes such as Ras, PI3K (phosphatidylinositol 3-kinase), and Src (*5*–*7*). HGF-induced scattering of MDCK cells occurs within 24 hours (*3*) and in three phases (Fig. 1, A and B): (i) cell spreading, (ii) weakening and disruption of cell-cell adhesions, and (iii) increased cell motility (*7*). The combined effect of these processes was reflected in the average cell speed, which started to rise ~2 hours after HGF stimulation, reaching a plateau within 8 to 10 hours, with a half-time of 5 to 6 hours (Fig. 1C). When the formation of cell-cell junctions was prevented in low-calcium conditions, the speed of cells increased more quickly after stimulation (half-time, ~3 hours) (Fig. 1C and movie S1). This suggests that the migration machinery is rapidly activated upon HGF stimulation, but that the migration speed is not increased efficiently until cell-cell adhesion is lost. The dissociation of adhesions is itself promoted by increased cytoskeletal contraction, which is part of the migratory response to HGF (*8*). Therefore, increased cell speed upon HGF stimulation is the combined response of adhesion loss and activation of the migration machinery. If a drug inhibits this increase of cell speed, it is not clear whether the drug prevents cell migration, cell-cell adhesion loss, or both.

To pinpoint the differential contributions of signaling pathways to cell motility and loss of cell-cell adhesion, which would enable the search for adhesion-specific inhibitors, we established a quantitative imaging assay of cell scattering. The assay is based on the analysis of cell trajectories acquired by low-magnification phase-contrast microscopy and automated cell tracking. The acquisition of individual cell tracks from phase-contrast images distinguishes our method from other nonfluorescence image analysis methods that have used population and clustering analyses to quantify cell scattering (*9*, *10*). Our approach avoids the complications of attempting to directly assay cell-cell contacts in low-magnification images of multicellular aggregates. Sampling at six frames per hour is sufficient to identify changes in cell-cell adhesion. Hence, the assay is suitable for image acquisition in a multiwell format on any robotic microscope. As a proof of concept and validation of the assay, we present a screen of small-molecule inhibitors in MDCK cell scattering, which identified 29 efficient

[1]Department of Cell Biology, Scripps Research Institute, 10550 North Torrey Pines Road, La Jolla, CA 92037, USA. [2]Hubrecht Institute for Developmental Biology and Stem Cell Research, Uppsalalaan 8, 3584 CT Utrecht, Netherlands.
*These authors contributed equally to this work.
†Present address: Department of Physics and Astronomy, University of Denver, 2112 East Wesley Avenue, Denver, CO 80208, USA.
‡Present address: Penguin Computing Inc., 45800 Northport Loop West, Fremont, CA 94538, USA.
§Present address: Novartis Pharma AG, Lichtstrasse 35, CH-4056 Basel, Switzerland.
¶Present address: Department of Cell Biology, Harvard Medical School, 240 Longwood Avenue, Boston, MA 02115, USA.
‖To whom correspondence should be addressed. E-mail: j.derooij@hubrecht.eu (J.d.R.); Gaudenz_Danuser@hms.harvard.edu (G.D.)

inhibitors, including 8 drugs that specifically affected cell motility and 9 drugs that specifically inhibited the loss of cell-cell adhesion. We confirmed inhibitor efficiency in a second HGF-responsive model cell line (DU145 prostate carcinoma cells) and directly assessed for specificity on cell-cell adhesion in MDCK cells with cell-cell junctions disrupted by knockdown of the junction protein α-catenin. Finally, several putative targets of efficient drugs were assessed by RNAi-mediated knockdown. These results support the notion that cyclooxygenase 2 (COX-2) functions in formation as well as dissociation of cell-cell junctions and identified the kinases cyclin-dependent kinase 1 (CDK1) and ribosomal S6 kinase (RSK) as signaling intermediates in HGF-induced epithelial cell scattering.

RESULTS

Three parameters derived from cell trajectories define the time course of cell scattering

The movement of individual cells was tracked in phase-contrast images using the dark area generated by the nucleus (note S1). Cell detection and tracking performance were validated with respect to a hand-tracked data set (note S1). Before HGF stimulation, the agreement between computer and manual tracking was 90 to 95%. This discrepancy can be partially explained by rounding of cells during mitosis, which leads to shielding of the dark nuclear area (note S1). After HGF stimulation, the morphological transformation of the cells decreased the detection efficiency to an overall accuracy of 80 to 85% (fig. S1). The field of view of the images typically contained 6 to 10 epithelial cell clusters, composed of 4 to 12 MDCK cells, and some single cells and smaller clusters (movie S1). Thus, at each time point, ~80 cell trajectories suitable for further processing could be harvested from one single time-lapse sequence. In each experiment, three separate time-lapse sequences were collected for each drug condition. This large pool of trajectories then allowed us to extract three parameters of cell motion that specifically reflected the three physical steps of cell scattering: increase in motility, spatial dispersion, and loss of adhesion. We confirmed that the increase of tracking error from before to after HGF stimulation had no systematic effect on any of these three parameters (note S1).

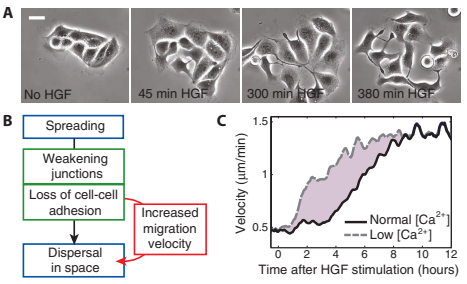

Fig. 1. Physical events during cell scattering. (**A**) Snapshots from a phase-contrast time-lapse image sequence of MDCK cells scattering in response to HGF stimulation. Scale bar, 50 μm. (**B**) Sequence of physical events during cell scattering. (**C**) Time course of average migration velocity (five-frame running average to increase smoothness of curves) in response to HGF stimulation, under normal (n = 1915 cells) and low-calcium conditions (n = 1454 cells).

The motility parameter measures the change in the average speed of cell migration (Fig. 2A and note S2) during cell scattering. Before HGF stimulation, the histogram of individual cell velocities shows a single slow population; after stimulation, a second fast population emerges, the size of which increases over time (Fig. 2B and movie S2). Because rounded cells were not detected, nonmigrating mitotic cells were generally not included in the motility parameter. Thus, unless a drug application strongly affects the rate of cell division rates and duration of mitosis, the motility parameter is robust against variation in cell cycle.

The spatial dispersal parameter measures the redistribution of cells during cell scattering. This parameter is based on the L function (*11*), which is derived from Ripley's K function (*12*) (note S2). In brief, the analysis tests in each time point of a movie whether the number of cells within a radially expanding distance from each cell in the field of view increases, on average, faster or slower than would be expected for a spatially random distribution of cells (Fig. 2C). Before HGF stimulation, adherent cells were clustered in groups, resulting in a distinct positive peak of the L function at distance d_2, which related to the average size of groups (Fig. 2D). For distances between 0 and d_1, the L function value was negative, indicating the exclusion of neighboring nuclei at distances less than the average cell diameter. After HGF stimulation, the function flattened in two phases. First, cell spreading causes radial movement of cells away from the cluster center. Second, cells completely disperse in random directions when cell-cell junctions are disrupted. The rate of flattening in this second phase is the combined result of the velocity and persistence of cell migration. Rapid dispersal rates thus indicate high values for either or both of these cellular behaviors. The flattening was quantified by the time course of the measured area under the L function curve between the characteristic distances d_1 and d_2 (Fig. 2D, fig. S2, and movie S3). Measurement of the L function required the correction of boundary effects caused by the systematic underestimation of the number of neighboring cells near the border of the field of view. Furthermore, the effects of increasing cluster size as a result of cell proliferation were corrected by simulation and subtraction of L function changes associated with cell division (note S3).

The adhesion loss parameter measures the degree of cell-cell adhesion in the cell population on the basis of the motion correlation of neighboring cells (Fig. 2E). For each cell, a correlation value between −1 and +1 was determined by averaging the cosine of the angle between the cell's displacement and the displacements of its nearest neighbors (note S3). Strongly adherent cells in a cluster, which have a high probability of moving locally in parallel, systematically generate correlation values close to 1. In contrast, cells that are detached from one another move independently and thus generate random correlation values with 0 mean. Accordingly, before HGF stimulation, the histogram of correlation values was skewed to positive values (Fig. 2F). Twelve hours after stimulation, the histogram was nearly symmetrical about 0. Hence, at any given time point, the histogram can be decomposed into a positively skewed mode produced by cells that adhere to their neighbors and a symmetrical mode produced by cells that do not adhere to their neighbors (fig. S3 and movie S4). The adhesion loss parameter is then defined as the ratio between the contributions of these two modes to the histogram.

To determine the potency of different drugs to inhibit scattering, we normalized the time courses of the three parameters to the 12-hour effect of a reference sample in which cells were stimulated by HGF only (without any additional drug treatment). Accordingly, in a sample not stimulated by HGF ("no HGF"), the values of the normalized parameters remained close to 0 for the entire experiment (Fig. 2, G to I). In the reference sample ("HGF"), the normalized parameter values increased from

0 to 1 over the course of 12 hours. The fastest increase was in the spatial dispersal parameter (half-time, <3 hours) followed by the adhesion loss parameter (half-time, ~4 hours) and the motility parameter (half-time, <5 hours). If a tested drug was a potent scattering inhibitor, the parameter time courses resembled the no HGF condition; for a weak scattering inhibitor, the parameter time courses resembled the HGF condition.

The parameter of adhesion loss specifically reports the state of cell-cell attachment during cell scattering and is independent of motility and spatial dispersal

To establish that the adhesion loss parameter reports the adhesive state of the cell population and that this parameter is independent of cell motility and spatial dispersal, we determined the parameters in MDCK cells in which the E-cadherin complex, and consequently all cell-cell junctions, was disrupted by short hairpin RNA (shRNA)–mediated knockdown of α-catenin. After the addition of HGF, the motility parameter increased substantially faster in the absence of cell-cell junctions, suggesting that these cells no longer needed to overcome initial resistance to motility (Fig. 3A and movie S5). Moreover, α-catenin–depleted cells also reached a higher speed than wild-type MDCK cells, which likely reflects that loss of cell-cell adhesion is never complete in a population of wild-type MDCK cells and that scattering cells that encounter one another form functional, albeit transient cell-cell junctions even in the prolonged presence of HGF (*8*). Although the junction-compromised cells did cluster in the absence of HGF (movie S5), the adhesion loss parameter under these conditions was already close to 1, consistent with the absence of motion correlation between adjacent cells (Fig. 3B). The motility parameter before HGF stimulation or under unstimulated conditions in α-catenin–depleted cells is similar to that in unstimulated and thus uniformly adherent wild-type cells (Fig. 3A). This confirms that the adhesion loss parameter specifically detects the status of cell-cell adhesion independently of the motility or spatial distribution of cells.

To validate that the observed two modes, correlated and uncorrelated (Fig. 2F and fig. S3), represented subpopulations of attached and detached cells and to further probe the relationship between cell velocities and cell-cell adhesion, we examined the difference in correlation value between

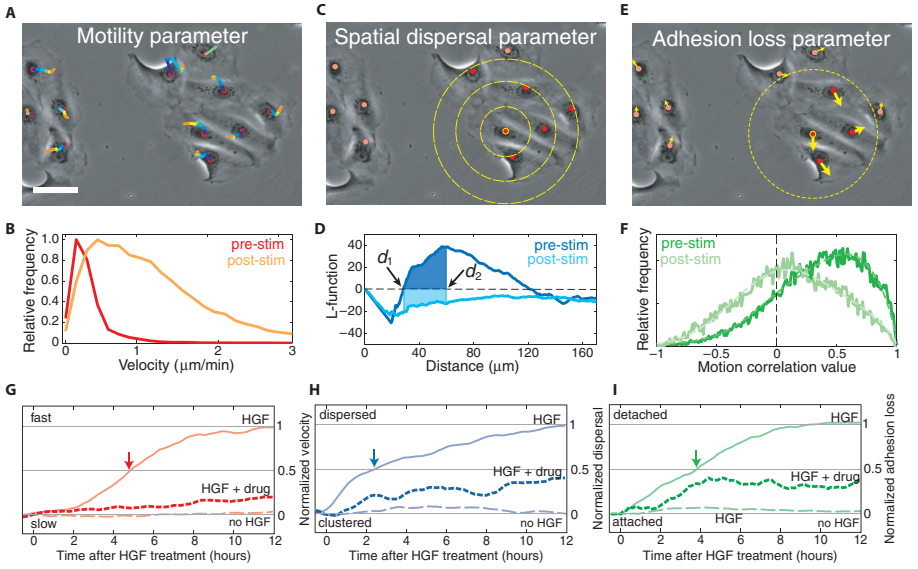

Fig. 2. Three parameters to describe physical phases of scattering. (**A** and **B**) Motility parameter. (A) Color-coded tails depict the cell positions in six previous movie frames, thus indicating the instantaneous cell velocity. Scale bar, 50 μm. (B) Histogram of velocities before and 12 hours after stimulation. (**C** and **D**) Spatial dispersal parameter. Ripley's K function measures the number of neighbors within a radially expanding distance *d* (C). L function before and 12 hours after stimulation (D). The spatial dispersal parameter is defined as the integral between d_1 and d_2 as explained in note S3. (**E** and **F**) Adhesion loss parameter. The adhesion loss parameter of a cell at one time point is derived from the correlation of the displacement vector of the cell with those of its immediately neighboring cells (E). Histogram of correlation values before and 12 hours after stimulation (F). The images and graphs in (A) to (F) are from a single experiment with >100 cells, representative of all (n > 20) unstimulated and HGF-stimulated samples used throughout this study. (**G** to **I**) Normalized time courses (seven-frame rolling average) of motility, spatial dispersal, and adhesion loss parameters for unstimulated (dashed line), HGF-stimulated (solid line), and HGF-stimulated and drug-treated (bold dashed line; PD98059) cells.

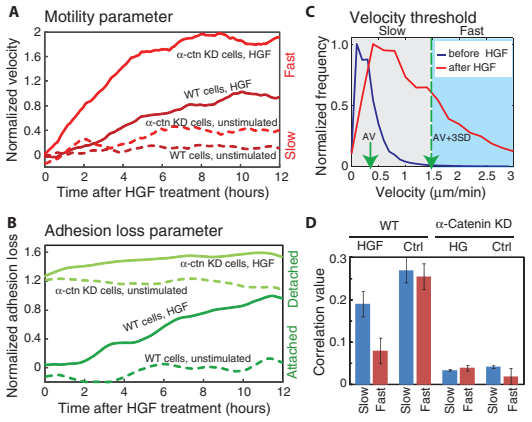

Fig. 3. Adhesion loss parameter reports the state of attachment of the cell population. (A to D) Effects of predissociation of cell-cell junctions (by α-catenin knockdown) on the different scattering parameters. (A) The motility parameter increases more quickly for predissociated cells (by α-catenin knockdown) than for attached cells. WT, wild type. (B) The adhesion loss parameter is high in predissociated cells. (C) Histograms of cell velocities (normalized to bin with maximal occurrence) before and 12 hours after stimulation to define partitioning of slow and fast cells that is used in (D). (D) Average motion correlation of slow and fast cells. HGF-stimulated cells: n = 1915; control (unstimulated) cells: n = 945; HGF-stimulated α-catenin knockdown cells (predissociated cells): n = 647. Unstimulated α-catenin KD cells: n = 761 (n = number of cells).

subpopulations of different velocities. We first pooled the trajectories from three to six movies before and after HGF stimulation, and with and without α-catenin knockdown, over several tens of frames and partitioned cells into "slow" and "fast" populations. The partition threshold was set to $v_{thresh} = \bar{v} + 3\sigma$, where $\bar{v}$ and σ are the average velocity and SD measured before HGF stimulation, respectively (Fig. 3C). Because prestimulation velocities approximate a normal distribution, less than 1% of the unstimulated cells have velocities above the partition threshold. Then, we tested whether the average motion correlation underlying the adhesion loss parameter was different between these two groups (Fig. 3D). We found that in unstimulated wild-type MDCK cells (which showed no loss of initial adhesion), the average correlation value (note S3) was high for both slow and fast populations (0.277 compared to 0.242); in unstimulated or HGF-stimulated α-catenin–negative cells (which did not show adhesion from the onset of the experiment), the average correlation value was low for both slow and fast populations (0.034 compared to 0.018). Thus, under these two conditions in which adhesion was uniform and cell velocity was independent of cell-cell adhesion, the adhesion loss parameter correctly reported equally strong adhesion in unstimulated cells and equally weak adhesion in α-catenin–depleted cells for the different velocity categories. In contrast, in HGF-stimulated samples (in which initial adhesion was lost over time), fast cells had a significantly lower average correlation score (0.074) than slow cells (0.194). This reflects the separation of HGF-treated MDCK cells into two subpopulations: (i) cells that have disrupted their adhesions to neighbors and are free to migrate at high speed and (ii) cells that maintain a certain degree of cell-cell adhesion that inhibits their full migratory potential. Thus, also under the condition in which velocity increase and loss of cell-cell adhesion were related (Fig. 1), the adhesion loss parameter specifically reported the state of cell-cell adhesion of subpopulations of MDCK cells. Thus, combined with the motility parameter and the spatial dispersal parameter describing the overall status of the scattering process, these measurements can be used to investigate the effect of interventions of cell scattering as a whole and to identify targets that differentially affect the motility or cell-cell dissociation response.

A screen of small-molecule inhibitors reveals motility- and adhesion-specific regulators of scattering

To identify signaling intermediates that are involved in the regulation of either cell motility or cell-cell dissociation, we used compounds from a commercially available library of small-molecule inhibitors with known targets (LOPAC 1280). We chose inhibitors of kinases, phosphatases, and mediators of calcium and lipid signaling that are putative intermediates of HGF-induced transformation. We complemented this selection with various commercially available inhibitors of kinases suspected to be activated downstream of the cMET receptor (table S1) and included the cMET inhibitor PHA-665752 as a positive control. The efficiency of an inhibitor was defined as the ratio of the normalized parameter values of the drug-treated condition ("HGF + drug") and that of the reference sample ("HGF") (fig. S4). Time-resolved efficiencies are shown as heat maps for all drug conditions at various concentrations (Fig. 4). These heat maps indicated that some drugs preferentially inhibited one parameter. For instance, the COX inhibitors nimesulide and diclofenac inhibited adhesion loss more efficiently than the increase in cell motility, whereas the protein kinase C (PKC) inhibitor GFX and the focal adhesion kinase (FAK) inhibitor PF573228 inhibited cell motility more efficiently. Some drugs (for example, the PKC activator oleic acid, the phosphatase inhibitor tetramisole hydrochloride, and the serine-threonine kinase inhibitor H-7 dihydrochloride) inhibited the spatial dispersal parameter at early time points, indicating a specific effect on the cell spreading. We speculate that this reflects the effect of isoquinaline sulfonamides on Rho-activated kinase (ROCK) and its downstream target actomyosin (*13*, *14*), but other explanations are possible. The mechanism for the effects by other drugs remains unclear. Here, we focused our analysis on adhesion loss– and motility-specific drugs.

Drugs were ranked on the basis of their maximum efficiency, which we defined as the efficiency 12 hours after stimulation (fig. S5). We referred to those 39 drug conditions that exceeded 66% efficiency for at least one of the three parameters as "effective inhibitors." Hierarchical clustering of all effective inhibitors (using the three efficiencies as the features to measure distances between inhibitors) distinguished three groups of drugs (Fig. 5A). The first group (green) contained inhibitors of targets implicated in the regulation of cell-cell adhesion because their strongest effect was on the adhesion loss parameters (also see Fig. 4 and fig. S6). The second group (red) contained inhibitors of targets implicated in the regulation of cell motility. The third group (brown) contained inhibitors that had similar effects on all three parameters. In the clustering tree, the branches of the unspecific third group merged first with the motility group, which underscores that inhibition of cell motility may affect scattering both directly (because the speed of migration affects the speed of spatial dispersal of the cells) and indirectly [because certain aspects of

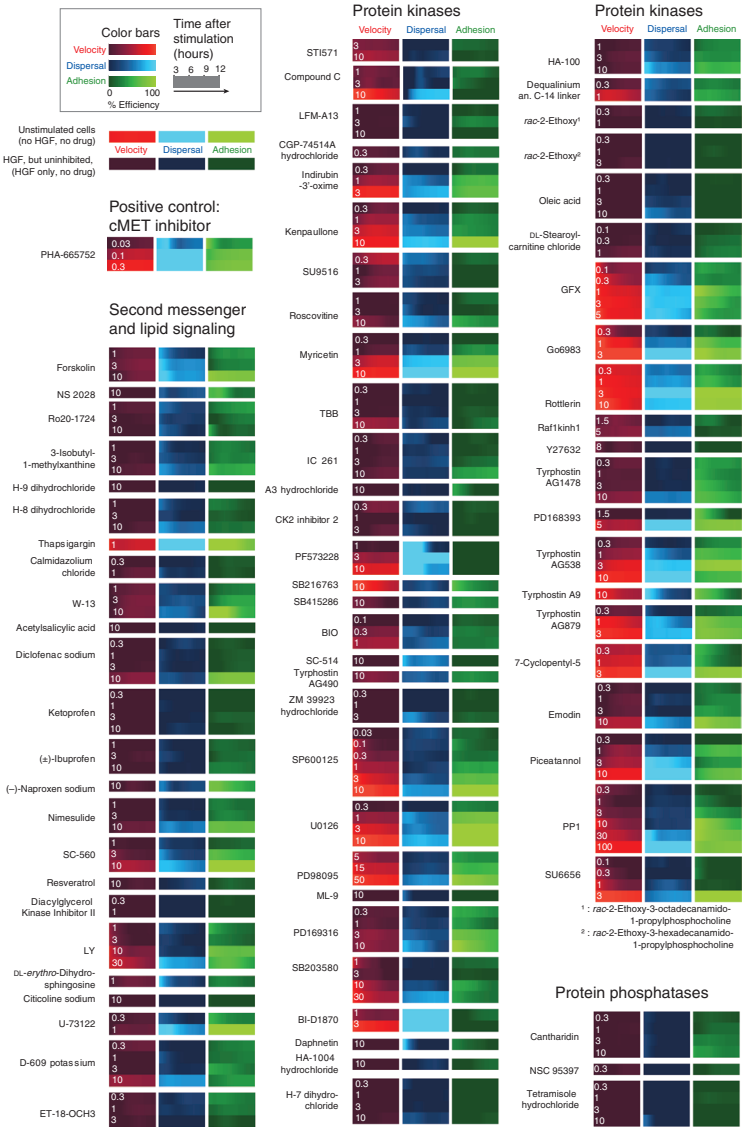

Fig. 4. A small-molecule screen for inhibition of HGF-induced cell scattering. Small-molecule inhibitors were used in a live-cell imaging–based screen of MDCK cell scattering. The resulting time-lapse image series (at least three per condition) was analyzed by the cell tracking software using the three parameters defined in Fig. 2. Color bars represent the inhibition efficiencies over time for all drugs and concentrations used in the screen (see legend). The inhibition efficiency in one parameter is defined as the time-resolved ratio of the normalized parameter values of the drug-treated condition compared to the reference sample. Drugs, targets, and specificity are summarized in table S1. Drug concentrations (μM) are indicated on the leftmost color bar in white.

the motility response, especially the induction of actomyosin contraction, are needed for efficient breakdown of cell-cell junctions (*8*)].

Some drugs were already effective at nonmaximal concentration and therefore yielded entries for multiple concentrations. In the case of the PKC inhibitor GFX, all efficient concentrations of the drug had a motility-specific effect. In other cases, such as the mitogen-activated or extracellular signal–regulated protein kinase kinase (MEK) inhibitor U0126, the PKC family inhibitor rottlerin, and the Src family inhibitors PP1 and piceatannol, specificity toward one parameter at lower concentration was lost at higher concentration. This could reflect a dual function with differential sensitivity to drug inhibition of the targeted protein in both aspects of scattering, or nonspecific targeting of the inhibitors at higher concentrations. Overall, these analyses demonstrate the sensitivity of the three implemented parameters of cell scattering to classify signaling intermediates at the interface between loss of cell-cell adhesion and increased motility.

Comparison of motility of clustered and single cells confirms the specificity of adhesion loss parameter

To further validate drugs classified by hierarchical clustering as adhesion-specific, we implemented an alternative readout of adhesion specificity, which relied only on the difference in cell velocity between clustered cells and single cells (those detected as distinctly isolated by the initial image segmentation). If a drug inhibited the loss of cell-cell adhesion but not the motility increase, isolated cells would be expected to migrate faster than clustered cells. On the other hand, if a drug blocked both the loss of adhesion and the increase in motility, the velocities of single cells and clustered cells would be expected to be similar (see fig. S7 for examples of velocity time courses). Thus, the difference in velocities between isolated and clustered cells was also indicative of the adhesion specificity (quantified by the P value of a two-sided t test of the means of the two velocity distributions). Using this analysis, we found that adhesion-selective drugs (green) had P values <0.05 (Fig. 5B), showing that single cells had significantly higher velocities than clustered cells in samples treated with these drugs. Nonselective drugs (brown) generally scored lower on the significance scale.

Myricetin, PP1, and U0126, which were classified by hierarchical clustering as nonspecific drugs, had high P values in this measurement, indicating a differential inhibitory effect on adhesion loss and motility. The different data interpretations by hierarchical clustering (Fig. 5A) and velocity-based analysis (Fig. 5B) were likely caused by the limitations of the purely velocity-based readout, which depends on an accurate segmentation of single cells compared to clustered cells. Due to stringent selection criteria, only a few fully noncontacting cells were found, which makes this measurement less robust. Also, a velocity-based readout is susceptible to motion artifacts caused by changes of cell morphology. Especially with isolated cells, changes in the cell shape induced by a subgroup of drugs can cause oscillations in the detected cell position. These two factors combined lead to an overestimation of single-cell velocity, and thus a high P value for the velocity difference between isolated and clustered cells. Thus, although this alternative approach of classifying inhibitors overall corroborates the distinction of adhesion-specific inhibitors, we suggest that the combination of all three efficiencies in a hierarchical clustering offers more robust results.

RNAi-mediated disruption of cell-cell adhesion confirms drugs that specifically inhibit adhesion

To directly test the predictive value of our classification, we examined the effects on velocity increase of a subset of efficient inhibitors in α-catenin–depleted MDCK cells (movie S5). Motility-selective drugs would be expected to have equally strong effects in these cell-cell adhesion-defective and wild-type cells, whereas adhesion loss–selective drugs would be expected to be less effective in adhesion-defective cells. Plotting the ratio between percentage inhibition in wild-type and adhesion-defective cells for each drug at a concentration that was in the dynamic range of inhibition showed that adhesion-specific drugs (PP1 and diclofenac) were less effective on adhesion-compromised cells than on adhesive cells (Fig. 5C and fig. S8). Most other drugs, including two drugs previously classified as motility-specific, clustered around a ratio of 0.5, indicating that they retained about 50% of their inhibitory potential in junction-compromised cells. This may reflect that engagement of the motility machinery to increase actomyosin contraction also contributes to the efficient breakdown of cell-cell junctions in MDCK cells after HGF (*8*). Adhesion-defective cells may therefore be less efficiently inhibited by motility-targeting drugs as well. In sum, these analyses validate our classification based only on cell migration dynamics as a powerful tool for the identification of drugs that specifically target the loss of cell-cell adhesion downstream of HGF.

E-cadherin staining confirms the adhesion loss specificity of inhibitors

To investigate whether the specificity of adhesion loss inhibitors was reflected in molecular markers of cell-cell adhesion, we performed immunofluorescence staining of E-cadherin. We quantified the relative intensity of the E-cadherin signal in remaining junctions (a ~400-nm-wide line scan along junctions) over the background signal near the junctions (a 2.6-μm-wide line scan along the junctions) (Fig. 5D). The relative abundance of E-cadherin in cell-cell junctions was variable among individual junctions and, on average, decreased only slightly in response to HGF before junction breakage occurred (Fig. 5E, upper panel). In the presence of the motility-specific inhibitor of FAK (PF573228), the abundance of E-cadherin decreased faster than in control cells. Conversely, in the presence of the adhesion loss–specific COX-2 inhibitor diclofenac, the abundance of E-cadherin decreased less rapidly and to a lesser extent. After 6 hours of HGF treatment, the remaining junctions in cells treated with the adhesion loss–specific inhibitors such as diclofenac and nimesulide or the cMET inhibitor PHA-665752 had higher amounts of E-cadherin in cell-cell junctions than uninhibited or FAK-inhibited cells (Fig. 5E, lower panel). These data indicate that differential effects on molecular parameters of cell-cell adhesion were exerted by adhesion loss– and migration-specific inhibitors. However, because of the minor loss of E-cadherin, it is questionable that this molecular measure is a reliable estimate of adhesion strength. This corroborates our earlier work on MDCK cell scattering in which we found that the buildup of physical forces, rather than a gradual loss of E-cadherin by internalization, precedes cell-cell junction disruption (*8*). For a second independent validation of the adhesion loss parameter, we quantified by immunofluorescence the number of cell-cell junctions at increasing times after HGF. The adhesion loss–specific inhibitors diclofenac and nimesulide and the cMET inhibitor PHA-665752 blocked the loss of cell-cell junctions after stimulation, whereas FAK inhibition did not (Fig. 5F). Together, these analyses not only further establish the validity of the migration-based readout of cell-cell adhesion strength used in our screen, but they also demonstrate that an assessment of adhesion strength by immunofluorescence of adhesion components is more ambiguous than the proposed live-cell assay.

Verification of efficient inhibitors in unrelated cells

DU145 cells are human prostate cancer cells that scatter in response to HGF. Because of the importance of HGF in prostate cancer and the possible use of this cell line as a model for drug- or small interfering RNA (siRNA)–based target discovery, we compared the scattering process between MDCK and DU145 cells. We tested 17 efficient drugs covering all

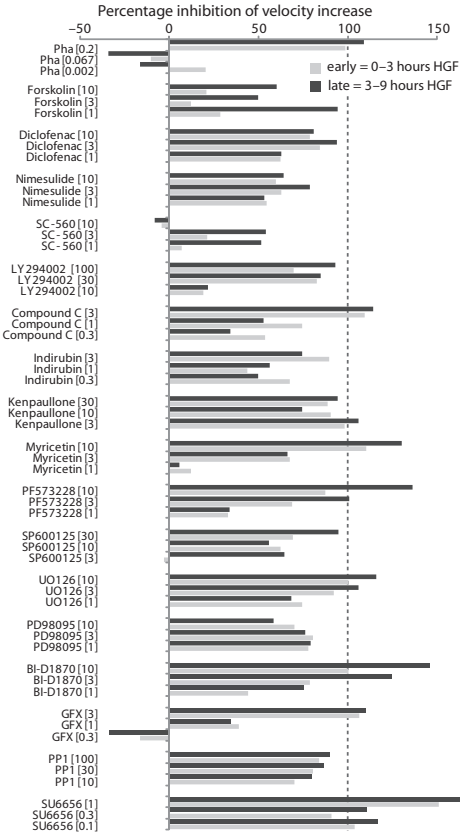

Fig. 6. Inhibition efficiency of MDCK-effective drugs on DU145 cell scattering. The average inhibition efficiency of the motility response in early (0 to 3 hours after HGF) and late phases (3 to 9 hours after HGF) of DU145 cell scattering is depicted for 18 efficient inhibitors of MDCK cell scattering, including the cMET inhibitor PHA-665752 as a positive control. Concentration of drugs in μM is indicated between brackets.

predicted intracellular signaling intermediates from the screen on the human DU145 cell line. Most drugs (except the COX inhibitor SC-560 and the adenylyl cyclase activator forskolin) reproduced their inhibitory effect on the HGF-induced scatter response as measured by velocity increase (Fig. 6), which suggests that cells from different species and from different organs respond to HGF through conserved molecular mechanisms that can be targeted by the same chemical inhibitors.

Validation of drug targets by RNAi

Several of the efficient inhibitors from our chemical screen target intermediates of scattering or cell migration such as Src, FAK, PI3K, and PKC. The screen also identified various less characterized drug targets, which we explored in more detail. Indirubin-3-oxime and kenpaullone, two efficient nonselective inhibitors of scattering, are CDK inhibitors with side effects on other kinases, including glycogen synthase kinase 3β (GSK-3β), LCK, and serum- and glucocorticoid-induced protein kinase (SGK). We eliminated some of these possible targets by showing that the CDK2 inhibitor roscovitine and the GSK-3β–specific inhibitor SB216763 (both included in the screen) did not inhibit scattering. Because CDK5 has been previously implicated in prostate cancer cell migration (*15*), we used siRNA-mediated knockdown in DU145 cells to directly test the role in HGF-induced scattering of CDK5 and a close homolog, CDK1, which is also targeted by these drugs. siRNA-mediated knockdown of CDK1, but not CDK5, significantly inhibited scattering (Fig. 7, A and B, and movie S6). Because CDK1 is a regulator of cell cycle progression, we were concerned that the effects of RNAi on the motility parameter could be related to an increased population of nonmigrating cells arrested in mitosis (note S2). The rate of cell division was affected by CDK1 RNAi (Fig. 7C). However, the percentage of tracked cells that undergo mitosis was too low to affect the average velocity and was not altered by CDK1 depletion (as judged from the individual velocity profiles of all cells that were fully tracked between 3 and 6 hours after HGF) (Fig. 7D). Also, the duration of mitosis was not altered by CDK1 RNAi as judged from the individual cell velocity profiles (Fig. 7E). Thus, these results identify CDK1, but not CDK5, as an intermediate in HGF-induced scattering of DU145 cells.

We also examined COX-2 inhibitors, several of which emerged as selective inhibitors of the loss of cell-cell adhesion in the screen. Indeed, COX-2 abundance was increased after 2 hours of HGF stimulation of MDCK cells (Fig. 7F). Using shRNA constructs against canine COX-2, we reduced its abundance in HGF-stimulated cells to below its abundance in unstimulated cells (Fig. 7F). The effect of COX-2 inhibition by RNAi, however, was opposite that of drug-induced inhibition of COX-2: COX-2 RNAi resulted in a more rapid and higher increase in cell velocity than in control cells, similar to the effect of E-cadherin depletion in MDCK cells (Fig. 7F and movie S7). Because two unrelated shRNAs targeting COX-2 showed the same effect, these results are unlikely due to an off-target effect of the shRNA constructs. We propose that COX-2 protects cell-cell junctions from HGF-induced disruption in MDCK cells, whereas chemical inhibition of COX-2 prevents the efficient breakdown of cell-cell junctions by HGF. Whether the latter effect is through inhibition of COX-2 enzymatic activity or due to off-target effects of these drugs remains to be investigated.

An effective motility-selective drug was BI-D1870, which targets p90RSK family members. HGF induced rapid and prolonged phosphorylation of several residues in RSKs (Fig. 7G, right panel), which is consistent with the upstream induction of mitogen-activated protein kinase (MAPK) signaling. Targeting the RSK1 and RSK2 by siRNA reduced the overall abundance and phosphorylation of RSKs and inhibited the HGF response in DU145 cells (Fig. 7G and movie S8). Thus, we conclude that the RSK family kinases are signaling intermediates in HGF-induced scattering that specifically mediate the cell motility response.

DISCUSSION

We have developed a quantitative assay for epithelial cell scattering based on phase-contrast imaging and tracking of cell nuclei and demonstrated its use in a screen of chemical inhibitors to identify specific regulators of cell

motility or loss of cell-cell adhesion downstream of HGF in MDCK cells. We identified 29 efficient inhibitors of scattering, including 8 inhibitors of motility response and 9 inhibitors of cell-cell dissociation. Using the human prostate carcinoma cell line (DU145), we verified that drugs targeting the HGF response are efficient in an unrelated cell line from a different species and organ. Furthermore, we have validated the predictive value of

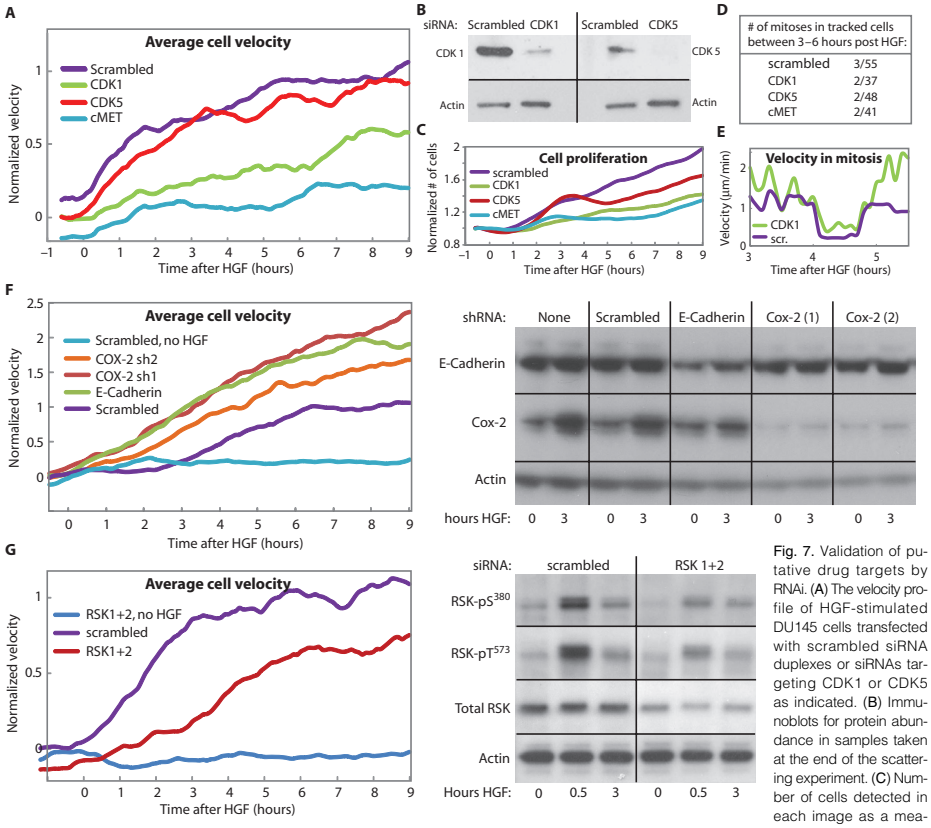

Fig. 7. Validation of putative drug targets by RNAi. (**A**) The velocity profile of HGF-stimulated DU145 cells transfected with scrambled siRNA duplexes or siRNAs targeting CDK1 or CDK5 as indicated. (**B**) Immunoblots for protein abundance in samples taken at the end of the scattering experiment. (**C**) Number of cells detected in each image as a measure of cell proliferation. (**D**) Number of cell velocity time courses with a substantial drop in velocity between 3 and 6 hours after HGF stimulation (which is indicative of cells in mitosis) compared to the total number of cell tracks in the same period. (**E**) Single-cell velocity time courses of a CDK1-depleted cell that goes through mitosis compared to a cell treated with scrambled siRNA. The data in (A) to (E) were taken from a single representative experiment that was repeated four times. The velocity graphs are an average of the analysis of three time-lapse image sequences for each condition from this experiment. (**F**) Left: The velocity profile of HGF-stimulated MDCK cells transfected with a nontargeting shRNA construct or shRNA constructs targeting E-cadherin or COX-2 as indicated. Right: Immunoblots for protein abundance in parallel samples taken at the indicated time points during this scattering experiment. Data are from a single representative experiment that was repeated six times. The velocity profile is an average of the analysis of three time-lapse image sequences for each condition from this experiment. (**G**) Left: The velocity profile of HGF-stimulated DU145 cells transfected with scrambled siRNA duplexes or siRNAs targeting RSK1, RSK2, or both, as indicated. Right: Immunoblots for protein abundance and phosphorylation of the two indicated sites in parallel samples taken at the indicated time points during this scattering experiment. Data are from a representative experiment that was repeated three times. The velocity profile is an average of the analysis of three time-lapse image sequences for each condition from this experiment.

the cell-cell adhesion specificity classifier with cell-cell junction-defective cells and by direct observation of E-cadherin aggregation in junctions. Finally, we have used RNAi to validate the drug targets CDK1 and RSK as signaling intermediates in HGF-induced cell scattering.

A key feature of our assay is the use of an indirect measure of cell-cell adhesion through the correlated movement of neighboring cells, following the notion that cell-cell junctions restrict and coordinate migration of cells in a cluster. If correlated cell movement is also promoted by mechanisms beyond cell-cell junctions, like polarized paracrine signaling, effects of drugs on such a mechanism would also affect this parameter. To our knowledge, such mechanisms have not been previously described for either the MDCK or the DU145 systems, but this possibility should be taken into account when using this assay. We have validated our assay by several alternative approaches (Fig. 5) including the use of junction-compromised (α-catenin–depleted) cells. Subsequently, we applied the assay to identify several drugs that specifically interfere with adhesion loss during HGF-induced cell scattering.

For all tested drugs, we considered the possibility that effects on scattering were due to inhibition of other yet unidentified targets (*13*, *14*). Controlling compound specificity in separate biochemical experiments was beyond the scope of this study, which aimed to provide a low-cost, high-yield screening method for the identification of drugs selective for inhibition of motility and loss of cell-cell adhesion. Nevertheless, in cases in which we identified several drugs targeting one protein family (such as Src, PKC, or COX), it is more likely that the observed effect was through inhibition of these specific proteins. It is interesting to note that inhibitors with different selectivity for the individual Src family members are classified as motility-specific (piceatannol), adhesion-specific (emodin, PP1), or nonspecific [su6656, 7-cyclopentyl-5-(4-phenoxy)phenyl-7*H*-pyrrolo[2,3-*d*]pyrimidin-4-ylamine]. This result underscores the differential roles these individual Src family members play and highlights the potential for developing member-specific drugs.

A prominent group of efficient inhibitors of cell-cell dissociation we identified belongs to the class of nonsteroidal anti-inflammatory drugs (NSAIDs), which target COX enzymes: nimesulide, SC-560, and diclofenac sodium (movie S7). Of the two mammalian family members, COX-2 is regulated at the level of protein expression and is increased in several types of invasive cancer including colon cancer (*16*). Consistent with our result that COX-2 inhibitors slow the loss of cell-cell adhesion upon HGF stimulation, COX-2 reduces E-cadherin–dependent cell-cell adhesion by activating RhoA (*17*) or by inhibiting expression of the gene encoding E-cadherin through the transcription factors Snail and ZEB1 (*18*). COX-2 has also been implicated in HGF-induced angiogenesis, which involves disruption of endothelial cell-cell junctions (*19*). Surprisingly, we found that knockdown of COX-2 resulted in increased scattering, comparable to the effect of E-cadherin knockdown. This suggests that COX-2 depletion is not compatible with the formation of stable cell-cell adhesion in MDCK cells. The difference in effects between chemical inhibition and RNAi-mediated interference could be caused by different effects of long-term reduction of protein abundance compared to short-term inhibition and suggests that COX-2 functions both in formation and in dissociation of cell-cell junctions. This also highlights the notion that target discovery by RNAi may yield different results from drug discovery by chemical screening. The alternative explanation for the difference in this case is that these NSAIDs target other enzymes to inhibit cell-cell dissociation. Nevertheless, NSAIDs are drugs that have a selective effect on the HGF-induced loss of cell-cell adhesion, which makes them interesting lead compounds for anti-metastasis drug development.

Drugs based on the natural compound indirubin have been extensively studied and have been used as anticancer treatment predominantly in chronic myeloid leukemia. Because their main targets are the CDKs (*20*), their effect is thought to be inhibition of cell division. However, indirubin-based drugs target several other kinase families including GSK-3 and the SGK family kinases. Our current results show that indirubin-3-oxime is a potent inhibitor of HGF-induced cell scattering, which adds a new spectrum to the clinical potential of indirubin-derived compounds. Whether indirubin-3-oxime's effect on scattering is mediated through inhibition of CDKs is not yet fully established. On the basis of our inhibitor screen, we can exclude most of the alternative kinase targets as well as the cell cycle member CDK2 as the indirubin-3-oxime target involved in inhibited scattering. Efficient knockdown of CDK5 did not affect scattering, and thus, we can also exclude a role of CDK5 in this process. On the other hand, knockdown of CDK1 inhibited DU145 cell scattering. CDK1 was previously shown to stimulate cell migration in a different prostate cancer cell line, LNCaP (*21*).

RSK family kinases have multiple downstream substrates and multiple intracellular functions (*22*). They are crucial for the Ras-MAPK–induced motility of MDCK cells (*23*), and pharmacological inhibition of RSKs inhibits the effect of 31 migration-inducing shRNA treatments (*24*). Our results show that RSK is phosphorylated downstream of HGF and that its pharmacological inhibition as well as knockdown of two of its isoforms inhibits HGF-induced cell scattering by decreasing cell motility. This places RSK at a crucial position in the signaling cascade leading from cMET activation to cell scattering and underscores the potential of RSK family kinases as drug targets in cMET-positive metastatic cancer (*23*).

In summary, we have developed a robust image analysis tool that can be used in any standard laboratory setting to track cells and distinguish inhibitory effects by drugs and RNAi on cell motility and cell-cell adhesion during epithelial transformation. The data from our screen confirms the involvement of a number of signaling molecules (such as MEK, PI3K, PKC, and Src) in HGF-induced metastatic cell behavior. They identify NSAIDs as drugs that specifically target the disruption of cell-cell adhesion downstream of HGF, indirubins as drugs that target cell motility downstream of HGF, and CDK1 and RSK as cMET signaling intermediates and putative drug targets.

MATERIALS AND METHODS

Phase-contrast microscopy

We used different microscope systems—Zeiss Axiovert 200M, Leica AF7000, and Nikon Ti—all similarly equipped with robotic stages and controlled by company software (AxioVision, LAS-AF, and NIS-Elements). Cameras on these systems were a 10-bit charge-coupled device (CCD) AxioCam camera (Zeiss), a 12-bit CCD DFC365 FX camera (Leica), and a 12-bit electron multiplying CCD (EMCCD) Luka camera (Andor). Images were acquired with comparable 10× 0.5 numerical aperture (NA) Plan objective lenses and compatible LWD condensers.

Cell culture

MDCK cells were plated in Dulbecco's modified Eagle's medium (DMEM) (Gibco) supplemented with 0.5% fetal calf serum (FCS) (Sigma) and 10 mM Hepes (pH 7) 24 hours before imaging at a density of 5500 cells/cm^2 in collagen type 1 (3 μg/ml; Sigma)–coated, non–tissue-culture–treated polystyrene 48- or 96-well plates (Nunc). DU145 cells were plated in RPMI medium (Gibco) supplemented with 10% FCS (Sigma) 48 hours before imaging at a density of 5000 cells/cm^2 in collagen type 1 (10 μg/ml; PureCol)–coated, non–tissue-culture–treated polystyrene 48-well plates (Nunc). Twenty-four hours before imaging, the medium was replaced by medium containing 0.5% FCS. Immediately before imaging, drugs were

added and wells were completely filled with medium and sealed with silicon grease and a glass plate. Cells were imaged for 2 hours before stimulation and then wells were opened briefly for HGF addition, after which imaging continued for at least 9 hours. To establish low-Ca^{2+} conditions, we used calcium-free DMEM (Gibco) supplemented with 0.06 mM $CaCl_2$, 0.5% FCS, and 10 mM Hepes (pH 7).

RNA interference

For RNAi in MDCK cells, 19 nucleotide target sequences were cloned into pSuper and transfected by two rounds of nucleofection (Lonza, DE) with buffer L and program T-020 4 and 2 days before imaging. Sequences were as follows: E-cadherin: 5′-AGCAGTATGTCTTGTACGT-3′, COX-2 sh1: 5′-ATGGGATGATGAGCGGTTA-3′, and COX-2 sh2: 5′-GGGAGTCTGGAACATTGTC-3′. MDCK cells stably expressing an α-catenin knockdown sequence were a gift from J. Nelson and was described previously (*25*). For RNAi in DU145 cells, RNA duplexes were transfected with HiPerFect (Qiagen) according to the manufacturer's protocols 3 days before imaging. We used the following sequences—for RSK-1, 5′-CCCAACATCATCACTCTGAAA-3′, and for RSK-2, 5′-AGCGCTGAGAATGGACAGCAA-3′—that were previously tested in (*26*). For CDK1 and CDK5, we used ON-TARGET plus SMARTpools from Thermo Scientific Dharmacon.

Western blotting

For the analysis of protein abundance, we performed SDS–polyacrylamide gel electrophoresis (SDS-PAGE) with NuPage gradient gels (Invitrogen) and standard Western blotting on polyvinylidene difluoride membranes. The antibody directed against CDK5 was from Cell Signaling; those directed against COX-2, CDK1, and E-cadherin (clone 36) were from BD Biosciences; and those directed against total RSK, pS^{380}-RSK, and pT^{573}-RSK were from Cell Signaling. Actin (clone C4) was from Millipore.

Immunofluorescence analysis of E-cadherin and junction disruption

The immunofluorescence staining and quantification of E-cadherin levels in junctions in Fig. 5, D to F, were as follows. Cells were grown on collagen (3 μg/ml)–coated coverslips for 24 hours and then stimulated for the indicated times with HGF. The appropriate drugs were added 10 min before addition of HGF (or 10 min before fixation if no HGF was added). Cells were washed once in ice-cold phosphate-buffered saline (PBS), once in ice-cold cytoskeletal buffer (*27*), and then once more in ice-cold PBS and fixed in 4% paraformaldehyde. The E-cadherin antibody used was clone 36 (BD Biosciences). Imaging was performed on a Nikon Ti epifluorescence microscope equipped with a 12-bit EMCCD Luka camera (Andor) and a 40× 1.3 NA Plan Fluor objective lens. The relative abundance of E-cadherin in cell-cell junctions was measured by drawing a line on top of a junction fragment (from one tricellular junction to the next or along the full junction between two cells) and dividing the average pixel intensity in a 3-pixel line scan (corresponding to 400 nm) along this line over the average pixel intensity in a 20-pixel line scan (2.6 μm) along this line. Values were normalized to the unstimulated, drug-treated conditions. To quantify the average number of cell-cell junctions per cell in Fig. 5D, we determined for each cell in these images the number of contacts with neighboring cells that showed discernible E-cadherin signal (irrespective of the length of contact).

Image analysis and parameter identification

Details of the methods for image analysis and cell tracking are in note S1. The identification of parameters that specify the diverse physical aspects of cell scattering is explained in notes S2 to S4. The metric used for hierarchical clustering of drug effects on cell scattering is defined in note S5 along with a discussion of cluster validation procedures.

SUPPLEMENTARY MATERIALS

www.sciencesignaling.org/cgi/content/full/5/231/rs5/DC1
Note S1. Phase-contrast image analysis, cell detection, and tracking.
Note S2. Quantifying cell migration and dealing with mitotic cells.
Note S3. Quantifying spatial dispersal using Ripley's K function.
Note S4. Quantifying cell-cell adhesion.
Note S5. Hierarchical clustering.
Fig. S1. Cell tracking.
Fig. S2. Definition of spatial dispersion parameter based on Ripley's K function.
Fig. S3. Definition of adhesion loss parameter based on motion correlation.
Fig. S4. Inhibition efficiency for motility, dispersal, and adhesion loss parameters.
Fig. S5. Ranked inhibition efficiencies.
Fig. S6. Validation of hierarchical clustering.
Fig. S7. Velocity differences indicate adhesion specificity.
Fig. S8. Inhibition efficiency of effective drugs on the scattering of normal and cell-cell junction-compromised MDCK cells.
Table S1. Target names and additional information on drugs used in screen.
References
Movie S1. The presence of cell-cell adhesions slows down HGF-induced cell motility.
Movie S2. Motility parameter.
Movie S3. Spatial dispersion parameter.
Movie S4. Adhesion loss parameter.
Movie S5. α-Catenin–depleted cells do not form functional cell-cell junctions.
Movie S6. Knockdown of CDK1 but not CDK5 inhibits the HGF-induced increase in cell motility.
Movie S7. Diclofenac inhibits the HGF-induced loss of cell-cell adhesion, whereas knockdown of COX-2 reduces the stability of cell-cell junctions.
Movie S8. Blocking RSKs by chemical inhibition or siRNA-mediated knockdown inhibits the HGF-induced increase in cell motility.

REFERENCES AND NOTES

1. J. P. Thiery, Epithelial–mesenchymal transitions in tumour progression. *Nat. Rev. Cancer* **2**, 442–454 (2002).
2. J. E. Fata, Z. Werb, M. J. Bissell, Regulation of mammary gland branching morphogenesis by the extracellular matrix and its remodeling enzymes. *Breast Cancer Res.* **6**, 1–11 (2004).
3. M. Stoker, M. Perryman, An epithelial scatter factor released by embryo fibroblasts. *J. Cell Sci.* **77**, 209–223 (1985).
4. C. Birchmeier, W. Birchmeier, E. Gherardi, G. F. Vande Woude, Met, metastasis, motility and more. *Nat. Rev. Mol. Cell Biol.* **4**, 915–925 (2003).
5. J. Behrens, L. Vakaet, R. Friis, E. Winterhager, F. Van Roy, M. M. Mareel, W. Birchmeier, Loss of epithelial differentiation and gain of invasiveness correlates with tyrosine phosphorylation of the E-cadherin/β-catenin complex in cells transformed with a temperature-sensitive v-SRC gene. *J. Cell Biol.* **120**, 757–766 (1993).
6. A. Khwaja, K. Lehmann, B. M. Marte, J. Downward, Phosphoinositide 3-kinase induces scattering and tubulogenesis in epithelial cells through a novel pathway. *J. Biol. Chem.* **273**, 18793–18801 (1998).
7. A. J. Ridley, P. M. Comoglio, A. Hall, Regulation of scatter factor/hepatocyte growth factor responses by Ras, Rac, and Rho in MDCK cells. *Mol. Cell. Biol.* **15**, 1110–1122 (1995).
8. J. de Rooij, A. Kerstens, G. Danuser, M. A. Schwartz, C. M. Waterman-Storer, Integrin-dependent actomyosin contraction regulates epithelial cell scattering. *J. Cell Biol.* **171**, 153–164 (2005).
9. M. D. Pope, N. A. Graham, B. K. Huang, A. R. Asthagiri, Automated quantitative analysis of epithelial cell scatter. *Cell Adh. Migr.* **2**, 110–116 (2008).
10. A. Zaritsky, S. Natan, J. Horev, I. Hecht, L. Wolf, E. Ben-Jacob, I. Tsarfaty, Cell motility dynamics: A novel segmentation algorithm to quantify multi-cellular bright field microscopy images. *PLoS One* **6**, e27593 (2011).
11. J. Besag, Contribution to the discussion of Dr Ripley's paper. *J. R. Stat. Soc. Ser. B* **39**, 193–217 (1977).
12. B. D. Ripley, The second-order analysis of stationary point processes. *J. Appl. Prob.* **13**, 255–266 (1976).
13. J. Bain, H. McLauchlan, M. Elliott, P. Cohen, The specificities of protein kinase inhibitors: An update. *Biochem. J.* **371**, 199–204 (2003).
14. J. Bain, L. Plater, M. Elliott, N. Shpiro, C. J. Hastie, H. McLauchlan, I. Klevernic, J. S. Arthur, D. R. Alessi, P. Cohen, The selectivity of protein kinase inhibitors: A further update. *Biochem. J.* **408**, 297–315 (2007).

15. C. J. Strock, J. I. Park, E. K. Nakakura, G. S. Bova, J. T. Isaacs, D. W. Ball, B. D. Nelkin, Cyclin-dependent kinase 5 activity controls cell motility and metastatic potential of prostate cancer cells. *Cancer Res.* **66**, 7509–7515 (2006).
16. C. S. Williams, M. Mann, R. N. DuBois, The role of cyclooxygenases in inflammation, cancer, and development. *Oncogene* **18**, 7908–7916 (1999).
17. Y. W. Chang, J. W. Marlin, T. W. Chance, R. Jakobi, RhoA mediates cyclooxygenase-2 signaling to disrupt the formation of adherens junctions and increase cell motility. *Cancer Res.* **66**, 11700–11708 (2006).
18. M. Dohadwala, S. C. Yang, J. Luo, S. Sharma, R. K. Batra, M. Huang, Y. Lin, L. Goodglick, K. Krysan, M. C. Fishbein, L. Hong, C. Lai, R. B. Cameron, R. M. Gemmill, H. A. Drabkin, S. M. Dubinett, Cyclooxygenase-2–dependent regulation of E-cadherin: Prostaglandin E_2 induces transcriptional repressors ZEB1 and Snail in non–small cell lung cancer. *Cancer Res.* **66**, 5338–5345 (2006).
19. S. Sengupta, L. A. Sellers, T. Cindrova, J. Skepper, E. Gherardi, R. Sasisekharan, T. P. Fan, Cyclooxygenase-2-selective nonsteroidal anti-inflammatory drugs inhibit hepatocyte growth factor/scatter factor-induced angiogenesis. *Cancer Res.* **63**, 8351–8359 (2003).
20. R. Hoessel, S. Leclerc, J. A. Endicott, M. E. Nobel, A. Lawrie, P. Tunnah, M. Leost, E. Damiens, D. Marie, D. Marko, E. Niederberger, W. Tang, G. Eisenbrand, L. Meijer, Indirubin, the active constituent of a Chinese antileukaemia medicine, inhibits cyclin-dependent kinases. *Nat. Cell Biol.* **1**, 60–67 (1999).
21. T. Manes, D. Q. Zheng, S. Tognin, A. S. Woodard, P. C. Marchisio, L. R. Languino, $\alpha_v\beta_3$ integrin expression up-regulates cdc2, which modulates cell migration. *J. Cell Biol.* **161**, 817–826 (2003).
22. R. Anjum, J. Blenis, The RSK family of kinases: Emerging roles in cellular signalling. *Nat. Rev. Mol. Cell Biol.* **9**, 747–758 (2008).
23. U. Doehn, C. Hauge, S. R. Frank, C. J. Jensen, K. Duda, J. V. Nielsen, M. S. Cohen, J. V. Johansen, B. R. Winther, L. R. Lund, O. Winther, J. Taunton, S. H. Hansen, M. Frodin, RSK is a principal effector of the RAS-ERK pathway for eliciting a coordinate promotile/invasive gene program and phenotype in epithelial cells. *Mol. Cell* **35**, 511–522 (2009).
24. G. A. Smolen, J. Zhang, M. J. Zubrowski, E. J. Edelman, B. Luo, M. Yu, L. W. Ng, C. M. Scherber, B. J. Schott, S. Ramaswamy, D. Irimia, D. E. Root, D. A. Haber, A genome-wide RNAi screen identifies multiple RSK-dependent regulators of cell migration. *Genes Dev.* **24**, 2654–2665 (2010).
25. J. M. Benjamin, A. V. Kwiatkowski, C. Yang, F. Korobova, S. Pokutta, T. Svitkina, W. I. Weis, W. J. Nelson, αE-catenin regulates actin dynamics independently of cadherin-mediated cell–cell adhesion. *J. Cell Biol.* **189**, 339–352 (2010).
26. R. Anjum, P. P. Roux, B. A. Ballif, S. P. Gygi, J. Blenis, The tumor suppressor DAP kinase is a target of RSK-mediated survival signaling. *Curr. Biol.* **15**, 1762–1767 (2005).
27. I. S. Näthke, L. Hinck, J. R. Swedlow, J. Papkoff, W. J. Nelson, Defining interactions and distributions of cadherin and catenin complexes in polarized epithelial cells. *J. Cell Biol.* **125**, 1341–1352 (1994).

Funding: A.K., M.M., and G.D. were supported by NIH grants P50GM68762 and U01GM067230, and G.D. by R01GM071868. D.L. was partially supported by the Dale Tooley Cancer Research Fund. J.d.R., I.B., and Q.I.D. were supported by grant 2006-3714 from the Dutch Cancer Society (KWF Kankerbestrijding). E.S. was supported by a grant from the Netherlands Genomics Initiative to J.d.R. **Author contributions:** D.L. wrote the software package with assistance from E.S., A.K., and M.M.; performed data analysis; and coauthored the manuscript. Q.I.D. and I.B. designed and performed live-cell interference experiments. G.D. and J.d.R. designed the study and authored the manuscript with D.L. J.d.R. performed the initial set of live-cell experiments and advised Q.I.D. and I.B. in further experimental studies. **Competing interests:** The authors declare that they have no competing interests.

Submitted 10 November 2011
Accepted 15 June 2012
Final Publication 3 July 2012
10.1126/scisignal.2002677
Citation: D. Loerke, Q. le Duc, I. Blonk, A. Kerstens, E. Spanjaard, M. Machacek, G. Danuser, J. de Rooij, Quantitative imaging of epithelial cell scattering identifies specific inhibitors of cell motility and cell-cell dissociation. *Sci. Signal.* **5**, rs5 (2012).

Science Signaling
AAAS

www.sciencesignaling.org/cgi/content/full/5/231/rs5/DC1

Supplementary Materials for

Quantitative Imaging of Epithelial Cell Scattering Identifies Specific Inhibitors of Cell Motility and Cell-Cell Dissociation

Dinah Loerke, Quint le Duc, Iris Blonk, Andre Kerstens, Emma Spanjaard, Matthias Machacek, Gaudenz Danuser,* Johan de Rooij*

*To whom correspondence should be addressed. E-mail: j.derooij@hubrecht.eu (J.d.R.); Gaudenz_Danuser@hms.harvard.edu (G.D.)

Published 3 July 2012, *Sci. Signal.* **5**, rs5 (2012)
DOI: 10.1126/scisignal.2002677

Note S1: Phase-contrast image analysis, cell detection, and tracking.

The ScatterTrack image-analysis software was developed to automatically process large data sets with minimal requirements for user interaction. The image processing consists of

- image segmentation to detect cell locations and clusters, based on adaptive intensity threshold selection in the intensity distribution of the raw images for the distinction of cell nucleus, cell area, and cell-free image background;
- cell tracking, using a global nearest neighbor method to resolve possible assignment conflicts between source and target points (1).

After cells were detected in a frame, their positions were associated by the global nearest neighbor method to the cell positions in the previous frame. The procedure yields a list of cells without correspondence in the previous frame (referred to as "new" cells), and a list of cell positions in the previous frame that could not be assigned to any of the available positions in the current frame (referred to as lost cells). New and lost cells are subsequently processed in a gap closing step, aimed at linking broken trajectories due to temporary detection errors. Thus, gap closing maximizes the length of the detected trajectories, while the detection step maximizes the number of cells. Both strategies are critical to the system's ability to accommodate cell division.

A flow-chart of the algorithm is shown in Fig. S1A. First, the overall intensity variance of the image was tested to determine whether the frame contained discernible objects. If the variance was close to 0, the segmentation algorithm will not find any objects in the image; this situation could occur due to shutter malfunction, overexposure, temporary defocus, or lack of cells present in the field of view. The frame was rejected and stored in a "bad frame" list. If the intensity variance as sufficient for segmentation, the image was corrected for shading in the background, a phenomenon typical for low magnification phase contrast images. After background correction, the image was segmented into three features associated with three intensities: dark nuclei, white halos, and grey background. The intensity thresholds were determined by k-means clustering (2) (Fig. S1B). Subsequently, cell coordinates were calculated as the centroids of the nuclei (red dots in Fig. S1B, panel II).

Second, cells were tracked by linking cell coordinates found in the current frame to the track heads of the growing tracks in the previous frame using the global nearest neighbor approach as

discussed (1). Using the lists of 'lost' and 'new' cells, gaps were closed if unassigned track heads existed within the past 5 frames that fell inside a search radius derived from the time gap to be closed and the typical cell speed. Detected halos were also stored and used to fill these gaps. This rescued tracking of cells lost in detection due to short periods of rounding which obscures the dark nuclear area. Cell coordinates in the gap were linearly interpolated. The last step was assigning cell properties, such as the number of cells in each segmented island, which defined if a cell was isolated or part of a cell cluster. Third, a pruning step restricted valid cell trajectories to those which were tracked for at least two consecutive frames.

To evaluate the efficiency of the automated detection algorithm, the results were compared to manual detection in one representative time lapse movie (the same used for movies S2 to S4). The fidelity of the automated detection was 90-95% before stimulation (Fig. S1C). Upon HGF stimulation, the fidelity first increased slightly during the cell spreading phase when nuclei were better separated from each other, and subsequently, as cells change morphology and detach from each other, it decayed to 80-85%. One explanation for inaccuracies in detection is the rounding of mitotic cells, which obscures their phase-dense nuclei. In resting MDCK cells, ~ 4% of the cells are in mitosis; this fraction increases to ~6% upon HGF treatment (see below). In DU-145 cells, division rates are lower.

To ensure that the three scattering parameters (described in more detail in notes S2 and S3) were not affected by a 10% reduction of the detection efficiency upon stimulation, we performed a 'jackknife' error estimation. In 100 iterations, 10% of the trajectories occurring 4 hours after stimulation were randomly deleted before parameter calculation. We found that this deletion caused only a slight underestimation of the normalized parameters, by 0.038 ± 0.011 at the reference timepoint 12 hours after stimulation. Thus, we conclude that the loss in detection efficiency during the progression of scattering does not affect the accuracy of the parameters.

For examples of tracking results from time lapse image series under different experimental conditions, see movie S1. Dragtails visualize the automatically determined cell positions in the last 6 frames.

Note S2: Quantifying cell migration and dealing with mitotic cells.

I. Quantifying cell migration.

The image segmentation and subsequent cell-centroid tracking yielded trajectories that were then processed to extract the three parameters quantifying the cell scattering behavior. We used a sampling rate of 10 min per frame, and our measured migration velocity is defined as the absolute displacement of cells in 20 min. This definition is based on 2 considerations:

1) Sampling rate: accuracy of tracking compared to technical limitations.

The sampling rate affects the accuracy of tracking when cellular displacements from frame to frame get close to half the mean distance between cells (3). In general, higher sampling rates will allow more accurate tracking; however, for practical reasons the sampling rate is limited to 10 min/frame in the multi-well microscopy setup used in our screening assay. The fastest population of MDCK cells after prolonged HGF treatment migrated at a velocity of 3 μm/min (see Figs. 2B and 3C). Within 10 minutes these cells have thus traveled about 30% of their minimal intercellular distance (MDCK cells have an average diameter of 100 μm). Therefore global nearest neighbor based tracking was still sufficient at this sampling rate even for fast-moving cells. We tested faster sampling rates (down to 1 min per frame) and did not observe differences in the migration velocities measured from the resulting tracks.

Migration velocity: persistent compared to instantaneous movement

Measuring the velocity in a short time window (for example, frame-to-frame) makes it possible to capture the instantaneous velocity and migration behavior of the cell, which may include random small-scale movement of the cell. However, frame-to-frame measurements are also inherently more sensitive to - and may be inflated by - noise in the measured cell positions. In contrast, velocities measured over longer time windows (for example, based on the net displacement over 10 frames) tend to 'smooth out' random frame-to-frame displacements, both those caused by positional noise and those that represent real undirected motion. Thus, measurements over larger time windows better describe the cells' ability to sustain motion into a specific direction over extended periods and distances (directional persistence). In this study, the choice of motility measurement over 20 min allowed some reduction of positional noise while still capturing instantaneous turns of cells. Our rationale was that even instantaneous motion with low directional persistence would be an important indicator of the migratory competence of cells. Although the motility parameter thus has low sensitivity to directional persistence of motion (or lack thereof), the effects of motion persistence were reflected in the spatial dispersal parameter, where - for a

given increase in the migration speed - more persistent motion will allow a population of cells to disperse faster.

An alternative approach to separate the effects of changes in instantaneous motion speed and directional persistence would be to fit trajectories with the persistent random walk model (4, 5). However, these models rely on the assumption that the trajectory is governed by stationary parameters over the duration of the time window. Moreover, stable fits require windows of 20 and more time points. Given the transient behavior of cells after HGF stimulation, we cannot assume that the trajectories fulfill the conditions of stationarity over long enough time windows. Therefore, the simpler approach of computing the velocity of cells over a time window of 3 time points is more appropriate in this case.

II. Dealing with mitotic cells

Cells in mitosis round up and temporarily stop migrating; thus, to prevent dividing cells from lowering the measured velocity, they should ideally be systematically excluded from velocity measurements. Our assay ignored most cells that were rounded for prolonged periods of time because they temporarily 'disappear' from detection (see above), but it did not systematically identify and subsequently discard all dividing cells; thus, in principle, stimulations and perturbations that increase the percentage of cells in mitosis (for example, those that block progression through mitosis or increase in cell division rates) could affect the cell velocity measurement. It should be noted however, that even in HGF stimulated conditions, MDCK cells divide once every 12 hours (DU145 cells once every 18 hours), and mitosis lasts about 40 min. Thus, the percentage of cells in mitosis at any given time point after HGF stimulation does not exceed 6%. This small percentage, together with the reduced detection probability of rounded cells, indicates that effects on mitosis are not likely to affect the motility parameter in our assay. Moreover, drugs that increase cell division rate are rare, and existing drugs that block cells in mitosis (like nocodazole and other microtubule drugs) cause all cells to round up, which is easily recognized from the tracking results because of the decrease in cell numbers. The software would thus detect those incidences and the associated agents should be further analyzed for mitosis defects and toxicity. As an example and verification of these considerations, we have performed extended analyses, using the output from the tracking algorithm to verify the migration specific effect of depletion of the cell cycle kinase CDK1 in Fig. 7A.

Note S3: Quantifying spatial dispersal using Ripley's K function

I. Ripley's K-function

The quantitative description of cells' spatial dispersal in this study is based on Ripley's K-function (6). The K-function is widely used as a statistical descriptor of spatial clustering in ecology and astronomy, and has recently been applied to microscopy data (7), for example to study the distribution of specific cell types in tissue (8), or the distribution of specific subcellular structures (9-14).

Ripley's K-function $K(r) = N_r / \pi\rho$ specifies how many neighbors *N* are found within a certain distance *r* of a given cell, averaged over all cells in the image and normalized by the total cell density ρ (see the example in Fig. S2, A and B). In a completely random spatial distribution, the average number of neighbors depended only on the search area and the cell density as $N_r = \rho \cdot \pi r^2$, hence $K(r) = r^2$ (dashed line in Fig. S2B). Deviations in the measured *K(r)* function from the r^2-parabola reflected deviations of the cell locations from spatial randomness: Significantly higher values indicated more neighbors for a cell than expected for spatial randomness (clustering); significantly lower values indicated less neighbors than expected for spatial randomness (exclusion). To visualize deviations from r^2, it was convenient to use a linearized version of the K-function, such as the L-function $L(r) = \sqrt{K(r)} - r$ (panel insert in Fig. S2B). In the L-function, a spatially random distribution corresponds to zero, so that positive values (here at distances 50-250 pixels) reflected cell clustering in islands, whereas negative values (here at distances 250-450 pixels) reflected exclusion (the 'empty' space between clusters).

II. Boundary Correction

Determining the K-function for objects near the border of the image poses the problem that not all of these cells' actual neighbors are visible in the field of view. Various boundary correction methods have been proposed in the literature to account for this effect. In this assay, we used Ripley's correction, which weighs the number of visible neighbors in the circle of radius *r* by a correction factor corresponding to the fraction of the circle's circumference that falls inside the field of view. In an image of size (l_x, l_y) and for an object with distance *(x,y)* from the nearest edge, this correction factor can be derived from simple geometrical considerations (15) as:

$$c(x,y,r)=\begin{cases}\dfrac{\pi/2+\sin^{-1}(y/r)+\sin^{-1}(x/r)}{2\pi} & \text{if } r>\sqrt{x^2+y^2}\\ \dfrac{2\sin^{-1}(y/r)+2\sin^{-1}(x/r)}{2\pi} & \text{if } \sqrt{x^2+y^2}\geq r>\max(x,y)\\ \dfrac{\pi+2\sin^{-1}(\min(x,y)/r)}{2\pi} & \text{if } \max(x,y)\geq r>\min(x,y)\\ 1 & \text{elsewhere}\end{cases}$$

This formula is valid for distances up to $r_{\max}=\min(l_x,l_y)/2$, for which the circle of radius r extends over no more than two of the image borders.

III. Dispersal parameter from Ripley's K-function

The L-function $L(r,t)$ was calculated for every frame of the movie. In stimulated cells, the measured function flattened out as the cells disperse (Fig. S2C). To capture the time course of spatial dispersal in a single parameter $p_{disp}(t)$, we extracted the partial integral of the $L(r,t)$ function

$$p_{disp}(t)=\int_{d_1}^{d_2}L(r,t)\,dr$$

between the distances d_1 and d_2. These distances were determined from the function $L(r,t_0)$ recorded prior to stimulation and then were kept fixed; d_1 represented the distance where $L(r,t_0)$ crosses from negative to positive values (approximating the average cell diameter), and d_2 was the position of the first maximum of $L(r,t_0)$ (approximating the average cluster diameter).

To ensure that this parameter responded to scattering as expected, we performed simulations (Fig. S2D): When a distribution of clustered points was allowed to move, but was kept together by attractive forces, the parameter did not change. When the attraction was removed and the points gradually dispersed in space by diffusion, the parameter decayed. When in addition the speed was increased, the decay became faster.

In cell measurements, the dispersal parameter is normalized with respect to the value prior to stimulation and to the end value measured in an HGF-only experiment. Therefore, the normalized parameter ranges between 0 and 1. Movie S3 shows an example of cell scattering, the associated flattening of the L-function, and the corresponding increase of the normalized spatial dispersal parameter over time.

IV. Growth Correction

The dispersal parameter is affected by cell division. Although the L-function is invariant with respect to cell density, new cells appearing over the course of the movie are not added in random positions; rather, cell division result in systematic growth of existing clusters, which 'stretches' the L-function in x-direction over time and causes a systematic distortion of the dispersal parameter.

To account for this effect, every measurement of the dispersal parameter in a frame was accompanied by a simulation of cluster growth (Fig. S2E). The cell distribution prior to HGF-stimulation defined the mean nearest-neighbor distance (NDD) probability function under clustered conditions. Throughout the movie, cell division was simulated by randomly adding new points to the edge of existing clusters, at positions allowed by the NDD distribution. The number of points added per frame was equal to the increase of cell positions detected in between two frames of the movie. Three separate simulations of cell division were performed per frame. The average difference between the L-functions and dispersal parameters with and without cell division indicated the distortion of these measures due to cell division. The distortion values were subtracted from the experimentally observed dispersal parameter to yield the growth-corrected parameter used for final analysis. The growth-corrected dispersal parameter of unstimulated cells (which divide but do not scatter) was constant over time (Fig. 2H), indicating the functionality of this growth-correction.

Note S4: Quantifying cell-cell adhesion

Cells attached to their neighbors tend to move together, whereas dissociated cells move independently from each other. This can be quantified through the motion correlation of neighboring cells, as defined by the cosine of the angle between the displacement vectors:

$$corr = \cos\alpha = \frac{u \cdot v}{|u| \cdot |v|} = \frac{(u_1 v_1 + u_2 v_2)}{\sqrt{(u_1^2 + u_2^2)} \cdot \sqrt{(v_1^2 + v_2^2)}}$$

where $u=(u_1,u_2)$ and $v=(v_1,v_2)$ are the displacement vectors of two neighboring cells from frame *n* to frame *n*+*s*, and the resulting correlation (*corr*) is a dimensionless number between -1 and 1. For uncorrelated motion, the average correlation value – averaged over all available point pairs in a population – is zero. For correlated motion, the average correlation value is positive.

Due to the pairwise analysis and statistical nature of the correlation measurement, averaging over a population was required. However, to relate the velocity of an individual cell to the adhesion status of the same cell, as measured by motion correlation, a correlation value had to be estimated for each cell. For this purpose, the correlation scores between the target cell and all its neighbors within the distance d_2 (see Note S2, section III) were averaged. If less than 3 neighbors fulfilled the distance criterion, the next neighbors were added until three correlation values per frame were available for averaging. In addition, the motion correlation with each neighbor was averaged over 5 consecutive frames to provide sufficient statistics for each individual cell and to capture correlation on various time scales. In assays with low positional noise, this time window can be reduced if higher time resolution is desired.

Before stimulation with HGF, the histogram of correlation values is skewed to positive values (Fig. S3A). 12 hours after stimulation, the mean motion correlation is shifted towards zero and the distribution is symmetric (Fig. S3B). To monitor the change of the histogram over time, the correlation histogram was fitted at each time point with the superposition of two distributions: A distribution of ‘detached’ cells represented by a zero-mean Gaussian, and a distribution of ‘attached’ cells represented by a positive-mean skewed Weibull function (see dashed magenta lines in Fig. S3, A and B). This superposition was motivated by the fact that (i) attached cells with a non-zero migration velocity have to display positive net motion correlation values (this requirement is physically necessary for cells in order to stay within each other's vicinity), so that attached cells are expected to give rise to a positive mean correlation 'mode'; (ii) detached cells that lack physical coordination with their neighbors (other than exclusion) are expected to display zero net correlation values, giving rise to a zero mean correlation 'mode'; (iii) attached and detached cells generally co-exist in these movies. Even in unstimulated conditions, there is usually a small subpopulation of single cells not attached to any cluster; in stimulated cells, individual cells

transform and detach (contributing to the zero-mean mode) whereas some clusters of attached cells remain stable for continued periods of time (contributing to the positive-mean mode).

In HGF-stimulated cells, the relative weight ratio of the two distributions (attached or detached) decays from typically ~0.9 prior to stimulation to ~0.1 at 12 hours following stimulation. Movie S4 shows an example of cell scattering, the gradual shift of the correlation histogram, and the corresponding increase of the normalized adhesion loss parameter over time.

Note S5: Hierarchical clustering

An inhibitor's efficiency was defined as one minus the ratio of the normalized parameter values of the drug-treated condition ('HGF+drug') compared to that of the reference sample ('HGF'), yielding an efficiency value ranging between 0 (0%, lowest efficiency, or no inhibition) and 1 (100%, highest efficiency, or complete inhibition) (Fig. S4). For each parameter (motility, adhesion, dispersal), a separate single value for the efficiency was extracted at 12 hours post-stimulation, so that each drug condition - drug X at concentration Y - was characterized by a triplet of efficiency values: efficiency in inhibiting adhesion loss, efficiency in inhibiting motility increase, and efficiency in inhibiting spatial dispersal.

After ranking drugs ranked based on their maximum efficiency (Fig. S5), we chose the 39 most efficient drug conditions - those that exceeded 66% (0.66) efficiency for at least one of the three parameters - for hierarchical clustering. We performed hierarchical clustering with single linkage as linkage method, which requires the definition of a metric or a semi-metric that defines the dissimilarity of data points. We used the Euclidian distance in the three-dimensional parameter space defined by the three inhibition frequencies.

The hierarchical clustering by itself does not provide a measure of the significance and the robustness of groups. Therefore, we performed a validation of the clustering results following previously described strategies (16).

As a first exploratory step, we visualized the clustering results in the 3D feature space (Fig. S6A). The data fall into three distinct groups with little to no significant overlap, in that the spread of

points within the cluster is small compared to the distance between neighboring clusters. Indeed, we find that the separation, or the mean distance between cluster centers (16), amounts to 0.60, whereas the compactness, or the mean distance of data points from their corresponding cluster center (16), amounts to 0.22. Next, we confirmed that the assignment of the individual data points to the three clusters is identical when the clustering is performed by k-means clustering instead of hierarchical clustering.

To quantitatively assess the quality of the clustering, we used the Dunn index as an internal measure (17). The Dunn index relates the minimum distance of points in one cluster from points in the nearest neighboring cluster to the maximum distance between points within the same cluster; a higher Dunn index value indicates better cluster separation, or a better quality of the partitioning. First, we confirmed that the selection of 3 clusters resulted in the best partition of the complete dataset. To accomplish this, we forcibly partitioned the data into 2-9 clusters and calculated the Dunn index for each solution (Fig. S6B). The Dunn index has a clear maximum at 3 clusters, indicating that with 2 clusters the data is under-partitioned and with 4 and more clusters the data is over-partitioned. Second, we performed simulations in which we took the full dataset, but assigned each data point randomly to one of the three clusters, and re-calculated the Dunn index for the new assignments. For 500 simulations, the Dunn index was an order of magnitude below that of the cluster assignment presented in Fig. 5A, underlining the high statistical significance of this result.

To test the robustness of the clusters, we established 'self-consistency' by drawing overlapping sub-samples of the complete data set (corresponding to randomly deleting 10% of the points), re-clustering with hierarchical clustering, and determining the center-of-mass of the updated clusters (Fig. S6D). In particular, this procedure would reveal adverse influences of data outliers. The deviation of the sub-sampled data sets from the full data sets was 0.0845 for the non-specific cluster, and 0.0432 and 0.0469 for the motility- and adhesion-specific clusters, respectively. It should be noted that this scatter is 3 to 5 times less than the compactness of the individual clusters, although the cluster of unspecific efficient inhibitors is somewhat unstable. This is mainly associated with the fairly low number of data points, where elimination of 2 to 3 individual points from the cluster may cause substantial shifts of the cluster centers. Nonetheless, even with the worst case scenario, the three clusters remain well separated. Together, these tests indicated that

the partitioning by hierarchical clustering of efficient inhibitors of cell scattering into 3 classes – ‘adhesion-specific’, ‘motility-specific’, and ‘unspecific’ – is valid and robust.

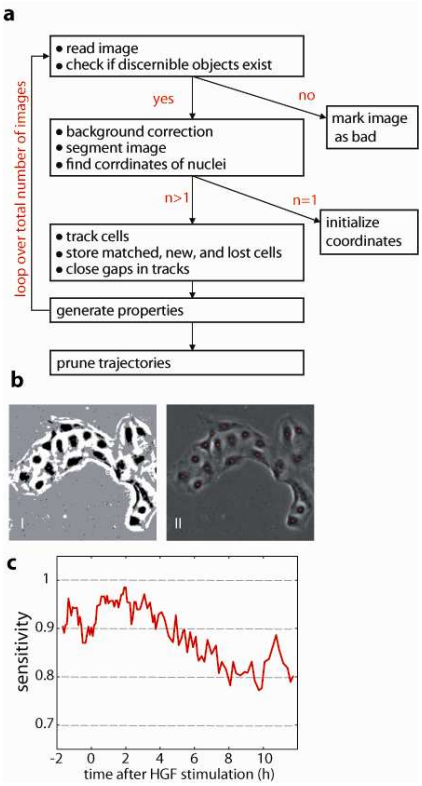

Figure S1. Cell tracking. a Schematic of the detection and tracking algorithm. **b** Segmented raw image (black: nuclear regions; white: cytoplasm; gray: background panel I) and extracted cell positions (red dots; panel II). **c** Sensitivity of automated detection: Ratio of automatically detected compared to manually detected cells over the course of a time lapse sequence double-tracked for the purpose of performance testing.

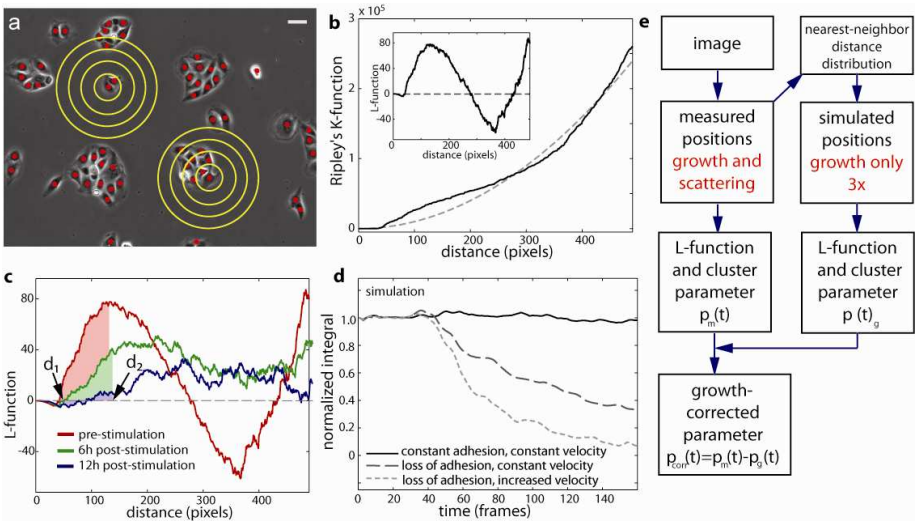

Figure S2. Definition of spatial dispersion parameter based on Ripley's K function. a Ripley's K-function measures the average number of neighbors within a circle of increasing radius *r*. Scale bar, 50 µm. **b** K-function and L-function (inset) for the distribution shown in a. **c** L-function at different time points before and after HGF-stimulation. d_1 is the distance at which the L-function prior to stimulation crosses zero (which corresponds to the average cell diameter); d_2 is the position of the first maximum of the L-function prior to stimulation (which corresponds to average cluster diameter). **d** Normalized partial integral of the L-function from d_1 to d_2 used to quantify spatial dispersal over time in simulated data sets of cell scattering. **e** Algorithm to compensate for distortion of the spatial dispersal parameter due to cell division.

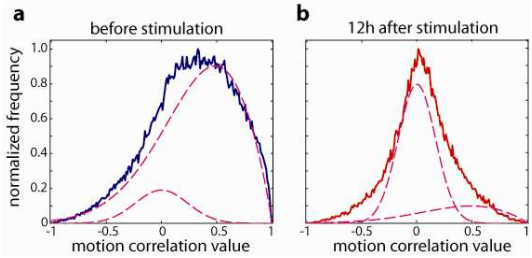

Figure S3. Definition of adhesion loss parameter based on motion correlation. a Histogram of correlation scores in a cell population before stimulation with HGF (n=358 cells measured for 20 frames). Fit of two superimposed distributions to determine the relative contributions of uncorrelated mode (Gaussian distribution with zero mean), or the subpopulation of detached cells; and correlated mode (positively skewed Weibull function), or the subpopulation of attached cells. **b** Histogram of correlation scores of cells between 10-12 hours after stimulation with HGF (n=792 cells measured for 20 frames).

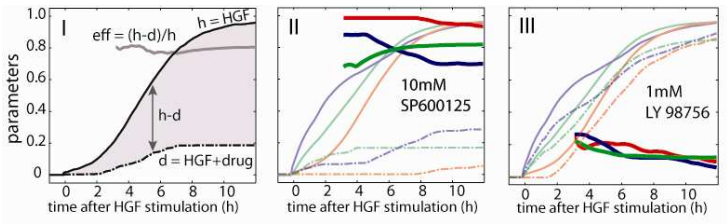

Figure S4. Inhibition efficiency for motility, dispersal, and adhesion loss parameters. Panel I: The inhibition efficiency of a drug ('HGF+drug') is calculated relative to a reference experiments with HGF stimulation only ('HGF'). Panels II and III: Parameter time courses (5 frame running average) for reference sample (dash-dotted lines) and drug-treated sample (solid lines) with calculated efficiency (bold lines; motility = red, adhesion loss = green, spatial dispersion = blue). Panel II displays a drug with strong inhibitory performance and panel III depicts a drug with weak inhibitory performance.

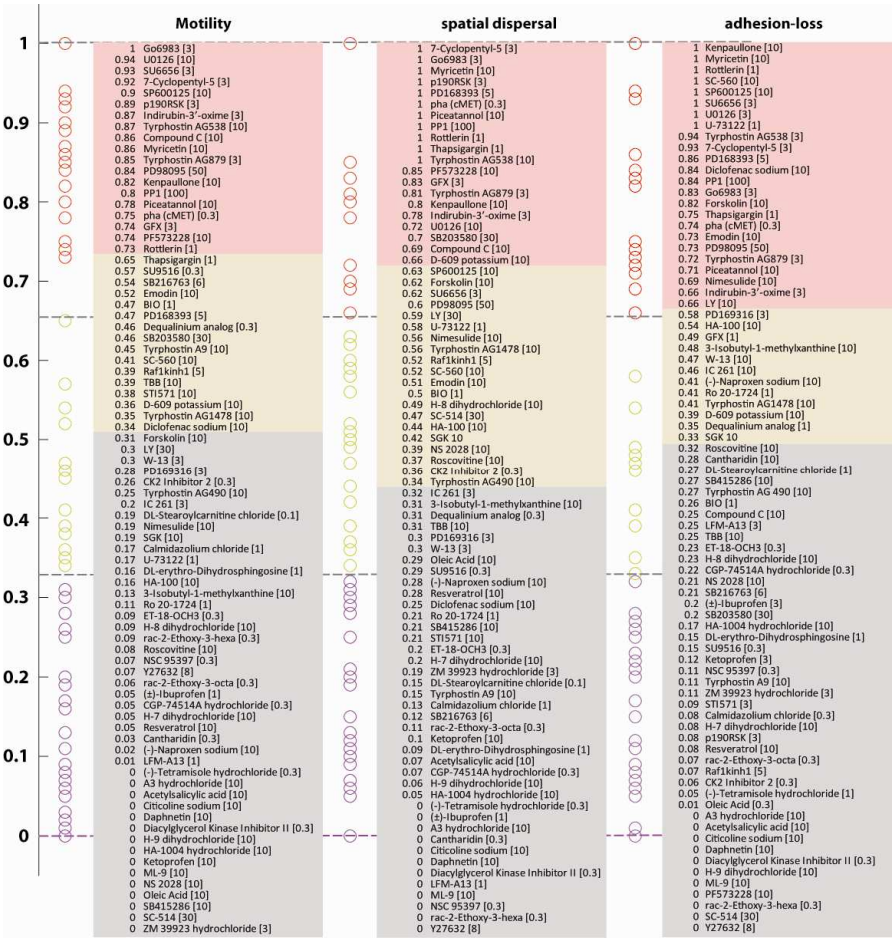

Figure S5. Ranked inhibition efficiencies. Inhibition efficiencies for motility increase, spatial dispersal, and adhesion loss of all screened drugs. Maximum efficiency is defined as the efficiency 12 hours post-stimulation (read out on the smoothed efficiency time course as shown in fig.Fig. S4). For graphical clarity, if multiple concentrations of a drug were used, only the efficiency of the most effective concentration is shown (concentration in square brackets in µM). Effective inhibitors were drugs with maximum efficiencies ranging from 67-100% (red); moderately effective inhibitors were drugs with maximum efficiencies ranging from 33-66% (yellow); ineffective inhibitors had maximum efficiencies below 33% (grey).

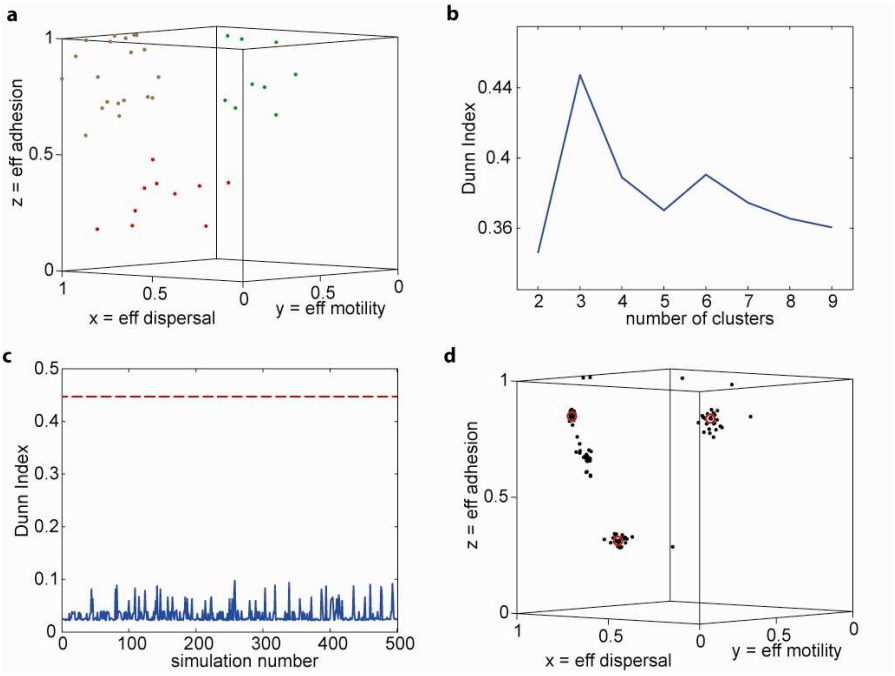

Figure S6. **Validation of hierarchical clustering**. **a** 3D scatter plot of the efficiencies of the drugs used for hierarchical clustering. Colors indicate the three identified clusters (green: adhesion-specific, red: motility-specific; brown: non-specific; see Fig. 5A). **b** The Dunn index for varying number of clusters. **c** The Dunn index for random assignment of data points to three clusters. Red dashed line indicates the Dunn index for the clusters selected in Fig. 5A**. d** 3D scatter plot of cluster centers for re-sampled data (black: re-sampled data sets; red: full dataset).

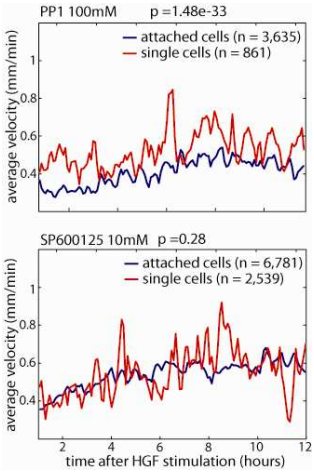

Figure S7. Velocity differences indicate adhesion specificity. Comparison of single-cell to clustered-cell velocities as an indicator for adhesion-specific effect of drugs. To test the significance of the velocity difference, a two-sided t-test was performed on the distributions of single-cell and clustered-cell velocities starting 1 hour after HGF stimulation. Upper panel: Example of high adhesion specificity (100 μM PP1); significant difference between velocities. Lower panel: Example of efficient, yet non-specific drug (3 μM Go6983); difference between velocities was not significant.

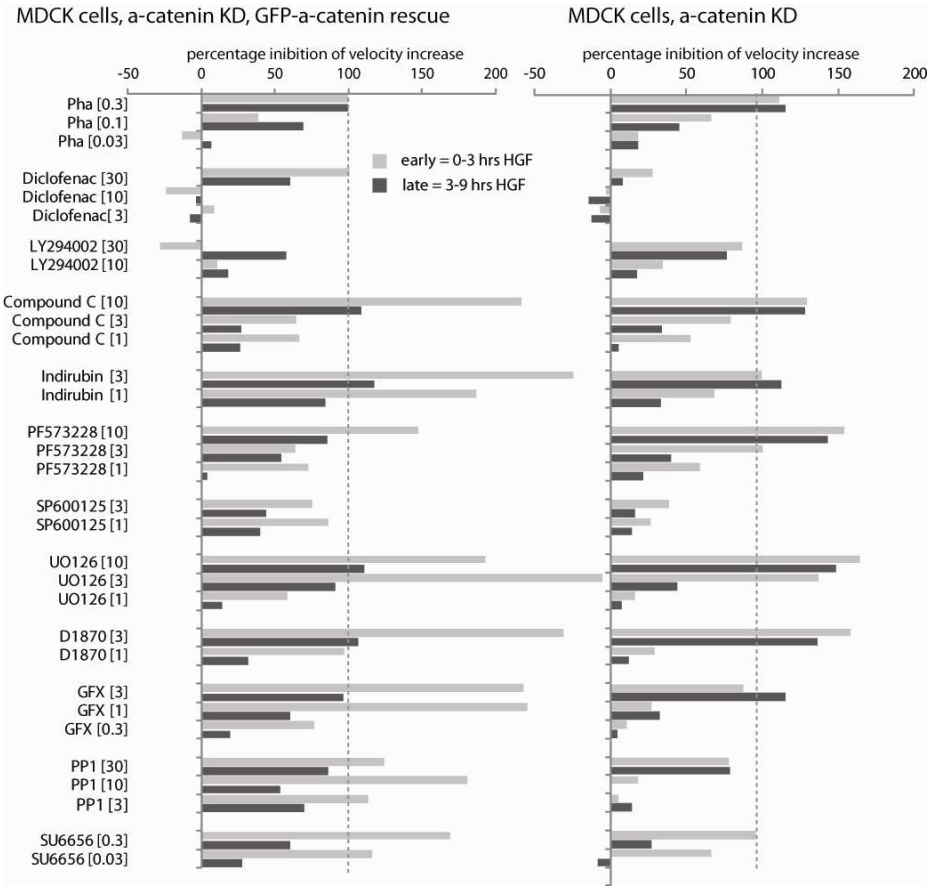

Figure S8: Inhibition efficiency of effective drugs on the scattering of normal and cell-cell junction-compromised MDCK cells. The average inhibition efficiency of the motility reponse in early (0-3 hours post HGF) and late phases (3-9 hours post HGF) of MDCK cell scattering is depicted for 12 efficient inhibitors, including the cMET inhibitor PHA-665752 as the positive control.

molcular target(s)	Name	further information (if available)
second messenger and lipid signaling		
AC	Forskolin	Activates adenylate cyclase;
GC	NS 2028	Specific soluble guanylyl cyclase inhibitor
PDE	Ro 20-1724	Potent and selective cAMP phosphodiesterase inhibitor
PDE	3-Isobutyl-1-methylxanthine	Potent phosphodiesterase inhibitor; more active than theophylline at adenosine receptors
PKA/PKG	H-9 dihydrochloride	Protein kinase inhibitor most effective for cAMP- and cGMP-dependent protein kinases
PKA/ PKG	H-8 dihydrochloride	
Ca2+	Thapsigargin	Potent, cell-permeable, IP3-independent intracellular calcium releaser
Ca2+ATPase	Calmidazolium chloride	Potent inhibitor of calmodulin activation of phosphodiesterase; strongly inhibits calmodulin-dependent Ca2+-ATPase
Calmodulin	W-13	
COX	Acetylsalicylic acid	COX inhibitor; antithrombotic, COX-3 > COX-1 > COX-2
COX	Diclofenac sodium	
COX	Ketoprofen	COX-1 selective non-steroidal anti-inflammatory (NSAID) drug
COX	(±)-Ibuprofen	non-selective COX inhibitor
COX	(-)-Naproxen sodium	COX-1 and COX-2 inhibitor
COX	Nimesulide	Highly selective COX-2 inhibitor
COX	SC-560	Selective COX-1 inhibitor
COX	Resveratrol	Prevents apoptosis in K562 cells by inhibiting lipoxygenase and cyclooxygenase activity
DAGK	Diacylglycerol Kinase Inhibitor II	
PI3-kinase	LY294002 (LY)	
PKC / PLA2 / PLD	DL-erythro-Dihydrosphingosine	
PLA2	Citicoline sodium	Phospholipase A2 inhibitor; neuroprotective in situations of hypoxia and ischemia
PLC, PLA2	U-73122	Phospholipase C and A2 inhibitor
PLD/PLC	D-609 potassium	inhibits phospholipase D and phosphatidylcholine phospholipase C (PIPLC)
PLC	ET-18-OCH3	Phosphoinositide-specific Phospholipase C (PI-PLC) inhibitor
protein kinases		
cMET	PHA-665752	c-MET inhibitor, serves as positive controle
Abl	STI571	
AMPK	Compound-C	selective AMPK inhibitor
BTK	LFM-A13	
CDK	CGP-74514A hydrochloride	Cdk1 inhibitor

CDK	Indirubin-3'-oxime	
CDK	Kenpaullone	Potent inhibitor of CDK1/cyclin B, CDK2/cyclin A, CDK2/cyclin E, and CDK5/p25
CDK	SU 9516	Cylcin-dependent kinase-2 (Cdk-2) inhibitor; induces apoptosis in colon cancer cells
CDK	Roscovitine	
CK	Myricetin	Casein Kinase II inhibitor
CK	TBB	Highly selective, ATP/GTP-competitive inhibitor of casein kinase 2 (CK2).
CK	IC 261	Casein kinase-1 (CK-1delta/epsilon) inhibitor.
CK	A3 hydrochloride	Non-selective casein kinase (CK) inhibitor.
CK	CK2 Inhibitor 2	High affinity, selective, ATP-competitive casein kinase 2 (CK2) inhibitor.
FAK	PF573228	
GSK3	SB216763	
GSK3	SB415286	
GSK3	BIO	ATP-competitive glycogen synthase kinase 3alpha/beta (GSK-3alpha/beta) inhibitor.
IKK	SC-514	
JAK	Tyrphostin AG 490	Jak-2 protein tyrosine kinase (PTK) inhibitor
JNK	ZM 39923 hydrochloride	Janus kinase 3 (JNK-3) inhibitor.
JNK	SP600125	
MEK	U0126	Specific inhibitor of MEK1 and MEK2 (MAP kinase kinase; MAPKK)
MEK	PD98059	
MLCK	ML-9	
MLCK	ML-7	
p38 MAPK	PD 169316	Potent, cell permeable and selective p38 MAP kinase inhibitor; nM potency
p38 MAPK	SB203580	
p90 RSK	BI-D1870	
PK	Daphnetin	
PK	HA-1004 hydrochloride	Potent inhibitor of cAMP- and cGMP-dependent protein kinases; because it has low affinity for protein kinase C, HA-1004 serves as an excellent negative control of H-7 HCl
PKA / PKC	H-7 dihydrochloride	
PKA / PKC / MLCK	HA-100	
PKC	Dequalinium analog, C-14 linker	Protein kinase C-alpha (PKC-alpha) inhibitor
PKC	rac-2-Ethoxy-3-octadecanamido-1-propylphosphocholine	
PKC	rac-2-Ethoxy-3-hexadecanamido-1-propylphosphocholine	
PKC	Oleic Acid	Activates protein kinase C in hepatocytes; uncouples oxidative phosphorylation
PKC	DL-Stearoylcarnitine chloride	
PKC	GF109203X (GFX)	similarly high affinities for PKC a, b, g, d, e

PKC	Go6983	similarly high affinities for PKC a, b, g, d
PKC / CaM Kinase III	Rottlerin	PKCd selective and CaM kinase III inhibitor
Raf	Raf1Kinh1	
ROCK	Y-27632	Rho-associated coiled-coil forming protein kinase (ROCK) inhibitor. Also inhibits ROCK-II.
RTK	Tyrphostin AG 1478	EGFR
RTK	PD168393	EGFR
RTK	Tyrphostin AG 538	IGF-1 R
RTK	Tyrphostin A9	PDGFR
RTK	Tyrphostin AG 879	Tyrosine kinase nerve growth factor receptor (TrkA) inhibitor; inhibits 140 trk protooncogene and HER-2
Src	7-Cyclopentyl-5-(4-phenoxy)phenyl-7H-pyrrolo[2,3-d]pyrimidin-4-ylamine	Potent and selective lck (src family tyrosine kinase) inhibitor.
Src	Emodin	p56lck Tyrosine kinase inhibitor
Src	Piceatannol	Non-receptor kinase Syk and Lck inhibitor
Src	PP1	high affinity for Lck and Fyn, lower for Src
Src	SU6656	high affinity for Src, Fyn, Yes, Lyn. Lower affinity for Lck
protein phosphatases		
PP2A	Cantharidin	Protein phosphatase 2A inhibitor
Cdc25	NSC 95397	Selective, irreversible Cdc25 dual specificity phosphatase inhibitor.
AP	(-)-Tetramisole hydrochloride	Inhibits multiple mammalian alkaline phosphatases

Table S1: Target names and additional information on drugs used in screen.

References

1. Ponti, A., A. Matov, M. Adams, S. Gupton, C. M. Waterman-Storer, and G. Danuser. 2005. Periodic patterns of actin turnover in lamellipodia and lamellae of migrating epithelial cells analyzed by quantitative Fluorescent Speckle Microscopy. *Biophys J* 89: 3456-3469.

2. MacQueen, J. 1967. Some methods for classification and analysis of multivariate observations. *Proceedings of 5-th Berkeley Symposium on Mathematical Statistics and Probability* 281-297.

3. Jaqaman, K., D. Loerke, M. Mettlen, H. Kuwata, S. Grinstein, S. L. Schmid, and G. Danuser. 2008. Robust single-particle tracking in live-cell time-lapse sequences. *Nat Methods* 5: 695-702.

4. Dunn, G. A., and A. F. Brown. 1987. A unified approach to analysing cell motility. *Journal of cell science. Supplement* 8: 81-102.

5. DiMilla, P. A., J. A. Quinn, S. M. Albelda, and D. A. Lauffenburger. 1992. Measurement of individual cell migration parameters for human tissue cells. *AIChE Journal* 38: 1092-1104.

6. Ripley, B. D. 1976. 2nd-Order Analysis of Stationary Point Processes. *Journal of Applied Probability* 13: 255-266.

7. Mattfeldt, T. 2005. Explorative statistical analysis of planar point processes in microscopy. *J Microsc* 220: 131-139.

8. Reilly, C., Schacker, T., Haase, A. T.,Wietgrefe, S., Krason, D. 2002. The clustering of infected SIV cells in lymphatic tissue. *J. A.. Sat. Ass.* 97: 943-954.

9. Beil, M., F. Fleischer, S. Paschke, and V. Schmidt. 2005. Statistical analysis of the three-dimensional structure of centromeric heterochromatin in interphase nuclei. *J Microsc* 217: 60-68.

10. Ehrlich, M., W. Boll, A. Van Oijen, R. Hariharan, K. Chandran, M. L. Nibert, and T. Kirchhausen. 2004. Endocytosis by random initiation and stabilization of clathrin-coated pits. *Cell* 118: 591-605.

11. Hess, S. T., M. Kumar, A. Verma, J. Farrington, A. Kenworthy, and J. Zimmerberg. 2005. Quantitative electron microscopy and fluorescence spectroscopy of the membrane distribution of influenza hemagglutinin. *J Cell Biol* 169: 965-976.

12. Philimonenko, A. A., J. Janacek, and P. Hozak. 2000. Statistical evaluation of colocalization patterns in immunogold labeling experiments. *J Struct Biol* 132: 201-210.

13. Prior, I. A., C. Muncke, R. G. Parton, and J. F. Hancock. 2003. Direct visualization of Ras proteins in spatially distinct cell surface microdomains. *J Cell Biol* 160: 165-170.

14. van Rheenen, J., E. M. Achame, H. Janssen, J. Calafat, and K. Jalink. 2005. PIP2 signaling in lipid domains: a critical re-evaluation. *EMBO J* 24: 1664-1673.

15. Haase, P. 1995. Spatial pattern analysis in ecology based on. Ripley's K-function: Introduction and methods of edge correction. *J. Veg. Science* 6: 575-582.

16. Handl, J., J. Knowles, and D. B. Kell. 2005. Computational cluster validation in post-genomic data analysis. *Bioinformatics* 21: 3201-3212.

17. Dunn, J. C. 1974. Well separated clusters and optimal fuzzy-partitions. *Journal of Cybernetics* 4: 95-104.

Movie S1. The presence of cell-cell adhesions slows down HGF-induced cell motility.
Time lapse image series of MDCK cell behavior under indicated conditions. Left panel – unstimulated cells; middle panel – HGF-stimulated cells; right panel – HGF-stimulated cells in low [Ca^{2+}] condition. Color-coded tails ('dragtails') indicate the automatically determined cell-positions in the previous 6 frames. Thus, the length of the dragtail is indicative of the instantaneous velocity. 5 ng/ml HGF was added to the indicated samples 115 min after the start of imaging (frame 19). Frame rate: 6 min.

Movie S2. Motility Parameter
Left panel: Phase-contrast image of cell distribution with detected cell positions as colored dots; scale bar 50 μm, frame rate 5 min. Middle panel: Normalized histogram of measured current average cell velocities, triangle denotes position of the mean. Right panel: Time course of normalized average velocity.

Movie S3. Spatial Dispersion Parameter
Left panel: Phase-contrast image of cell distribution with detected cell positions as colored dots; scale bar 50 μm, frame rate 5 min. Middle panel: L-function of measured current cell distribution; shaded area denotes the distances over which the partial integral is performed. Right panel: Time course of normalized partial integral.

Movie S4. Adhesion Loss Parameter
Left panel: Phase-contrast image of cell distribution with detected cell positions as colored dots; scale bar 50 μm, frame rate 5 min. Middle panel: Normalized histogram of correlation values in the current frame; red and magenta curves indicate the fitted attached (zero-mean) and detached (positive-mean) distributions. Right panel: Time course of the normalized ratio of the respective areas of the fitted attached or detached distributions.

Movie S5. α-Catenin–depleted cells do not form functional cell-cell junctions
Time lapse image series of HGF-induced scattering in MDCK cells stably expressing an aE-catenin targeting shRNA. In the left panel, cell-cell junction formation was rescued in these cells by overexpression of GFP-α-catenin. 5 ng/ml HGF was added to the indicated samples 2 hours after the start of imaging (frame 20). Frame rate: 6 min.

Movie S6. Knockdown of CDK1 but not CDK5 inhibits the HGF-induced increase in cell motility.

Representative areas from time lapse image series of cell scattering in response to HGF of DU145 cells transfected with siRNAs directed against cMET, CDK1, or CDK5 as indicated. 5 ng/ml HGF was added 2 hours after the start of imaging (frame 20). Frame rate: 6 min.

Movie S7. Diclofenac inhibits the HGF-induced loss of cell-cell adhesion, whereas knockdown of COX-2 reduces the stability of cell-cell junctions.

Representative areas from time lapse image series of HGF-induced cell scattering of MDCK cells transfected with scrambled (non-targeting) or COX-2-targeting shRNA compared to untransfected MDCK cells treated with 10 μM diclofenac just prior to the start of imaging. 5 ng/ml HGF was added 1.5 hours after the start of imaging (frame 15). Frame rate: 6 min.

Movie S8. Blocking RSKs by chemical inhibition or by siRNA-mediated knockdown inhibits the HGF-induced increase in cell motility.

Representative areas from timelapse image series of HGF-induced cell scattering of untransfected DU145 cells in the absence or presence of 3 μM BI-D1870 (added just prior to the start of imaging) and DU145 cells transfected with scrambled or RSK1- and RSK2-targeting siRNAs. 5 ng/ml HGF was added 2 hours after the start of imaging (frame 20). Frame rate: 6 min.

General Discussion

General Discussion

The view of the cadherin-complex as a mere static adhesion structure belongs to the past. Cadherin and the intercellular binding partners like α-, β- en P120- catenin form a core complex that is required for the formation and loss of cell-cell junctions, however recent studies show that this structure can be accredited a lot more. The complex is responsible for very dynamic processes that entail the sensing and concurrent directing of the cell status. For instance, N-cadherin was shown to function as a mechanosensor, the tension forces of N-cadherin mediated adhesions on micropillars varied with the micropillar stifness (Ladoux, Anon et al. 2010) Furthermore, pulling forces on endothelial VE-cadherin based c-c junctions lead to increased junction length without the loss of junctional tension (Liu, Tan et al. 2010). These studies attribute mechanosensing properties to classical cadherin mediated junctions. Such a mechanosensing function was also identified in the epithelial variant of the classical cadherins. In our study in collaboration with D. Leckband, magnetic twisting cytometry of E-cadherin-coated magnetic beads revealed that The E-cadherin complex is a genuine mechanosensor (le Duc, Shi et al. 2010). The degree in which the junction to the bead was reinforced after twisting was dependent on the initial twisting force applied to the bead, this linearity defines true mechanosensors, see chapter 3 (le Duc, Shi et al. 2010).

In our model, cadherin adhesions are physically pulled by perpendicular actomyosin bundles which likely brings α-catenin under tension, and alters its conformation to allow recruitment of vinculin to reinforce cell-cell adhesions (Yonemura, Wada et al. 2010). This force dependent junction reinforcement is dependent on the connection with the actomyosin network, as disturbance of actin or myosin by inhibitors resulted in the loss of these properties. Other classical cadherins seem to depend on the same mechanism. Inhibition of actomyosin activity in cells expressing N-cadherin (astrocytes) and VE-cadherin (Human Umbilical Vein Endothelial Cells, HUVEC's) gave the same effect: disruption of vinculin recruitment to junctions, see chapter 5 and Huveneers et al (Huveneers, Oldenburg et al. 2012). This suggests that the mechanosensing properties observed in N- and VE-cadherin mediated junctions (Ladoux, Anon et al. 2010; Liu, Tan et al. 2010) are based on the same molecular mechanism proven for E-cadherin mediated junctions. Probably this specific mechanosensing mechanism is conserved among all members of the classical cadherins. This mechanosensing property reveals an intricate form of dynamic regulation of classical cadherin's. This novel property really dusts of the appearance of the classical cadherins as a static adhesion receptor and thereby invigorates the inveterate field of cell adhesion studies.

Molecular design of the mechanosensor

a-catenin allosteric regulation by force and/or interacting proteins

Molecular details concerning the make up of the cadherin mechanosensor are also coming to light. The core of the sensor is α-catenin. It is capable of binding to both cadherin, via β-catenin, and the actin cytoskeleton, through its own actin binding site and through vinculin. The specific perturbation of α-catenin's vinculin binding site, results in the total loss of force dependent reinforcement in the magnetic twisting cytometry assay, chapter 4. This indicates that the mechanosensing properties of the cadherin-complex are lost once vinculin is unable to bind to α-catenin and thereby incapable to establish a link with the actin cytoskeleton.

So how is vinculin recruitment regulated, in other words, why does vinculin bind α-catenin and actin exclusively when reinforcement is initiated? Accessibility of the binding domains in α-catenin and

vinculin appear to be the key means of regulation within this mechanism. To start with α-catenin, the vinculin binding domain (VBD) of α-catenin is sterically hindered in the native/inactive conformation. The isolated VBD-peptide binds vinculin a 1000-fold stronger than the full length α-catenin where the VBS is obstructed (Choi, Pokutta et al. 2012). Thus α-catenin itself needs to be activated before it is capable to recruit vinculin. α-Catenin itself has an actin binding domain that could mediate VBD accessibility for subsequent vinculin binding, actomyosin mediated tension could stretch α-catenin so the VBS becomes available (Yonemura, Wada et al. 2010). Alternatively, activation through binding of the proteins I-afadin (Pokutta, Drees et al. 2002), ZO-1 (Itoh, Nagafuchi et al. 1997) or EPLIN (Abe and Takeichi 2008) could otherwise be an option. Chervin-Petinot et al recently reported that EPLIN can link α-catenin to actin, independent of actomyosin activity, a probable route for the transduction of tension needed to uncover the VBD of α-catenin (Chervin-Petinot, Courcon et al. 2012).

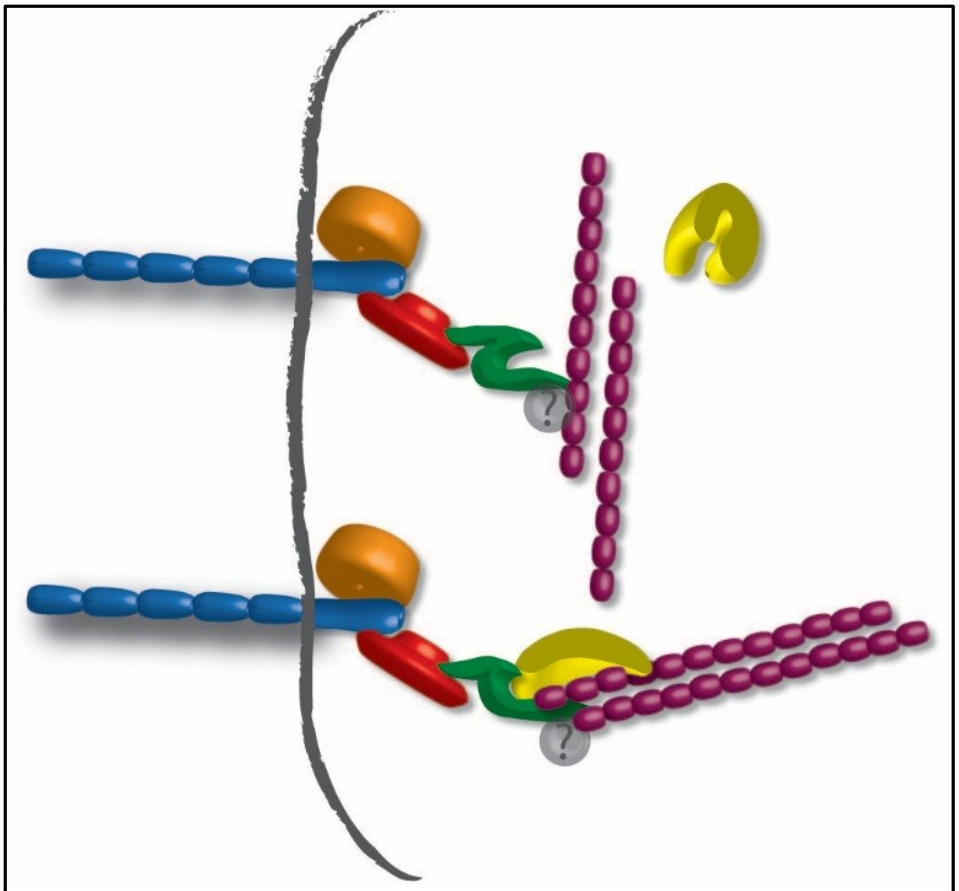

Figure 1
Schematic overview of vinculin (yellow) recruitment to the cadherin (blue), p120- (orange), β- (red) and α-catenin (green) upon tension build-up by the actin (purple) myosin network. Possible unknown partners ("?") could be at play.

Allosteric activation and regulation of vinculin recruitment

To make things even more complicated, even if α-catenin is activated and able to bind vinculin, vinculin needs to be activated before being able to bind to both α-catenin and F-actin. Both the F-actin and the α-catenin binding sites, the tail and head region respectively, are autoinhibited in vinculin's unbound state. The head region has a strong affinity for the tail region and this keeps vinculin in the closed conformation. Thus this poses an interesting problem; before vinculin can bind to F-actin and α-catenin simultaneously, it needs to open up, but in order to open up it first needs to bind to F-actin and α-catenin simultaneously.,

Maybe vinculin tackles this conundrum by its abundance in the cytoplasm. Although vinculin's preference for the closed conformation, high abundance increases the absolute fraction of open vinculin in the cytoplasm, because there is always an equilibrium. Therefore, abundance increases the chances for an activated vinculin molecule being in close proximity of an activated α-catenin in the cadherin complex. In contrast to this passive hypothesis, vinculin could possibly be actively positioned to the tensed cadherin complex. Proteins like ponsin, vinexin and VASP bind to a domain of vinculin that is even accessible in the autoinhibited state; the proline rich region between the tail and head domain. Furthermore, these proteins locate to c-c junctions and associate with the actin cytoskeleton for actin remodeling activities, processes activated in c-c junction reinforcement; Vinexin and Ponsin induce the formation of F-actin stress-fibers (Kioka, Sakata et al. 1999) and VASP stimulates the formation of filamentous actin (Bear and Gertler 2009). Tension generated damage at actin stress fibers recruits ZYXIN and its binding partners α-actinin and VASP to reinforce the actin bundles (Smith, Blankman et al. 2010). Although only shown for cell-matrix adhesions, this actin damage repair mechanism could very well be taking place in cell-cell junctions as well. The cadherin complex is supposed to be linked to the actin cytoskeleton, even in the steady state. Initial tugging forces could induce damage through this connection with f-actin. This damage recruits the above mentioned actin repairing proteins which on their turn could aid in the recruitment of vinculin to cell-cell junctions, although it should be noted that in the above mentioned study (Smith, Blankman et al. 2010) ZYXIN does not recruit vinculin in these cell-matrix junctions. However, it has been reported that ZYXIN and VASP can act upstream of vinculin. During spontaneous nucleation and polymerization of actin along the substrate-attached surface of the cell, called F-actin waves, integrin adhesion are initiated in a reverse order wherein vinculin localization follows that of ZYXIN and VASP (Case and Waterman 2011). Moreover, unreported observations in our lab show that after the induction of tension on cell-cell junctions, VASP and ZYXIN are recruited independently of vinculin recruitment to α-catenin. So VASP locates to tensed cell-cell junction independent of vinculin, creating the opportunity for a supporting role in vinculin binding to α- catenin. Taken together the above observations, suggest an actin damage driven recruitment of ZYXIN and VASP that is able to deliver vinculin at the right place and time (Figure 2).

Conceivably the binding of VASP (or similar proteins) to the proline rich region could also turn out to prime vinculin activation in order to facilitate α-catenin binding. That would really complete a large part of the puzzle. Another vinculin activation mechanism functions by means of interaction with the lipid bilayer, a Polyphophoinositides lipid, PIP2, binds to the tail region of vinculin and thereby exposing the binding sites in the head region. Although the actin binding site in the tail is concurrently blocked in this procedure, vinculin's autoinhibited state is overcome and α-catenin's binding site exposed (Steimle, Hoffert et al. 1999). Therefore PIP2 activation could be an intermediate state where initial α-catenin binding is followed by release from the bilayer and consecutive binding to F-actin.

In conclusion, the key players of this specific mechanosensor are clear; α-catenin, vinculin and actin, however supporting roles of other proteins still have to be filled in. Studies in the next few years will definitely reveal these mechanisms and/or supporting proteins for α-catenin and vinculin activation.

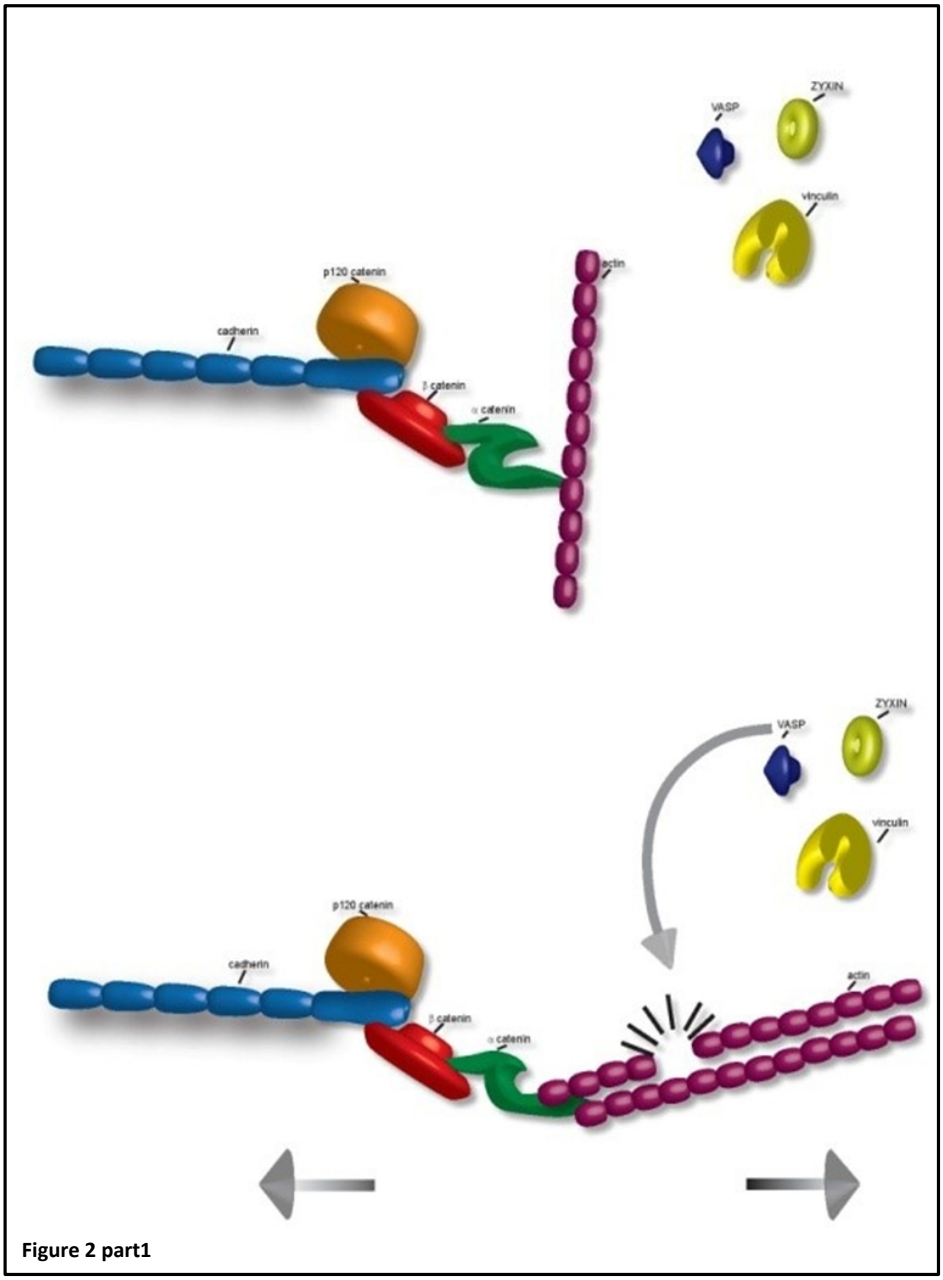

Figure 2 part1

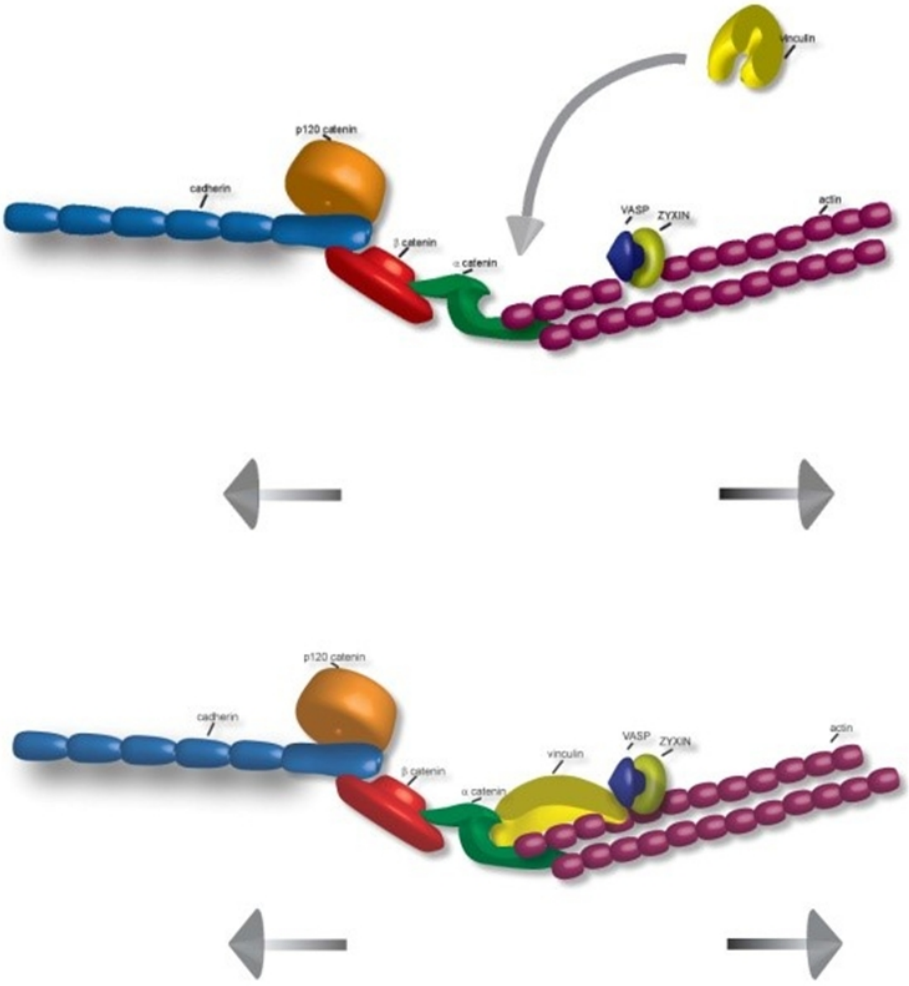

Figure 2
Schematic overview of a possible vinculin recruiting mechanism in in cell-cell junctions. The indicated arrows represent tension upon the complex, whereby actin damage results in VASP and ZYXIN recruitment, who subsequently recruit vinculin.

Open questions.

The mechanosensing properties shown in the magnetic twisting cytometry experiments in DLD1-R2/7 cells ((Twiss, Le Duc et al. 2012),chapter 4), were fully dependent on an intact vinculin binding domain in a-catenin (a-catenin-DVBS was the mutant used). This suggested that α-catenin-dependent vinculin recruitment was the only mechanosensitive mechanism present at cell-cell junctions. Putting things in perspective, the magnetic beads used in the assay are only 4.5μM in size

while the cells have a size of approximately 50-100μM. Thus forces actuated at the bead-cell contact are distributed over a much smaller area in comparison to the physiological cell-cell contact.
Although mechanosensing at the local level seems α-catenin-vinculin binding dependent, this might not necessarily be true for the cell-cell contact at a global level. In our initial experiments comparing WT F9 cells to vinculin deficient F9 cells, force dependent reinforcement was not totally abolished in the absence of vinculin, so other mechanosensitive systems could be involved here. The discrepancy with the complete abrogation of mechanosensing by α-catinin-VBS disruption could also be explained by possible disruption of additional α-catenin interactions in this mutant. Alternatively the vinculin deficient F9 cells are not completely deprived of all vinculin, minimal amounts of vinculin are detected by western blotting (unreported observation), possibly the result of alternative splicing.

A vinculin independent mechanosensing model.

In a recent study by N. Borghi et al, a FRET based tension sensor in the cytoplasmic part of the E-cadherin molecule shows that E-cadherin is under constitutive actomyosin generated tension. Even when E-cadherin is present at the cell surface without engaging in a trans-homophilic interaction, and therefore no contra force from the neighboring cell is exerted, tensile forces are still measured (Borghi, Sorokina et al. 2012). The cadherin complex seems therefore to be linked to the actin cytoskeleton during its whole lifetime at the membrane surface by a constitutive link, even when the cadherin complex is in the steady state. So possibly the cadherin complex is linked to the cortical actin network running parallel to the cell membrane which is present in the steady state. In our model, mechanosensing is established by tugging forces on this constitutive link and the subsequent recruitment of vinculin, which forms an additional link to the actin cytoskeleton. Possibly alternative mechanosensing processes modify the constitutive link independent of the recruitment of vincullin. The earlier discussed F-actin damage repair system could also function as an independent mechanosensitive mechanism. Upon initial exertion of force on c-c junctions the actin cytoskeleton conveys damaging tensile forces via this constitutive link and therefore recruits actin remodeling proteins (Smith, Blankman et al. 2010). F-actin binding proteins like Zyxin, Vasp and α-actinin could remodel the cortical actin fibers of this constitutive link into a stiffer and stronger tension enduring radial actin network. This model describes a mechanism were cadherin mediated junctions could be reinforced independ of the formation of extra connections to the actin cytoskeleton.

Alternatives to the vinculin-cadherin mechanosensing model.

Alternative force sensing mechanisms dependent on other c-c junction receptors than cadherin, could exist because, several other c-c junction receptors physically connect to the cytoskeleton. During shearflow alignment of endothelial cells, PECAM-1 was identified to be the mechanosensor while VE-cadherin merely played an adaptor role (Tzima, Irani-Tehrani et al. 2005).The PECAM-1 receptor may not be as widespread among tissue types as cadherin, however other Cell Adhesion Molecules like L1-CAM and N-cam (for review see Gibson 2011) could substitute for PECAM in other cell types. So, in parallel of the VE-cadherin PECAM mechanosensor other cadherin CAM combinations could produce a similar mechanism.
The c-c junction receptor Nectin is closely associated with the cadherin complex (Tachibana, Nakanishi et al. 2000). It's know that both cadherins and Nectins are crucial for c-c junction formation (Tachibana, Nakanishi et al. 2000; Mizoguchi, Nakanishi et al. 2002) (Takai and Nakanishi 2003; Morita, Nandadasa et al. 2010) and it has therefore remained unclear whether cadherins or Nectins form the mechanical connection to actomyosin involved in the organization of junction formation. In chapter 4 of this thesis

(Twiss, Le Duc et al. 2012) we showed that the α-catenin-cadherin fusion is capable of mechanosensing, but this doesn't exclude Nectin from participation. Nectin's heterophilic association with cadherin in cis could be crucial for the functioning of cadherin dependent mechanosensing, independent of intercellular Nectin bonds.
Whereas these alternative c-c adhesion receptors still incorporate the actomyosin network into the tension-sensor, it doesn't look like actomyosin has a monopoly on providing force generation.
A different example of cadherin-based mechanotransduction, where tension generation did not directly depend on actomyosin, is found in Xenopus cells. The pulling of C-cadherin coated beads binding to isolated cells resulted in protrusion formation at the side of the cell opposing the bead-cell contact site (Weber, Bjerke et al. 2012). The system allows clustered xenopus cells to synchronize cell protrusions needed for simultaneous migration during gastrulation. This mechanosensation was dependent on both the keratin intermediate filament and their connection, through plakoglobin, to the C-cadherin complex, which leaves no role for a-catenin and actomyosin.
Another possible alternative mechanosensory mechanism does involve α-catenin, with the discrepancy being that the actual tension sensing is performed by a mechanosensitive ion channel. The calcium channel TRPV4 that can interact with α-catenin, may localize at cell-cell contact sites (Ko, Arora et al. 2001; Sokabe and Tominaga 2010; Janssen, Hoenderop et al. 2011). This opens the possibility that calcium influxes are generated by force at cell-cell junctions.
How these alternative tension-sensing mechanisms interplay with the Cadherin- α-catenin-vinculin mechanism is fascinating. How are these systems integrated and who dominates in the cell?

Evolutionary design

A seniority battle; c-c or c-m

The dynamics of the force-actuated response of classical cadherins permits a comparison with the dynamics of the highly actomyosin regulated focal adhesions (FA). The force dependent reinforcement of integrin-matrix junction shows similarities with the cadherin mediated junctions. Proteins like actin and vinculin are the most prominent examples of shared proteins in mechanotransduction. Others like vinexin, ponsin, VASP, ZYXIN remain suspects, until their function in mechanotransduction is further elucidated. Interestingly, endogenous forces measured at FAs and cadherin mediated junctions appear to be of the same magnitude (Ganz, Lambert et al. 2006; Maruthamuthu, Sabass et al. 2011). But are both systems really related to each other?
Was evolution smart enough to not invent the wheel twice or did the formation of multicellular organisms demand more than just one universal adhesion mechanosensing system could provide?

Cell adhesion predates multicellular organisms

The origin of either cell adhesion system predates multicellular, metazoan, organisms: homologues of current cell-cell and c-m adhesion proteins are found in pre-metazoan Dictyostelium discoideum and choanoflagellates (King, Hittinger et al. 2003; Cornillon, Gebbie et al. 2006; Abedin and King 2008: Dickinson et al 2011). However, the homologues of the c-c junction members found in these "simple" organisms do not form a functional adhesion complex whereas the homologues for the c-m junctions do as talin and paxillin homologues associate with the integrin in D. discoideum (Tsujioka, Yoshida et al. 2008). In D. discoideum the β-catenin and α-catenin homologues are involved in cytoskeletal organization and epithelial cell polarity, however no cadherin like protein capable of binding these proteins has been detected in this organism (Stadler, Keenan et al. 1989; Wong, Brar et al. 1996; Wang and Chakrabarty 2001). In the metazoan phylogeny/family tree the sponge A.

queenslandica is the first branch to contain a form of cadherin that has a putative β-catenin binding domain (Srivastava, Simakov et al. 2010), suggesting the capacity to form a complex with β- and α-catenin. However, C. elegans and M. drosophila are the simplest organism in evolutionary hierarchy where cadherins have been been functionally characterized as c-c receptors and catenins actually have been found in complex with cadherin (for review see Nichols, Roberts et al. 2012). So while protein complexes associated with integrins appear in pre-metazoan organisms, a complex associated with cadherins appeared only after the formation of multicellular organisms. Taking everything in consideration it does seem like the evolution of the metazoan c-m system has had a jump start in single cell organisms in comparison to the classical c-c junctions which are only present in multicellular organisms, (even though isolated members of both c-c and c-m systems appeared simultaneous during evolution), giving us so far no signs that c-c and c-m junctions share a common ground.

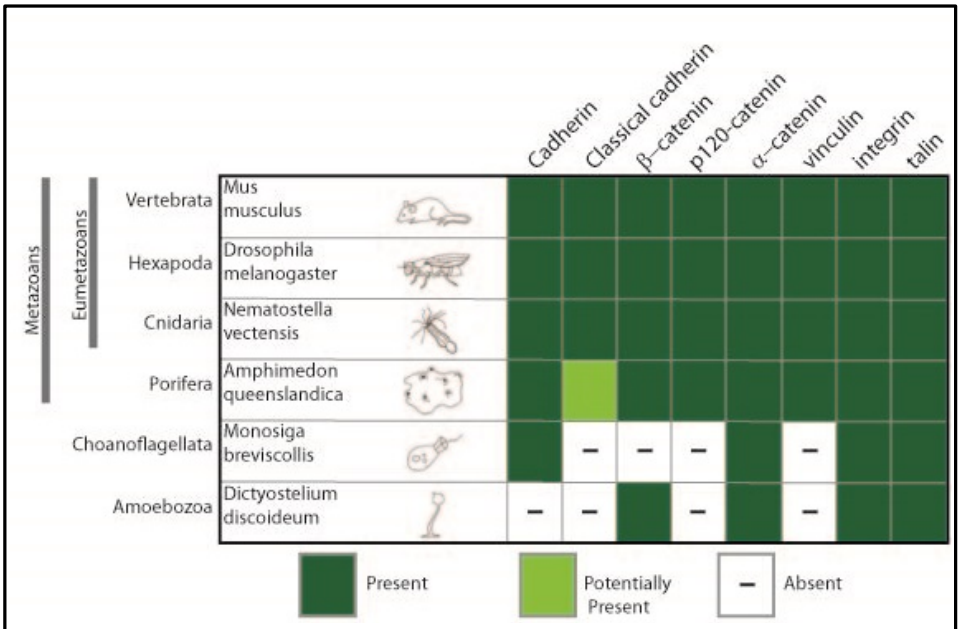

Figure 3
A table depicting organisms in subsequent appearance on the evolutionary timescale, ranging from single cell organisms up to complex multicellular mammals on the Y-axis and the presence or absence of several proteins involved in either cell-cell or cell-matrix adhesions.

When does vinculin appear on stage

Interesting to know is when vinculin, a mechanosensitive protein shared by c-c and c-m junction systems, entered the stage. Vinculin is related to α-catenin. Since α-catenin homologues appear in pre-metazoan organisms and close vinculin homologues are only found within the metazoan phylum, α-catenin is the ancestral protein of vinculin. This relation of α-catenin and vinculin might suggest a co-evolution of both proteins in c-c junctions, however the functioning of early vinculin homologues appears to be restricted to c-m junctions. Surprisingly, even though a vinculin homologue is present in C. elegans, it is not expressed in its epithelia and has therefore no function in c-c adhesion (Kwiatkowski, Maiden et al. 2010). On the other hand, vinculin is present in C. elegans c-m adhesion

display disrupted embryonic elongation and muscle development ((Barstead and Waterston 1991). Furthermore, vinculin homologues have been identified in simpler organisms than C. elegans, suggesting that it could have been functioning in c-m junctions for a long time in evolutionary history. So when did vinculin then get involved in c-c adhesions? Next to c. elegans we know from personal communications with other labs that vinculin is also not essential in the c-c adhesions of D. melanogaster either. This suggests that vinculin is actually quite a novice to the c-c junction system in evolutionary history, since all known reports of vinculin involvement in c-c junctions are in cells of vertebrate origin. This suggests that vinculin was initially exclusively involved in c-m adhesion before turning to c-c adhesion.

Are c-c and c-m systems interconnected?

So, if at all, where did both c-c and c-m systems interconnect, did α-catenin maybe adopt the molecular vinculin activating mechanism that was evolved in the c-m system? Actually, the vinculin binding partners α-catenin and Talin for c-c and c-m junctions respectively, show no structural similarities, for instance the number of putative vinculin binding sites differ substantially between α-catenin (1) and c-m talin (11) (Critchley 2009). Underscoring the fundamental differences in vinculin binding between c-m and c-c junctions, the A50 residue in vinculin is essential for talin binding, but not for α-catenin binding (Peng, Zhong et al. 2009), further suggesting separate development of vinculin incorporation between c-c and c-m systems. In conclusion, although vinculin and actomyosin are utilized by both types of adhesion, in current knowledge of both their pathways strong similarities seem aberrant.

By drawing a parallel between the c-c and c-m adhesion systems , similarities found could be used to extrapolate working mechanism from c-m to c-c adhesion systems or vice versa. So knowledge from one system could be used to accelerate the study of the other system. On the other hand, one must not unnecessarily invest into the quest of revealing similarities when they do not exist. Current understanding of both systems reveal no big similarities evidence found is still circumstantial. Future research has to show if vinculin is the only member present in both systems or that more interactors are shared by these systems, thereby showing features of one universal system. It is possible that similarities found between c-c and c-m adhesion system are just coincidental. A recent study shows that myocytes on a N-cadherin substrate enhance myofibril organization while myocytes on fibronectin/ integrin mediated adhesions disrupt this organization(Chopra, Patel et al. 2012). Maybe the two systems differ too much to utilize a similar mechanosensing-system. For instance the high number of adhesion receptors numbers for c-c in comparison to those for c-m adhesion, make it far more complex to regulate in a similar manor. In many tissues multiple cell-cell adhesion proteins co-exist: cadherins, nectins, CAM's, occludins, claudins and JAM's to name a few. Most have been reported to link to the cytoskeleton and some even have mechanosensing properties, as described above. Wouldn't (Tachibana, Nakanishi et al. 2000)it be too much juggling for such a single universal system to keep all these different connections up in the air?

Maybe there is only a single mechanosensitive adhesion system for both c-c and c-m

In defense of the single universal design hypothesis: during endothelial junction formation it was shown that integrin adhesion complexes and cadherin adhesion complexes are in close proximity(references!! Birukov work? Others?). These observations open up the intriguing possibility that the actin cytoskeleton could even swap directly from integrins to cadherins, in this case there would actually only be one system which is shared by both c-m and c-c. In this view, the integrin-connected actomyosin bundles would be directly transferred to the cadherin mediated junctions at specific sites where cell-matrix intersects with the cell-cell borders. Indeed fibronectin binding

integrins have been observed in cell-cell contact areas and a direct complex formation between a3b1 and the E-cadherin complex has been postulated in epithelial cells as well endothelial cells? (Chattopadhyay, Wang et al. 2003). Thus, there is anecdotal evidence for close contact between integrins and cadherins that underscores the possibility of the existence of transfer regions where integrins and cadherins share or transfer their cytoskeletal connection. The existence of such a region could be intermediated by cadherins that can mediate weak heterophilic interactions with integrins. For instance, both E and N-cadherin can interact with the intergrin αEβ7.(Cepek, Shaw et al. 1994). Possible exchange of the constructed actomyosin network between these adhesion receptors could prevent the major (unfavorable) remodeling of actomyosin network, during migration over substrates and other cells, which would happen if adhesion-actomyosin anchorage is completely lost.

Summarizing the current understanding of both c-c and c-m mechanosensing systems, similarities are found in functional output, however identification of molecular similarities does not reach much further than the presence of vinculin and the actomyosin network. Other components do locate to both c-c and c-m junctions, like ZYXIN, VASP and ponsin for example, however their relation to either c-c or c-m mechanosensing systems is not yet fully established. Even without all the pieces in place, some researchers see enough reason to name the actomyosin regulated c-c junctions “Focal Adherens Junctions” (FAJ). By using that name, they wish to convey the notion that there is a clear analogy to cell-matrix junctions that are named FAs. As argued above however, it could very well be that one mechanism evolved for integrin mediated mechanosensing while a distinct mechanism separately evolved for the c-c adhesion proteins. So far undiscovered mechanomachinery proteins and mechanisms hold the key; will they refute additional homologies between c-c and c-m sytems or actually confirm that “Focal adherens junction” is correct nomenclature.

References

Abe, K. and M. Takeichi (2008). "EPLIN mediates linkage of the cadherin catenin complex to F-actin and stabilizes the circumferential actin belt." Proc Natl Acad Sci U S A **105**(1): 13-19.

Abedin, M. and N. King (2008). "The premetazoan ancestry of cadherins." Science **319**(5865): 946-948.

Barstead, R. J. and R. H. Waterston (1991). "Vinculin is essential for muscle function in the nematode." J Cell Biol **114**(4): 715-724.

Bear, J. E. and F. B. Gertler (2009). "Ena/VASP: towards resolving a pointed controversy at the barbed end." J Cell Sci **122**(Pt 12): 1947-1953.

Borghi, N., M. Sorokina, et al. (2012). "E-cadherin is under constitutive actomyosin-generated tension that is increased at cell-cell contacts upon externally applied stretch." Proc Natl Acad Sci U S A **109**(31): 12568-12573.

Case, L. B. and C. M. Waterman (2011). "Adhesive F-actin waves: a novel integrin-mediated adhesion complex coupled to ventral actin polymerization." PLoS One **6**(11): e26631.

Cepek, K. L., S. K. Shaw, et al. (1994). "Adhesion between epithelial cells and T lymphocytes mediated by E-cadherin and the alpha E beta 7 integrin." Nature **372**(6502): 190-193.

Chattopadhyay, N., Z. Wang, et al. (2003). "alpha3beta1 integrin-CD151, a component of the cadherin-catenin complex, regulates PTPmu expression and cell-cell adhesion." J Cell Biol **163**(6): 1351-1362.

Chervin-Petinot, A., M. Courcon, et al. (2012). "Epithelial protein lost in neoplasm (EPLIN) interacts with alpha-catenin and actin filaments in endothelial cells and stabilizes vascular capillary network in vitro." J Biol Chem **287**(10): 7556-7572.

Choi, H. J., S. Pokutta, et al. (2012). "alphaE-catenin is an autoinhibited molecule that coactivates vinculin." Proc Natl Acad Sci U S A **109**(22): 8576-8581.
Chopra, A., A. Patel, et al. (2012). "alpha-Catenin localization and sarcomere self-organization on N-
Cornillon, S., L. Gebbie, et al. (2006). "An adhesion molecule in free-living Dictyostelium amoebae with integrin beta features." EMBO Rep **7**(6): 617-621.
Critchley, D. R. (2009). "Biochemical and structural properties of the integrin-associated cytoskeletal protein talin." Annu Rev Biophys **38**: 235-254.
Ganz, A., M. Lambert, et al. (2006). "Traction forces exerted through N-cadherin contacts." Biol Cell **98**(12): 721-730.
Gibson, N. J. (2011). "Cell adhesion molecules in context: CAM function depends on the neighborhood." Cell Adh Migr **5**(1): 48-51.
Huveneers, S., J. Oldenburg, et al. (2012). "Vinculin associates with endothelial VE-cadherin junctions to control force-dependent remodeling." J Cell Biol **196**(5): 641-652.
Itoh, M., A. Nagafuchi, et al. (1997). "Involvement of ZO-1 in cadherin-based cell adhesion through its direct binding to alpha catenin and actin filaments." J Cell Biol **138**(1): 181-192.
Janssen, D. A., J. G. Hoenderop, et al. (2011). "The mechanoreceptor TRPV4 is localized in adherence junctions of the human bladder urothelium: a morphological study." J Urol **186**(3): 1121-1127.
King, N., C. T. Hittinger, et al. (2003). "Evolution of key cell signaling and adhesion protein families predates animal origins." Science **301**(5631): 361-363.
Kioka, N., S. Sakata, et al. (1999). "Vinexin: a novel vinculin-binding protein with multiple SH3 domains enhances actin cytoskeletal organization." J Cell Biol **144**(1): 59-69.
Ko, K. S., P. D. Arora, et al. (2001). "Cadherins mediate intercellular mechanical signaling in fibroblasts by activation of stretch-sensitive calcium-permeable channels." J Biol Chem **276**(38): 35967-35977.
Kwiatkowski, A. V., S. L. Maiden, et al. (2010). "In vitro and in vivo reconstitution of the cadherin-catenin-actin complex from Caenorhabditis elegans." Proc Natl Acad Sci U S A **107**(33): 14591-14596.
Ladoux, B., E. Anon, et al. (2010). "Strength dependence of cadherin-mediated adhesions." Biophys J **98**(4): 534-542.
le Duc, Q., Q. Shi, et al. (2010). "Vinculin potentiates E-cadherin mechanosensing and is recruited to actin-anchored sites within adherens junctions in a myosin II-dependent manner." J Cell Biol **189**(7): 1107-1115.
Liu, Z., J. L. Tan, et al. (2010). "Mechanical tugging force regulates the size of cell-cell junctions." Proc Natl Acad Sci U S A **107**(22): 9944-9949.
Maruthamuthu, V., B. Sabass, et al. (2011). "Cell-ECM traction force modulates endogenous tension at cell-cell contacts." Proc Natl Acad Sci U S A **108**(12): 4708-4713.
Mizoguchi, A., H. Nakanishi, et al. (2002). "Nectin: an adhesion molecule involved in formation of synapses." J Cell Biol **156**(3): 555-565.
Morita, H., S. Nandadasa, et al. (2010). "Nectin-2 and N-cadherin interact through extracellular domains and induce apical accumulation of F-actin in apical constriction of Xenopus neural tube morphogenesis." Development **137**(8): 1315-1325.
Moulder, G. L., M. M. Huang, et al. (1996). "Talin requires beta-integrin, but not vinculin, for its assembly into focal adhesion-like structures in the nematode Caenorhabditis elegans." Mol Biol Cell **7**(8): 1181-1193.
Nichols, S. A., B. W. Roberts, et al. (2012). "Origin of metazoan cadherin diversity and the antiquity of the classical cadherin/beta-catenin complex." Proc Natl Acad Sci U S A **109**(32): 13046-13051.

Peng, H., X. Y. Zhong, et al. (2009). "Expression and significance of adenomatous polyposis coli, beta-catenin, E-cadherin and cyclin D1 in esophageal squamous cell carcinoma assessed by tissue microarray." Ai Zheng **28**(1): 38-41.
Pokutta, S., F. Drees, et al. (2002). "Biochemical and structural definition of the l-afadin- and actin-binding sites of alpha-catenin." J Biol Chem **277**(21): 18868-18874.
Smith, M. A., E. Blankman, et al. (2010). "A zyxin-mediated mechanism for actin stress fiber maintenance and repair." Dev Cell **19**(3): 365-376.
Sokabe, T. and M. Tominaga (2010). "The TRPV4 cation channel: A molecule linking skin temperature and barrier function." Commun Integr Biol **3**(6): 619-621.
Srivastava, M., O. Simakov, et al. (2010). "The Amphimedon queenslandica genome and the evolution of animal complexity." Nature **466**(7307): 720-726.
Stadler, J., T. W. Keenan, et al. (1989). "The contact site A glycoprotein of Dictyostelium discoideum carries a phospholipid anchor of a novel type." EMBO J **8**(2): 371-377.
Steimle, P. A., J. D. Hoffert, et al. (1999). "Polyphosphoinositides inhibit the interaction of vinculin with actin filaments." J Biol Chem **274**(26): 18414-18420.
Tachibana, K., H. Nakanishi, et al. (2000). "Two cell adhesion molecules, nectin and cadherin, interact through their cytoplasmic domain-associated proteins." J Cell Biol **150**(5): 1161-1176.
Takai, Y. and H. Nakanishi (2003). "Nectin and afadin: novel organizers of intercellular junctions." J Cell Sci **116**(Pt 1): 17-27.
Tsujioka, M., K. Yoshida, et al. (2008). "Overlapping functions of the two talin homologues in Dictyostelium." Eukaryot Cell **7**(5): 906-916.
Twiss, F., Q. Le Duc, et al. (2012). "Vinculin-dependent Cadherin mechanosensing regulates efficient epithelial barrier formation." Biol Open **1**(11): 1128-1140.
Tzima, E., M. Irani-Tehrani, et al. (2005). "A mechanosensory complex that mediates the endothelial cell response to fluid shear stress." Nature **437**(7057): 426-431.
Wang, H. and S. Chakrabarty (2001). "Requirement of protein kinase Calpha, extracellular matrix remodeling, and cell-matrix interaction for transforming growth factorbeta-regulated expression of E-cadherin and catenins." J Cell Physiol **187**(2): 188-195.
Weber, G. F., M. A. Bjerke, et al. (2012). "A mechanoresponsive cadherin-keratin complex directs polarized protrusive behavior and collective cell migration." Dev Cell **22**(1): 104-115.
Wong, E. F., S. K. Brar, et al. (1996). "Molecular cloning and characterization of DdCAD-1, a Ca2+-dependent cell-cell adhesion molecule, in Dictyostelium discoideum." J Biol Chem **271**(27): 16399-16408.
Yonemura, S., Y. Wada, et al. (2010). "alpha-Catenin as a tension transducer that induces adherens junction development." Nat Cell Biol **12**(6): 533-542.

Nederlandse samenvatting voor leken

Het lichaam bestaat uit miljarden cellen en de reden dat deze niet uit elkaar vallen is gestoeld op twee biologische aspecten, de contacten tussen cellen zelf en de contacten tussen cellen en hun ondergrond. Een sprekend voorbeeld is de huid, dit zijn meerdere lagen van huidcellen die als mozaïek aan elkaar liggen en als geheel steun vinden aan de bindweefsel-laag van de onderhuid.

Het tot stand komen van cel-cel contacten verloopt via vele eiwitten die zich aan de buitenkant van de cellen bevinden, als een soort armen die uitreiken naar naburige cellen. In diezelfde analogie kan men de eiwitten, die contact met de ondergrond vormen, zien als de voeten die stabiliteit zoeken op de ondergrond. Aangezien de miljarden cellen waar wij uit bestaan voortkomen uit de samenkomst van maar twee cellen, een zaad- en een ie-cel, kan men voorstellen dat nieuwe contacten gevormd moeten kunnen worden en oude afgebroken. Gedurende verscheidene veranderingen in lichaamsweefsel, zoals wondgenezing, maar ook de uitzaaing van kankercellen zullen deze cel contacten onderhevig zijn aan processen van formatie en afbraak. Dus hoe weet de arm of voet van de cel nu wanneer hij een contact moet aangaan of juist verbreken. Hiervoor geef ik eerst een globale uitleg over de opbouw van de cel-cel contact, arm van de cel. De buitenkant van de cel zelf is een dun vliesje dat net zoals onze huid zonder skelet geen sterke trekkrachten kan weerstaan. Gelukkig heeft de cel zijn eigen skelet, gevormd door lange strengen eiwitten. En de brug tussen dit skelet en de arm aan de celwand is opgebouwd uit een complex van verschillende soorten eiwitten. En juist in deze brug lijkt veel aansturing van de “armen” plaats te vinden door middel van variaties in samenstelling van de eiwit-bouwstenen.

Wat wij voornamelijk aan hebben getoond is dat een bepaald eiwit genaamd Vinculin gedirigeerd word naar de brug zodra de cel-contacten meer trekkrachten te verduren krijgen. Hierdoor word de brug in staat gesteld om meer trekkrachten te weerstaan. Het lijkt erop dat de cel-contacten in verschillende stadia kunnen verkeren. Een rust stadium waarbij weinig krachten uitgeoefend worden op de onderlinge contacten en andere waarbij de cellen ten opzichte van elkaar bewegen en dus aan elkaar trekken. In dit laatste stadium wordt de brug versterkt met het eiwitten waarin vinculin een prominente rol vervult.

Hoofdstuk 1 geeft een kort overzicht van wat er in de meest recente jaren in ons vakgebied ontdekt is. Voornamelijk de beschrijving van verschillende biologische processen waarin de aansturing van cel-cel contacten een hoofdrol vervullen, zoals de reorganisatie van weefsel tijdens de ontwikkeling naar een volwassen wezen. Daarnaast worden ook de ontwikkelingen op het niveau van de individuele bouwstenen binnen de cel-cel contacten besproken. Voornamelijk het bestaan van een brug tussen de arm en het skelet krijgt veel aandacht omdat het bestaan hiervan door sommige wetenschappers betwijfeld werd, maar ook de specifieke opbouw en regulering van deze brug is een “heet” onderwerp waar veel belangstelling naar is.

Hoofdstuk 2 laat duidelijk zien dat vinculin betrokken is bij de regulatie van cel-cel contacten. Het feit dat Vinculin niet alleen betrokken is bij cel-cel contacten, de armen van de cel, maar ook de voeten maakt het een hele lastige opgave om deze twee functies van elkaar te scheiden. Door hele kleine magnetische kraaltjes met “arm”-eiwitten te bedekken kunnen wij ze cel contacten aan laten gaan met

cellen. En met behulp van de magnetische eigenschappen van de kraaltjes kan er aan getrokken worden en dus bepaalt worden hoe stevig de arm aan het skelet vast zit. Dit geeft informatie over de sterkte van de brug tussen de arm en het cel-skelet, onder normale omstandigheden maar ook als we cellen gebruiken waar ons eiwit van interesse niet voorkomt. En wat blijkt;cellen zonder het eiwit vinculin hebben een minder stevige verankering aan het skelet dan cellen met dit eiwit.

Hoofdstuk 3 beschrijft de rol van vinculin en cel-"armen" in betrekking tot barriere vormende cel-lagen, zoals bijvoorbeeld de huid. Als cellen een laag vormen zullen ze elkaar vast moeten pakken willen ze een stevige laag kunnen vormen, hierbij zijn de "armen" cruciaal. Als de cellen elkaar vastpakken is vinculin in het begin heel belangrijk om de cel-cel contacten in staat te stellen de cellen naar elkaar toe te trekken, maar als eenmaal een dichte barrière gevormd is , verdwijnt vinculin uit het 'arm'-complex en ontstaat er een stabiele situatie.

Hoofdstuk 4 bouwt voort op hoofdstuk 2 en 3 door te laten zien dat het eiwit Vinculin zijn functie uitoefent in vele celtypen. De armen van de cel zijn niet voor elk celtype hetzelfde, cellen van de bloedvaten hebben bijvoorbeeld een andere vorm van de arm dan een huidcel of zenuwcel. Om aan te tonen dat de functie van Vinculin belangrijk is voor alle vormen van armen word in dit hoofdstuk aangetoond dat Vinculin daar inderdaad aanwezig. Doormiddel van geavanceerde microscopie kunnen de locaties van verschillende eiwitten toonbaar gemaakt worden in de cel. Naast dat Vinculin aanwezig is in cel-cel contacten waar trekkrachten op uitgeoefend worden laten we ook duidelijk zien dat Vinculin niet aanwezig is als de trekkrachten in de cel plat gelegd worden doormiddel van chemische stofjes.

Hoofdstuk 5 beslaat onderzoek naar cellen die onder invloed van een “verspreidings” factor hun buurmannen verlaten en zich gaan verplaatsen door de ruimte. Deze “verspeidings” factor word dus ingezet zodat wij het proces van cel-cel contact afbraak kunnen aanzetten. Er is nog veel onduidelijk rondom dit proces van afbraak en doormiddel van deze factor kunnen wij dit nader bestuderen. Ten eerste word besproken hoe de software ontwikkeld is om speciaal deze cellen te volgen in de tijd. Een menselijk oog zou dit prima kunnen, maar de hoeveelheid data en het feit dat de observaties omgezet moeten worden naar harde cijfers maakt deze software onmisbaar. Daarnaast wordt er gekeken of wij dit proces kunnen saboteren met behulp van onder andere chemische stofjes. Dit via het principe van: als je een onderdeel uit een auto haalt en hij doet het niet meer zal het vast wel belangrijk zijn.

Hoofstuk 6 bespreekt in het kort de resultaten van de voorgaande hoofdstukken en kijkt naar wat de toekomst in dit onderzoeksgebied gaat brengen. Vooral het mechanisme waarop het complex van eiwitten dat de brug vormt de informatie van de cel verwerkt is nog niet volledig opgehelderd. De eiwitten, waarvan Vinculin er één is, moeten op een bepaalde manier geactiveerd worden waardoor ze in staat zijn om aan de ene kant het skelet te kunnen binden en aan de andere kant contact kan maken met de armen van de cel. Zodra de processen rond cel-cel contacten verder ontrafeld worden zullen er ook aangrijpingspunten ontstaan waardoor middelen ontwikkeld kunnen worden die verstoringen naar aanleidingen van ziektes kunnen verhelpen.

Curriculum Vitae

Quint le Duc werd geboren te Meliskerke op 28 mei 1980. In 1998 behaalde hij zijn VWO diploma aan het Stedelijk Scholen Gemeenschap Middelburg. In 1999 begon hij aan de opleiding biologie van de universiteit Utrecht. In 2004 studeerde hij af en begon hij aan een promotietraject bij het VUMC en Brandwondenstichting voor het ontwikkelen van huidvervanging voor brandwonden.
Na een jaar heeft hij deze vroegtijdig beeindigd en is in 2007 begonnen aan een nieuwe aio-positie bij het NKI en later het Hubrecht instituurt onder leiding van J. de Rooij. De resultaten van deze studie naar de dynamische eigenschappen van cel-cel contacten staan beschreven in dit proefschrift.

List of publications

Twiss F, **Le Duc Q**, Van Der Horst S, Tabdili H, Van Der Krogt G, Wang N, Rehmann H, Huveneers S, Leckband DE, De Rooij J.
Vinculin-dependent Cadherin mechanosensing regulates efficient epithelial barrier formation.
Biol Open. 2012 Nov 15;1(11):1128-40

Loerke D, **le Duc Q**, Blonk I, Kerstens A, Spanjaard E, Machacek M, Danuser G, de Rooij J.
Quantitative imaging of epithelial cell scattering identifies specific inhibitors of cell motility and cell-cell dissociation.
Sci Signal. 2012 Jul 3;5(231)

Leckband DE, **le Duc Q**, Wang N, de Rooij J.
Mechanotransduction at cadherin-mediated adhesions.
Curr Opin Cell Biol. 2011 Oct;23(5):523-30.

le Duc Q, Shi Q, Blonk I, Sonnenberg A, Wang N, Leckband D, de Rooij J.
Vinculin potentiates E-cadherin mechanosensing and is recruited to actin-anchored sites within adherens junctions in a myosin II-dependent manner.
J Cell Biol. 2010 Jun 28;189(7):1107-15.

Klooster R, Eman MR, **le Duc Q**, Verheesen P, Verrips CT, Roovers RC, Post JA.
Selection and characterization of KDEL-specific VHH antibody fragments and their application in the study of ER resident protein expression.
J Immunol Methods. 2009 Mar 15;342(1-2):1-12.

le Duc Q, Breetveld M, Middelkoop E, Scheper RJ, Ulrich MM, Gibbs S.
A cytotoxic analysis of antiseptic medication on skin substitutes and autograft.
Br J Dermatol. 2007 Jul;157(1):33-40.